NOTICE

The quality of this microform is heavily dependent upon the quality of the original thesis submitted for microfilming. Every effort has been made to ensure the highest quality of reproduction possible.

If pages are missing, contact the university which granted the degree.

Some pages may have indistinct print especially if the original pages were typed with a poor typewriter ribbon or if the university sent us an inferior photocopy.

Reproduction in full or in part of this microform is governed by the Canadian Copyright Act, R.S.C. 1970, c. C-30, and subsequent amendments.

AVIS

La qualité de cette microforme dépend grandement de la qualité de la thèse soumise au microfilmage. Nous avons tout fait pour assurer une qualité supérieure de reproduction.

S'il manque des pages, veuillez communiquer avec l'université qui a conféré le grade.

La qualité d'impression de certaines pages peut laisser à désirer, surtout si les pages originales ont été dactylographiées à l'aide d'un ruban usé ou si l'université nous a fait parvenir une photocopie de qualité inférieure.

La reproduction, même partielle, de cette microforme est soumise à la Loi canadienne sur le droit d'auteur, SRC 1970, c. C-30, et ses amendements subséquents.

ISBN 0-315-56067-3

Canada

Photochemical Charge Transfer Across the Electrolyte/Electrode Interface Mediated by Polymers Doped with Dithiolene Complexes

David Anthony Biro

A Thesis

in

The Department

of

Chemistry and Biochemistry

Presented in Partial Fulfillment of the Requirements
for the Degree of Doctor of Philosophy at
Concordia University
Montréal, Québec, Canada

December 1989

ABSTRACT

Photochemical Charge Transfer Across the Electrolyte/Electrode Interface Mediated by Polymers Doped with Dithiolene Complexes

David Anthony Biro, Ph.D.
Concordia University, 1989

The photochemical and photoelectrochemical behaviour of two metal maleonitriledithiolate ($M(mnt)_2$) complexes was investigated in homogeneous solution and in electroactive polymer films on SnO_2 electrodes. Acetonitrile solutions of $Ni(mnt)_2^{2-}$ and $Pt(mnt)_2^{2}$ undergo photo-oxidation to the monoanion under visible light irradiation. Transient absorption spectroscopy of the above complexes suggests that the excited state of the platinum complex is longer lived than its nickel counterpart.

Irradiation in a metal to ligand charge transfer band of $M(mnt)_2$ in a $[MV^{2+}][M(mnt)_2^{2}]$ (where MV^{2+}= methyl viologen) salt produces emission associated with a partially reduced viologen species indicating photoinduced charge transfer between the mnt and the viologen.

The photoelectrochemical behaviour of polymer modified electrodes containing the dithiolene complexes was investigated to gain insight on the charge transport processes involved following irradiation of the films with visible light. An ion-exchange polymer blend based on quaternized poly(chloromethylstyrene-co-styrene) and poly(vinylpyridine-co-styrene) was used to incorporate $Ni(mnt)_2^{2}$ and $Pt(mnt)_2^{2-}$.

Anodic photocurrents in the μA range were observed under white light illumination. This polymer film displayed high ionic conductivity with diffusion coefficients for $Fe(CN)_6^{3-/4-}$ from 0.5→6.0 X 10^{-7} cm^2/sec. Composite films of the polymer appear to segregate into hydrophobic and hydrophylic domains. The mechanism of photoconduction in the polymer films was treated using a molecular-ion state model where charge carriers can migrate by a trap controlled mechanism The photogenerated carriers migrate in localized states associated with defect sites in the polymer matrix. These states may trap or partially stabilize a charge carrier. Other ion-exchange polymers based on quaternized poly(chloromethylstyrene-co-styrene) displayed similar results with smaller photocurrents. The photoelectrochemistry of composite modified electrodes with polyviologens and $M(mnt)_2^{2-}$s exhibited charge transport and diffusional characteristics associated with a hopping mechanism between adjacent redox sites. Electronically conducting polypyrrole modified electrodes containing $Ni(mnt)_2^{2-}$ displayed photocurrents in the μA range with trap-controlled characteristics similar to other electroactive polymer described in this study.

Acknowledgements

I wish to express my sincere gratitude to Dr. Cooper H. Langford for his guidance and ideas. His dedication to research and teaching will always an inspiration to me in science and in life.

I want to thank Dr. Marcus Lawrence for helping me understand some physics concepts and for being there as a friend and researcher.

I also wish to thank all the individuals in my research group who helped, assisted, and supported me over the past four years. Without a strong interactive research group, post graduate studies can be hell.

To all my friends who kept telling me to "go for it" when the work was long and hard, thank you for the encouragement.

To my family, for their love and caring at all times, and for financial and moral support during critical stages of the work.

A special thanks to all the secretaries of the chemistry department who knit together the undergraduate students, the faculty, the graduate students and the department into a working fabric.

To Diane, my girlfriend, for her love and support.

To Mama, Mommy, Daddy, Wendy, Scott, and Saffron

TABLE OF CONTENTS

CHAPTER 3
RESULTS AND DISCUSSION I

CHAPTER 4
RESULTS AND DISCUSSION II

CHAPTER 5
RESULTS AND DISCUSSION III

LIST OF FIGURES

PAGE

CHAPTER 5

LIST OF TABLES

CHAPTER 1

INTRODUCTION

1.1 Overview

The investigation of photo-processes in polymeric systems has applications in the synthesis of photoresists for microcircuitry, photocuring of paints and resins, photopolymerization, photodegradation and stabilization of plastics, and xerography, to name some notable ones. A novel area of research is in the use of polymers for various solar energy conversion devices. The significant potential use of such devices includes photovoltaic and/or photogalvanic systems, sensors, and photocatalytic degradation of refractory waste materials. The stability of the polymer systems to solar radiation often becomes a restricting factor in trying to mimic the success of plant photosynthesis. The purpose of chlorophyll *a* in green plants is to use sunlight to absorb and transfer photon energy to well-organized reaction centers. Typically, the efficiency of plant photosynthesis has been estimated between 75% to 95% for transfer of energy or electrons from the "antenna" pigment to the reaction centers. Man-made polymers which mimic the antenna effect can stabilize or enhance polymers against photodegradation, become photocatalysts or provide a host of other uses. New polymeric systems and composites are being developed worldwide in order to improve solar energy conversion without significant deterioration of the polymer system/composite.

Organic materials in thin films form or embedded in polymer matrices have been used in areas such as photography and electrophotography. Both photoprocesses involve the collection and use of light energy. Induced generation of charge and its movement through the film or polymer resembles the photovoltaic and the photosynthetic process. Over the years work in this field has focused mainly on porphyrins, chlorophylls, and similar structures like the phthalocyanines. These planar molecules possess desirable properties as photovoltaic dyes. Part of the work presented here involves the study of photochemical and photophysical properties of two square planar anionic metal-sulfur complexes. The dyes can be incorporated into electroactive polymer films (ion-exchange or redox) in order to elucidate electrochemical and photophysical processes in the films and at the electrode surfaces. These processes are governed chiefly by the nature and morphology of the polymer film, as well as the photophysics of the dyes and their interaction with the polymeric host. Furthermore, the interaction between the support (semiconducting or metallic) and the polymer composite must be favorable in order to obtain rapid charge transfer characteristics and kinetics. These latter factors are important parameters governing the use of such polymer composites as photoactive devices.

In order to gain further insight into these processes, charge transport schemes and energy levels in polymer films will be described. The mechanisms of charge transport in electronically conductive, redox conductive, and ion-exchange polymer films will be examined as well as the physical and chemical properties of chromophores incorporated into polymer films. Finally, some concepts on chemically

modified electrodes and background on the metal maleonitriledithiolates will be described in the introduction.

1.2 The Charge Transport Scheme

1.2.1 Energy and Charge Transfer in Polymer Films

Organic polymers are generally considered to be electrically insulating materials. Most commercial applications relate to packaging, clothing, transportation materials, containers, communications and other non-conducting uses. Polymers tend to be poor conductors of electricity with the exception of polymeric systems with delocalized π-orbitals and/or highly conjugated double bonds. These materials can form complexes with either strong electron acceptors or donors to yield conductivities in the semiconducting to metallic range ($10^{-6} \rightarrow 10^{4}$ ohm^{-1} cm^{-1})(1,2,3,4). Unfortunately, many of these polymers are not processible by conventional solvent or melt techniques, and may possess undesirable mechanical and physical properties which may limit practical applications.

One application of polymeric materials relates to their use in xerography. This stems from the result that polymers, when exposed to light of sufficient energy, develop charged species which can migrate under an electric field, thereby conducting electricity. A photoconductive material is one whose conductivity increases upon illumination. For commercial applications in electrophotography a photoconductive material must exhibit an increase of at least three orders of magnitude when illuminated in the spectral region of interest.

A surprising number of common vinyl and condensation polymers show a substantial increase in conductivity when exposed to light. These include polystyrene (5,6), poly(ethylene terephthalate) (7), and most notably poly(N-vinyl carbazole) (PVK)(8,9,10). The photophysical processes which occur in solid polymer matrices differ considerably from similar reactions in solution on account of limitations of diffusion, and of reduced translational and rotational freedom. Most photophysical processes in a polymer matrix depend on free volume, chemical structure, macroscopic and microscopic viscosity, and glass transition temperature.

These polymers and similar ones are virtually transparent in the visible region of the electromagnetic spectrum. It is desirable for photoconduction and sensitization schemes to enhance the response to visible light. By doping PVK with dyes such as 2,4,7-trinitro-9-fluorenone (TNF), the sensitivity of the material can be increased and extended into the visible region. New absorption bands appear as a result of charge-transfer from the highest occupied molecular orbital of carbazole to the lowest unoccupied molecular orbital of TNF (11). The effect of sensitizers on photoconduction in polymers is illustrated in Figure 1.1.

In the first type of sensitization the response is due to the absorption of the charge-transfer complex between the donor and acceptor. The PVK-TNF system is an example of this type of sensitization. Charge transfer complex crystals of N-isopropylcarbazole with TNF are not photoconductive in the charge-transfer region which implies that traps unique to the polymer are responsible for the effect in the polymer film.

The second type of sensitization, develops when the visible spectrum of the dye is reproduced along with the polymer, and photoconduction presumably occurs by energy or electron transfer from the excited state of the dye molecule to that of a chromophore unit in the host polymer. This case is often called "optical sensitization" (12).

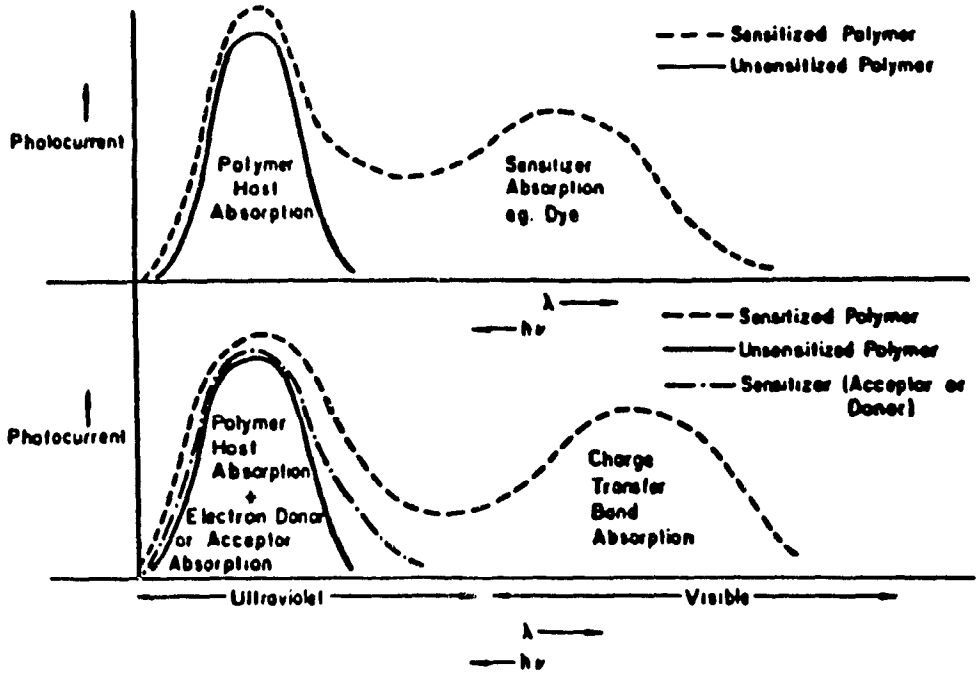

Figure 1.1 Effect of sensitizers on photoconduction action spectrum in polymers (from ref. 12).

Electronic energy transfer between chromophores attached to a polymer chain has been used to explain excimer formation and energy transfer to chemically bound traps (13,14). Electronic energy transfer is the one-step transfer of electronic energy

from an excited donor molecule (D*) to an acceptor molecule (A) (Equation 1.1).

$$\begin{aligned} D + h\nu &\longrightarrow D^* \\ D^* + A &\longrightarrow D + A^* \end{aligned} \qquad [1.1]$$

Various factors affect the type of energy transfer in solid polymer matrices. Energy transfer may also occur in solids under conditions where molecular diffusion is highly reduced or not possible. Intermolecular energy or charge migration in a solid polymer matrix may lead to processes dominated by multi-step migration of the excitation among molecules of the host followed by transfer to a guest impurity (12,15). Intramolecular energy migration can occur in vinyl polymers with pendant chromophore groups by two methods: either from group to group along the chain and/or from group to group in a coiled chain (also called intracoil energy migration). In either case of intramolecular or intermolecular energy migration, the energy absorbed by an aromatic chromophore group attached to polymeric chains can be transferred to trap sites distributed in the polymer matrix (13-19). These traps could be impurity sites such as physical defects due to chain folding or strain points in a solid polymer, or chemical irregularities like different oxidation states, or chain ends. Traps may also be regions in the solid of high local dielectric constant (multiplets and clusters (20)), excimer forming sites or even charge transfer complex sites (21). Charge carriers may be trapped in these sites. Energy accumulated in a trap site can be transferred to another trap or dissipated non-radiatively in the matrix. Only recently has trap controlled migration in polymer systems become an

interesting field of photoconductivity and polymer photophysics.

1.2.2 Energy Level Diagram for Polymers

Photoprocesses in inorganic and organic semiconductors have been well described in terms of ordered, covalent, molecular crystals. These well-defined materials can have a definite band structure, band-gap, as well as some shallow and deep impurity traps. Polymers are not the simple covalent crystals of conventional solid state physics. A solid polymer is a complex structure which can exist as an amorphous material, a crystalline material, or a mixture of both. Each polymer chain is unique with different conformations. Like molecularly ordered materials such as anthracene crystals, polymers generally have weak interactions between molecules or chains. Disordered molecular materials or polymers may not have a definite band structure, but rather a distribution of positive and negative molecular ion states in addition to localized dipole states associated with the disorder (21).

Many transport properties are therefore unique to these polymer systems. Free or injected charge carriers may migrate easily through regions of low polarization or may be trapped in highly charged areas of the medium. However, other scenarios involving charge or energy transport cannot be discounted.

Theoreti al approaches to determine important parameters such as oxidation potential, band gap, and band width in electrically conductive polymers (i.e. poly-(pyrrole)) have yielded good agreement with experimental results (22).

Band theory applies in low dimensional systems. Molecular materials, such as anthracene or perylene, are at about the limit to which band theory applies simply. Polymers can be discussed in these terms only in single chains with simple

carbon-hydrogen interactions, and only over short distances.

Transport properties in a band model are related to electrical conductivity σ [1.2] ,

$$\sigma = ne\mu \qquad [1.2]$$

where n is the charge carrier density, e is the electrical charge, and μ is the carrier mobility. This latter quantity is an important parameter in the overall conductivity of a polymer since mobilities of most carriers are reduced in polymer matrices.

A polymer containing crystalline and amorphous regions can have many localized states. These may be chain ends, ionic impurities, bulk dipole states, chain branches, interfacial states between amorphous and crystalline zones, interfacial states between hydrophilic and hydrophobic states, etc.. Temperature can greatly affect the nature and distribution of these states since molecular motions of chain segments or whole chains would affect the local environment of the states. The localized states may act in trapping carriers. These states may be considered as regions in the polymer matrix which can trap or partially stabilize a charge carrier. The charge carrier can be a charged species electron, a hole, an exciton, or even an ion.

In analogy to semiconductor band theory, a neutral acceptor state or an ionized donor state will trap electrons, and a neutral donor state or an ionized acceptor state will trap holes (22). Duke (23) has described localized states for pendant-group polymers in terms of a molecular ion model. The electronic structure of the polymer is basically that of an ensemble or group of molecular subunits since the bandwidth due to overlap of pendant groups is so small. In an effort to under-

stand these molecular ion states, Duke and Fabish performed metal-polymer contact charging experiments (23,24). They measured charge transferred to polymers from metals with different work functions. The results suggest that each metal transferred charge only to particular polymer states which were localized in a narrow window (≈0.4 eV) near the metal Fermi level.

The molecular-ion state model (25) can be represented as two gaussian distributions of acceptor states (E_{anion}) and donor states (E_{Cation}) (Figure 1.2). The relative densities of the bands is a measure of the bulk density of states. These bands should be regarded as broad continuous distributions of donor and acceptor states, in which injected charges can travel by a tunneling or hopping mechanism from one localized trap to another (Figure 1.3). It would therefore be more favorable for charge transport processes to inject electrons into a state of high acceptor density. These molecular ion states were calculated from contact charge measurements between metal surfaces and polymers, and is not known how the shape and position of these levels might be influenced under visible or UV-illumination. However, the model would still remain valid for a polymer in contact with a solution of ions, since polarization energies appears to a dominant factor in the intrinsic charge-carrying states of polymers. A variation of this model has recently been adapted to the discussion a photoinduced electron migration in a polymer blend in contact with a redox solution (26).

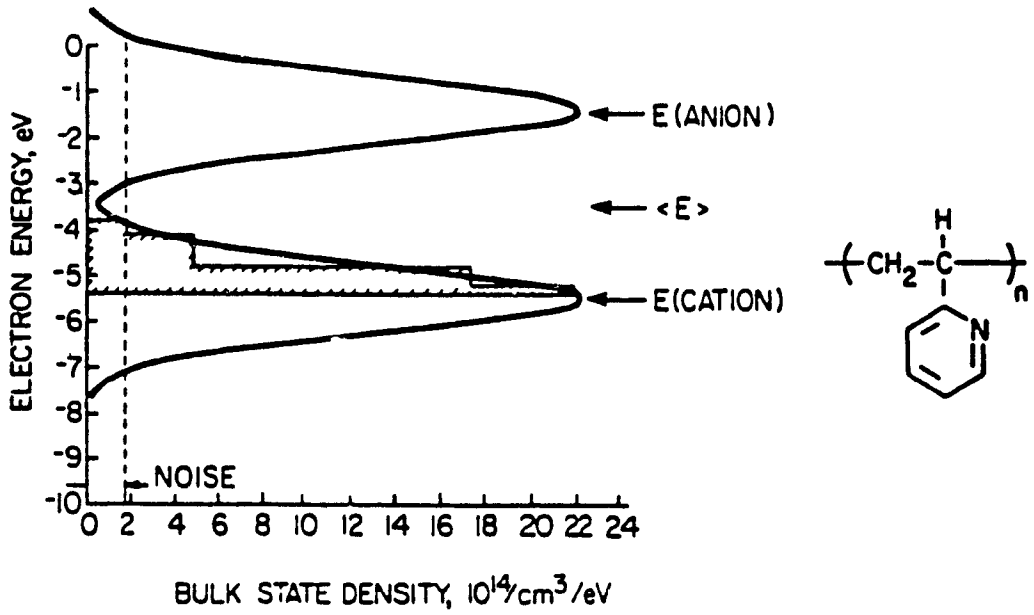

Figure 1.2 Continuous Gaussian distributions of molecular-ion state energies for poly(2-vinylpyridine) as determined from contact charge experiments. The measured densities are represented by the hatched area and the fitted densities of molecular-ion states by the solid curve (from ref. 21).

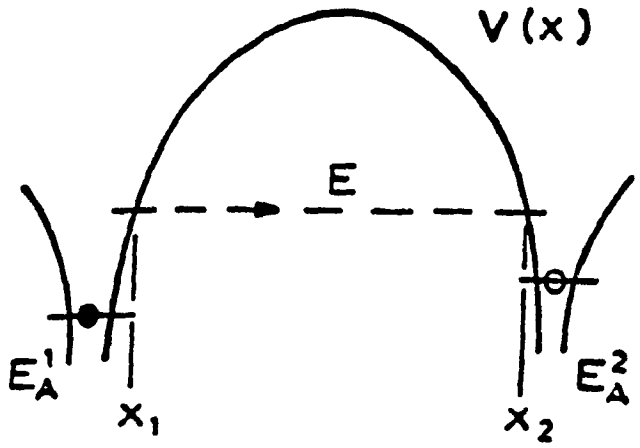

Figure 1.3 Electron tunnelling through a barrier V(x) at energy E from an occupied acceptor state E_A^1 to an empty acceptor state E_A^2 (from ref. 128).

1.3 Requirements for Polymers

In many polymer films supported on electrodes, redox centers in electroactive and photoelectroactive films cannot rapidly contact the electrode surface. There are basically three types of charge transport mechanisms which exist in rigid and semi-rigid electroactive polymeric systems. The first is electron transport in broad bands, the second is redox ion transport, referred to in solid state language as the "hopping" mechanism, and finally ion transport in polymer films. Each mechanism will be briefly discussed below.

Electron and/or charge transport in these polymers is highly dependent on the particular physical morphology and chemical properties of the polymer system. Electroactive polymers include all types mentioned above, in addition, they are dynamic matrices which can accommodate the movement and inclusion of various counterions and chemical species. This fact must be remembered throughout the discussion of all charge transport processes in polymer films.

1.3.1 Electron transport in polymers

Electronically conductive organic polymers with conjugated π-networks and delocalized electronic states have been reported over the past decade. The most promising commercial materials are polyacetylene (27), polypyrrole (28), polythiophene (29,30), and polyaniline (31,32). The high electronic conductivity of these materials arises from the oxidative or reductive doping of the polymer using chemical agents such as halogens, perchlorates, As_2F_5 , SO_4^{2-} and its derivatives, Na, and Li. Electronic conductivity refers to electron transport through the polymer by delocalized band structures and is distinct from other types of charge transport to be

discussed. Such electron transport and similar phenomena has even been reported in disordered insulating polystyrene systems (33,34,35,36). Insulating polymers can conduct charge once sufficiently doped or excited.

1.3.2 Redox Charge Transport in Polymers

Electroactive polymers with redox sites bound directly to the polymer backbone are termed redox polymers. Poly(vinylferrocene) (37,38,39) is one such example.

In contrast to electronically conductive polymer films, charge transport in redox polymers is governed by site to site hopping between one oxidation state and another. This mechanism has also been called electron self-exchange since the redox sites are considered fixed and immobile in the film, but adjacent, in order to allow apparent charge diffusion by electron exchange with its nearest neighbor. Such an example is shown in a poly[-Ru(vbpy)$_3$]$^{2+}$ film (40,41,42).

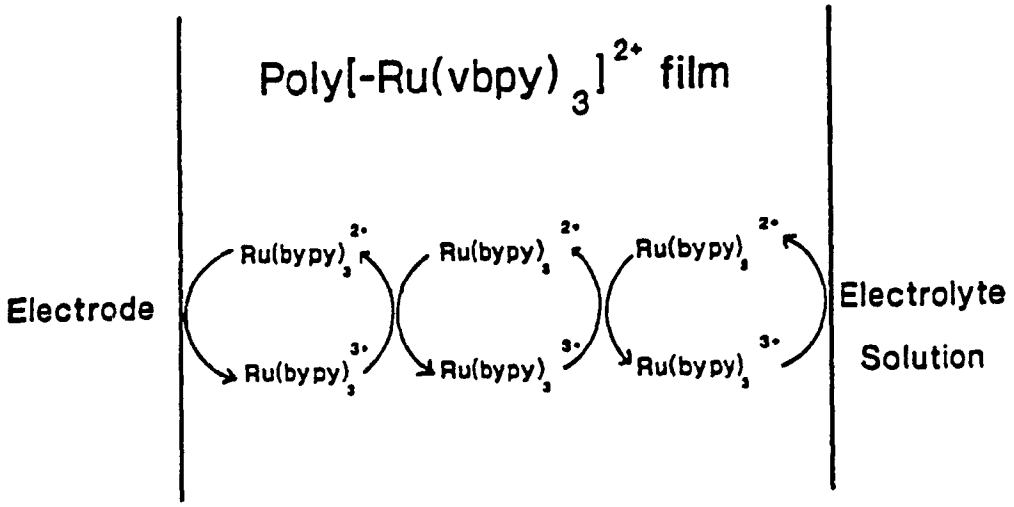

Figure 1.4 Schematic representation of electron self-exchange charge transport in a poly[Ru(vbpy)$_3$]$^{2+}$ polymer film (adapted from ref. 45).

In order to preserve electroneutrality, the propagation of electrons is accompanied by the displacement of mobile electroinactive counterions. Thus there can be mixed kinetic control of charge transport by electron hopping and the movement of these counterions. Electron hopping under a chemical potential gradient has been shown to be equivalent to the diffusion of the fixed redox centers with the same diffusion coefficient for the oxidized and reduced states (43,44). One part of the diffusional process is thus expressed by the electron diffusion coefficient,

$$D_e = k_e C_e^\circ d^2 \qquad [1.3]$$

where k_e is the bimolecular isotropic electron transfer rate, C_e° is the concentration of redox sites, and d is the mean distance between two adjacent redox sites. Charge transport in many redox polymers has been analyzed in this way (45,46). The electron diffusion coefficient, D_e, of a polymer film modified electrode is a measure of the rate of reaction of electron transport in the film. It is an important parameter for describing the kinetic behaviour of a polymer modified electrode. In cases where redox sites are not strictly fixed, but where diffusion is slow, ionic diffusion and electron hopping can significantly contribute to charge transport through these polymers.

1.3.3 Ionic charge transport in polymers

Another category of electroactive polymers include those whose redox active components are counterions in poly-ionic (cationic or anionic) films. These polymers rely on the incorporation of redox species by ion-exchange with charge compensating ions such as Cl^-, SO_4^{2-}, and I^- already in the film. The pioneering work of Oyama and Anson (47,48) in 1980 led to the term "electrostatic binding".

Large multi-charged anions such as $Fe(CN)_6^{3-/4-}$ and $Ir(Cl)_6^{2-/3-}$ were incorporated into protonated polyvinylpyridine modified electrodes. The modified carbon electrodes could be placed in a solution containing only supporting electrolyte and an electrochemical signal due to the incorporated redox ions was observed. A drawback of this earlier work was the reversible partitioning of the redox species leading to gradual leaching of the species into the background electrolyte. Even at the limit of maximum leaching, there was a large partition coefficient for redox ion incorporation since an observed discernable electrochemical response which could be assigned to the electrostatically bound redox ions was recorded. Work in this field has experienced rapid growth, mainly with respect to quaternized or crosslinked polyvinylpyridines, polyviologens, polystyrene sulfonates, polyacrylic acids, and especially Nafion.

Dupont's Nafion (49) is a perfluosulfonate ionomer capable of cation exchange. Unlike most sulfonate ion-exchange resins, Nafion has virtually no crosslinking, a low density of exchange sites in comparison to typical sulfonate resins, and a fluorocarbon backbone providing a hydrophobic environment.

There is substantial evidence that Nafion exists in segregated hydrophilic and hydrophobic domains (50,51). The sluggish motion of ions in ion-exchange polymers follows the same diffusion laws as in solution, but contains contributions for film thickness. Typical apparent diffusion coefficients for large ions like $Ru(NH_3)_6^{3+}$ in Nafions, and $Fe(CN)_6^{3-/4-}$ in protonated polyvinylpyridine are about 10^{-9} - 10^{-10} cm^2/sec. Smaller ions diffuse at a faster rate, but their motions are still much reduced in polymer films on electrodes. More recently, Anson and co-workers have

reported a polyelectrolyte material which exhibits high ion retention and apparent diffusion coefficients of 1 X 10^{-6} cm^2/sec for the hexacyanoferrate(II/III) couple (52). These results were rationalized in terms of the polymer's internal morphology leading to segregated hydrophobic and hydrophilic domains. The latter structures appeared to provide adequate channels for facile diffusion of redox species in a more solution-like environment.

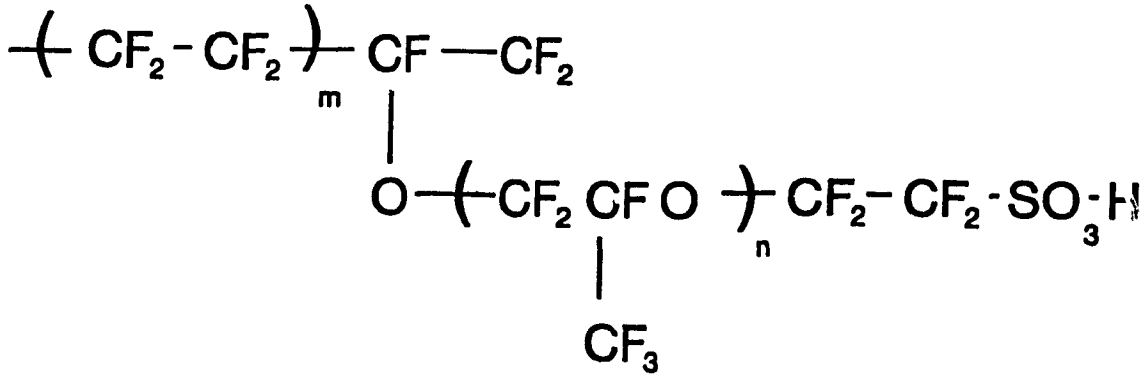

Nafion

Figure 1.5 Structure of Dupont's Nafion.

1.3.4 Diffusion of Electroactive Species in Polymers Films on Electrodes.

Solution electrochemical equations have been extended to polymeric systems to evaluate D_{app} since diffusion phenomenology is similar. The apparent diffusion

coefficients of redox materials in polymeric films on electrodes can be measured by electrochemical techniques such as rotating disc voltammetry (RDE), cyclic voltammetry at different scan rates, and chronoamperometry (45,53,54).

In a chronoamperometric experiment, a potential step of sufficient amplitude depletes the effective surface concentration of electroactive species at the electrode/-polymer interface. Then, under conditions of semi-infinite planar diffusion (53), charge transport under the influence of the concentration gradient of redox species in the film produces a redox reaction, which is monitored as a current decay-time profile. The Cottrell equation [1.4] describes the current-time behavior, where i is the diffusion current in amperes, n is the number of electrons, F is Faraday's constant, A is the electrode area in cm^2, C is the concentration of redox species in the film in moles/cm^3, and D is the diffusion coefficient in conventional units of cm^2/sec (55).

$$i = nFACD^{1/2} / (\pi t)^{1/2} \qquad [1.4]$$

The apparent diffusion coefficient is dependant on the concentration of redox species in the film and accurate quantitation must account for all electroactive species in the film. Film thickness may vary greatly since a polymer film might swell or contract under different experimental conditions such as solvent or electrolyte concentration. At long times (i.e. t>1 sec.), the diffusion coefficients calculated by the potential step chronoamperometric method and by a cyclic voltammetry method are almost identical.

Voltammetric data acquired at different scan rates are also helpful for determining diffusional characteristics of a polymer modified electrode. Plots of

peak current versus the square root of the scan rate should be linear for diffusion limited processes at planar electrodes under conditions of semi-infinite diffusion.

1.4 Requirements for Chromophores

1.4.1 Redox Potentials

The photochemical redox behavior of man-made dyes is controlled by their excitation energies and their ground-state redox potentials (56). The charge transport scheme outlined in the preceding sections places restrictions on the type of chromophores to be used for evaluations in photoelectrochemical systems that use the solar spectrum. Optical sensitization of semiconductor electrodes using polymer supported chromophores is one method that can be employed to achieve charge separation and vectorial electron transfer across the matrix. Photo-excited molecules possess different reactivities and properties than their ground state counterparts. The simplest energy diagram of an electronically excited state shows that electron transfer may occur to acceptor or donor sites in the system (Figure 1.6).

The excited species can transfer an electron to a lower energy acceptor state nearby. In photoelectrochemical terms, the redox potential of the excited chromophore has shifted in two directions. First, it has produced a state of greater reducing power where the molecule is a better electron donor in its excited state than its ground state. Second, absorption of a photon by the redox chromophore creates an electron "hole" and the molecule is a better electron acceptor (or oxidizer) in its excited state than its ground state. For both these reasons, it is important that the photo-excited state of the chromophore be stabilized in order for charge

separation to occur and not simple recombination of the excited species returning to the ground state.

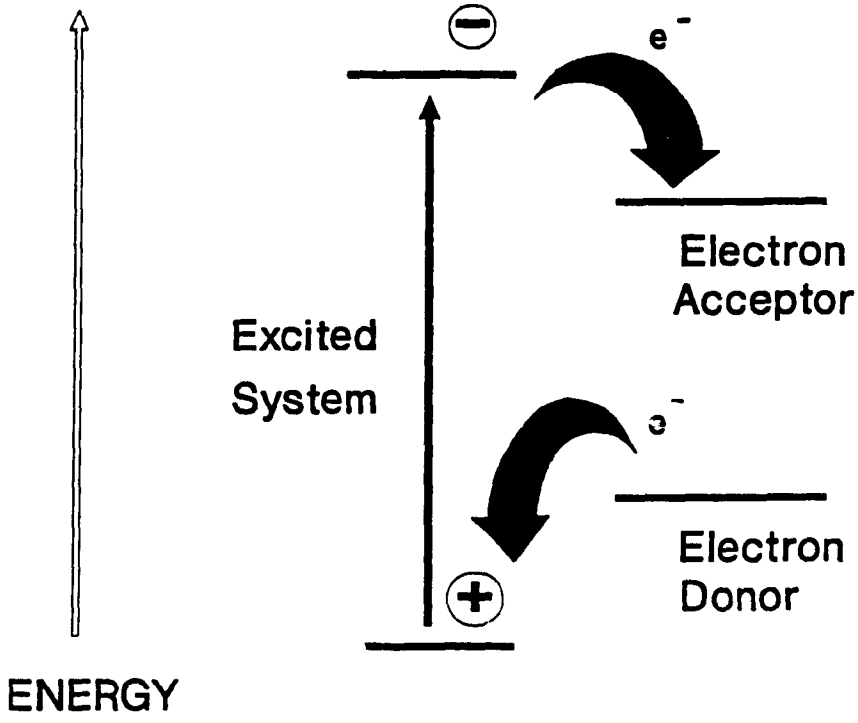

Figure 1.6 Schematic representation of electron transfer between a suitable electron donor and acceptor.

Therefore there are two limits for redox potentials in the charge transfer scheme. Either the reducing potential is raised or the oxidizing potential is lowered to provide electronic excited states capable of being good electron donors or acceptors, respectively.

1.4.2 Absorption Characteristics of Chromophores

Most commercial applications for photochemical energy conversion and light driven devices rely on materials which absorb solar radiation. These chromophores

must be strong absorbers of light for a given photochemical reaction. That is, highly colored materials should be used for visible light sensitization. The molar extinction coefficient of a suitable electronic transition in the visible region should be at least 10^4 $M^{-1}cm^{-1}$. The energy corresponding to this absorption maxima, λ_{max}, is usually an upper limit on the excited singlet state. Excited triplet states of dyes are usually about 0.2 to 0.6 eV below that of the singlet state (57). The quantum yield of any process producing excited states should be high (close to unity). Finally, the chromophores must be able to exist in more than one oxidation state and be stable with respect to its environment. Highly air-sensitive dyes would not be suitable candidates for practical uses of photochemical reactions using sunlight.

1.4.3 Excited State Lifetimes

The excited state lifetime of dyes in photophysical reaction schemes is a crucial factor towards determining whether efficient charge separation and charge transport will occur in polymer based systems. Electronically excited states have a limited lifetime and can dissipate energy by several modes. Photophysical energy dissipation can occur via energy transfer, internal conversion between states, or radiative dissipation. Photochemical dissipation processes include free radical formation, cyclization, and intramolecular rearrangement (15). According to the Franck-Condon principle, absorption of a photon requires about 10^{-15} seconds. Internal conversion to a lower excited state of the same spin usually takes about 10^{-13} to 10^{-11} seconds. Lifetimes of excited singlet states ranges from 10^{-8} to 10^{-12} seconds. Metallic organic complexes based on porphyrins, phthalocyanines, and tris(2,2'-bipyridyl) have been successfully employed as photosentizers. Their

relatively long-lived excited states (τ > 1 nsec) can be used to separate photo-generated charge to reactive sites for the photoreduction of water (58,59,60).

The maleonitriledithiolate complexes of nickel and platinum have short excited lifetimes in solution. However, long lived excited states are not a necessity for productive energy conversion. The chloroplasts of green plants have bypassed the pathway of long lived excited states and rely on a efficient organization of components which rapidly separates the photo-generated charges by a series oxidations and reductions that make up electron transfer in the electron transfer chain. Thus, the organization of components which can rapidly capture and separate the photo-generated excited states is beneficial to the harvesting of the photon energy. Polymers possess sites such as pendant chromophores and localized states which can act as organizational centers which separate and trap photo-generated carriers. It should be possible therefore to use chromophores and polymers in a concerted fashion in order to achieve rapid charge separation, even if the excited state lifetime of the chromophore is rather short. The problem remains of transporting these charge carriers (without many losses) to a region where they can do useful work such as catalysis or energy storage.

1.5 Background on Polymer Modified Electrodes

1.5.1 Advantages of Chemically Modified Electrodes

Electroanalytical techniques have been developed over the past twenty years by the analytical chemist for qualitative and quantitative determinations, and by the physical chemist for obtaining thermodynamic and kinetic information about electro-

chemical systems.

In the past decade, there has been considerable effort in the development of a new class of electrochemical devices called chemically modified electrodes (CMEs). The concept of CMEs probably arose in part from the electrochemist's frustration in grasping direct control of the chemical nature of the electrode surface (63). By attaching certain reagents to the electrode surface, desirable properties such as freedom from adsorptive and coating effects, and excited state features or optical properties may be gained.

Conventional electrodes such as platinum, carbon, and mercury generally display non-specific electrochemical behaviour, that is, they serve mainly as a site for heterogeneous electron transfer. Chemically modified electrodes may be tailored to kinetically amplify desired redox processes over others. These modifications may result in an enhancement of electroanalytical specificity and sensitivity, an increased electrochemical reaction rate, a protective coating for electrodes, and opto-electrical phenomena. The latter result of electrode modification will be examined more closely with regards to transport and photoelectrochemical processes in modified electrode systems.

1.5.2 Types of Chemically Modified Electrodes

The concept of chemically modified electrodes has been extensively reviewed (45,46,64). Several methods can be used to incorporate a redox component on an electrode surface. These include: (I) adsorption or chemisorption, (II) covalent bonding, and (III) polymer films.

Methods of preparing CMEs using electroactive polymers include film casting, electrochemical polymerization, or ion-exchange to preformed polymers on electrodes. Electroactive polymers are of particular interest because of their potential as catalysts and their ability to store electrical charge. They are dynamic matrices that can have variable composition and charge. The study of transport of electrons and ions through polymer films continues to be an important research topic.

1.5.3 Applications of Chemically Modified Electrodes

Adsorption of redox species on electrodes has led to greater selectivity and electrochemical sensitivity. Studies in this field have been directed towards electrocatalytic applications, especially the reduction of molecular oxygen using porphyrins and phthalocyanines (65,66).

Covalent bonding of redox species to electrodes has been examined mainly by silane linkages to surfaces. Wrighton and co-workers have immobilized quinones (67), viologens (68), and ferrocenes(69) on a variety of substrates.

Polymer modified electrodes have been discussed in electrocatalysis, electroanalysis, photocatalysis, and photoelectrochemistry (27-48,53,54,62,68,70). Ease of preparation and high selectively have made polymer modified electrodes the choice for specific analytical determinations.

Electrodes of micron dimensions can be made into "molecular transistors" (64,71,72,73), chemical field effect transistors (CHEMFETs) (74,75,76), or gas sensors (77). These structures are of particular importance in the field of macromolecular electronics.

Large bandgap semiconductor electrodes such as ZnO, TiO_2, and SnO_2 have been chemically modified using dyes or polymer supported dyes in order to increase the amount of visible light absorbed (45,53,54). Narrow band gap semiconductors like CdS, CdSe, and GaAs photocorrode in most redox electrolytes. Polymer coated semiconductors of this type can retard the photodissolution of the semiconductor (46,70).

1.6 Background on Metal 1,2 Dithiolene Complexes (mnts)

1.6.1 History and General Preparation

The study of the chemistry of transition metal complexes containing sulfur ligands has grown phenomenally over the past thirty years. These compounds have interest as model complexes for biological systems containing metal sulfur bonds with numerous possible commercial applications (78). Even as early as 1936, Clark and Mills (79) studied the analytical uses of toluene 3,4-dithiol with the metal halides of Zn, Cd, and Hg among others. It was not until the late 1950's and the early 1960's that research interest on the 1,2 dithiol ligands shifted from their analytical uses to coordination chemistry. The sodium salt ligand, $Na_2S_2C_2(CN)_2$, designated Na_2(mnt) [Figure 1.7] was first isolated by Bähr and Schleitzer (80,81). This light yellow light-sensitive powder was prepared by dimerization of dithiocyanoformate followed by spontaneous desulfurization.

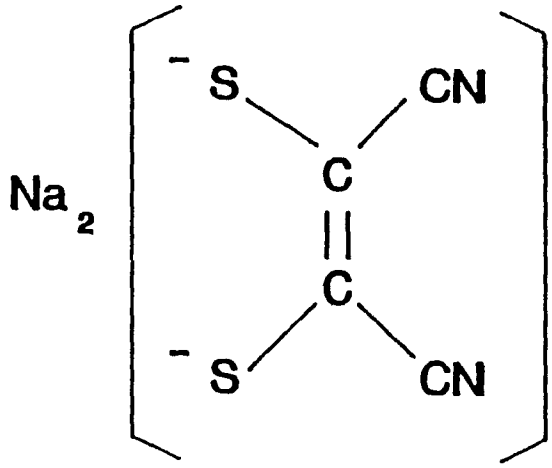

Figure 1.7 Structure of $Na_2(mnt)_2$.

Dithiolenes are noninnocent ligands. There are no usual formal oxidation states of ligands and metals in dithiolene complexes, since the ring system can change oxidation state as well as the metal. The ligand can be visualized in two oxidation states, the neutral or dianionic form [Figure 1.8]. The neutral dithione form (A) has four π-electrons, while the dianionic dithiol form (B) has six. Either form has four sulfur σ lone pairs (82). In molecular orbital terms, the extent to which electrons are delocalized over the ligand will determine the oxidation states of the ligand and the metal. Generally, extensive delocalization occurs which explains the wide range of possible oxidation states.

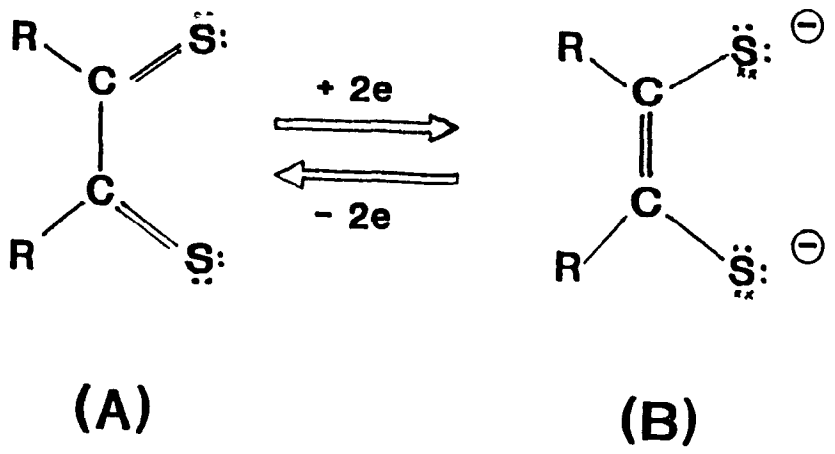

Figure 1.8 Two possible oxidation states of the maleonitriledithiolate ligand, (A) dithione form, and (B) dithiol form.

Stable anionic metal complexes were prepared from aqueous solutions of Na_2(mnt) and metal halides by Gray and co-workers (83). The ligand formed four coordinate complexes represented by the general formula $M(mnt)_2^{n-}$ (Figure 1.9).

The deeply colored metal complexes could be collected by precipitation from aqueous solution as alkyl ammonium salts. Oxidation states of the metal complexes may vary from 0 to -3, with the -1 and -2 species being the most stable. An interest in these complexes arose mainly from the inability to assign formal oxidation states to the transition metal. Great care must be taken in order to avoid any uncertainty when discussing the formal oxidation states of the metals in the complexes.

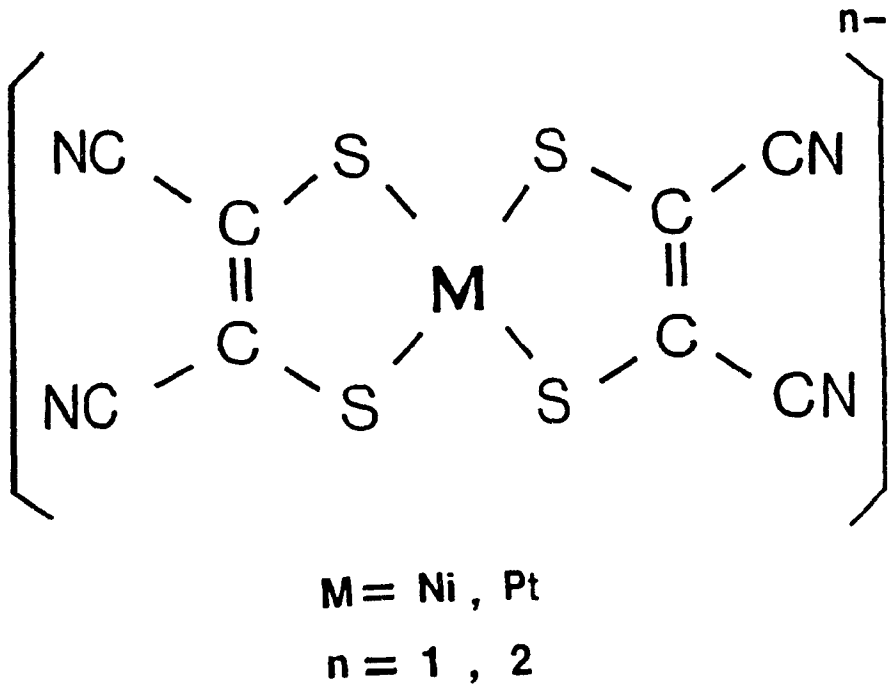

Figure 1.9 General structure for a metal maleonitriledithiolate.

1.6.2 Physical and Chemical Properties of M(mnt)'s

The crystal structure of the metal complexes has been analyzed by X-ray diffraction and determined to be square planar in both the monoanionic and dianionic species (86). The change in overall charge (either 0,-1,-2,-3) does not affect the planar molecular geometry of the complex but it does modify the bond lengths slightly to accommodate the change. This observed invariance in planarity implies rapid electron transfer which occurs with little structural reorganization. The Ni-S and S-C bond distances increase from the $Ni(mnt)_2^{1-}$ to the $Ni(mnt)_2^{2-}$ complex, while the ethylenic bond length decreases slightly [Table 1.1] (87).

Table 1.1 Average values of the bond distances in tetraethylammonium salt complexes of $[Ni(mnt)_2]^{n-}$ (adapted from reference 87)

Type of Bond	n=1 (angstroms)	n=2 (angstroms)
Ni-S	2.149	2.174
S-C	1.720	1.742
C=C	1.369	1.350
C-C	1.440	1.407
C≡N	1.131	1.173

It can be concluded that the overall charge (or oxidation state of the Ni atom) of the $Ni(mnt)_2^{n-}$ plays a role in the case of the Ni-S and S-C bonds. If reduction of the complex (from n= -1 → -2) arose solely from the delocalized orbitals of the ligand, while the oxidation state of the metal remained in the normal Ni(II) state, then there should be a decrease in the C=C and an increase in the S-C bond lengths. If the changes are due primarily to the metal or molecular orbitals of the metal, then small changes in bond lengths of the ligand are expected, while the reduction of the monoanion complex to its dianion should increase the Ni-S bond length. The observed changes in the crystallographic data suggest that changes in the oxidation state of the complex are related to both the metal and the delocalized ligand system of the maleonitriledithiolate. Infra-red studies on 1,2 dithiolenes complements the crystallographic data in terms of calculated force constants and band positions (88). Again, one must be very careful in the assignment of any

oxidation state with $M(mnt)_2$'s since there are strong metal-ligand interactions.

The neutral $Ni(mnt)_2^0$ form can be thought as a Ni(IV) metal atom surrounded by mnt ligands in a highly dithioketonic form. This unstable species can undergo reduction to a Ni(III) ("d^7") system lending to a more dithiol type ligand arrangement, while the dianion with Ni(II) ("d^8") has a substantial amount of dithiolate character in the ligands. The air-sensitive trianion adds an electron to a primarily metal based orbital, which has a high degree of metal-ligand delocalization, leading to the uncommon Ni(I) ("d^9") configuration (89). This is in agreement with ESR data (89).

The electronic structures of these 1,2 dithiolenes is somewhat controversial. A number of MO calculations on the metal bis-dithiolenes have been reported (90,91,92,93). Workers believe that stabilization of the square planar geometry involves the metal d_{xz}, d_{yz}, and p_z orbitals in an extensive π-network across the entire complex.

The rapid one electron transfers observed in the solution electrochemistry is strongly dependant on the type of metal present in the cases of the 2- to 3-transition. This point is in agreement with observations that the Ni-trianion has an orbital with substantial metal character. The $-1 \rightarrow -2$ reduction waves are quite similar for most $M(mnt)_2^{n-}$ complexes and appears to be independent of the type of metal in the mnt.

The metal complexes display intense absorption bands from the ultraviolet to the near infrared. The complexes have been studied by several other techniques including Infrared (88), ESR (86,89,94), Resonance Raman (95), X-ray photoelectron

spectroscopy (96), and Mössbauer spectrometry (97).

The rich electronic spectra of the $M(mnt)_2$ complexes has been known and studied for almost three decades. The photochemistry of the complexes was not examined until the early eighties when Kisch and Hennig (98) obtained hydrogen from water using $Zn(mnt)_2^{2-}$ and UV-light. It was later discovered that $Zn(mnt)_2^{2-}$ decomposes under UV-irradiation to ZnS which was ultimately responsible for the photocatalytic production of hydrogen (99). Photo-oxidation of metal maleonitrile-dithiolates by UV-light was investigated in chloroform by Dooley and Patterson (100). Similar work done by Vogler and Kunkeley (101) at about the same time in halocarbon solvents showed that they the quantum yield for photo-oxidation increased with decreasing wavelength, and that the photo-oxidation may proceed via a charge transfer to solvent (CSST) band. Both groups suggested that the photo-oxidation of the dianion in halocarbon solvents produces the corresponding mono-anion, a chloride ion, and a radical halocarbon moiety which may undergo secondary reactions. The researchers did not examine the visible light photochemistry of these metal complexes. A more recent paper presented a photoelectrochemical study of $M(mnt)_2^{n-}$ complexes where M = Ni, Pd, Pt, Cu and n = 0 to -3 (102). These same complexes were then ion-exchanged into quaternized poly(vinylpyridine) films on transparent SnO_2 electrodes so that the films may be better illuminated than in solution (62).

CHAPTER 2

EXPERIMENTAL

2.1 Materials

Commercially available starting materials were used as received, without purification, in syntheses and physical measurements. Common solvents such as acetone (A&C Chemicals), chloroform (A&C Chemicals), iso-propanol (Mallinckrodt), ethanol (Commercial alcohols) and toluene (A&C Chemicals) were reagent grade and used without further purification unless otherwise specified. Water was distilled and deionized in glass before usage in synthetic procedures and in physical measurements. Acids (HCl (Caledon) and HNO_3 (Anachemia reagent)) and bases (NaOH and KOH (Fischer reagent)) were obtained from the Concordia stockroom and used as received. Tetraalkyl-ammonium salts, silver nitrate, and hydroscopic polymers were vacuum dried in a an oven at 60°C prior to use. Microanalyses of the metal maleonitriledithiolate dyes was performed by Galbraith Laboratories, Tenn, U.S.A.. Elemental analysis of selected polymers was done at Guelph Laboratories, Guelph, Ont.. The composition of the synthesized random co-polymers was estimated from elemental analyses. The identity of other products was established by the UV-visible and/or FTIR spectrum in comparison to previously published spectra. Prepurified nitrogen or argon was used for degassing in the synthetic, photochemical, and electrochemical work.

2.2 Preparation of Complexes, Polymers, and Solutions

2.2.1 Preparation of Sodium Maleonitriledithiolate (Na_2mnt)

Sodium maleonitriledithiolate was prepared by a modification of the procedure of Bahr and Schleitzer (80). 2.5 grams of sodium cyanide (Aldrich, reagent) was suspended in 30 mls of dimethylformamide (Aldrich,reagent). 12 mls of carbon disulfide (Fischer,reagent) was added and the mixture was stirred overnight until a blackish red mass of sodium dithioformate was obtained. This product was collected by filtration and recrystallized from 1:1 butyl and isopropyl alcohol. Sodium mnt (Na_2mnt) was obtained by spontaneous desulfurization (1 week) of the salt in chloroform. The salt was purified twice by recrystallization from methanol/-ethanol (1:1 v/v) solution. The light sensitive bright yellow product was vacuum dried and stored in a dessicator over $CaCO_3$ in the dark.

2.2.2 Preparation of $[(C_2H_5)_4N]_2Ni(mnt)_2$.

The $[(C_2H_5)_4N]_2Ni(mnt)_2$ salt is denoted $Ni(mnt)_2^{2-}$ for simplicity and was prepared by the method of Billing *et al.* (103). A 50 ml solution of aqueous methanol (1:1 v/v) containing 12 grams of Na_2mnt was gently warmed on a hot plate. To this stirred solution, 12 mls of a 2.6 M aqueous $NiCl_2 \cdot 6H_2O$ (Aldrich, 99%) was added dropwise. The red solution was filtered and a saturated solution of tetraethylammonium bromide (A&C,reagent) was slowly added. The precipitate was filtered and washed with cold water. The product was recrystallized from an aqueous acetone solution to yield bright red crystals.

2.2.3 Preparation of $[(C_2H_5)_4N]_2Pt(mnt)_2$.

The related platinum complex was prepared by the method of Benson *et al* (104). Equal molar amounts of hexachloroplatinate(IV) (Aldrich, reagent) and Na_2mnt were dissolved in deaerated water. The red solution was warmed and treated with 2.0 grams of saturated ethanolic tetraethylammonium bromide. The red precipitate was filtered and recrystallized from an ethanol/water solution.

2.2.4 Preparation of $[MV^{2+}]Pt(mnt)_2$.

This platinum complex was prepared using a slight modification of the method of Benson *et al.* (104). Hexachloroplatinate(IV) (2.44 X 10^{-3} moles) was dissolved in deoxygenated water to which was added Na_2mnt (5.38 X 10^{-3} moles). The red solution was gently warmed on a hot plate and treated with an aqueous solution containing 2.5 X 10^{-3} moles of methylviologen chloride (Aldrich, reagent). The brownish-red precipitate that formed was collected by filtration and washed several times with water, methanol and acetone. The solid was dried in vacuo at 60° overnight. The resultant viologen-Pt(mnt) product was soluble only in DMF (Aldrich, spectrograde) and DMSO (Aldrich, spectrograde).

2.2.5 Preparation of $[MV^{2+}]Ni(mnt)_2$.

The corresponding nickel complex was prepared by slight modification of the published procedures (103). Na_2mnt (5.38 X 10^{3} moles) was dissolved in 7 mls of aqueous methanol (1:1) and warmed on a hot plate. To this solution, 2.45 X 10^{3} moles of $NiCl_2.6H_2O$ in 2 mls of water was added The deep red solution was filtered and a solution containing 2.60 X 10^{-3} moles of methylviologen was added. The precipitate was collected and washed in the same manner as the platinum

complex.

2.2.6 Synthesis of Ion-Containing Polymer P1

Styrene (Aldrich, 99.9%) and chloromethylstyrene (Eastman Kodak Ltd., reagent) were distilled under reduced pressure prior to use. Alternatively, the monomers were purified by chromatography using DEHIBIT100 (Polysciences) to remove inhibitors. Triethylamine (Aldrich, reagent) and triethanolamine (Aldrich, reagent) were used as received. Azoisobutyronitrile (AIBN) (Chemical Dynamics, high purity) was recrystallized twice from ethanol and dried under vacuum prior to use. The random ternary copolymer was prepared according to a modification of the procedure described by Montgomery and Anson (52). A random binary copolymer was prepared first from a benzene solution containing 2.4 M chloromethylstyrene, 0.6 M styrene, and 0.06 M AIBN as free radical initiator. The solution was thoroughly degassed with prepurified nitrogen. The polymerization was carried out at 60°C for 24 hours. The styrene-chloromethylstyrene copolymer was precipitated with methanol. The Menschutken reaction (105,106) was used to quaternize the alkyl chloride moieties of the copolymer. A 10-fold molar excess of triethylamine was added to a benzene solution of the copolymer and refluxed for one hour. This was followed by the addition of a 10-fold molar excess of triethanolamine, and continued reflux for another hour. The yellow solution became viscous until the ion-containing polymer precipitated from solution forming a gel-like mass at the bottom of the flask. Two methods were used to recover the polymer from this point.

In the first, concentrated HCl was added to the resulting polymer to neutralize the unreacted amines. The solution was then dialyzed against distilled water for

3 days. After the dialysis, THF was added to improve the solubility of the polymer. Subsequently, the ion-containing polymer was reprecipitated using cold 2-propanol to yield a pale yellow powder which was dried in vacuo at 60°C.

In the second recovery method, the gel-like mass was dissolved in a minimum amount of methanol and precipitated using cold 2-propanol to yield a pale yellow powder which was rinsed several times with the non-solvent to remove any unreacted amines. The polymer was dried at 60°C in a vacuum oven. This ion-containing polymer shall be denoted **P1** (Figure 2.1).

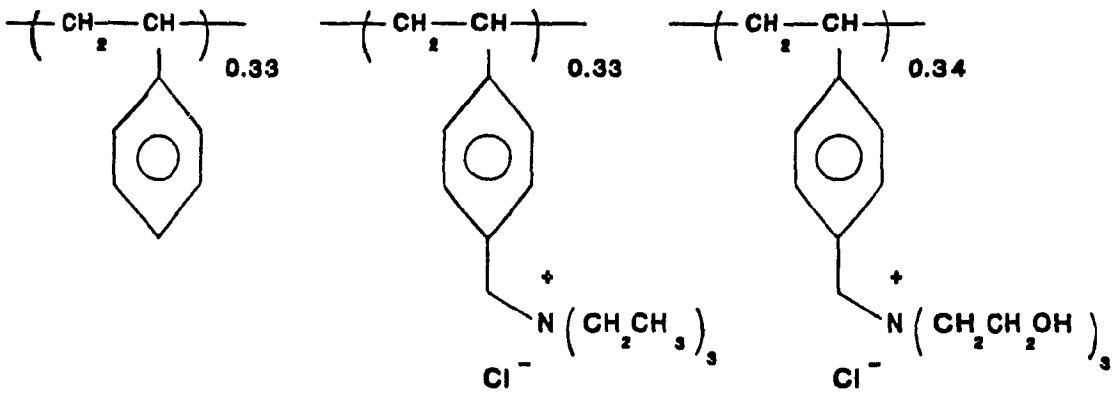

Figure 2.1 Structure of quaternized co-polymer P1.

2.2.7 Polymer Blend of Poly(vinylpyridine co-styrene) with Ion-Containing Polymer P1.

A 2% (w/v) solution of poly(vinylpyridine co-styrene) was prepared in spectrograde methanol. A similar 2% solution of **I** was prepared. Polymer blends were prepared by slowly mixing 2:1 (v/v) quantities of the ion-containing polymer and the PVP-co-styrene solutions with vigorous stirring. This blend shall be denoted **PB1** (Figure 2.2).

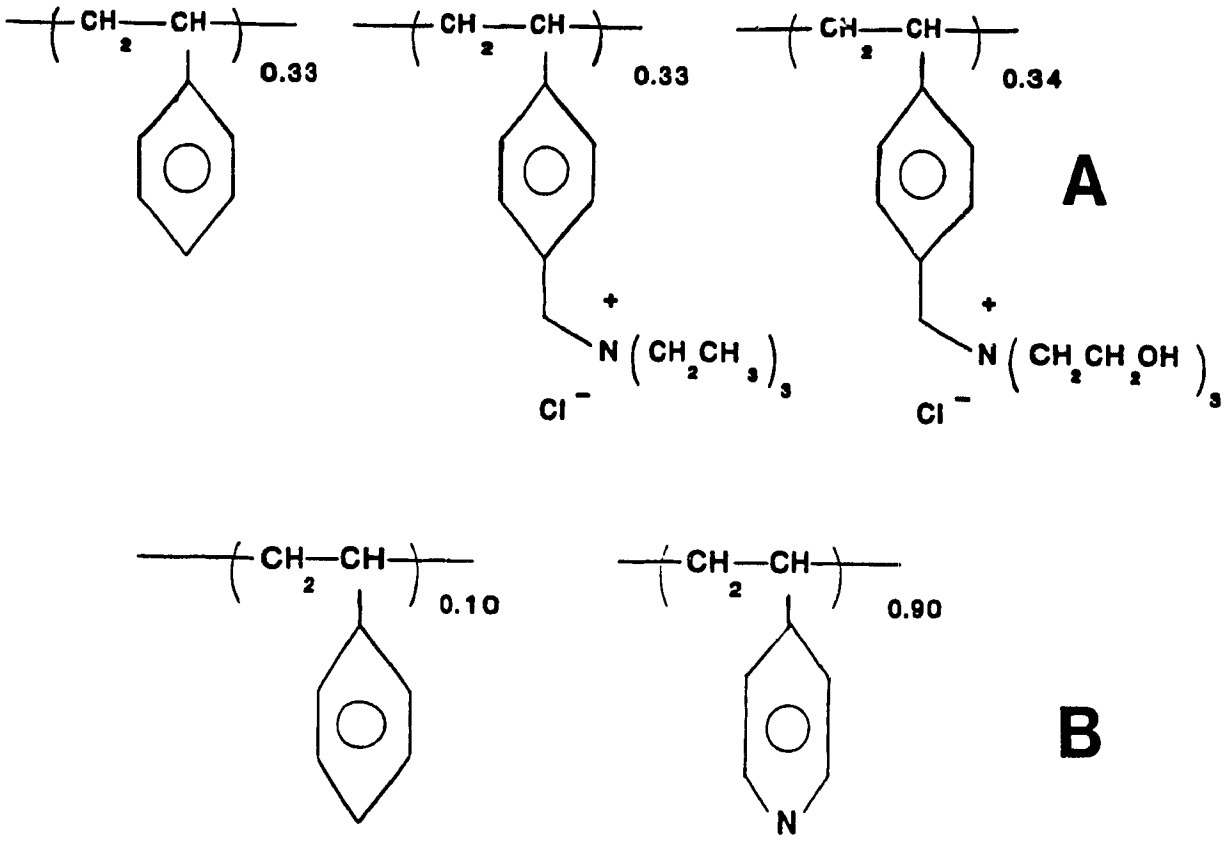

Figure 2.2 Structure of polymer blend **PB1** where (A) and (B) are mixed in a 2:1 ratio.

2.2.8 Synthesis of Ionically Conductive Polymer P2

A random ternary ion-containing copolymer was prepared according a modified procedure of that described in Section 2.2.5. A random binary copolymer was prepared first from a benzene solution containing 4.8 M chloromethylstyrene, 1.2 M styrene, and 0.12 M AIBN as free radical initiator. The solution was thoroughly degassed with prepurified nitrogen. The polymerization was carried out at 65°C for 24 hours. The styrene-chloromethylstyrene copolymer was precipitated with excess methanol. The alkyl chloride moieties of the copolymer were quaternized with triethylamine and triethanolamine. A 5-fold molar excess of triethylamine was added to a benzene solution of the copolymer and refluxed for two hours. This was followed by the addition of a 5-fold molar excess of triethanolamine, and continued reflux for another two hours. The yellow solution became viscous until the ion-containing polymer precipitated from solution forming a gel-like mass at the bottom of the flask. The gel-like ion-containing polymer was dissolved in methanol, concentrated by evaporation under reduced pressure, then precipitated into cold isopropyl alcohol (0°C). The polymer was dried in vacuo at 60°C. Its solubility in water or methanol was limited to less than 1% (w/v) in contrast to **P1** which was much more soluble (i.e. >> 2%). This polymer shall be denoted **P2**. A 0.56% (w/v) methanolic solution was prepared as a casting solution (Figure 2.3).

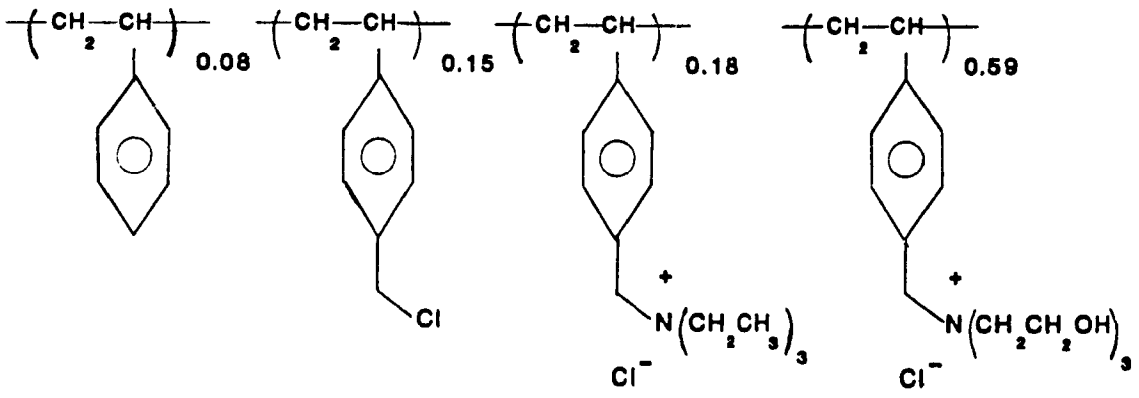

Figure 2.3 Structure of ion-containing polymer P2.

2.2.9 Synthesis of Random Co-Polymer P3.

Monomers were purified by chromatography as described in section 2.2.5 above. To a solution containing 200 mls of dry benzene, 1.47 X 10^{-1} moles of chloromethylstyrene and 4.45 X 10^{-2} moles of styrene were added. 6 X 10^{-3} moles of AIBN was added as initiator. The solution was thoroughly deoxygenated with prepurified nitrogen, then heated to 72°C for 24 hours. The resulting random binary copolymer was precipitated in excess methanol (yield 85%). The composition of the polymer was estimated to be 25%:75% polystyrene to chloromethylstyrene by elemental analysis. This polymer shall be denoted **P3** (Figure 2.4).

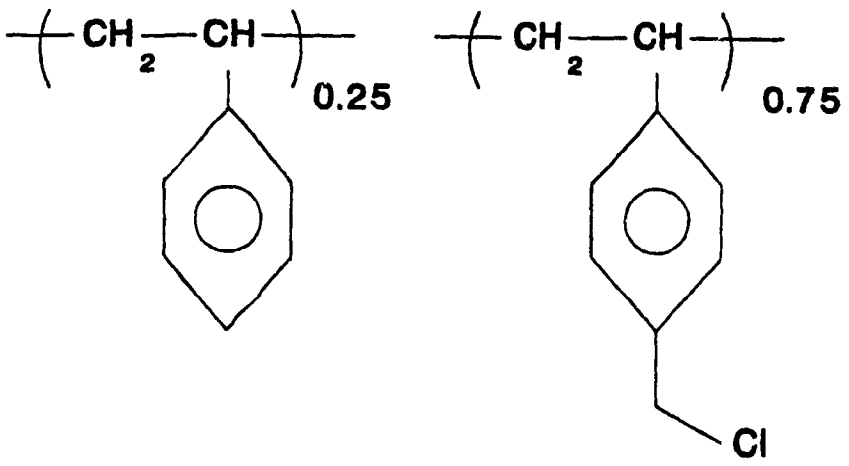

Figure 2.4 Structure of random co-polymer P3.

2.2.10 Quaternization of P3 with Triethylamine & Triethanolamine.

A 6.5% (w/v) benzene solution (200 mls) of the random copolymer **P3** was degassed and heated to a gentle reflux. Triethylamine (7.1 X 10^{-2} moles) was added using a dropping funnel and refluxed for 1 hour. This was followed by the addition of 7.5 X 10^{-2} moles of triethanolamine and continued reflux for another hour. The solution became slightly yellow and a sticky polymer precipitated from the benzene solution. The ion-containing polymer moiety was dissolved in methanol, and reprecipitated using isopropyl alcohol at 0°C. The polymer shall be denoted **P4** (Figure 2.5).

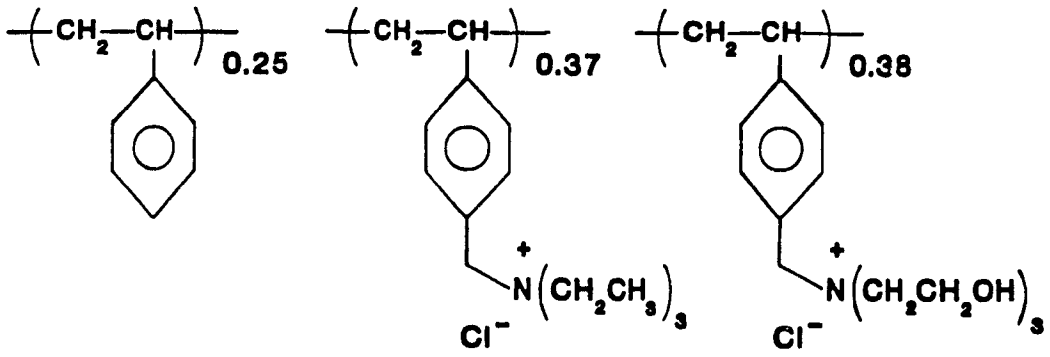

Figure 2.5 Structure of ion-containing polymer P4.

2.2.11 Quaternization of P3 with 4-4' Bipyridyl.

A 3.1% (w/v) solution of binary copolymer **P3** was prepared in 50 mls of benzene and reacted with 2 X 10^{-3} moles of 4-4' bipyridyl (Aldrich, 98%). The mixture was deoxygenated and refluxed for 3.5 hours. The solution became yellow and the polymer remained soluble in benzene. This was used directly as a casting solution denoted **PV1** (Figure 2.6).

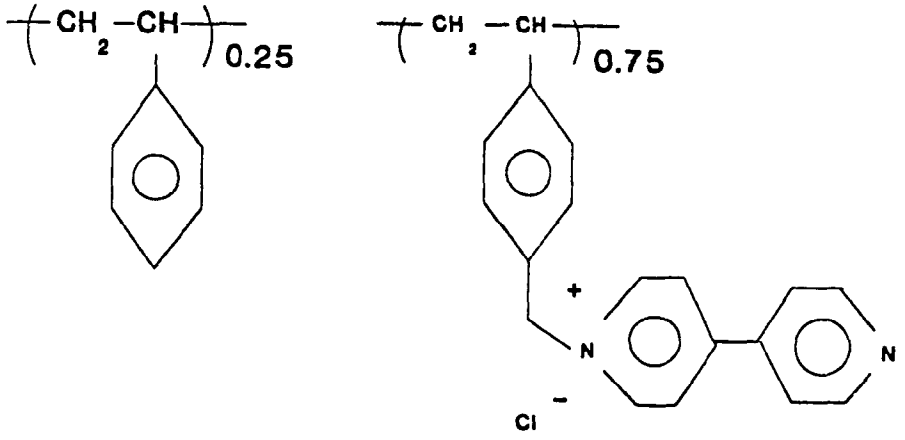

Figure 2.6 Structure of polymer PV1.

2.2.12 Synthesis of Poly(xylyl viologen) Bromide, PXV.

The poly(xylyl viologen) redox polymer was prepared by a simple one step synthesis (108) by reacting equimolar amounts of ortho- α,α'-dibromoxylene (Aldrich, 98%) and 4,4'-bipyridyl in 5% concentration in acetonitrile for 24 hours at room temperature. The resulting poly(xylylviologen bromide) was recovered as a bright yellow powder in 85% yield by filtration. This polymer was dried under vacuum at 60°C. The polymer was water soluble to an extent of 1-2% at room temperature. A 1% (w/v) aqueous casting solution was prepared and shall be denoted **PXV** (Figure 2.7).

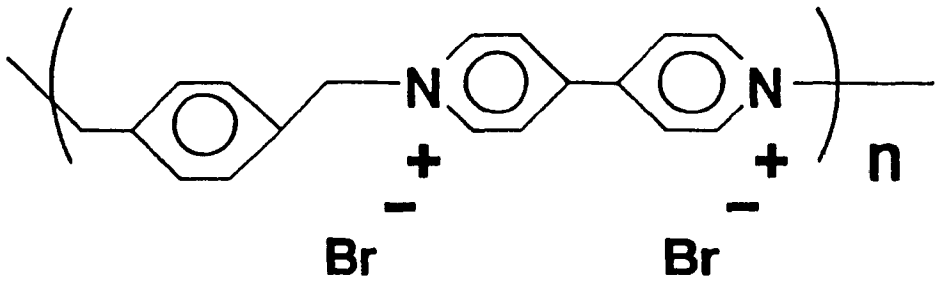

Figure 2.7 Structure of poly(xylyl viologen) bromide, PXV.

2.2.13 Preparation of Polypyrrole Modified Electrodes

Pyrrole (Aldrich, 98%) was fractionally distilled under a blanket of nitrogen and stored in a freezer at -5°C before use. Preparation of SnO_2 substrates will be described in a later section of this chapter. Polypyrrole was prepared either by electrochemical polymerization directly on SnO_2 electrodes, or by chemical oxidation of pyrrole to produce a casting solution. Each preparation will be outlined.

a) *Electrochemical Polymerization*

Polypyrrole was electropolymerized at +0.80 Volts vs. Ag/Ag^+ onto SnO_2 electrodes from deoxygenated acetonitrile solution containing 1% (v/v) water, 0.1 M pyrrole, 0.1 M tetraethylammonium perchlorate. Alternatively, pyrrole (0.1 M) was electropolymerized at the same potential vs. Ag/AgCl in aqueous 0.1 M KCl. Both methods afforded smooth green-black films into which the $Ni(mnt)_2^{-2}$ complex could be ion-exchanged for perchlorate or chloride from either acetonitrile or acetone

solutions.

b) *Chemical Oxidation*

Polypyrrole was prepared by chemical oxidation of 0.1 M pyrrole in acetone with 0.01 M $FeCl_3$. A black polymer was formed within 45 minutes and could be solution cast onto SnO_2 substrates. Excess iron and chloride could be leached out by soaking the modified electrodes in distilled water. $Ni(mnt)_2^{2-}$ was ion-exchanged into the film by the same method described above. Alternatively, $Ni(mnt)_2^{2-}$ was added directly to the acetone solution and cast on SnO_2 substrates. Films prepared by the chemical oxidation method were generally thicker and more robust than those prepared by electrochemical polymerization.

2.2.14 Preparation of Poly(4-vinyl pyridine) solutions

A 2% poly(4-vinyl pyridine) (PVP) (Polysciences) solution was prepared by slowly dissolving 2 grams of PVP in 100 mls of spectrograde methanol. A 1% solution of PVP was prepared in a similar fashion.

2.2.15 Preparation of Polycarbonate solution.

A 1% Polycarbonate solution was prepared by dissolving 0.25 grams of polycarbonate resin ($-C_6H_4-4-C(CH_3)_2C_6H_4-O-CO_2-$) (Aldrich) in 25 mls of methylene chloride.

2.3 Preparation of Polymer Modified Electrodes.

2.3.1 Preparation of SnO_2 electrodes

Optically transparent disk shaped electrodes were cut from n-doped SnO_2 coated pyrex (O.H. Johns Co., Industrial Glass Division). The dimensions of the disks were

fashioned such that the diameter of the disks was 25 mm and the thickness 6.25 mm. These disks could then be fitted into a specially designed electrochemical cell (108). The typical resistance of the electrodes was 20 → 35 Ω sq^{-1}.

Optically transparent slide shaped electrodes were cut from n-doped SnO_2 coated pyrex (Swift Glass Co.). The dimensions of the slides was 50 mm X 15 mm X 2.5 mm. The transparent electrodes were clamped and used in a conventional electrochemical cell. Typical surface resistance of this coated glass was 30 - 60 Ω sq^{-1}. Both disk and slide shaped electrodes were scrupulously cleaned before use or polymer modification. The slides were immersed in chromic acid or 1:1 HNO_3:HCl for 20-30 minutes, rinsed with lots of distilled water, and stored in ethanol. Prior to use, electrodes were rinsed with distilled water, then dried in an oven at 80°C.

2.3.2 Polymer modification of electrodes

Polymer modification of electrodes without the $M(mnt)_2^{2-}$ dyes was carried out by drop-evaporation of aliquots (0.5-1.0 mls) of the appropriate polymer casting solution onto levelled SnO_2 electrodes. The electrodes were then covered with an inverted crystallization dish to reduce the rate of solvent evaporation and to prevent dust particles from settling on the surface of the films. Solvent evaporation under normal conditions at room temperature took between 4 to 24 hours to produce satisfying films depending on the solvent. Alternatively, the time required for the solvent evaporation step was shortened by evaporation under reduced pressure using a water vacuum. This procedure was particularly effective when benzene or water was used as solvent for casting solutions.

The $M(mnt)_2^{2-}$ complexes were incorporated into the ion-containing polymer **P1**, poly(4-vinylpyridine) (PVP), and the blend **PB1** by slowly mixing different volumes (typically 2-8 mls) of a 1 X 10^{-3} M solution of the metal complex in methanol (Caledon, HPLC grade) to a previously prepared polymer solution also in methanol. The resulting mixture was stirred and heated gently until the final volume was reduced to that of the original polymer solution. This dye-polymer mixture was then solution cast onto levelled SnO_2 electrodes using the methods outlined above. Once dry, the composite polymer film electrodes were characterized by visible spectroscopy and the film thickness determined using a micrometer (Mitutoyo, Model 193-111).

The metal complexes were incorporated into polymers P2, P4, PV1, PXV and polypyrrole by ion-exchange against charge compensating counterions in the cationic films. Typically, the polymer coated electrodes were immersed in 0.5 $\rightarrow$ 1.0 X 10^{-3} M solutions of either $Ni(mnt)_2^{2-}$ or $Pt(mnt)_2^{2-}$ for 15 minutes to 1 day to incorporate the appropriate amount of dye into the film. Spectral characterization and film thickness were measured as before.

The $Ni(mnt)_2^{2-}$ was incorporated into polycarbonate films by dissolving as much of the complex as possible in the dichloromethane (Caledon, Spectrograde) polymer solutions, followed by the drop-evaporation method of film casting. Small particles of the red dye became visible upon drying. The translucent red films were characterized as described above.

The amount of dye in the polymer films was determined by dissolving the polymer and dye off the electrode, diluting in the suitable solvent and measuring its

optical absorbance. The concentration was then determined knowing the extinction coefficient of the complex in solution. It was possible to approximate the concentration of dye loading of the polymer modified electrodes by integrating the cyclic voltammetry peaks at slow scan rates. This method was useful only for films displaying voltammograms of the complex.

2.4 Electrochemical and Photoelectrochemical methods

2.4.1 Electrochemical Techniques

Once the solvent had evaporated, the red transparent films coated on the conductive glass disks were placed in the teflon flow cell (108) equipped with a platinum wire counter electrode and an Ag/AgCl (sat. KCl) reference electrode. The latter electrode was separated from the electrolyte by a glass frit. Electrolyte and redox solutions were pumped through silicone tubing (Cole Palmer) to the cell by using a locally constructed peristaltic pump. The solutions were circulated from a closed reservoir to the flow cell at a rate of 1.6 ml/min. Background electrolyte was either 1 M or 0.1 M KCl. The $Fe(CN)_6^{3-/4-}$ redox couple was incorporated via ion-exchange with the chloride counterions of the copolymer moiety.

The polymer modified slide shaped electrodes were coated with a commercially available clear lacquer (Annabelle) to expose an area of approximately 1 cm^2. The actual area was measured once the resin had dried. The lacquer was electroinactive and provides an easy way of controlling the exposed area of the electrode. The electrode was then mounted in a conventional 30 mls electrochemical cell along with a Ag/AgCl (sat. KCl) reference electrode and platinum counter electrode.

Cyclic voltammetric measurements and single-step chronoamperometric measurements were made using a Metrohm E-506 potentiostat coupled with a Methrohm E-612 scanner. A PAR-363 potentiostat was used to electropolymerize pyrrole onto SnO_2 substrates. Voltammetry was recorded on an X-Y recorder for cyclic voltammetry and on an X-t recorder for chronoamperometry. Solutions were deoxygenated with prepurified nitrogen prior to electrochemical measurements.

2.4.2 Photoelectrochemical Techniques

The modified electrode was illuminated from the SnO_2 side of the flow cell with either an Ar ion laser (Spectra-Physics) or a tungsten white light source filtered by a 5.5 cm water filter and a 400 nm cut-off filter to remove IR and UV radiation respectively. The white light source was either a Kodak slide projector (300 W tungsten bulb) or a locally constructed light source (GTE-Sylvania EKN tungsten projector bulb 120 W) equipped with a variable power supply to control the intensity of white light. Short circuit photocurrents and open circuit photovoltages were recorded using a Keithley (Model 177) multimeter in conjunction with an X-t strip chart recorder (Servogoer or Fischer recordall). The photon flux impinging on the photoelectrochemical cell was determined using a Coherent power meter (Model 210) placed at the position of the cell (Figure 2.8). The power meter was calibrated by ferrioxalate actinometry at 365 nm using interference filters, and at 472 nm and 488 using a laser. The actinometry values agreed with the power meter within 10% (134). For white light measurements, the electrode area exposed was $\approx$ 1 cm^2 for the slide-shaped electrodes and 2.0 cm^2 for the disk shaped electrodes. The white

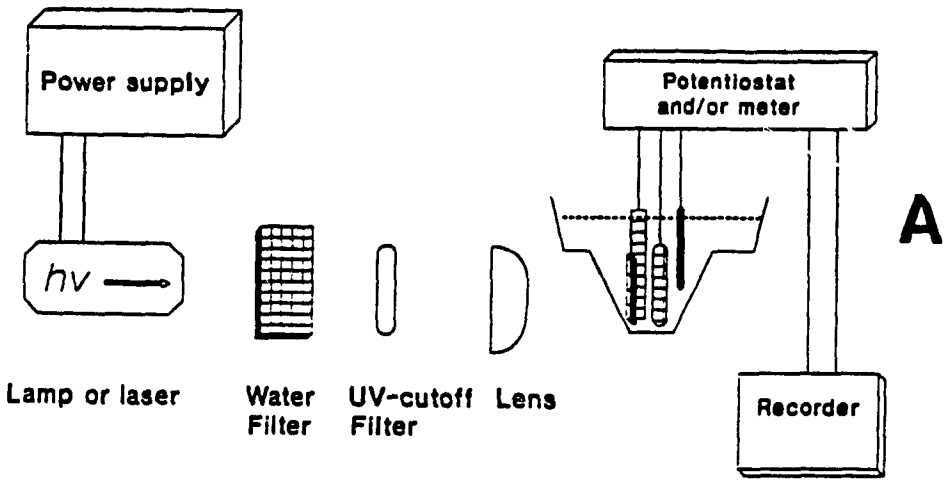

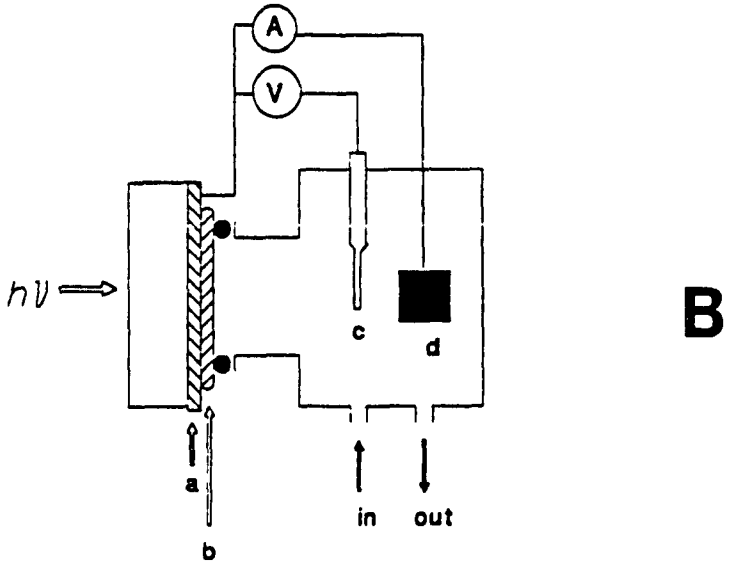

Figure 2.8 Schematic of photoelectrochemical setup, (A) Schematic for white light or laser illumination of slide-shape electrodes (filters and lens were removed for laser irradiations), (B) schematic of flowcell used for disk-shaped electrodes where (a) is the SnO_2 electrode, (b) the polymer coating, (c) the reference electrode, (d) the platinum counter electrode.

light impinges on an area of 2.5 cm^2 of the power meter.

All photocurrents were measured at short circuit between the working and counter electrode. Photovoltages were measured at open circuit between the same electrodes. Biased photocurrent measurements were obtained using a conventional three electrode design and monitoring the output on an X-t recorder.

2.5 Electronic Spectroscopy

2.5.1 Absorption Spectra

Absorption spectra of solutions and solid films were obtained using an HP8452A diode array spectrophotometer (2 nm resolution) interfaced to an IBM-PC computer. Near IR spectra were taken using a Shimadzu UV-'60 spectrophotometer at a resolution of 2 nm. Solution spectra were recorded in conventional cells with a pathlength of 1 cm or 2 mm. Spectra of polymer modified films were recorded on optically transparent SnO_2 electrodes (OTEs) in the path of the sample holder. Solid state and solution spectra were background corrected with a suitable blank.

2.5.2 Fluorescence Spectra

Solution fluorescence spectra were recorded with a Perkin-Elmer MPF-44B spectrofluorimeter in 1 cm quartz fluorimeter cells. A solid sample holder was used for polymer modified films on OTEs which allowed the incident beam to impinge at 30° to the solid sample.

2.6 Infrared Measurements

Fourier transform infrared spectra (FTIR) were obtained in either CsI or KBr pellets using a Bomem Michelson 102 FTIR at a resolution of 4 cm^{-1}.

Polymer films were also solution cast on Irtran or AgCl disks for FTIR measurements.

2.7 Electron Microscopy

2.7.1 Scanning Electron Microscopy

Scanning electron micrographs of polymer films were obtained using an ISI-SX30 electron microscope. Polymer modified electrodes were supported on aluminum stubs. Electrical contacts were made using silver epoxy and silver paint. Specimens were subsequently sputtered with gold. Modified films were observed at a +15° tilt with dynamic focus under 15kV electron acceleration voltage.

2.7.2 Transmission Electron Microscopy

Transmission electron microscopy of polymer films was done in Nanjing, China. Samples were cast on copper grids from methanolic solutions. We thank Profs. Zhai Hongru and Hu Meisheng, Centre for Materials Analysis, Nanjing University, Nanjing, China.

2.8 Continuous Photolysis Techniques

Solutions of $Pt(mnt)_2^{2-}$ and $Ni(mnt)_2^{2-}$ were photolysed in a 1 cm quartz cuvette modified to accommodate a septum cap. A constant temperature of 25.0°± 0.1°C was maintained using an HP-89054A water jacketed cell holder in conjunction with a MAW-Lauda circulating water bath. Samples were irradiated using a Spectra-Physics Model 2003 argon ion laser in single line mode or a Bausch & Lomb 75 W Xenon lamp with a 5.0 cm water filter and a 420 nm cut-off filter to

remove IR and UV radiation respectively. White light intensities were approximated using a Coherent 210 power meter placed at the position of the cell. The power meter was calibrated as described in section 2.4.2. Ferrioxalate actinometry was used in addition to thermopile measurements for laser irradiations and agreed within 10% of each other.

2.9 Flash Photolysis Techniques

2.9.1 Picosecond Absorption Spectroscopy

Picosecond transient absorption spectra were obtained in the Canadian Centre for Picosecond Flash Photolysis located at Concordia University. This system used a Quantel YG 402G Neodymium-doped YAG (Yttrium-Aluminum-Garnet) laser. The 1064 nm fundamental yielded 30 ps pulses at a maximum rate of 10 pulses per second. Frequency doubling and tripling of the fundamental using KDP type I and II crystals respectively, produced harmonic frequencies of 532 nm and 355 nm. Both frequencies were used as pump beams for excitation in picosecond absorption spectra.

Since the frequency doubling or tripling technique is not 100% efficient, the unconverted light (1064 nm) was focused into an aqueous solution of dilute H_3PO_4 which produced a white continuum from 425 nm to 675 nm with a pulse width comparable to that of the pump beam. A portion of this white beam was split to the sample to act as the probe beam while the other portion served as a reference beam.

The transmitted light from both pump and probe beams were each directed towards a section of a multichannel silicon enhanced vidicon array. Measurements were taken at probe delays from 20 ps to 1 ns. All data manipulation was performed using an EG&G PAR computer and then off-line on a PDP-11 minicomputer.

For each delay period, three data sets were collected and signal averaged. A data set consisted of one blank shot and three sample shots. For example, a curve for a probe delay of 50 ps was an average of nine sample shots and three blank shots. A transient absorption spectrum was presented as the average difference between the sample shots and blank shots. All picosecond absorption spectroscopy was carried out using fresh solutions in 2 mm quartz cell.

2.9.2 Picosecond Fluorescence Measurements

Transient fluorescence measurements were carried out using a modification of the system described in section 2.9.1. A Hammamatsu (model HTV N895) streak camera with a resolution of 10 ps was used to detect fluorescent traces following single laser shots at 355 nm. Glass cut-off filters, an interference filter and neutral density filters were placed before the entrance slit of the camera to select the fluorescent band and reject the laser pulse. The emission signal was recorded and displayed using a temporal analyzer (Hammamatsu C 1098). Samples were freshly prepared the day of the experiment in 2 mm quartz cells.

2.9.3 Microsecond Transient Absorption Spectroscopy

Transient spectra of $Pt(mnt)_2^{2-}$ in acetonitrile on the microsecond time scale was done using the laser flash photolysis instrumentation at the Center for Fast

Kinetic Research (CFKR), University of Texas at Austin, Austin, Texas.

A Quantel YG481 Nd:YAG Q-switched laser generated frequency tripled 355 pulses with a 0.2 ns duration. This excitation beam was focused through a 1 cm cell and the analysing beam through a 1 mm pinhole at right angles to the cell. All spectra and kinetics were analysed from an average of at least five shots. We thank Dr. Lalchan Persaud for performing these experiments while in Texas.

Chapter 3

Results and Discussion

Overview of Results and General Remarks

The results and discussion sections are split into 3 parts. The first includes the photochemistry and photophysics of $Ni(mnt)_2^{2-}$ and $Pt(mnt)_2^{2-}$. The second and third section describes the electrochemical and photoelectrochemical behaviour of polymer modified electrodes with these chromophores.

The photochemistry of $M(mnt)_2^{2-}$ was investigated in acetonitrile and mixed acetonitrile/water solutions in the spectral region of the metal to ligand charge transfer (MLCT) band. The photophysics of the complexes was studied using picosecond absorption and fluorescence spectroscopy. The visible light photoelectrochemistry of $M(mnt)_2^{2-}$ (M = Cu, Ni, Pt) at transparent SnO_2 electrodes has been studied by Persaud (62). It was suggested that the excited state lifetime of the complex might be prolonged by incorporation into a polymer matrix supported on the photoelectrode. The complexes were ion-exchanged into quaternized polyvinylpyridine films supported on SnO_2 (110). The work presented here reflects an extension of the photoelectrochemistry in quaternized polyvinylpyridine films. In the present case, much more stable performance is achieved. Ion-exchange polymers, redox polymers, and electronic polymers were evaluated as solid supports for the maleonitriledithiolate complexes. The electrochemical and photoelectrochemical charge transport processes were investigated for these polymers.

3.1 Photochemistry and Photophysics of $Pt(mnt)_2^{2-}$ and $Ni(mnt)_2^{2-}$

3.1.1 Visible Light Photolysis

The photochemical behaviour of $Pt(mnt)_2^{2-}$ and $Ni(mnt)_2^{2-}$ was studied in acetonitrile and acetonitrile/water (1:1) solutions. The photolysis of the complexes in solution can be related to the photoprocesses which occur when the dianions are immobilized in polymer films supported on optically transparent electrodes to be presented later. Upon irradiation with visible light (λ>400 nm), the spectral features of the dianionic metal complexes change to a species which resembles the monoanion. Photolysis using the xenon lamp setup was described in section 2.8. For irradiation periods resulting in less than 10 % conversion, photolysis of $Pt(mnt)_2^{2-}$ produces only two species as indicated by the well defined isosbestic points at 365 ± 2 nm and 452 ± 2 nm (Figure 3.1). The appearance of a characteristic low energy absorption band at 855 nm is indicative of the monoanion (111). Photolyses for greater than 10% conversion resulted in two peaks at 855 nm and 452 nm, two shoulders at 600 nm and 390 nm, and a corresponding decrease in the peaks at 310 nm and 336 nm (Figure 3.2).

The effect of oxygen on the photolysis of $Pt(mnt)_2^{2-}$ is shown in Figure 3.3 during a prolonged photolysis (3 hours). The cuvette was modified to accommodate a rubber septum. Deoxygenation of acetonitrile solutions was accomplished by passing a stream of prepurified nitrogen through a solvent bubbler into the cuvette using a syringe needle. The exhaust gas was released by means of a second needle inserted into the cuvette above the liquid phase. In the absence of oxygen, photolytic conversion of $Pt(mnt)_2^{2-}$ and $Ni(mnt)_2^{2-}$ to their corresponding monoanions

Figure 3.1 Electronic absorption changes for $Pt(mnt)_2^{2-}$ in acetonitrile under visible light irradiation. Irradiation times from reactant A to product B were 0, 2, 4, 6, 8, 10 minutes.

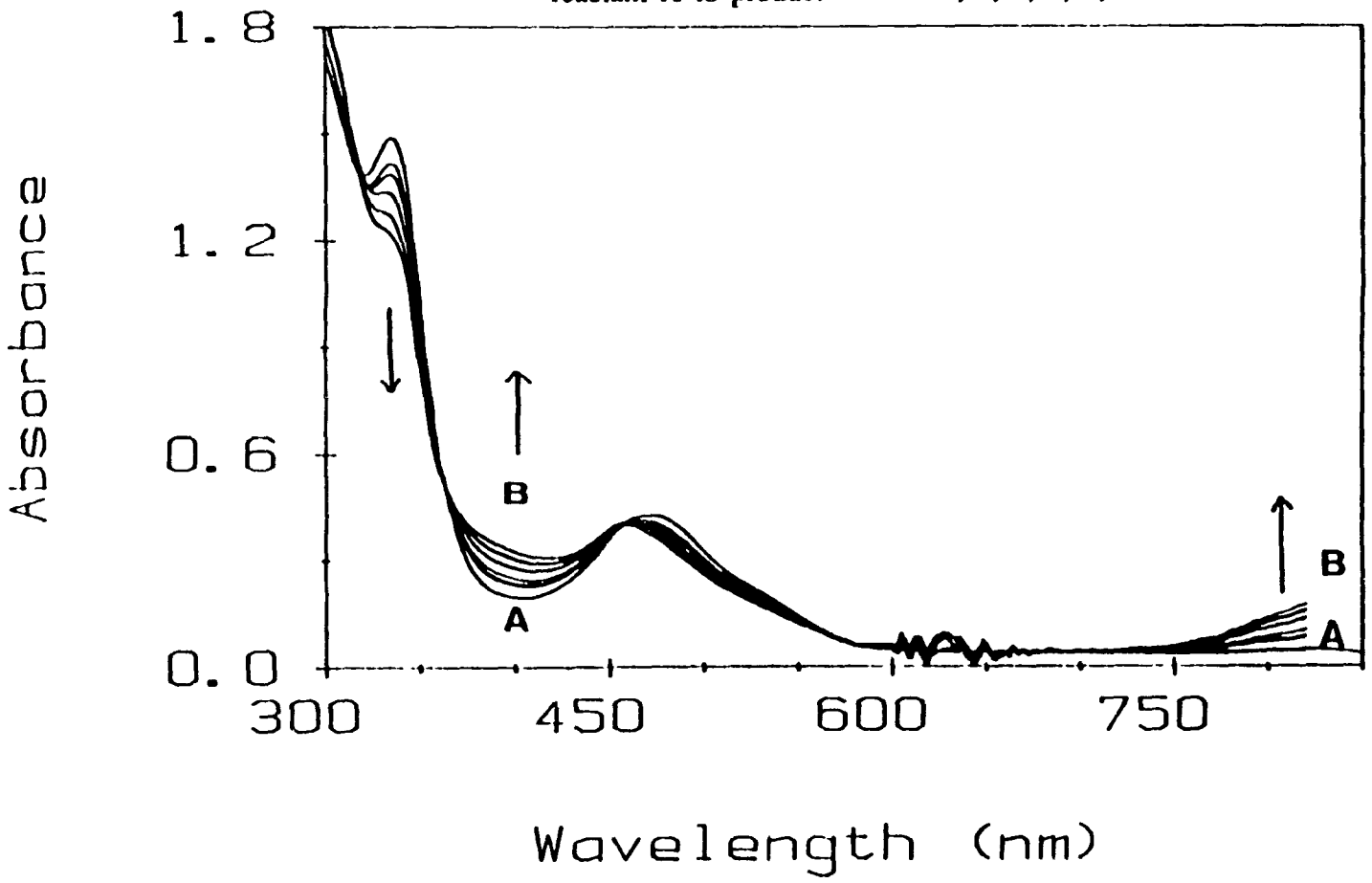

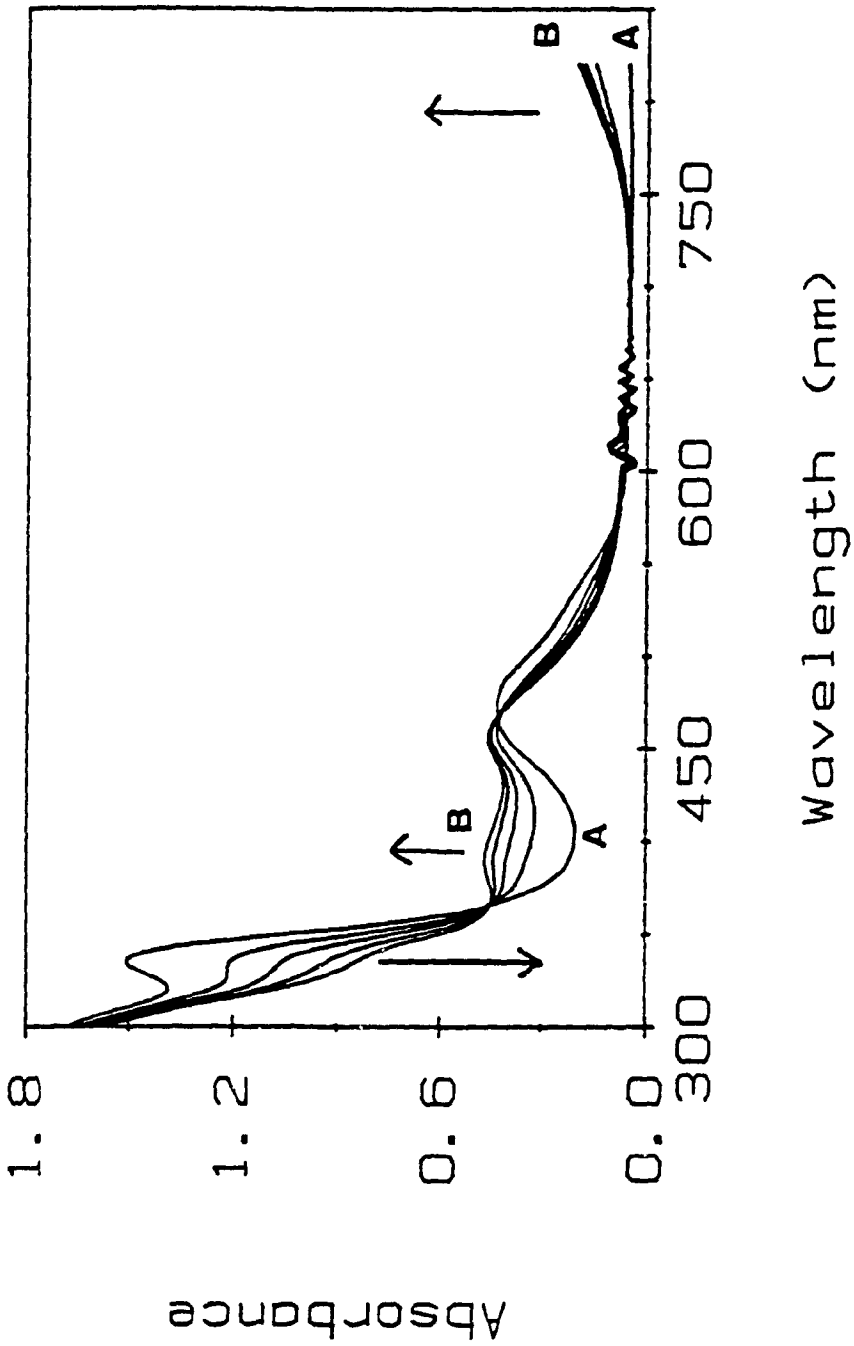

Figure 3.2 Electronic absorption changes for $Pt(mnt)_2^{2-}$ in acetonitrile under visible light irradiation. Irradiation times from reactant **A** to product **B** were 0, 15, 25, 35, 40 minutes.

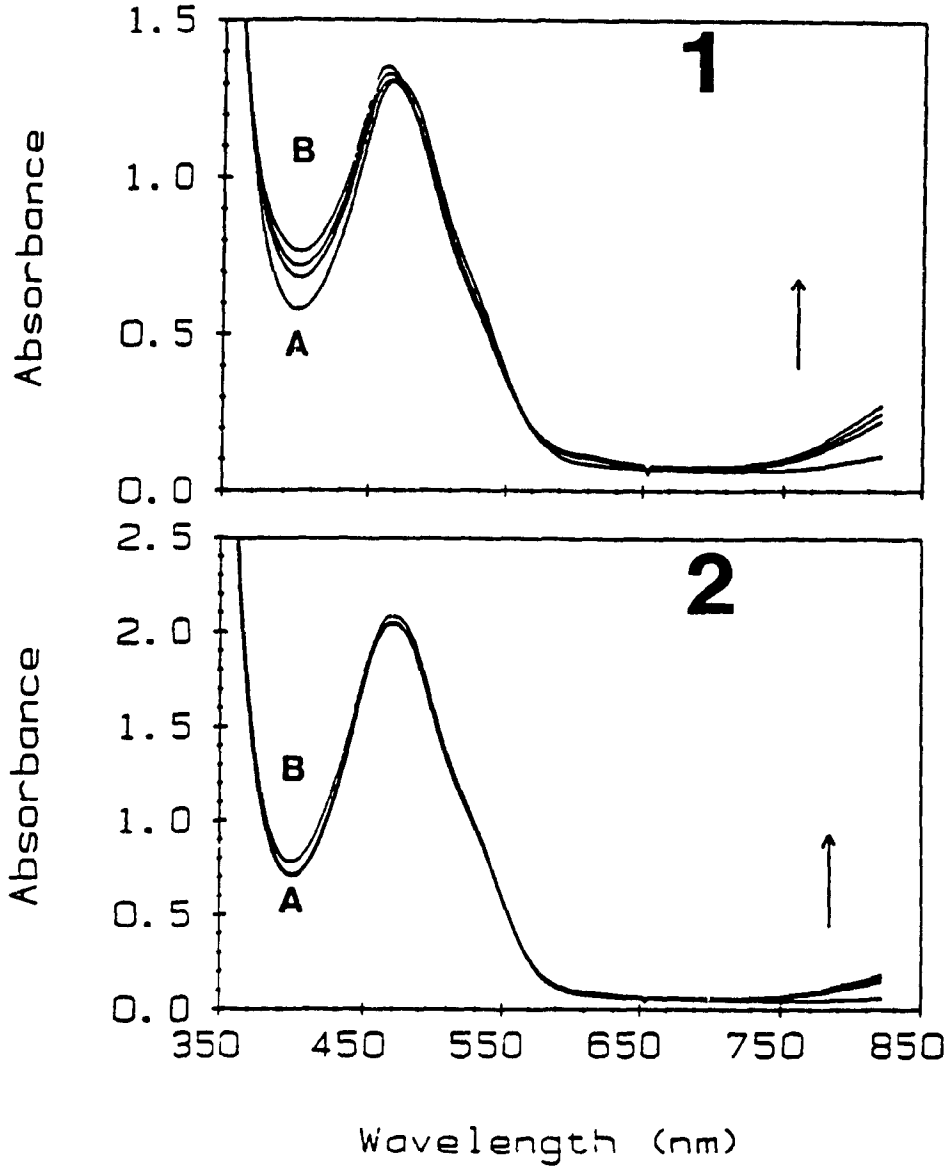

Figure 3.3 Electronic absorption changes for $Pt(mnt)_2^{2-}$ in acetonitrile under visible light irradiation. (1) Photolysis in the presence of atmospheric oxygen, (2) photolysis in deoxygenated acetonitrile. Irradiation times from reactant A to product B were 0, 1, 2, 3 hours.

proceeded slowly. Solutions which were not degassed underwent photo-oxidation more rapidly. The reaction is believed to proceed with oxygen as final oxidizing agent. Workers who studied the photo-oxidation of these complexes and other $M(mnt)_2^{2-}$ (M= Pt,Pd,Ni,Co,Cu) (100,101) did not indicate any degassing procedures or O_2 levels in their experimental sections. It should be noted however that the halocarbon solvents used in those experiments are better electron acceptors than acetonitrile in this study. Most other experiments to be described were performed without degassing since dissolved oxygen is present in the polymer films (15,21). The oxygen in the films probably acts only as an electron acceptor trap which reduces the overall photon to electrical current conversion efficiency. Water which can act as a weaker electron acceptor than oxygen is present in the neat acetonitrile to an extent of 150 ppm.

Steady state photolysis experiments were also carried out using an argon ion laser in single line mode. 472 nm irradiation into a low lying metal to ligand charge transfer band (MLCT) of $Pt(mnt)_2^{2-}$ photooxidized the complex more rapidly than with the xenon lamp light source without deoxygenation.

In the presence of acetonitrile/water mixtures (1:1), the photoreaction proceeded faster than in neat acetonitrile (Figure 3.4). The appearance of the shoulder at 390 nm was more rapid in this case.

The monoanion was the only photoproduct observed during the first 10 minutes of the photolyses. Further photolysis results in the loss of an isosbestic point at 452 nm. The products of any secondary photolyses have not yet been identified. The photo-behaviour of the $M(mnt)_2^{1-}$ anions has never been investigated.

Figure 3.4 Electronic absorption changes for $Pt(mnt)_2^{2-}$ in acetonitrile/water mixture (1:1) under visible light irradiation. Irradiation times from reactant A to product B were 0, 14, 65, 97, 140, 200 minutes.

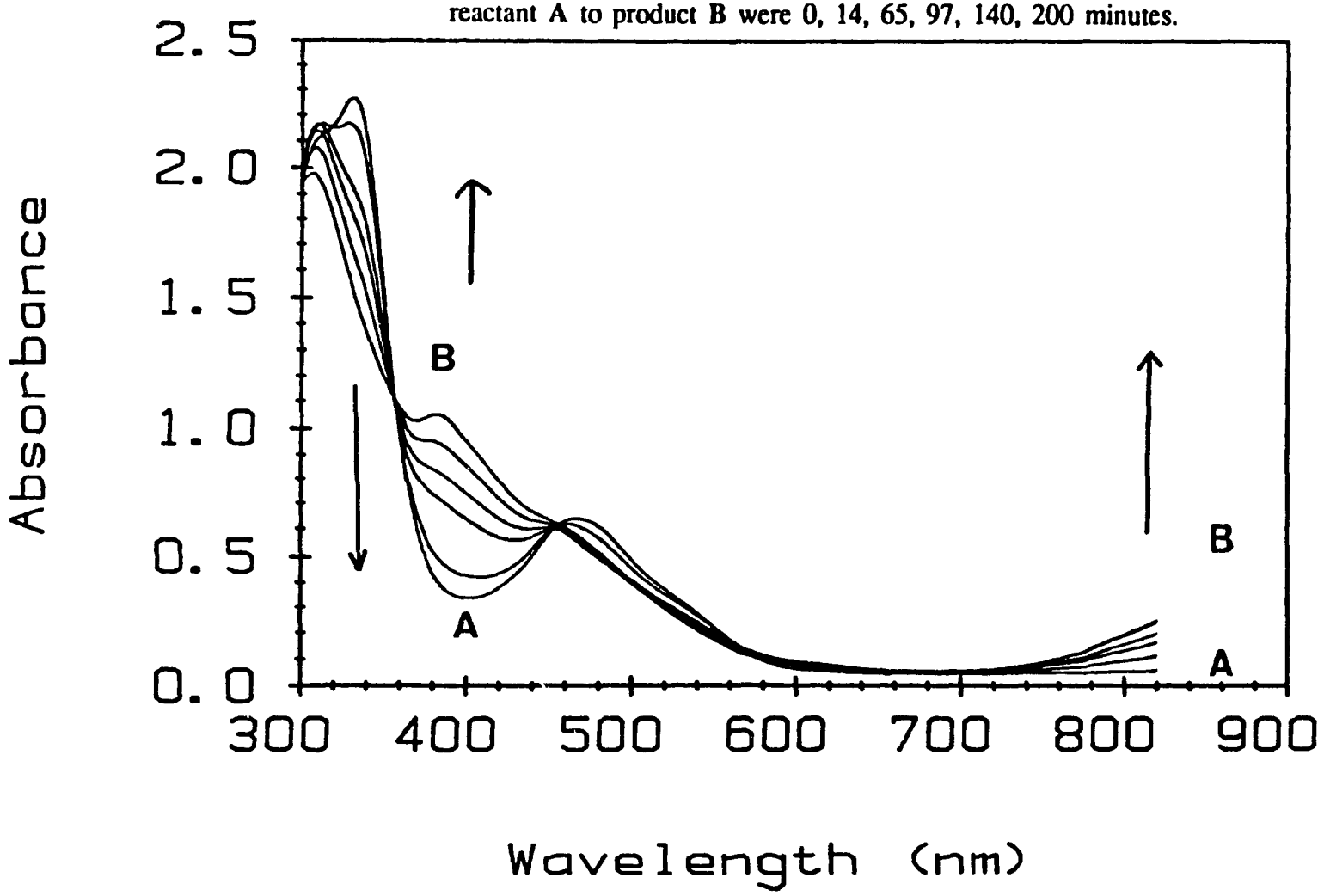

The primary photoproduct was identified by its absorption spectra. The characteristic near-IR transition of the $Pt(mnt)_2^{1-}$ occurs at λ = 855 nm (111), while the monoanion of the nickel complex absorbs at λ = 878 nm (91). The visible and near-IR spectra of $Pt(mnt)_2^{2-}$ and $Pt(mnt)_2^{1-}$ is shown in Figure 3.5. Similar spectra for $Pt(mnt)_2^{1-}$ and the photoproduct are depicted in Figure 3.6. The near-IR transition is the only published absorption band available for the characterization of the monoanion of the Pt complex. In addition, the photoproduct was characterized by its IR absorption, which compares closely to that of the monoanion (Figure 3.7). Assignments of the major IR absorption bands are provided in Table 3.1. The electronic and infrared spectra of the $M(mnt)_2^{n-}$(n= 1-, 2-) complexes of Ni and Pt are similar.

The electronic absorption spectra of $[(C_2H_5)_4N]_2[Pt(mnt)_2]$ and $[(C_2H_5)_4N]_2$-$[Ni(mnt)_2]$ complexes have been previously studied by Shupack and co-workers (91) and by Mayweg and Schauzer (90). The main spectroscopic features and their assignments are reported in Table 3.2. A simplified molecular orbital diagram of $Ni(mnt)_2^{2-}$ according to Shupack and co-workers is shown in Figure 3.8. Previous work by Persaud and Langford (110) has indicated that there is some photoelectrochemical precedent for using this scheme. A modification of this scheme has been proposed by Chandramouli and Manoharan based on single crystal measurements (85)(Figure 3.9). The scheme is comparable to the one proposed by Shupack *et al.* (91) except for the interchange of x^2-y^2 and xy+L levels which corresponds to $4a_g$ and $4b_{2g}$ (85). This scheme will be used in discussion of experimental results.

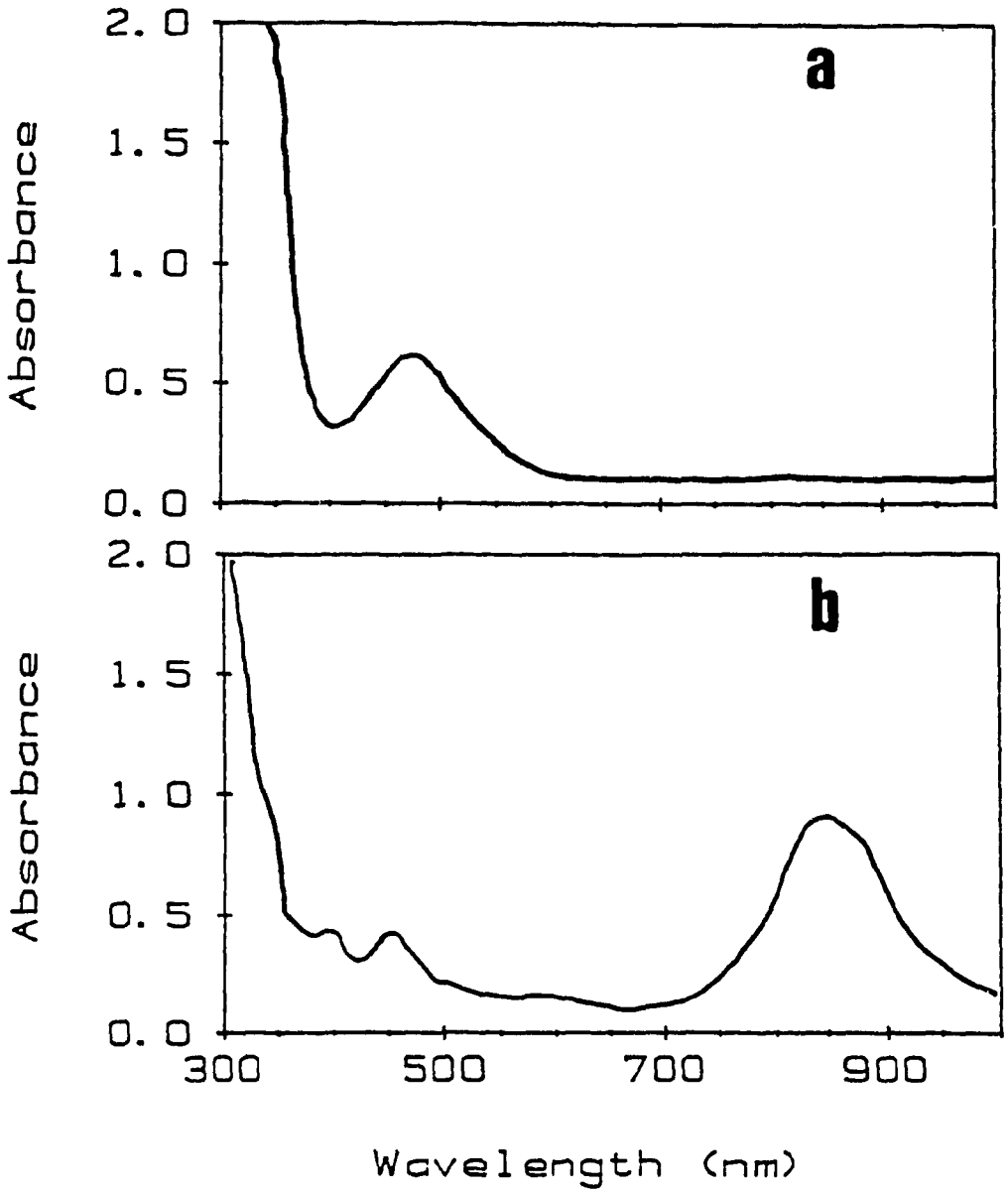

Figure 3.5 Visible and near-IR absorption spectrum of (a) $Pt(mnt)_2^{2-}$ in acetonitrile, and (b) $Pt(mnt)_2^{1-}$ in acetonitrile.

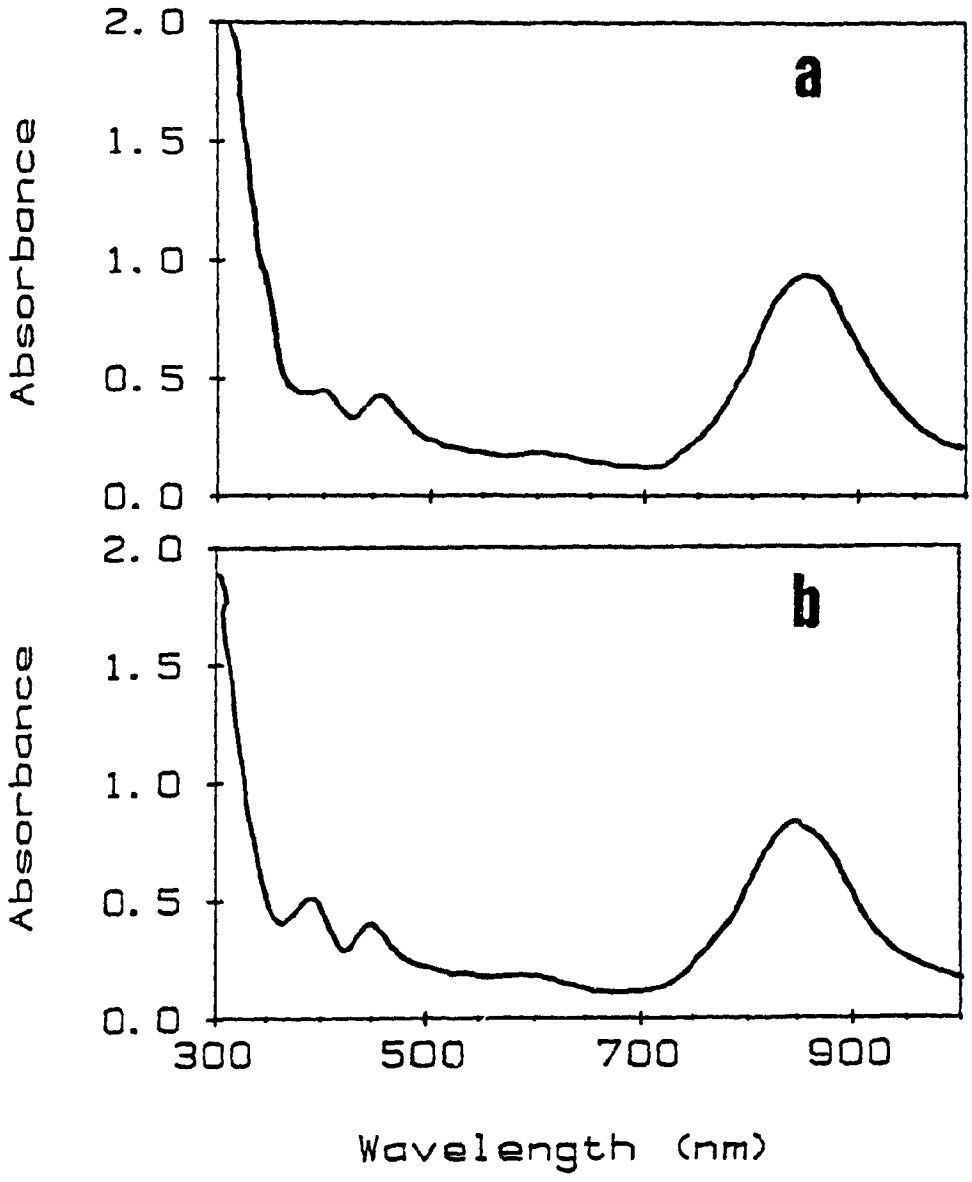

Figure 3.6 Visible and near-IR absorption spectrum of (a) $Pt(mnt)_2^{1-}$ in acetonitrile, and (b) photoproduct of $Pt(mnt)_2^{2-}$ in acetonitrile.

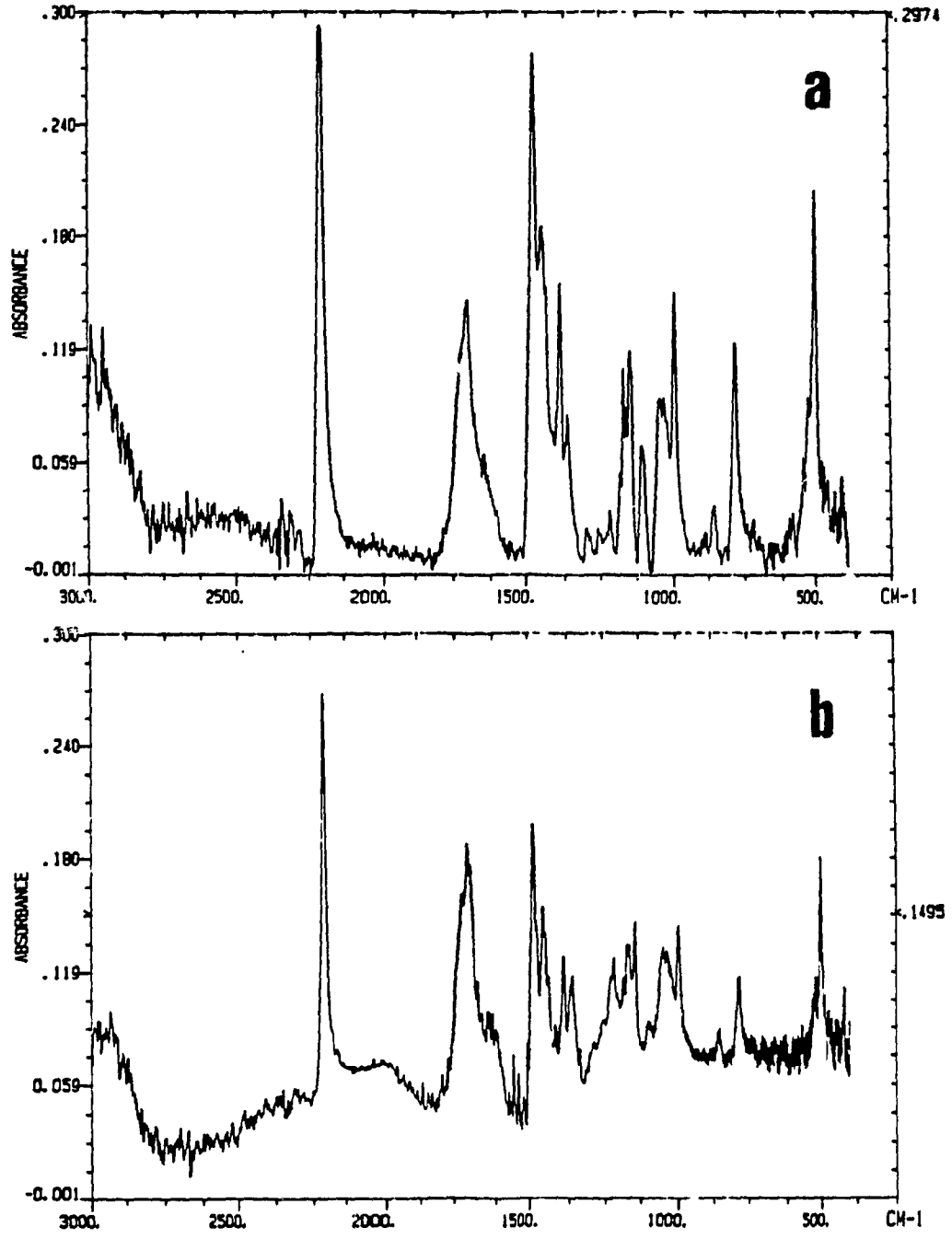

Figure 3.7 FTIR spectra of (a) primary product from photolysis of $Pt(mnt)_2^{2-}$ in acetonitrile, and (b) $Pt(mnt)_2^{1-}$. Both samples were prepared on AgCl plates with 100 scans at 4 cm^{-1} resolution.

Table 3.1 Comparison of infrared frequencies for $Pt(mnt)_2^{1-}$ and its primary photoproduct[a].

Assignment[b]	$Pt(mnt)_2^{1-}$ (cm^{-1})	Photoproduct (cm^{-1})
ν(C≡N)	2206 (s)	2202 (s)
ν(C=C)	1485 (s) 1436 (s)	1482 (s) 1438 (s)
ν(C-C) + ν(C-S)	1143 (s)	1145 (s)
ν(C-S) + ν(C-C)	1050 (m)	1052 (m)
ν(C-S)	855 (w)	857 (w)
ring def + δ(CCN)	501 (s)	501 (s)

a) ± 4 cm^{-1}

b) assignments adapted from ref.(88) using $Ni(mnt)_2^{1-}$ data.

Table 3.2 Electronic absorption maxima of $M(mnt)_2^{n-}$ and assignments.

Complex	Frequency ν (cm^{-1})	Wavelength[a] λ (nm)	Extinction coefficient ε (M^{-1} cm^{-1})	Assignment[b]
$Ni(mnt)_2^{2-}$	11,690	855	30	$^1A_g \rightarrow {}^1B_{1g}$ (x^2-$y^2 \rightarrow xy$)
	17,500	571	570	$^1A_g \rightarrow {}^1B_{3g}$ ($xz \rightarrow xy$)
	19,250	519	1,250	$^1A_g \rightarrow {}^1A_g$ (x^2-$y^2 \rightarrow L\pi^*$)
	21,000	476	3,800	$^1A_g \rightarrow {}^1B_{2u}$ ($xz \rightarrow L\pi^*$)
	26,400	378	6,600	$^1A_g \rightarrow {}^1B_{2u}, {}^1B_{3u}$ ($L\pi \rightarrow xy$)
	31,300	319	30,000	$^1A_g \rightarrow {}^1B_{2u}$ ($L\pi \rightarrow L\pi^*$)
	37,700	270	50,000	$^1A_g \rightarrow {}^1B_{2u}, {}^1B_{3u}$ ($L\sigma \rightarrow xy$)
$Pt(mnt)_2^{2-}$	14,410	694	49	$^1A_g \rightarrow {}^3B_{1g}$ (x^2-$y^2 \rightarrow xy$)
	15,650	639	56	$^1A_g \rightarrow {}^3B_{3g}$ ($xz \rightarrow xy$)
	18,500	540	1,220	$^1A_g \rightarrow B_{1g}$ (x^2-$y^2 \rightarrow xy$)
	21,100	473	3,470	$^1A_g \rightarrow {}^1B_{2u}$ ($xz \rightarrow L\pi^*$)
	29,700	336	15,600	$^1A_g \rightarrow {}^1B_{2u}$ ($L\pi \rightarrow L\pi^*$)
	32,300	309	13,400	$^1A_g \rightarrow {}^1B_{2u}, {}^1B_{3u}$ ($L\pi \rightarrow L\pi^*$)
	38,500	260	17,000(sh)	c
	43,800	228	43,500	$^1A_g \rightarrow {}^1B_{2u}, {}^1B_{3u}$ ($L\sigma \rightarrow xy$)
$Ni(mnt)_2^{1-}$	8,330	1,200	329	$4b_g \rightarrow 4a_g$ ($xz \rightarrow x^2$-y^2)
	11,790	848	8,000	$3b_{1u}, 2b_{2u,3u} \rightarrow 4a_g$ ($L\pi \rightarrow x^2$-y^2)
	16,666	600	668	$3b_{3g} \rightarrow 4a_g$
	18,349	545	798	$3a_g \rightarrow 4a_g$
	20,964	477	2,500	$1b_{2u,3u} \rightarrow 4a_g$ ($L\sigma \rightarrow x^2$-y^2)
	27,027	370[d]	7,114	$2b_{2,3u} \rightarrow 3b_{1g}$ ($L\pi \rightarrow xy$)
	32,154	311	33,870	$3b_{1u} \rightarrow 4b_{3g}$ ($L\pi \rightarrow L\pi^*$)
	37,037	270	34,017	$1b_{2u,3u} \rightarrow 3b_{1g}$ ($L\sigma \rightarrow xy$)
	43,478	230	19,000	c
$Pt(mnt)_2^{1-}$	11,700	855	11,700[e]	$3b_{1u}, 2b_{2u,3u} \rightarrow 4a_g$ ($L\pi \rightarrow x^2$-y^2)

a) Calculated from frequencies
b) From reference 84 and 91
c) not assigned
d) appears as a shoulder
e) From reference 111

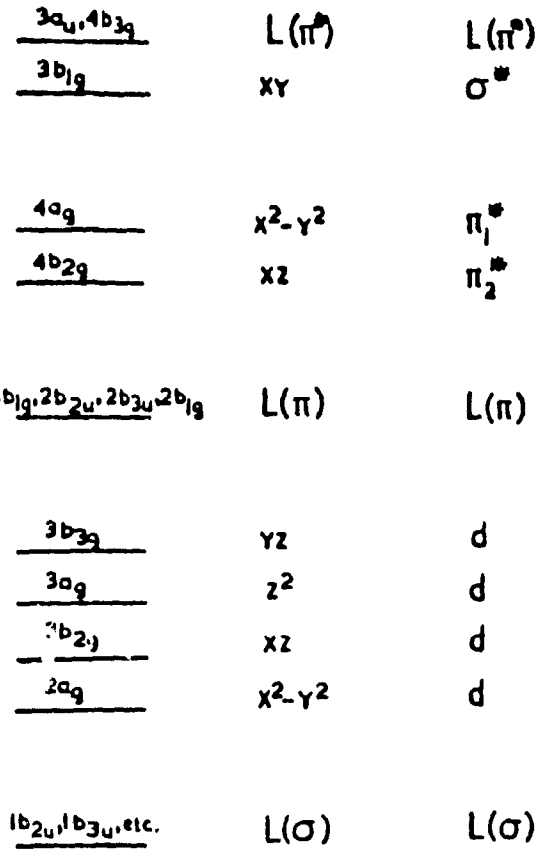

Figure 3.8 Simplified molecular orbital diagram for $Ni(mnt)_2^{n-}$ (n=1,2) according to Stiefupack *et al.* (taken from reference 91).

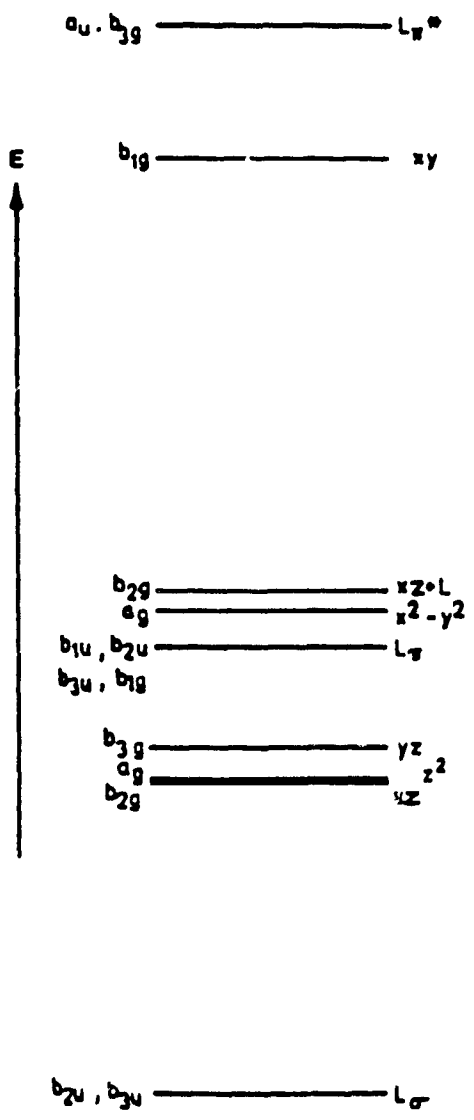

Figure 3.9 Energy level diagram for $[(n\text{-}Bu)_4N]_2[Ni(mnt)_2]$ according to Chandramouli and Manoharan (taken from reference 85).

3.1.2 Transient Absorption Spectroscopy

The transient absorption and emission spectra of $[N(C_2H_5)_4^+]_2[Pt(mnt)_2^{2-}]$ and $[N(C_2H_5)_4^+]_2[Ni(mnt)_2^{2-}]$ were investigated to gain more insight on the primary photochemical processes of these molecules which are involved in the generation of photocurrents from polymer modified electrodes.

Picosecond transient absorption of $Ni(mnt)_2^{2-}$, $Pd(mnt)_2^{2-}$, $Pt(mnt)_2^{2-}$, and $Pt(mnt)_2^{1-}$ have been briefly investigated by Persaud and Langford (61). The palladium complex and the monoanionic platinum complex displayed no excited state absorption despite strong absorbance of LMCT bands in the visible. However, $Pt(mnt)_2^{2-}$ and $Ni(mnt)_2^{2-}$, displayed excited state absorption and ground state bleaching. The excitation wavelength used in previous work was 355 nm. The work described here used both 355 nm and 532 nm as excitation wavelengths for $Pt(mnt)_2^{2-}$ and $Ni(mnt)_2^{2-}$. Excitation of $Pt(mnt)_2^{2-}$ at 355 nm corresponds to the initial population of $L\pi \rightarrow L\pi^*$ states while similar excitation of $Ni(mnt)_2^{2-}$ corresponds to initial population of orbitals with primarily $L\pi \rightarrow M$ and $L\pi \rightarrow L\pi^*$ character. A 532 nm pump beam excites transitions which are primarily MLCT and/or metal centered (*d-d*) transitions in both $Ni(mnt)_2^{2-}$ and $Pt(mnt)_2^{2-}$.

The transient absorption spectra for $Ni(mnt)_2^{2-}$ using 355 nm and 532 nm excitation are shown in Figure 3.10 and 3.11 respectively. The overall shape of the transient remained similar in both cases.

Transients are longer lived for 355 nm excitation than 532 nm excitation. Approximate lifetimes were estimated by fitting the spectra to first-order kinetic plots of Ln $(\Delta A_t - \Delta A_\infty)$ versus time. The lifetime of the transient following 532 nm

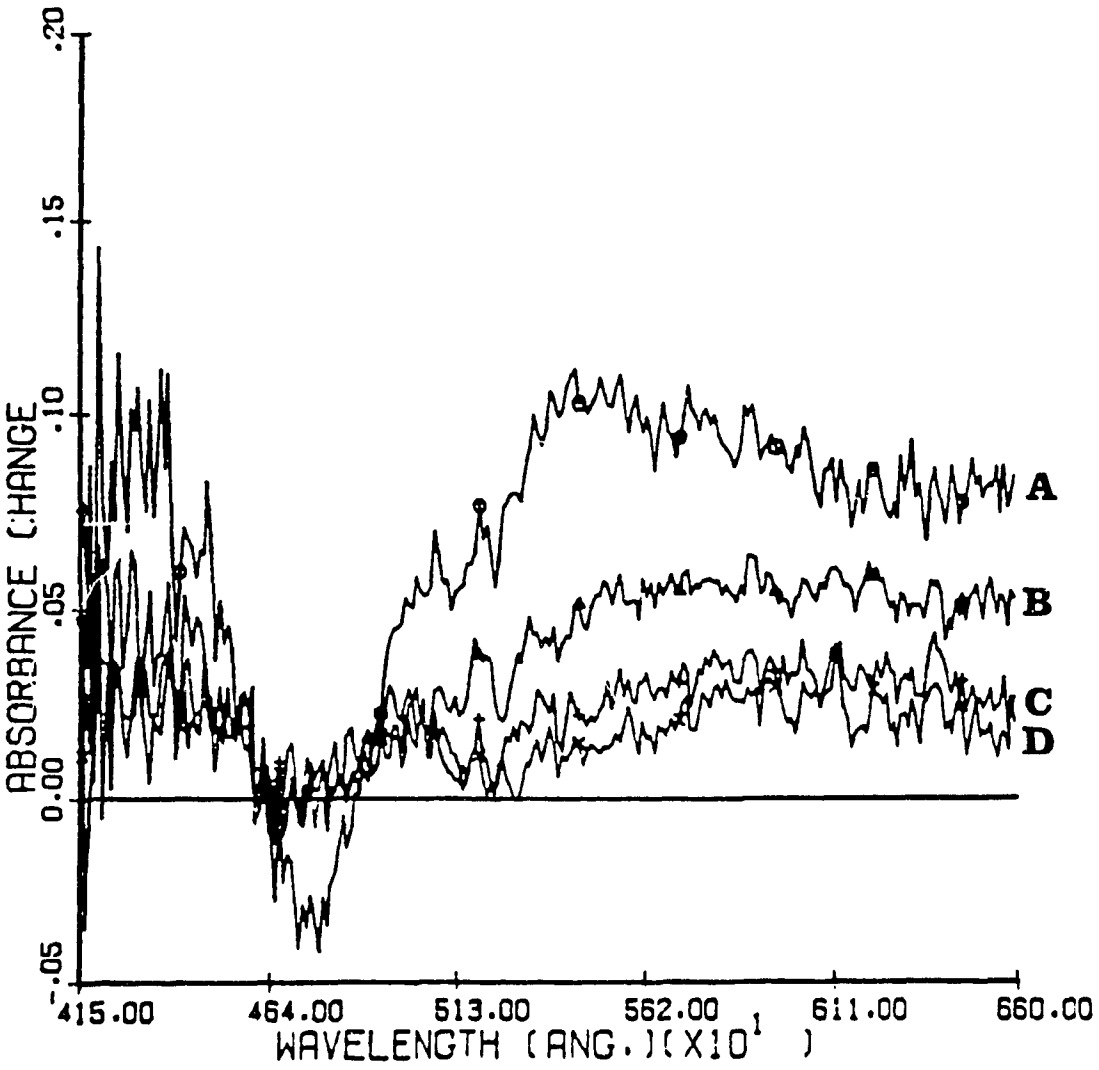

Figure 3.10 Transient absorption spectra for $Ni(mnt)_2^{2-}$ in acetonitrile using 355 nm excitation at probe delays of (A) 20 ps, (B) 50 ps, (C) 100 ps, and (D) 200 ps.

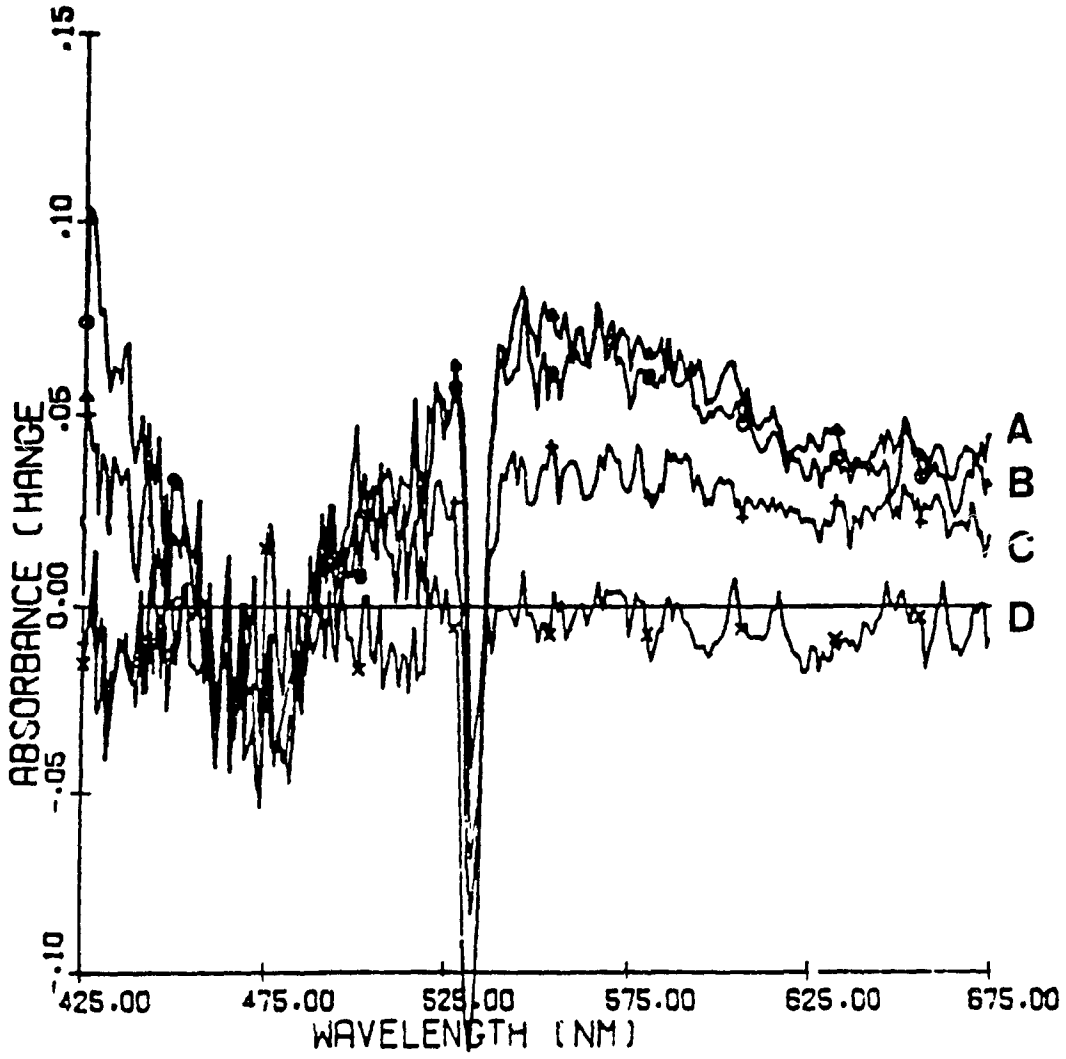

Figure 3.11 Transient absorption spectra for $Ni(mnt)_2^{2-}$ in acetonitrile using 532 nm excitation at probe delays of (A) 0 ps, (B) 20 ps, (C) 50 ps, and (D) 100 ps.

excitation was determined to be 40 ± 25 ps. There is minimal bleaching of the ground state remaining at 100 ps probe delay in this case indicating that no other processes are likely to occur at longer probe delays. The spectra obtained with 355 nm excitation displayed excited states even beyond 200 ps probe delays. In the blue region of Figure 3.10 (425→450 nm) there was similar excited state absorption following the same trend as the transient behaviour more to the red. The lifetime of the first transient centered at 540 nm was determined to be 100 ± 23 ps. The transient absorption signal observed at longer probe delays (i.e. 3,5,7, and 10 ns) indicate that another excited state species was growing in with broad band characteristics (Figure 3.12). The lifetime of this transient was not determined since the upper limit of probe delays is 10 ns at the picosecond flash photolysis center.

$Pt(mnt)_2^{2-}$ in acetonitrile was examined using both 355 nm and 532 nm excitation pulses. The Pt complex appeared to behave similar to the Ni complex but with longer lived excited states. The transient absorption spectra obtained using a 355 nm pulse displayed a constant ground state bleaching of the MLCT band at 480 nm (slight red shift) from 20 ps until a delay time of 500 ps. There was excited state absorption from 575 to 675 nm (Figure 3.13) which does not decay beyond 10 nanoseconds, although there is considerable recovery of the ground state in the bleaching region during the same period. The decay of transient signals for the platinum complex was not analyzed quantitatively since a reliable estimate of A_- could not be determined. $Pt(mnt)_2^{2-}$ does not return completely to its ground state within the time limits of this experimental setup of the picosecond centre.

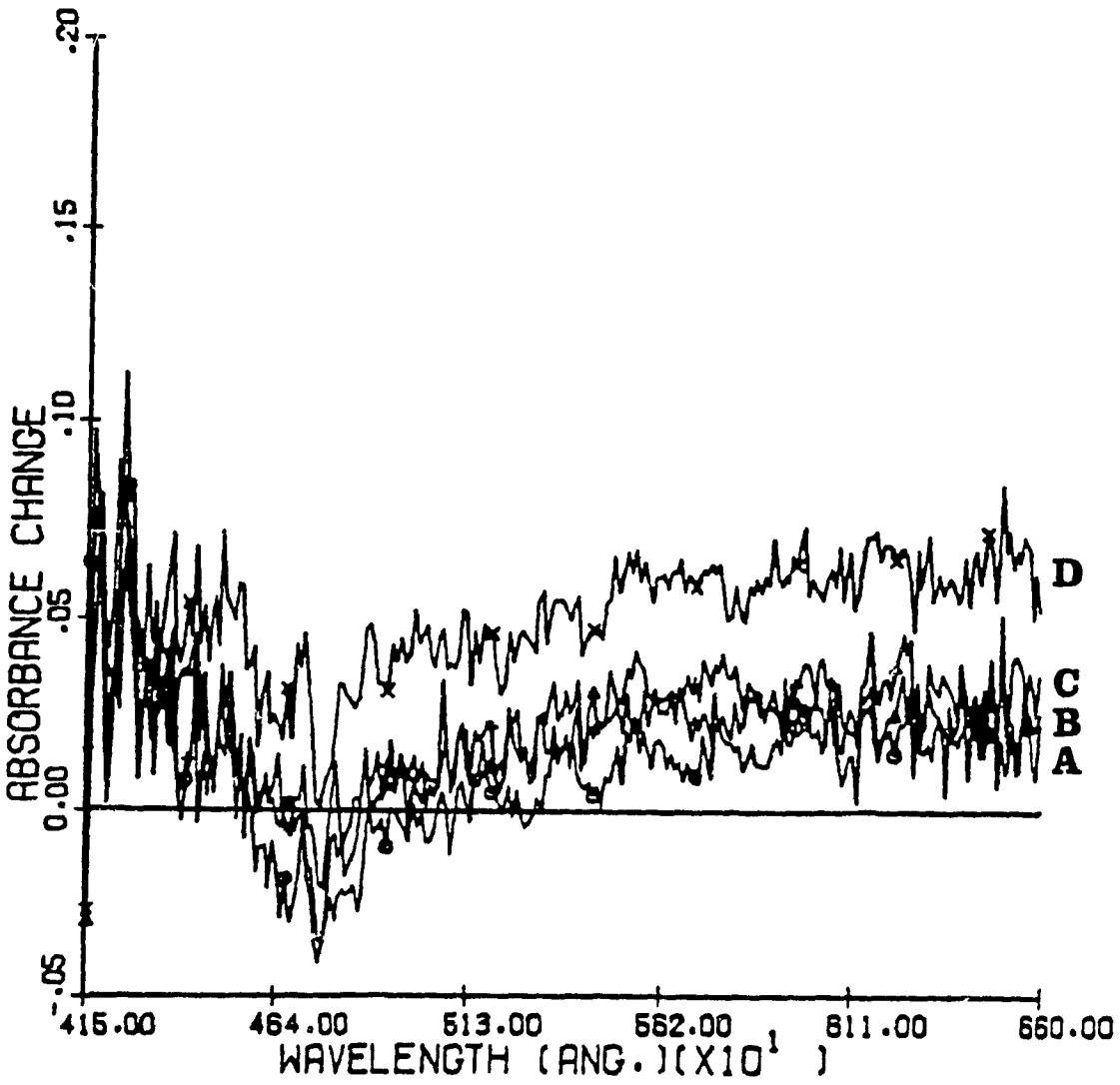

Figure 3.12 Transient absorption spectra for $Ni(mnt)_2^{2-}$ in acetonitrile using 355 nm excitation at probe delays of (A) 3 ns, (B) 5 ns, (C) 7 ns, and (D) 10 ns.

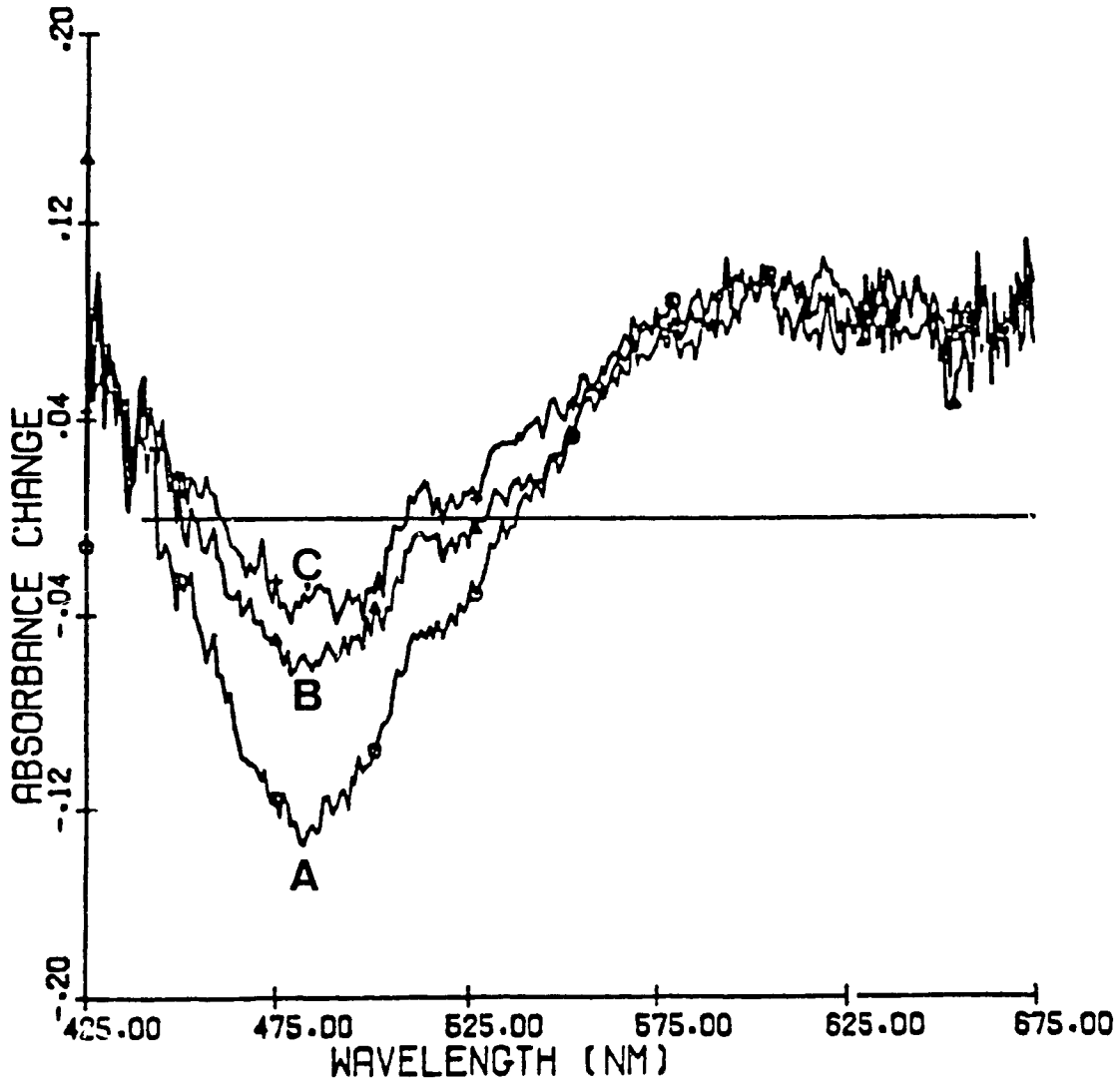

Figure 3.13 Transient absorption spectra for $Pt(mnt)_2^{2-}$ in acetonitrile using 355 nm excitation at probe delays of (A) 500 ps, (B) 5 ns, and (C) 10 ns.

It is suggested that the excited state initially populated by a 355 nm pulse partitions rapidly into a low lying singlet and triplet. The singlet decays on the picosecond timescale, whereas the triplet with an absorption in the red (575→670 nm) is longer lived species.

The transient behavior of the triplet was examined more closely on the micro-second timescale. Figure 3.14 shows the absorbance changes recorded between 3.2 μs and 430 μs in deoxygenated acetonitrile. There was bleaching of the ground state (shifted to 490 from 475 nm) and transient absorption centered at 625 nm and at 742 nm. These transients can be monitored at times shorter than a few micro-seconds. The decay of the transient absorption and the recovery of the ground state do not follow the same kinetics. Upon excitation the excited state generated decays via two routes: the first regenerates the ground state while the second pathway produces a species with absorption at 625 nm. Analysis of the transient absorption signal at 602 nm fitted very well to the sum of two first-order exponential decays. The fast component decays with a rate of 3.05 X 10^5 sec^{-1} corresponding to a lifetime of 3.2 μs. The longer lived component exhibited a rate constant of 4.14 X 10^4 sec^{-1} or 24.2 μs. The picosecond spectroscopy suggested that the absorption in the red could be the triplet. If so, it is not unlikely that the transient species with a lifetime of 3.2 μs is a triplet, while the longer lived species may be a primary photoproduct. Flash photolysis of $Pt(mnt)_2^{2-}$ in the presence of excess water (30%) in acetonitrile quenches the triplet state and only the longer lived photoproduct (24.6 μs) was observed.

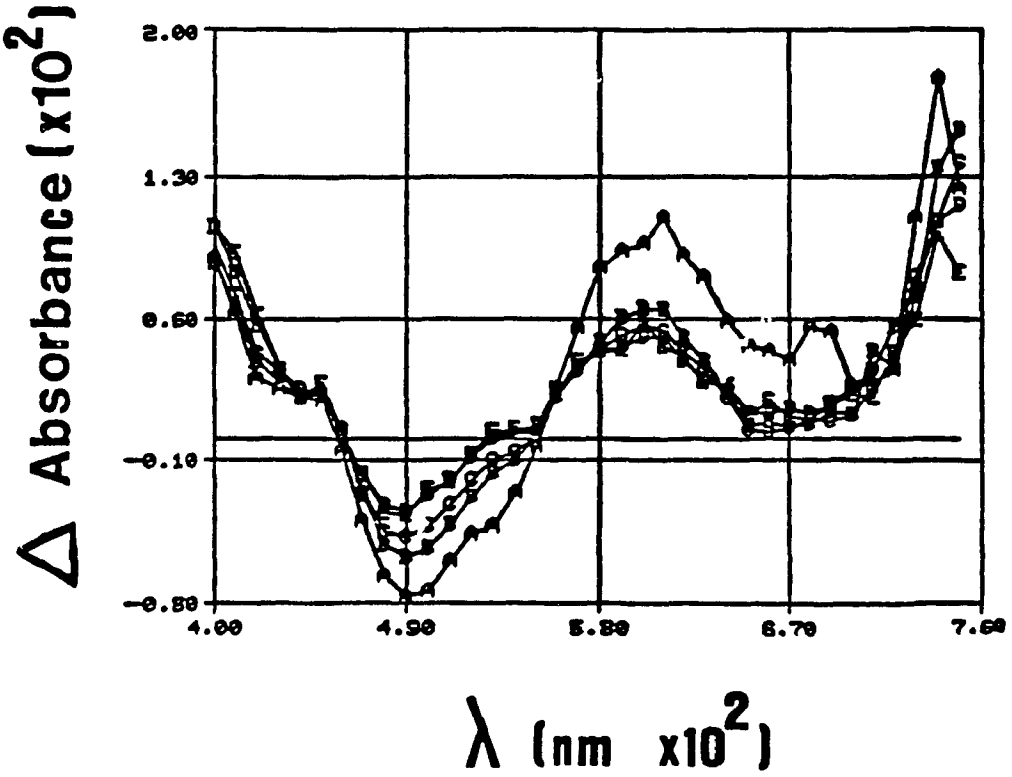

Figure 3.14 Transient absorption spectra for $Pt(mnt)_2^{2-}$ in acetonitrile using 355 nm excitation at probe delays of (A) 3.2 μs, (B) 12.8 μs, (C) 22.4 μs, (D) 118.4 μs, and (E) 430.4 μs.

A 532 nm pulse excites a MLCT band and *d-d* bands of $Pt(mnt)_2^{2-}$. Transient absorption spectra obtained at 20 ps and 1 ns were very similar to each other. At probe delays >1 ns the transient absorption and bleaching begin to recover towards the ground state (Figure 3.15). Similar decay of transient absorption was observed in the blue region at 425 nm to 435 nm. There is an indication that only two absorbing species were present since two isobestic points (444 nm and 564 nm) close to 0 absorbance change were obtained for probe delays from 1 to 10 ns.

In contrast to excitation with 355 nm light, for 532 nm excitation the transient species in the red decays as the ground state recovers. The triplet yield for 355 nm excitation is much greater than for 532 nm excitation. Only a very small amount of $Pt(mnt)_2^{2-}$ goes to the triplet excited state using 532 nm excitation. Excited state lifetimes were longer for $Pt(mnt)_2^{2-}$ than for $Ni(mnt)_2^{2-}$ in all cases. Approximate lifetimes were estimated from the data using the 10 ns delay spectrum as a final spectrum and plotting Ln (A_t-A_∞) versus time. The first order fit of the transient decay at the centre of the bleaching region gave a rate constant of 6.78 X 10^8 sec^{-1} with a corresponding lifetime of 1.5 ± 0.4 ns. Analysis of the transient decay in the red (667 nm) yielded a rate constant of 3.60 X 10^8 sec^{-1} with a corresponding lifetime of 2.8 ± 0.1 ns. These are considerably longer lived transients than obtained for $Ni(mnt)_2^{2-}$ in acetonitrile (i.e. 40 ± 25 ps).

The photophysical pathways of $Ni(mnt)_2^{2-}$ and $Pt(mnt)_2^{2-}$ are similar in many respects except for excited state lifetimes. 355 nm excitation excites Lπ based orbitals while 532 nm excitation excites metal based orbitals in both cases.

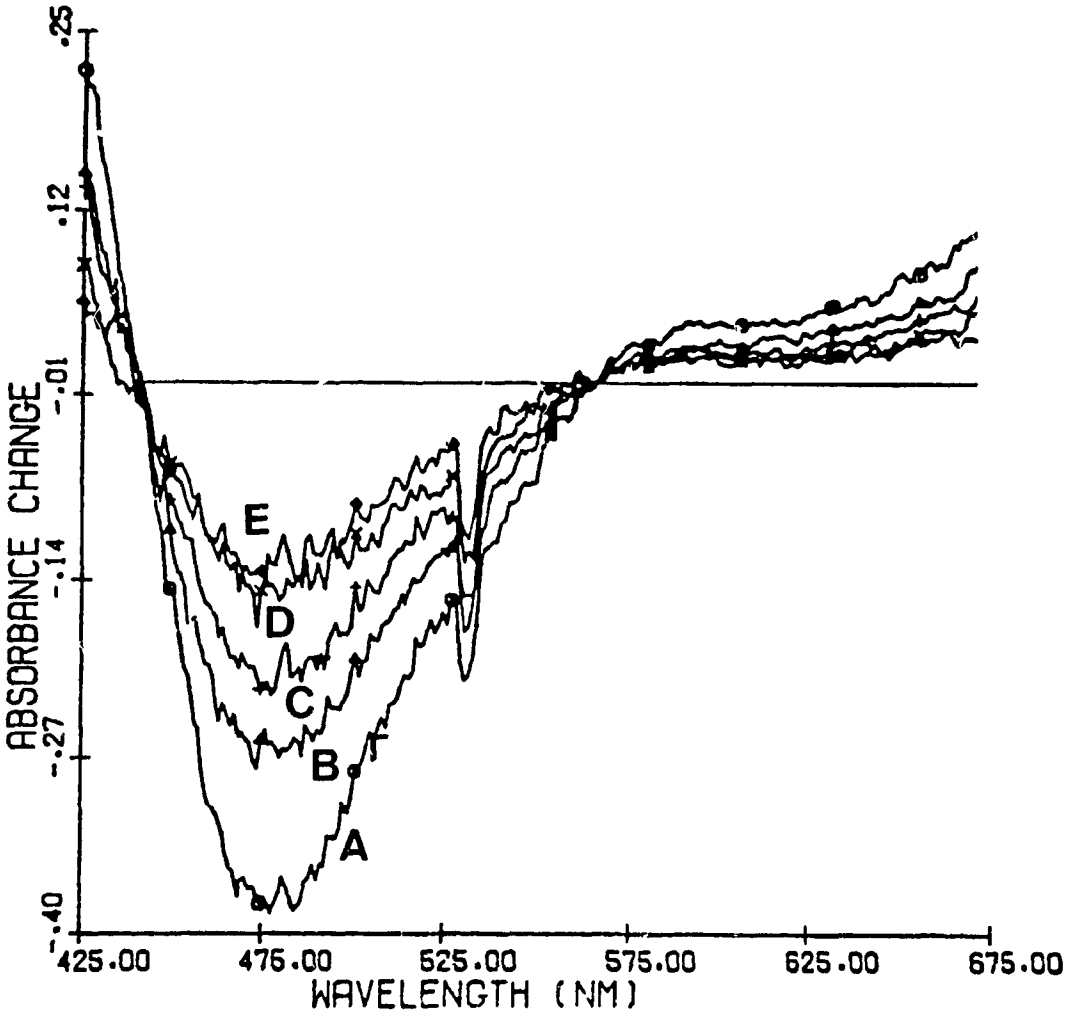

Figure 3.15 Transient absorption spectra for $Pt(mnt)_2^{2-}$ in acetonitrile using 532 nm excitation at probe delays of (A) 1 ns, (B) 3 ns, (C) 5 ns, (D) 7.5 ns, (E) 10 ns.

The information obtained so far using transient absorption spectroscopy for $Ni(mnt)_2^{2-}$ in acetonitrile have indicated that excitation into metal based bands produced short lived excited states at 550 nm with minimal bleaching of the M $\rightarrow$ Lπ^* band. Flash photolysis into ligand based bands produced two transients, one with a lifetime of about 100 ps and the other a longer lived species greater than 10 ns. The origin of the transition will determine the photophysical pathway and the excited state lifetime of complex. The ground state of $Ni(mnt)_2^{2-}$ is $..(4a_g)^2(4a_{2g})^2$. Population of the upper *xy* and Lπ^* orbitals while removing electron density from the Lπ orbital (i.e. 355 nm excitation) resulted in longer lived excited states (see Figure 3.8 and 3.9). Removal of an electron from the HOMO of $Ni(mnt)_2^{2-}$ or an orbital below (i.e. $4a_{2g}$ or $4a_{1g}$) produced short lived excited states, while removal of an electron from a Lπ based orbital results in the longer lived excited states as well as ground state bleaching of the MLCT band at 476 nm. The nickel complex has short excited state lifetimes in comparison to the platinum complex which is related, at least partially, to the Δ_1 splitting between the b_{2g} and b_{1g} ($xy \rightarrow x^2\text{-}y^2$) orbitals. The Δ_1 here is analogous to the Δ_1 ($xy \leftrightarrow x^2\text{-}y^2$) splitting in planar tetrahalides and tetracyanides (132). A value of 14,410 cm^{-1} was determined as the splitting for $Pt(mnt)_2^{2-}$ and 11,690 cm^{-1} for $Ni(mnt)_2^{2-}$ by Shupack *et al.* (91). A comparison of several Δ_1 values gives the spectrochemical series mnt^{2-}<Br<Cl<CN in a planar situation which places the mnt dianion ligand as a weak field ligand (91, 103).

The photophysical behaviour of $Ni(mnt)_2^{2-}$ and $Pt(mnt)_2^{2-}$ is consistent with scheme shown in Figure 3.16, where population of states by 355 nm excitation produces a singlet (Lπ^*) and intersystem crossing to a triplet (*xy*), while 532 nm

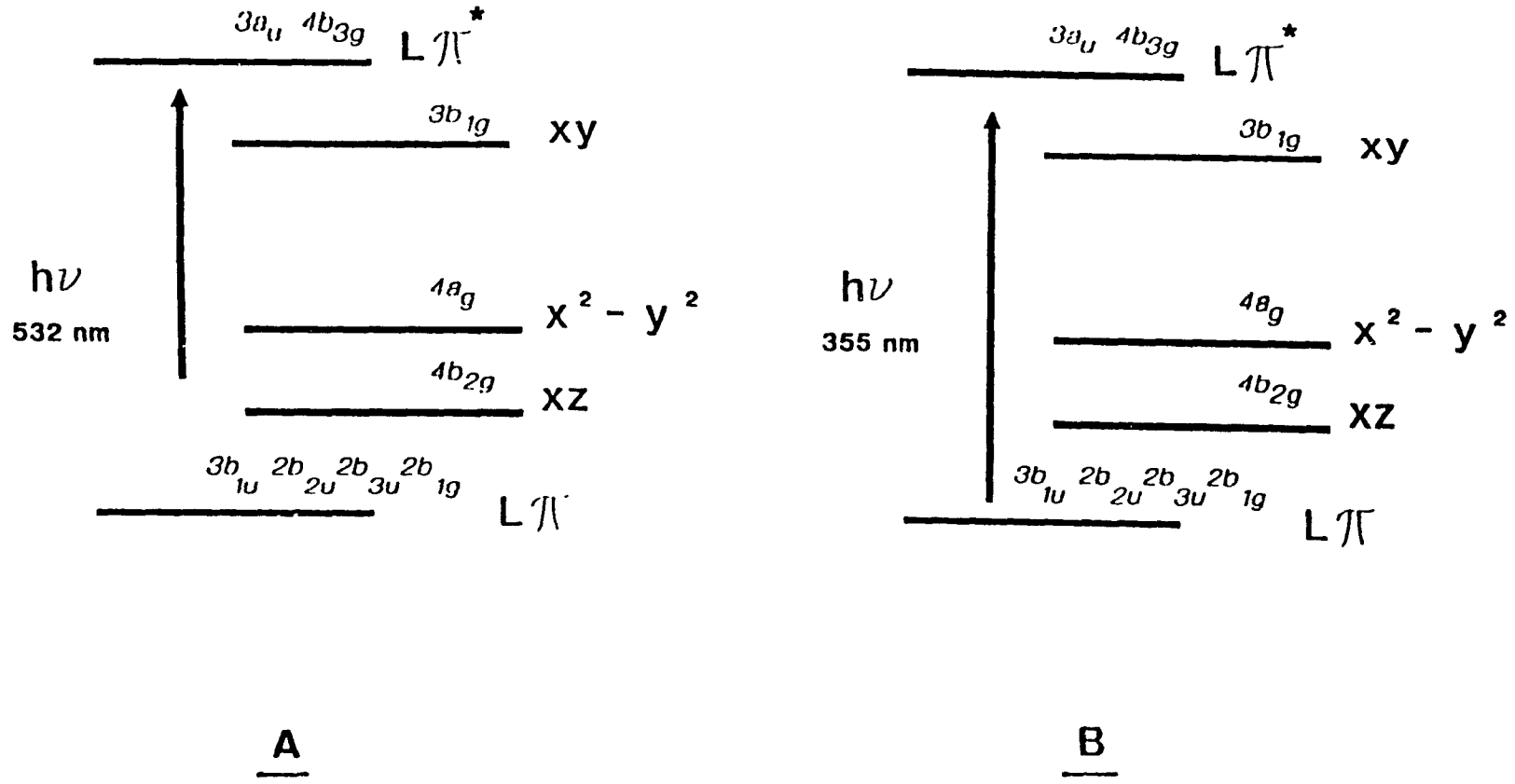

Figure 3.16 Simplified energy level diagram for $Ni(mnt)_2^{2-}$ and $Pt(mnt)_2^{2-}$ using (A) 532 nm and (B) 355 nm excitation. Only important levels are shown.

excitation generates the singlet with very little triplet yield in both cases. The extended lif times of the platinum complex versus the nickel complex is consistent with the energy gap law with respect to the splitting in Δ_1 (133).

A simple explanation for the behaviour of $Pt(mnt)_2^{2-}$ using 355 nm excitation is that initially populated $L\pi^*$ state relaxes rapidly and partitions into a triplet state and a ligand field state and/or photoproduct.

3.1.3 Steady-State and Transient Emission Spectra

Picosecond emission profiles and steady-state fluorescence spectra were obtained for the tetraethylammonium salts of $Pt(mnt)_2^{2-}$, $Pt(mnt)_2^{1-}$, and $Ni(mnt)_2^{2-}$ as described in sections 2.9.2 and 2.5.2, respectively. This is the first report of transient emission spectra for these complexes. Pulse fluorescence measurements were carried out in neat acetonitrile, a mixture of acetonitrile/water (70:30), and pure water. In the latter case, samples of $Pt(mnt)_2^{2-}$ and $Ni(mnt)_2^{2-}$ were shaken vigorously to obtain a "saturated solution" just before obtaining a spectrum, since the solubility of these complexes is quite limited in water. All pulse fluorescence experiments were carried out using 355 nm excitation.

Fluorecence emission was undetectable in steady-state room temperature fluorescence measurements of $Ni(mnt)_2^{2-}$. Resonance raman experiments performed by Clark and Turtle (95) indicated no fluorescence emission for this complex at λ_{ex}=635 nm althought weak fluorescence in the raman spectrum was observed at λ_{ex}= 457.9 nm. A picosecond pulse fluorescence profile of $Ni(mnt)_2^{2-}$ in neat acetonitrile is shown in Figure 3.17. The experiment consisted of flashing the

Figure 3.17 Transient emission decay of $Ni(mnt)_2^{2-}$ in acetonitrile following excitation at 355 nm. Luminescence was limited to λ>475 nm using 385 nm and 475 nm cut-off filters. Fitted curve shows first-order exponential decay. Residuals of fitted data shown in inset.

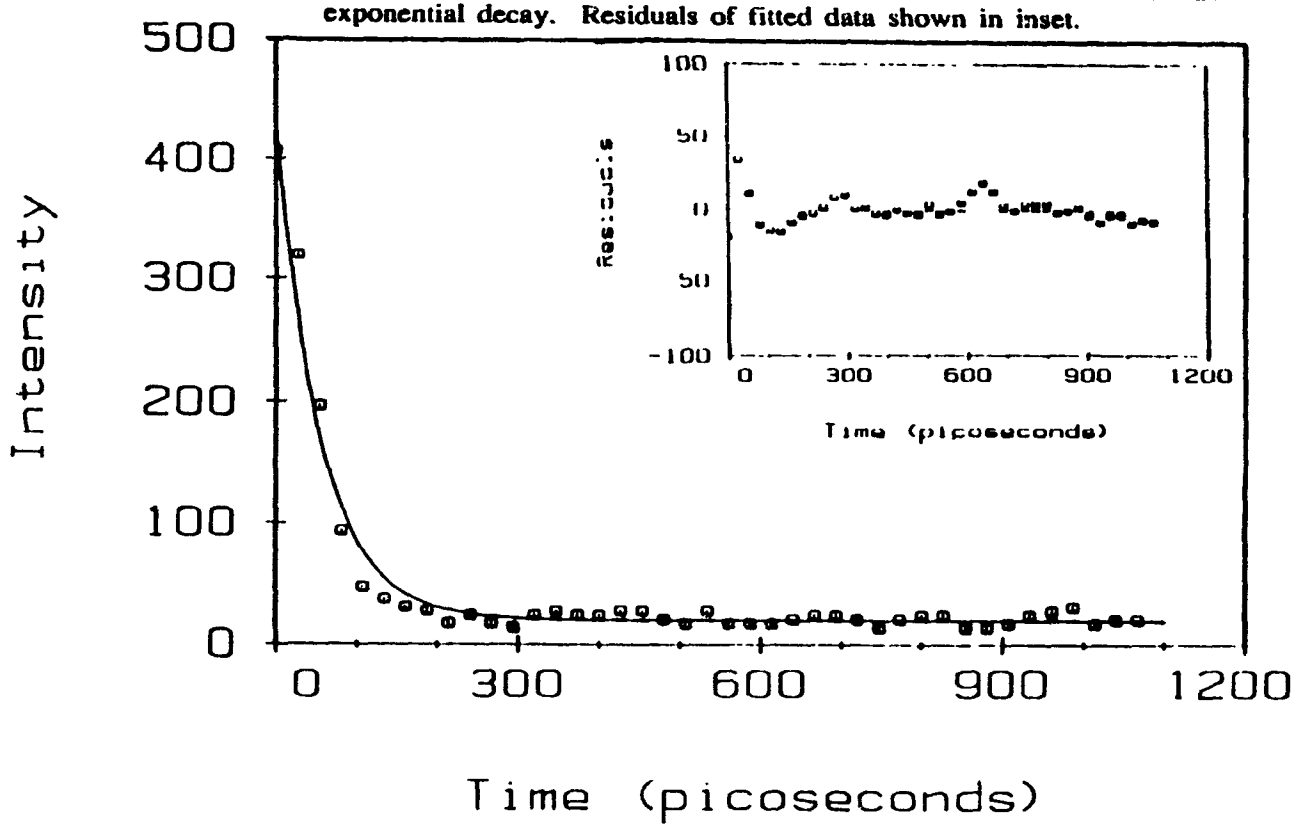

solution with a 3.13 mJ 30 ps pulse at 355 nm and luminescence was filtered using 385 nm and 475 nm cut-off filters. Luminescence was still observed with a 515 nm cut-off filter. The data was fitted to a first order exponential decay using the simplex method. The software used to obtain the best fitted curve was F-CURVE (113). The calculated rate constant was 1.8 X 10^{10} sec^{-1} which corresponds to a lifetime of 55 ps. Results of pulse fluorescence measurements for $Ni(mnt)_2^{2-}$, $Pt(mnt)_2^{2-}$, and $Pt(mnt)_2^{1-}$ are presented in Table 3.3.

The fluorescent lifetime for $Ni(mnt)_2^{2}$ in MeCN, MeCN/H_2O, and H_2O "saturated" solutions was about 60 ± 6 ps. There appeared to be no significant difference in fluorescent lifetimes among all three $Ni(mnt)_2^{2}$ samples listed in Table 3.3. These lifetimes are in agreement with the transient absorption results presented in the previous section. This shows that the singlet lifetime is in the picosecond domain (more precisely 40→70 ps). The fluorescent lifetime of $Ni(mnt)_2^{2}$ supported in a polymer film of **PB1** is extended in comparison to results obtained in the solution phase. The pulse fluorescence measurements were obtained by flashing a polymer modified SnO_2 electrode containing $Ni(mnt)_2^{2}$ at 355 nm and recording the luminescence in a similar manner as described above using a combination of 355, 435 and 550 nm cut-off filters. The fluorescent profile is shown in Figure 3.18. The data could not be fit to a single exponential decay, rather a sum of two exponential functions fit the data very well. The lifetimes of the dye in the polymer film were determined to be 96 ps and 2.8 ns. The first lifetime is extended in comparison to 60 ps in acetonitrile solution. It is quite possible that more than two processes may be occuring in the polymer film. These results are

Table 3.3 Pulse fluorescence results of $Ni(mnt)_2^{2-}$, $Pt(mnt)_2^{2-}$, and $Pt(mnt)_2^{1-}$ in acetonitrile, acetonitrile/water mixtures, and "saturated" water solution.

Complex	Type of decay[a]	MeCN (ps)	MeCN/water (70:30) (ps)	Water[b] "saturated" (ps)	Polymer film (ps)
$Ni(mnt)_2^{2-}$	single	55	61	63	-
$Ni(mnt)_2^{2-}$	double	-	-	-	τ_1= 96 τ_2= 2780
$Pt(mnt)_2^{2-}$	double	τ_1= 70 τ_2= 1970	τ_1= 76 τ_2= 1700	τ_1= 71 τ_2= 1870	- -
$Pt(mnt)_2^{1-}$	double	τ_1= 77 τ_2= 913	τ_1= 79 τ_2= c	- -	- -

a) Data was fitted to either a single exponential decay or to a sum of exponentials (double).
b) See text for experimental description.
c) Transient quenched by water.

Figure 3.18 Transient emission decay of a **PB1** polymer film containing $Ni(mnt)_2^{2-}$ supported on an SnO_2 electrode following 355 nm excitation. Luminescence was limited to λ>435 nm using 385 nm and 435 nm cut-off filters. Fitted curve shows the sum of two first-order exponential decays. Residuals of fitted data shown in inset.

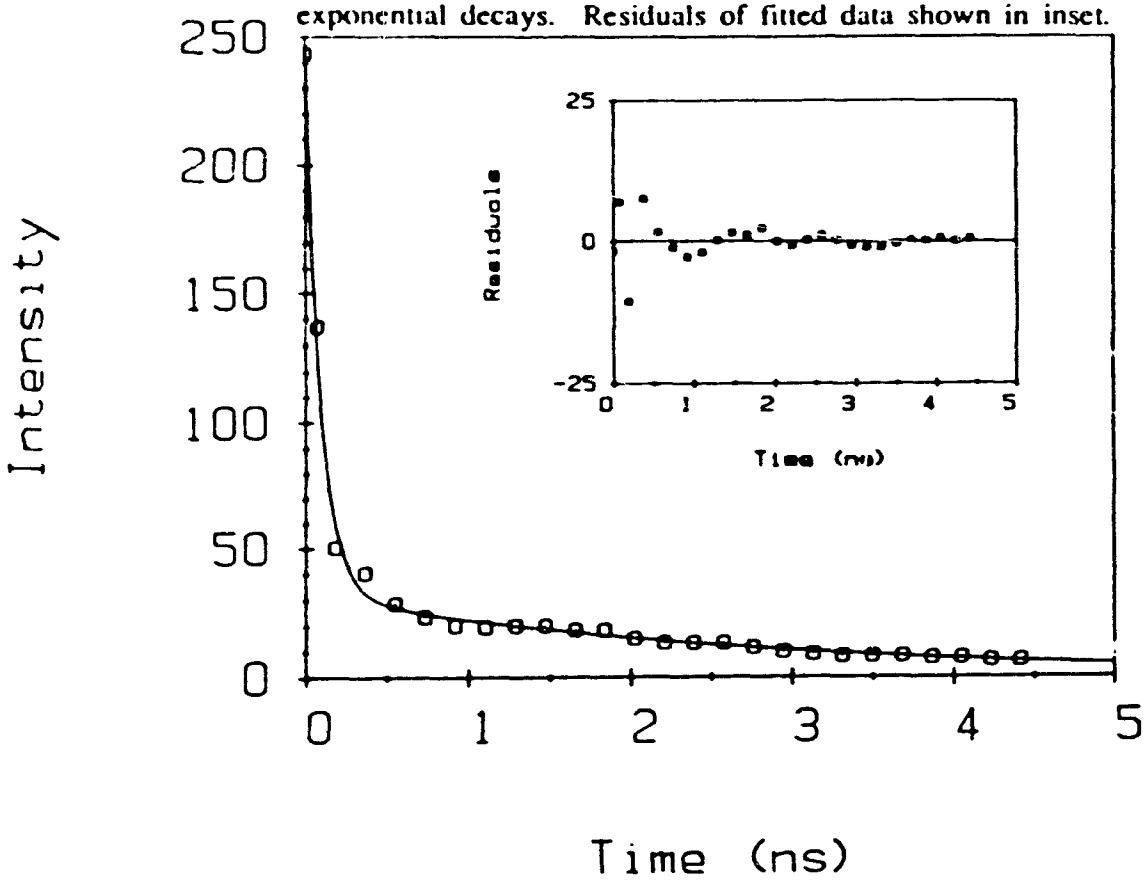

consistent with the transient absorption experiments indicating that the singlet lifetime for $Ni(mnt)_2^{2-}$ is less than a nanosecond.

Very weak fluorescence was observed for $Pt(mnt)_2^{2-}$ (small signal at gain=100) at 400 nm using 355 nm excitation. No fluorescence was observed when light of longer wavelengths was employed. Moreover, Clark and Turtle (95) reported that resonance raman measurements below 19,000 cm^{-1} could not be done because of strong fluorescence which obscured the raman spectrum (λ_{ex}=526 nm).

A transient emission profile of $Pt(mnt)_2^{2-}$ in acetonitrile is shown in Figure 3.19. Emission profiles for the $Pt(mnt)_2^{2-}$ and $Pt(mnt)_2^{1-}$ differ from those obtained for $Ni(mnt)_2^{2-}$ in that 385 nm & 435 nm filters were used for the platinum complexes while 385 nm & 475 nm filters were used for the nickel complex. This should not affect the lifetimes significantly. The transient emission intensity of $Pt(mnt)_2^{2-}$ follows the order {$Pt(mnt)_2^{2-}$/(MeCN)} > {$Pt(mnt)_2^{2-}$/(MeCn:water(70:30))} > {$Pt(mnt)_2^{2-}$/("water saturated")}. The order is reversed in the case of the mono-anionic $Pt(mnt)_2^{1-}$. The transient decays of $Pt(mnt)_2^{2-}$ in pure acetonitrile and in a mixture of water/acetonitrile are shown in Figure 3.20.

The pulse fluorescent measurements of $Ni(mnt)_2^{2-}$ and $Pt(mnt)_2^{2-}$ were consistent with the results obtained with transient absorption spectroscopy in that the platinum complex was longer lived than the nickel. Moreover, the bleaching recovery times in the transient absorption experiments for both $Ni(mnt)_2^{2-}$ and $Pt(mnt)_2^{2-}$ in the previous section compare well with the pulse fluorescence experiments presented here. $Ni(mnt)_2^{2-}$ displayed short lifetimes of about 60 ps, while the longer lived $Pt(mnt)_2^{2-}$ displayed biphasic emission with average lifetimes

Figure 3.19 Transient emission decay of $Pt(mnt)_2^{2-}$ in acetonitrile following 355 nm excitation. Luminescence was limited to λ>435 nm using 385 nm and 435 nm cut-off filters. Fitted curve shows the sum of two first-order exponential decays. Residuals of fitted data shown in inset.

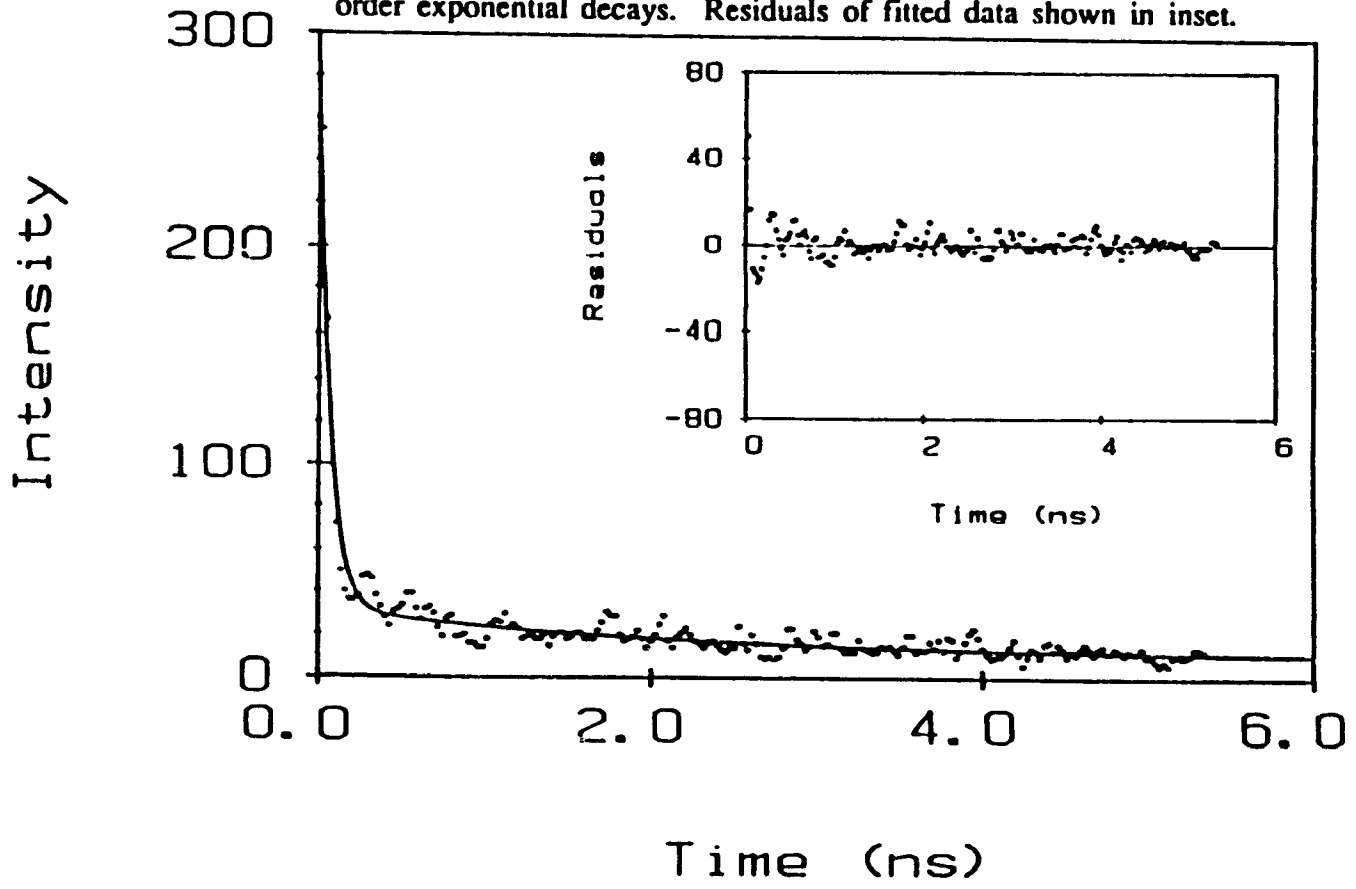

Figure 3.20 Transient emission decays of $Pt(mnt)_2^{2-}$ in acetonitrile (-----) and acetonitrile/water (70:30) (····X····) mixture following excitation with a 355 nm pulse. Luminescence was limited to λ>435 nm using 385 nm and 435 nm cut-off filters. Fitted curves show the sum of two exponential decays.

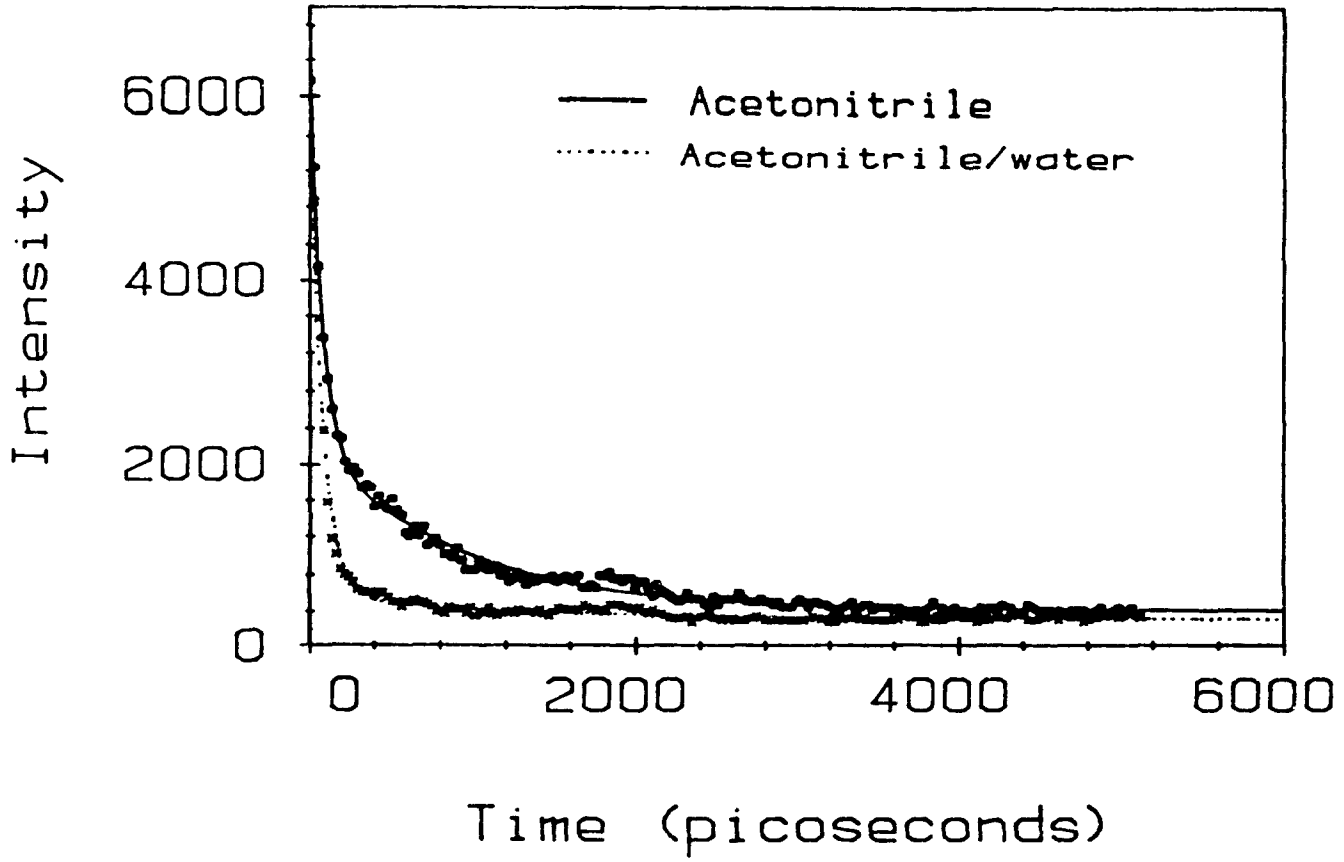

of 73 ps and 1.85 ns. This latter lifetime of 1.85 ns is in agreement with 1.5±0.4 ns from bleaching recovery times of transient absorption experiments for $Pt(mnt)_2^{2-}$. The fluorescent quenching of the $Pt(mnt)_2^{2-}$ by water is consistent with microsecond transient absorption results. The emission in most cases was at wavelengths longer than 475 nm indicating that there were lower energy states which participate in the photophysical processes of the dianionic mnt's. These states are most likely metal based orbitals which lie between the $L\pi \rightarrow L\pi^*$ transition from 355 nm excitation (Figure 3.17). Again the fluorescent lifetimes agree quantitatively with transient absorption measurements and difference in Δ_1 splitting between $Pt(mnt)_2^{2-}$ and $Ni(mnt)_2^{2}$ are in qualitative agreement with the energy gap law (133).

3.2 Steady-state and transient electronic spectra of $M(mnt)_2^{2-}$ (M=Ni,Pt) as methyl viologen complexes.

The spectra of these complexes have been investigated as simple models for those obtained from polyviologen polymer films containing $Ni(mnt)_2^{2}$ and $Pt(mnt)_2^{2-}$. It is thought that the viologen moiety of the composite polymer matrix acts as a better acceptor state (lower on an energy scale) than the pyridinium ion of the polymer blend, **PB1**. It was hoped that energy and/or electron transfer between the metal maleonitriledithiolate complexes and the viologen counterions could be observed on the picosecond timescale. Studies in this direction were aimed at a better understanding of the physical and photophysical processes which occur in polyviologen/$M(mnt)_2^{2}$ films supported on electrodes when illuminated in the $M \rightarrow L\pi^*$ region of the metal complex. This is the first report of the spectra of a methyl

viologen-$M(mnt)_2^{2-}$ complex (M= Ni, Pt).

3.2.1 Absorption and Fluorescence spectra of $[MV^{2+}][Ni(mnt)_2^{2-}]$ and $[MV^{2+}]$-$[Pt(mnt)_2^{2-}]$.

The visible absorption spectra of these complexes in DMSO is shown in Figure 3.21 and 3.22. The nickel complex displayed only slight red shifts (4 nm) in the charge transfer bands. The platinum complex exhibited similar displacements in band position (+8 nm) with the addition of a shoulder at 388 nm. This latter shoulder can be attributed either to the presence of some partially or fully reduced methyl viologen type species (λ=396 nm, ε= 42,000 $M^{-1}cm^{-1}$)(114). The absorption bands in both complexes were broader as compared to the alkylammonium salts. The near-IR absorption spectra of both complexes display a small but significant absorbance in the 875 nm and 913 nm region for the platinum and nickel complexes respectively. It is quite probable that these are ion-pair charge transfer bands. Much more intense outer-sphere charge transfer bands have been obtained by Vogler in solutions of square planar complexes of opposite sign, notably $Ni(tim)^{2+}$ (*tim= tetramethyl-1,4,8,11-tetraazatetradecatetraene)* and $M(mnt)_2^{2-}$ (M= Ni, Pd, Pt) (115). The synthesis of $M(mnt)_2^{n-}$ (n= 1,2) salts with other non-innocent type cations such as phenoxazine (116), tetrathiafulvalene (117), and ferrocenium (118) has yielded compounds with interesting physical and electrical properties.

The room temperature fluorescence of the $[MV^{2+}][Pt(mnt)_2^{2-}]$ complex dissolved in DMSO is shown in Figure 3.23. Even though the fluorescence intensity was weak at λ_{ex} = 480 nm (gain factor=10), minimal fluorescence was observed when λ_{ex} = 355 nm (the wavelength used in the transient spectroscopy).

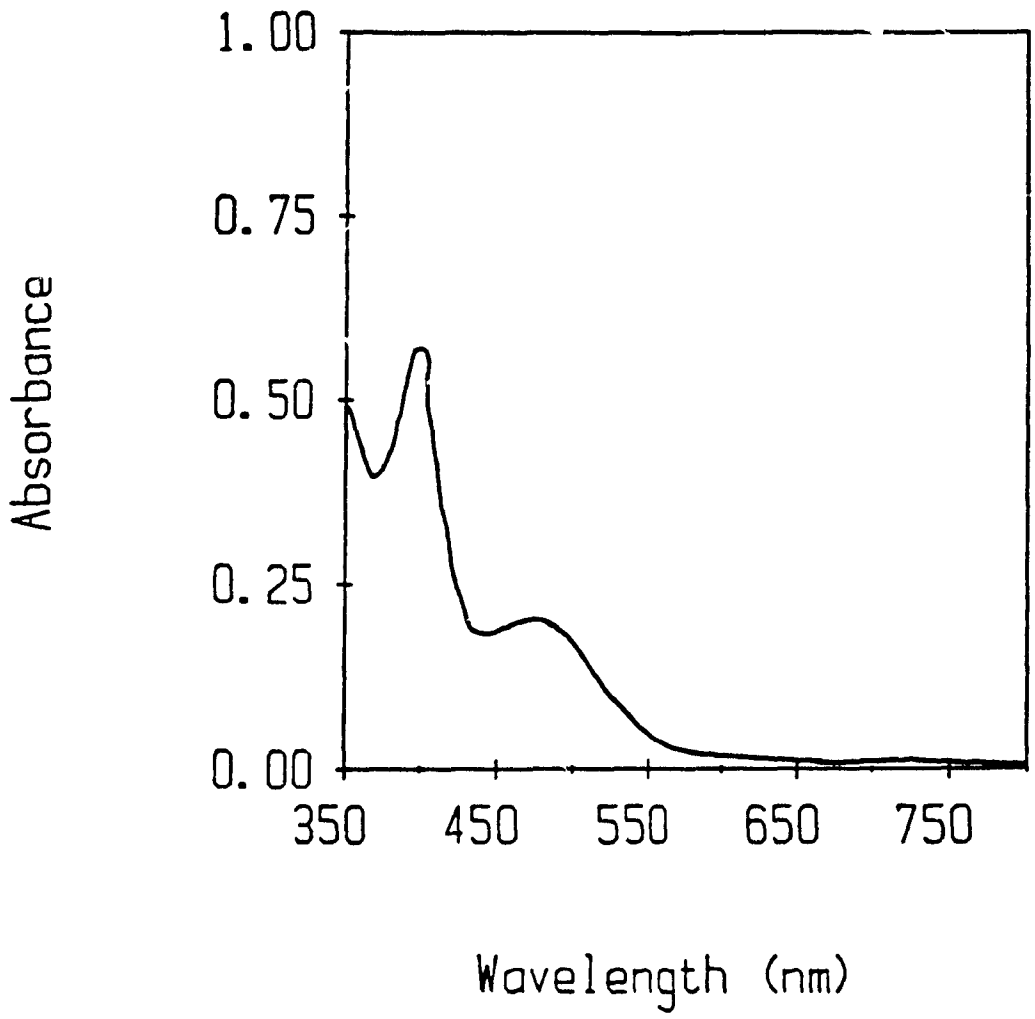

Figure 3.21 UV-visible absorption spectrum of $[MV^{2+}][Pt(mnt)_2^{2-}]$ in DMSO.

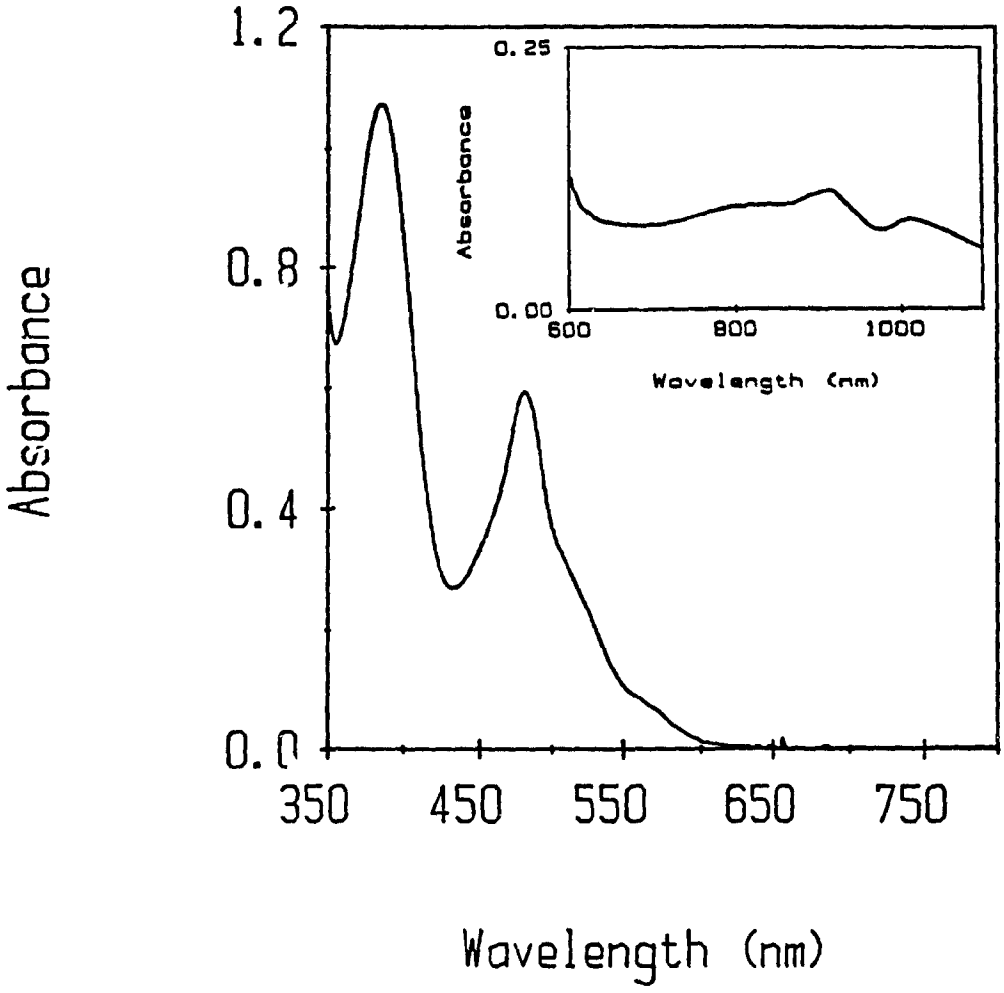

Figure 3.22 UV-visible absorption spectrum of $[MV^{2+}][Ni(mnt)_2^{2-}]$ in DMSO. Near-IR absorption spectrum shown in inset.

Figure 3.23 Room temperature fluorescence spectra of $[MV^{2+}][Pt(mnt)_2^{2-}]$ in DMSO. Emission spectra are shown for excitation at (——) 430 nm, (- - - -) 480 nm, and (-·-·-·) 380 nm. Excitation spectrum shown for $\lambda_{emission}$ at 575 nm (·····).

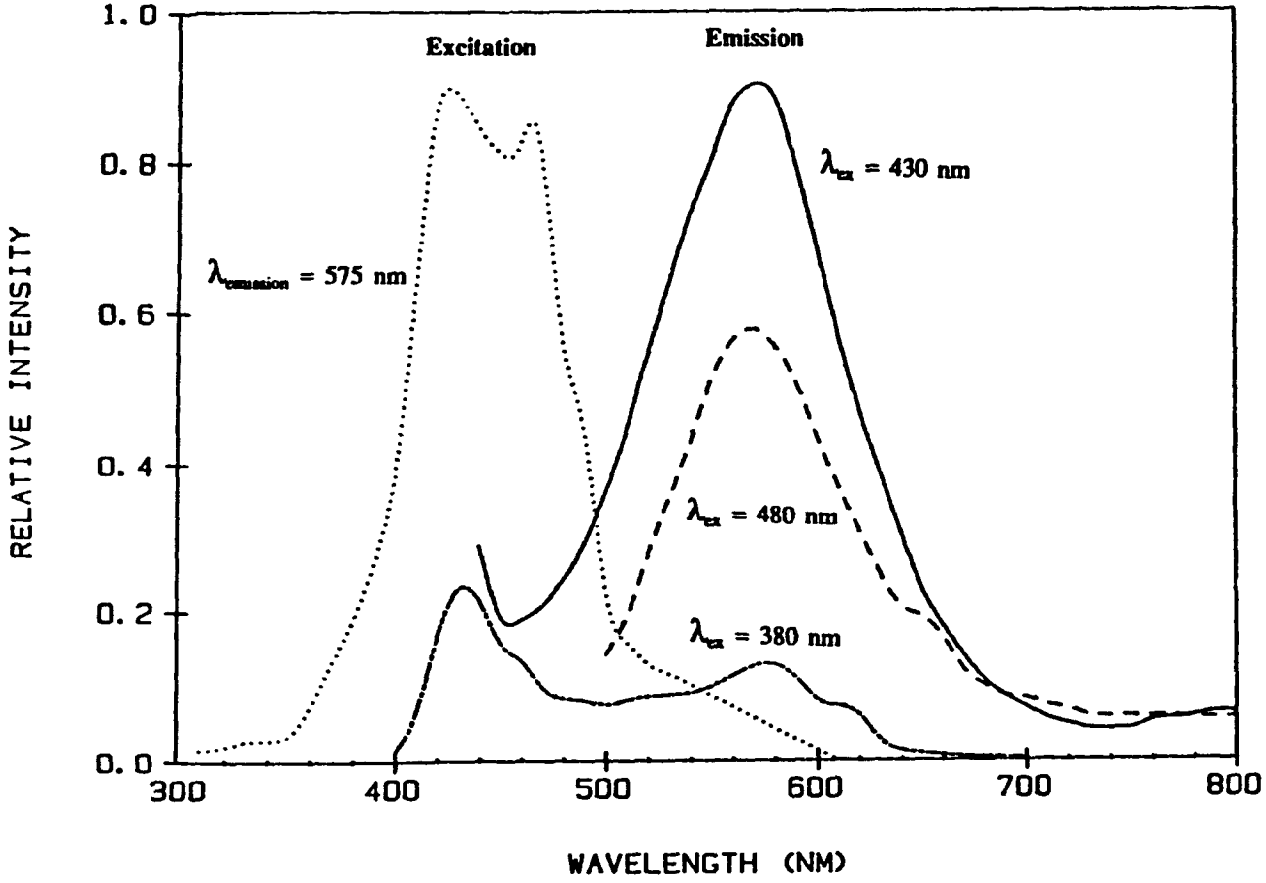

An excitation spectrum of the solution with the emission wavelength set at 572 nm revealed a two humped spectrum with discernable peaks at 430 nm and 480 nm. The strong emission at 572 nm has been assigned to a spectrum similar to a dimeric viologen cation radical species (119,120). Excitation of the MLCT band at 480 nm ($M \rightarrow L\pi^*$) is responsible for some of the emission at 572 nm. The remaining contribution of the emission is associated with the 430 nm band of the excitation spectrum.

This emission is to be the fluorescence under discussion. The excitation wavelengths reported are 480 nm, 430 nm, 380 nm, and 355 nm. At an excitation of 430 nm, strong fluorescence at 572 nm was observed. A similar shape was obtained when the excitation wavelength was changed to 480 nm, with exception to the presence of a small shoulder around 650 nm. A further bathochromic shift in excitation wavelength to 380 nm revealed a richer, but weaker fluorescence spectrum characterized by a peak at 430 nm and a broader peak at 572 nm with a shoulder at 620 nm.

It is not surprising that such complexes exhibited room temperature fluorescence. There are other examples of dianionic mnts complexes (M = Zn,Cd,Hg) which fluoresce and phosphoresce at 77°K (121). These are the first to exhibit room temperature visible light fluoresecence. Since the MLCT band of $[MV^{2+}]$-$[Pt(mnt)_2^{2-}]$ was shifted to the red by 8 nm from 472 nm, there probably exists some intermolecular interactions which perturb the transition slightly. It is known that certain MLL'-$(mnt)^{n-}$ complexes luminesce brightly in rigid media, but that emission is quenched in fluid solution (122). The emitting state in these MLL'-$(mnt)^{n-}$

complexes was found to be a MLCT band of d-π^* character. The intermolecular interactions that exist in the $[MV^{2+}][Pt(mnt)_2^{2-}]$ complex may give rise to similar behaviour in DMSO. The 430 nm peak in the excitation spectrum is not present in the absorption spectrum of the ion-pair and no tentative assignment to the origin of this band has been made. Also, upon excitation at 380 nm, an emission band at 430 nm is observed in analogy to complexes studied in liquid nitrogen (121). The emitting state for this complex is not known.

The observed Stokes shift of the luminescence is 5864 cm^{-1} and 3443 cm^{-1} for excitation at 23,256cm^{-1} (430 nm) and 20,833cm^{-1} (480 nm), respectively. This is a rather large Stokes shift.

3.2.2 Transient Absorption Spectroscopy

The transient spectra for the $Pt(mnt)_2^{2-}$ complexes with the tetraethyl-ammonium cation and the methyl viologen dication were recorded at probes delays of 20, 50, 500 picoseconds, and 1 nanosecond (Figures 3.24 & 3.25 respectively) following an excitation pulse at 355 nm. The overall shape of the transient spectra differed as cations changed. The transient bleaching signal of the complex with the tetraethylammonium salt was more pronounced than its viologen counterpart. The spectrum of $[MV^{2+}][Pt(mnt)_2^{2-}]$ at a probe delay of 5 ns is quite similar to a probe delay of 1 ns. It reveals a broad growth of a species resembling a partially reduced dimeric viologen component at 530 to 540 nm (114,123) and monomeric MV^{+} at around 618 nm (114,119). The broad absorption at 540 nm can be the result of extensive intramolecular association of the reduced viologens in solution (124). The transient absorption in the 530→540 nm region could also be attributed to a charge

transfer band between the $Pt(mnt)_2^{2-}$ and the MV^{2+}. There is precedent for such a charge transfer band in the outer-sphere charge transfer system of $[MV^{2+}][Fe(CN)_6^{2-}]$ which displays a broad absorption band at 530 nm (109). The spectra were corrected for absorption of light as well as laser intensity. The slight growth in the 450 nm region of Figure 3.24 and 3.25 is attributed to a partial oxidation to give $Pt(mnt)_2^{1-}$. The transient spectra of $[MV^{2+}][Pt(mnt)_2^{2-}]$ displays characteristics which are consistent with a viologen-mnt charge transfer complex which has an excited state beyond 1 ns. The transient absorption characteristics of this complex can be used to describe the behaviour of a polyviologen-$M(mnt)_2^{2-}$ composite on an SnO_2 electrode.

Figure 3.24 Transient absorption spectra for $[(C_2H_5)_4]_2[Pt(mnt)_2^{2-}]$ in DMSO using 355 nm excitation at probe delays of 20, 50, 500 ps, and 1 ns.

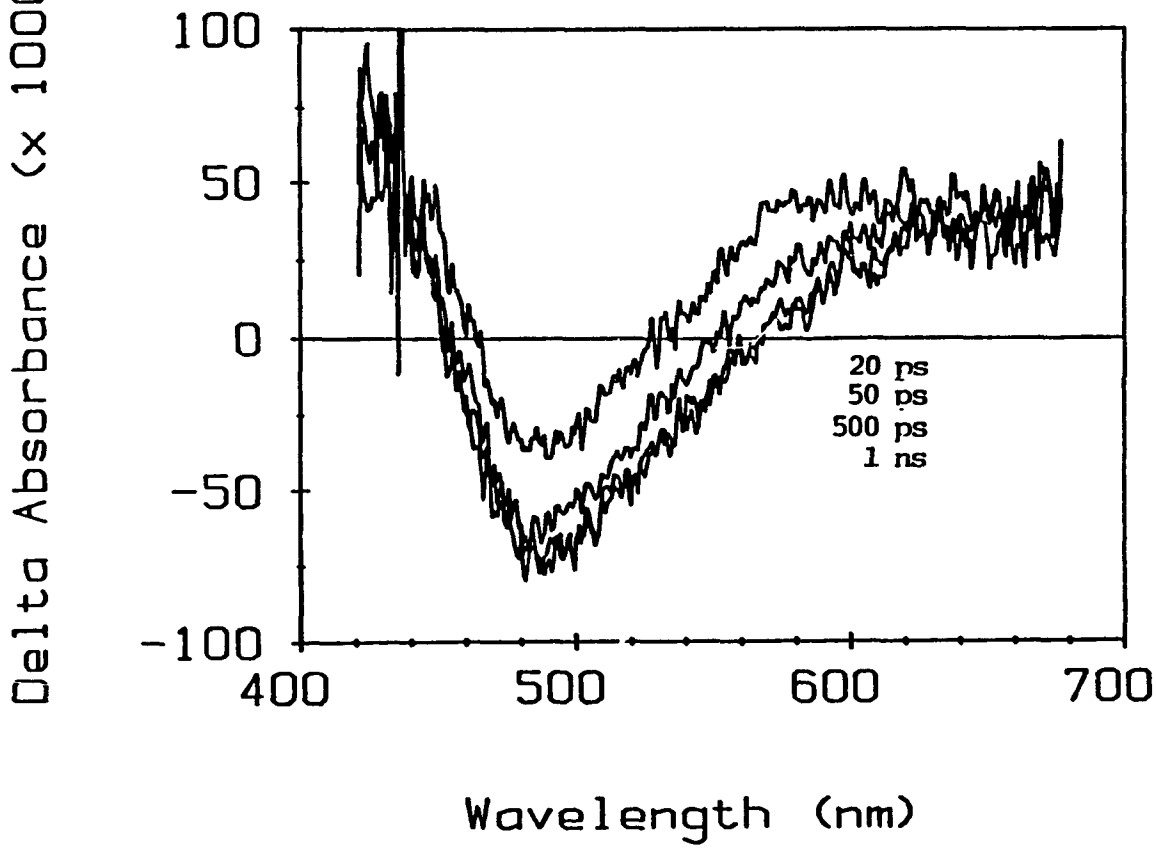

Figure 3.25 Transient absorption spectra for $[MV^{2+}][Pt(mnt)_2^{2-}]$ in DMSO using 355 nm excitation at probe delays of 20, 50, 500 ps, and 1 ns.

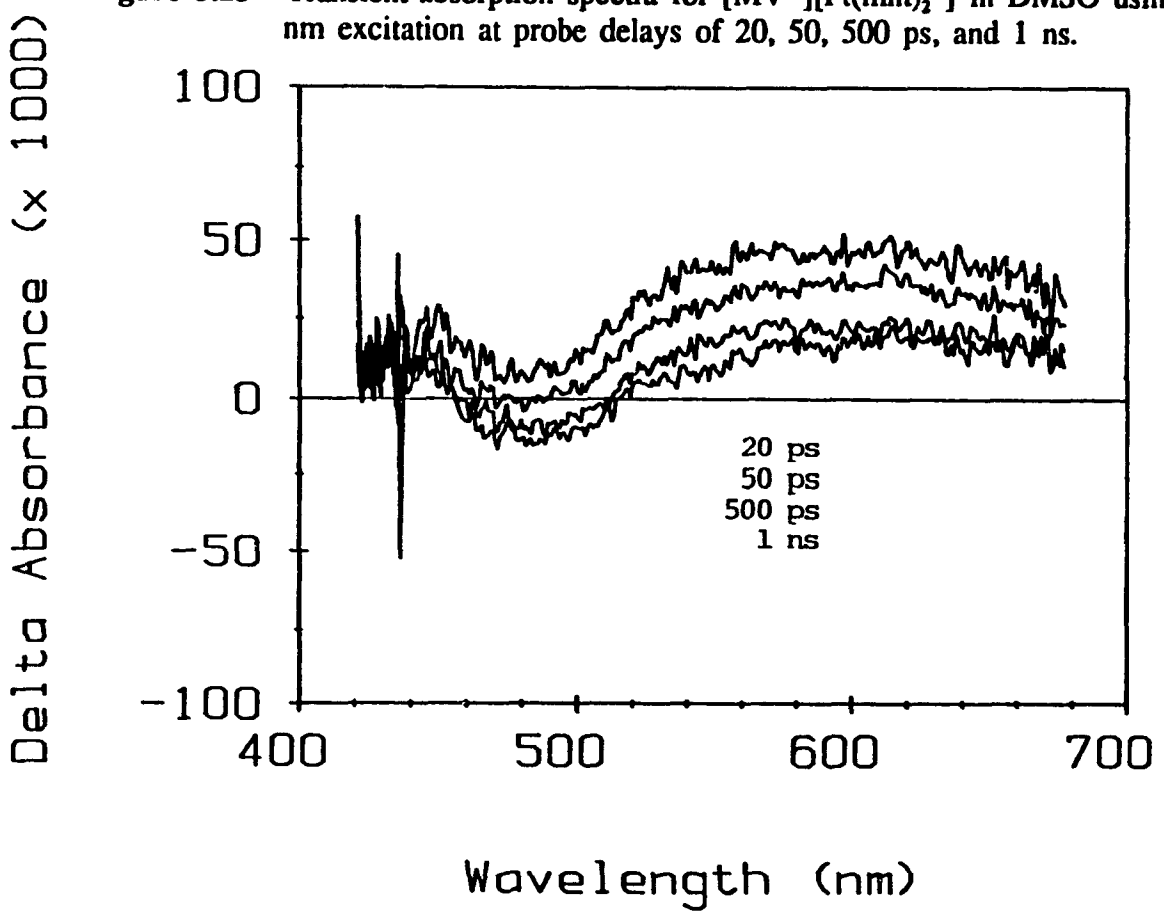

Chapter 4

Results and Discussion II

Electrochemical and Photoelectrochemical Properties of $Ni(mnt)_2^{2-}$ and $Pt(mnt)_2^{2-}$ in Polymer Blend PB1.

The **PB1** polymer matrix is known to retain anions of high charge against ion exchange with bulk solution electrolyte (52). The modified polymer film should allow sufficient transport of charge through the film. This section describes the behaviour of $M(mnt)_2^{2-}$ (M=Ni,Pt) complexes incorporated into **PB1** polymer blend films supported on SnO_2 electrodes.

4.1 Electronic Absorption of Complexes in PB1 films.

The near-UV and visible absorption spectrum of $Ni(mnt)_2^{2-}$ in acetonitrile and in **PB1** supported on SnO_2 is shown in Figure 4.1. Incorporation of the dye in this polymer broadens the spectrum. The band assigned (91) as MLCT ($xz \rightarrow L\pi^*$) is red shifted by 14 nm from 474 to 488 nm. Similarly, the band of the Pt complex is red shifted from 476 to 486-8 nm. The present result is in contrast to observation for a quaternized PVP film where the shift was smaller (110). It is not unlikely that this red shift is a consequence of coordination of a pyridine group from the polymer to an axial position on the metal. The relative intensity of the band may be used to estimate roughly the amount of dye in the film. Accurate quantitation must account for the scatter arising from the polymer film and SnO_2 electrode. The amount of dye incorporated was determined by dissolving the film from the electrode in methanol or DMF as described in section 2.3.4.

Figure 4.1 Visible absorption spectra of PB1 polymer film loaded with $Ni(mnt)_2^{2-}$ (dotted), and $Ni(mnt)_2^{2-}$ in methanol (solid).

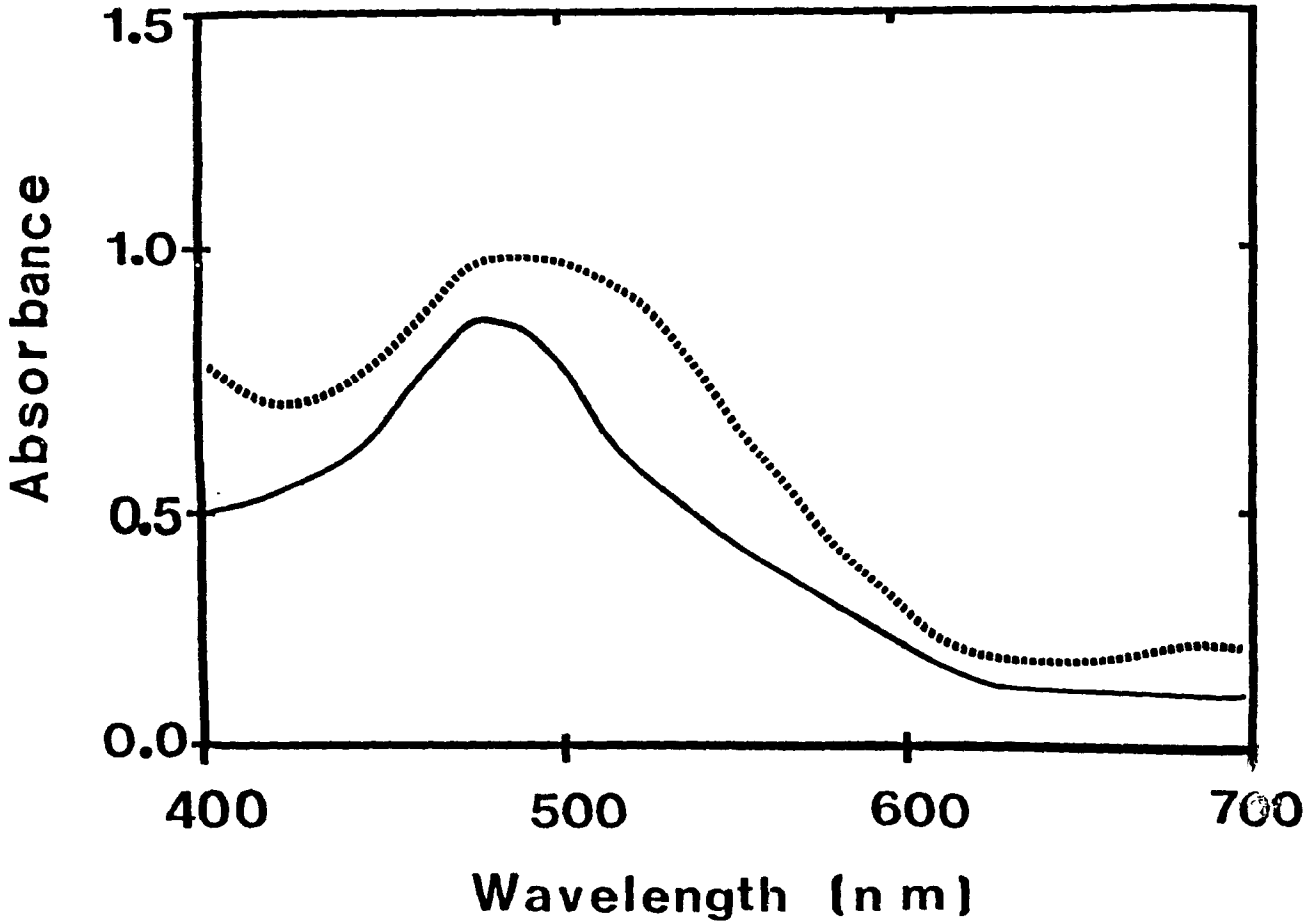

4.2 Dark Electrochemistry

Steady-state cyclic voltammograms of the polymer blend films without the metal complexes in 1.0 M KCl indicated a well defined irreversible reaction of the pyridinium ion to pyridine radicals at a $E_{1/2}$ = -0.65 V. The quaternized random ternary copolymer moiety of the blend was inactive over the electrochemical window in aqueous solution.

Polymer modified electrodes containing either $Ni(mnt)_2^{2-}$ or $Pt(mnt)_2^{2-}$ exhibit similar electrochemical behaviour (Figure 4.2). The characteristic rapid one electron transfers between $M(mnt)_2^{2-/1-}$ which are normally seen in the solution electrochemistry of the complexes are absent; at most a minimal signal attributable to the layer in direct contact with the SnO_2 is seen. This can be attributed to strong electrostatic interactions binding the complexes to the cationic polymer sites. The complex is immobile and only complexes immediately adjacent to the electrode can react. This result is in sharp contrast to readily observable electrochemistry of $M(mnt)_2^{2-/1-}$ in QPVP films (110).

As the redox couple is circulated through the cell, the cationic polymer blend incorporates a substantial amount of $Fe(CN)_6^{3-/4-}$ by ion-exchange with the initial chloride counterions. Voltammetry is shown in Figure 4.3. The separation between the anodic and cathodic hexacyanoferrate peaks, ΔE_p, is 120-240 mV at a scan rate of 100 mV/sec depending on film preparation. The scan rate dependence of a modified electrode in contact with the redox couple is also shown in Figure 4.3. The peak separation increases as the film thickness is increased. Thick films (20 μm or greater) exhibit peak separations in the range of 300-400 mV under the same

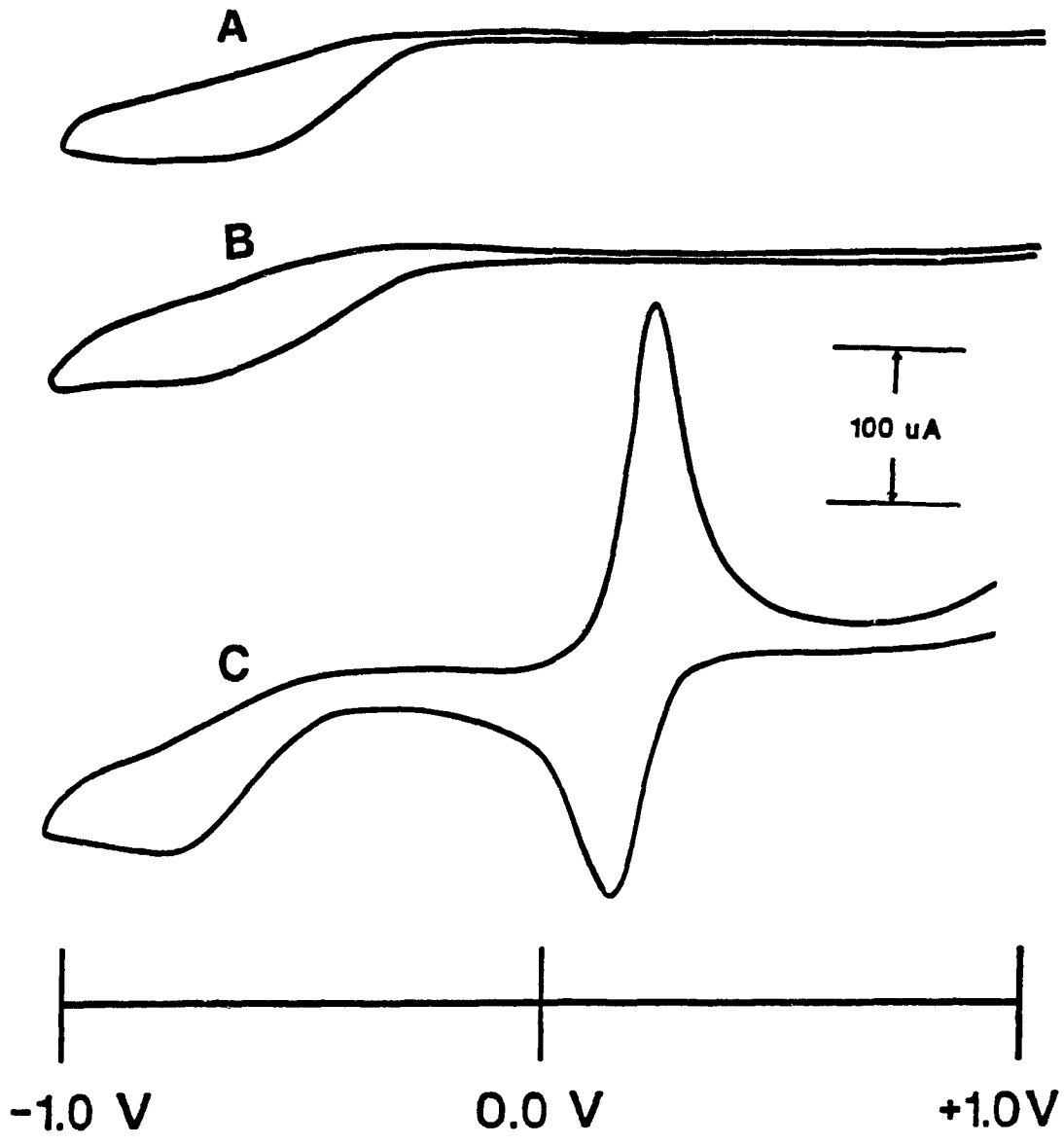

Figure 4.2 Cyclic voltammograms of (A) **PB1** polymer film in contact with 0.1 M KCl, (B) **PB1** polymer film loaded with $Ni(mnt)_2^{2-}$ in contact with 0.1 M KCl, (C) and in contact with 2 mM $Fe(CN)_6^{3-/4-}$ in 0.1 M KCl. Scan rate was 100 mV/sec. Anodic currents are upwards.

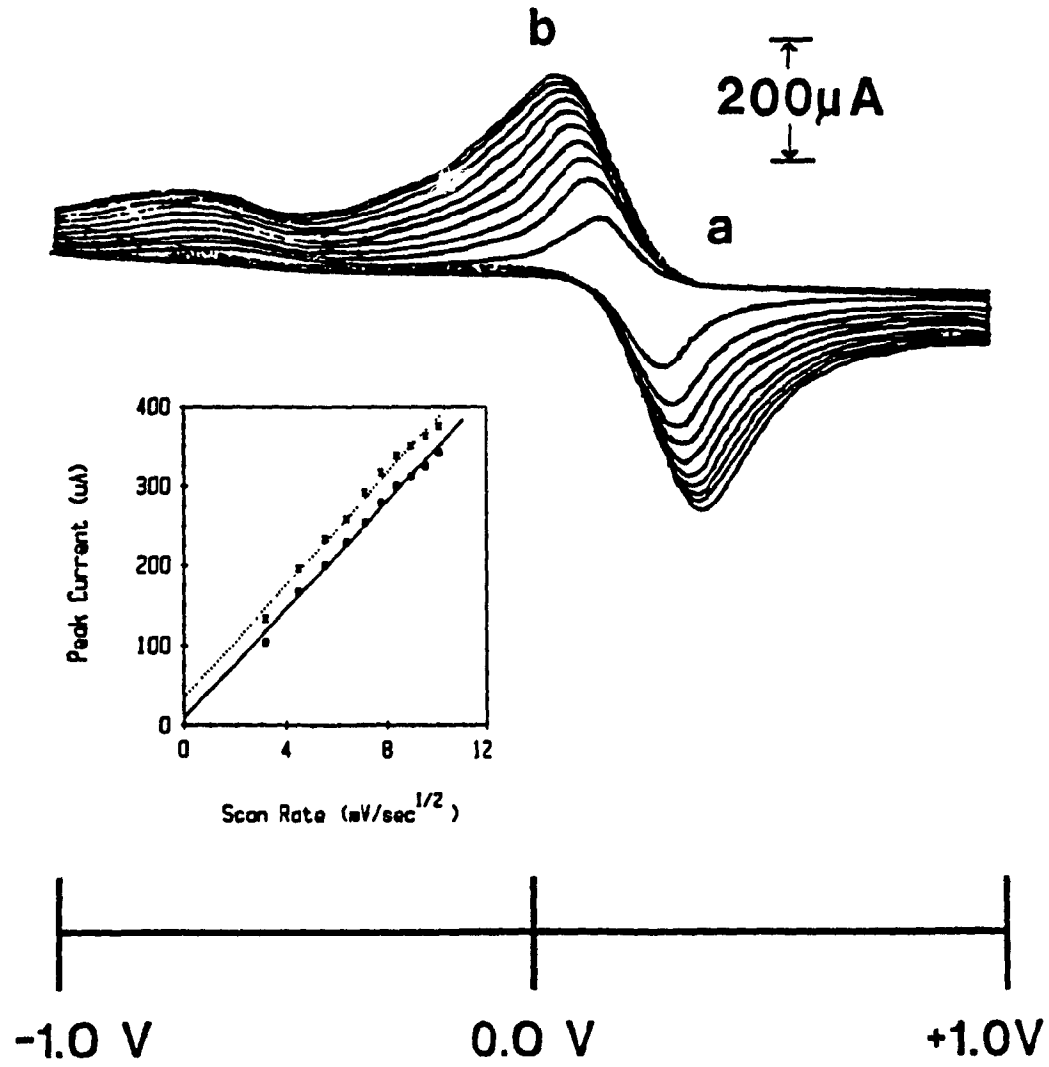

Figure 4.3 Cyclic voltammograms of **PB1** polymer film loaded with $Ni(mnt)_2^{2-}$ in contact with 2mM $Fe(CN)_6^{3-/4-}$ in 0.1 M KCl at scan rates from 10 to 100 mV/sec (a to b).

conditions. Selected electrochemical parameters for a **PB1** modified electrode are presented in Table 4.1.

The rate of charge transport across the polymer blend film by the redox couple in the film (in the dark), is determined by the apparent diffusion coefficient, $D_{app}(125)$. Chronoamperometric measurements were performed on polymer films **PB1** in both the absence and presence of dye. $Fe(CN)_6^{3-/4-}$ was ion-exchanged from a 2 mM solution until a steady voltammogram was obtained with maximum peak amplitudes. The contents of the flow cell's reservoir were changed from a solution containing the redox couple to a solution containing only the background electrolyte. The background electrolyte was pumped through the tubing and the flow cell until the $Fe(CN)_6^{3-/4-}$ was completely flushed from the solution phase of the system, leaving only the redox couple species and the dye in the film. Chronoamperometric measurements were conducted by stepping the potential of a non-flowing system from $+0.6 \rightarrow -0.6$ V. Under the conditions of the experiment, semi-infinite linear diffusion may be assumed and Cottrell plots can be used to evaluate D_{app} if all other parameters are known. A representative chronoamperometric decay is shown in Figure 4.4. The concentration of the incorporated redox couple was calculated by chronocoulometry. Film thicknesses were measured with a micrometer. The apparent diffusion coefficient of $Fe(CN)_6^{3-/4-}$ in the films were evaluated and are listed in Table 4.2.

Table 4.1 Selected electrochemical parameters for a **PB1** modified electrode.

Scan rate (mV/sec)	I_{pc} (μA)	I_{pa} (μA)	E_{pc}[a] (V)	E_{pa}[a] (V)	ΔE_p (mV)	$E_{1/2}$[a] (V)
10	104	133	.130	.260	130	.195
20	166	196	.100	.290	190	.195
30	200	233	.090	.305	215	.198
40	229	258	.085	.315	230	.200
50	254	292	.060	.325	265	.193
60	279	317	.050	.335	285	.193
70	300	338	.040	.345	305	.192
80	313	350	.035	.355	320	.195
90	325	363	.025	.360	335	.193
100	342	375	.020	.365	345	.193

a) Potentials given vs. Ag/AgCl (sat. KCl) electrode.

Figure 4.4 Typical chronoamperometric response for a **PB1** polymer modified electrode loaded with $Fe(CN)_6^{3-/4-}$ in contact with 0.1 M KCl as background electrolyte. Inset: peak current versus $1/time^{1/2}$ indicating diffusion limited characteristics.

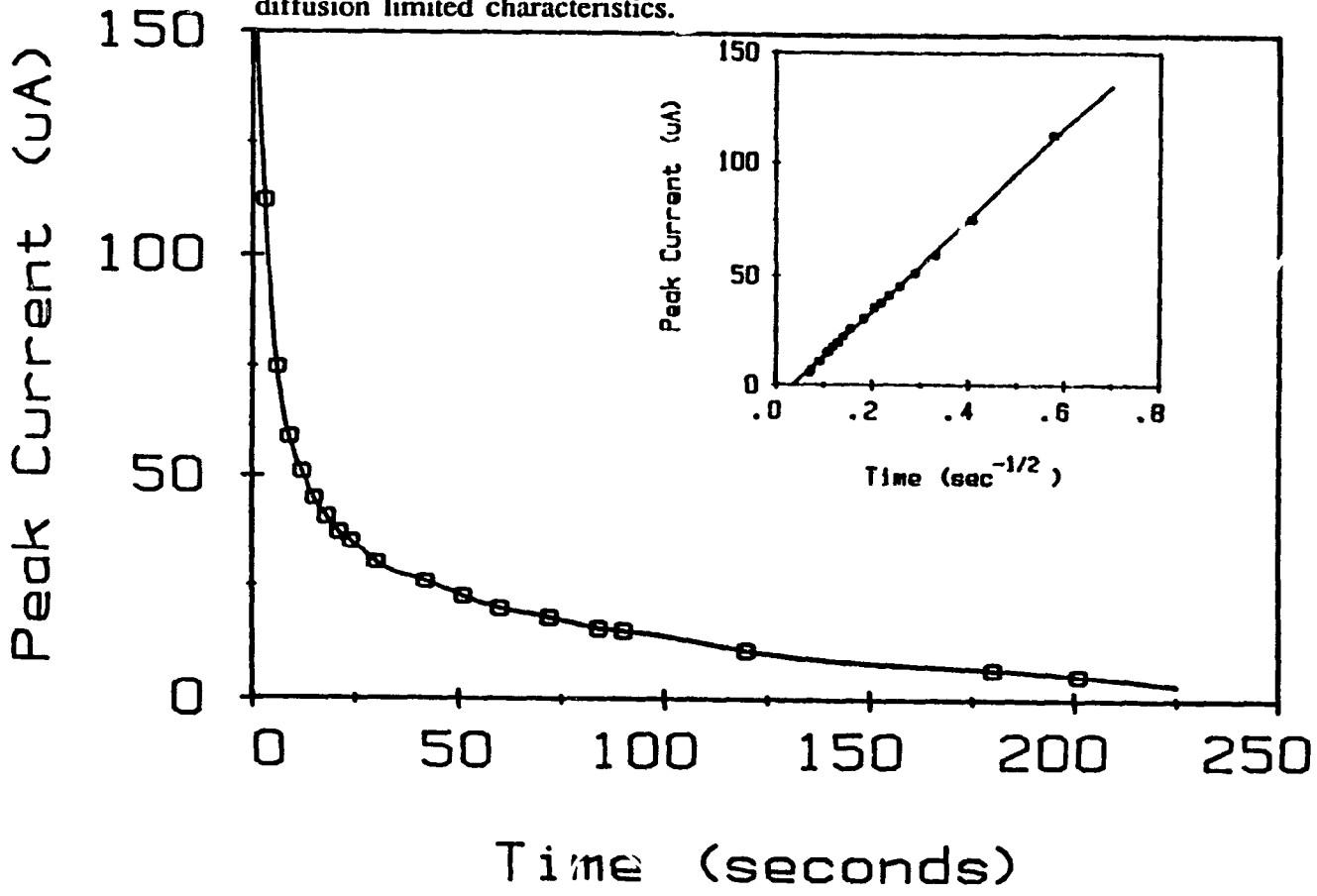

Table 4.2 Apparent diffusion coefficients of $Fe(CN)_6^{3-/4-}$ in **PB1** polymer blend films.

Electrode	Thickness (μm)	Diffusion coefficient ($cm^2/sec \times 10^7$)
1	10	6.0
2	11	1.0
3	16	0.42
4	20	0.67
5	20	0.45

The values are somewhat smaller in these thick films than values reported for thin films of this polymer blend on carbon electrodes (52). The apparent diffusion coefficient of $Fe(CN)_6^{3-/4-}$ in the films does not follow a simple film thickness dependence. The selected values in Table 4.2 are representative of the D_{app} in these films and depend on electrode preparation.

The hexacyanoferrate redox couple remains in the polymer film at a high concentration for some time after the electrode is placed in contact with the background electrolyte. Cyclic voltammograms of polymer films which were soaked in 10-50 mM $Fe(CN)_6^{3-/4-}$ are similar to those shown in Figure 4.3. This is an indication that the film incorporates a maximum amount of $Fe(CN)_6^{3-/4-}$ from the solution. Continuous CV scanning over a period of four hours reveals a gradual leaching of the $Fe(CN)_6^{3-/4-}$ into the background electrolyte solution. The leaching of the redox couple from the polymer reaches a limit at 45 to 50% of the initial concentration in the film. In contrast, the water-insoluble $M(mnt)_2^{2-}$ complexes do not appear to leach from the polymer film. Polymer modified electrodes containing the $Pt(mnt)_2^{2-}$ or the $Ni(mnt)_2^{2-}$ complexes were soaked in 1M KCl for 2 days

without any leaching of the complexes to the solution as indicated by absorption spectroscopy.

4.3 Polymer Blend Morphology

4.3.1 Transmission Electron Microscopy

The polymer film swells to accommodate electrolyte. The high retention values and diffusion coefficients of the $Fe(CN)_6^{3-/4-}$ in the composite film have been linked to the internal morphology of the film. Transmission electron micrographs (TEM) of a thin polymer film in the absence of dye are shown in Figure 4.5. The polymer film appears to segregate into hydrophilic and hydrophobic domains (126). The hydrophobic domains appear as small spherical globules with an approximate diameter of 500-1000 Å. The globules can be envisaged as a hydrophobic film surrounding a hydrophilic interior. The globules seem to form an interconnecting network with larger hydrophilic regions filling the voids. It is believed that the electrolyte and the redox couple can circulate in this network of channels. TEMs of the polymer blend containing another planar dye, zinc (II) mesotetra(4-sulfonatophenyl) porphyrin (i.e. $ZnTPPS^{4-}$), is also shown in Figure 4.5. In this case, the polymer film has an altered morphology with collapsed globules and channels, but displays self-similarity at different levels of magnification (Figure 4.6). This fractal-like characteristic (127) suggests that randomly attached planar anions have knitted together different points on the film surface of the original globules.

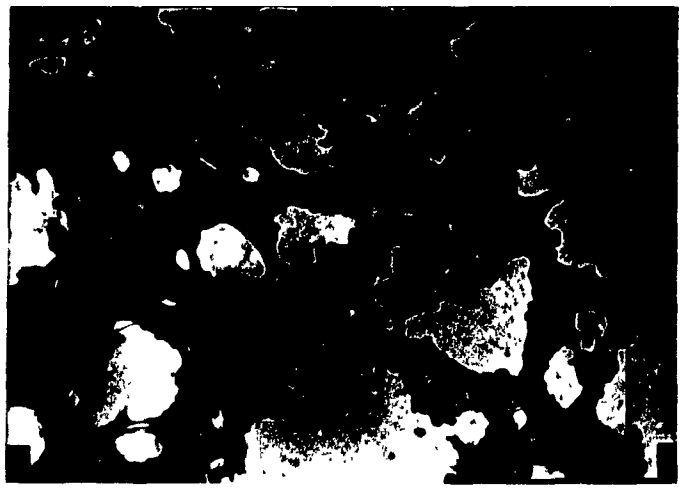

A

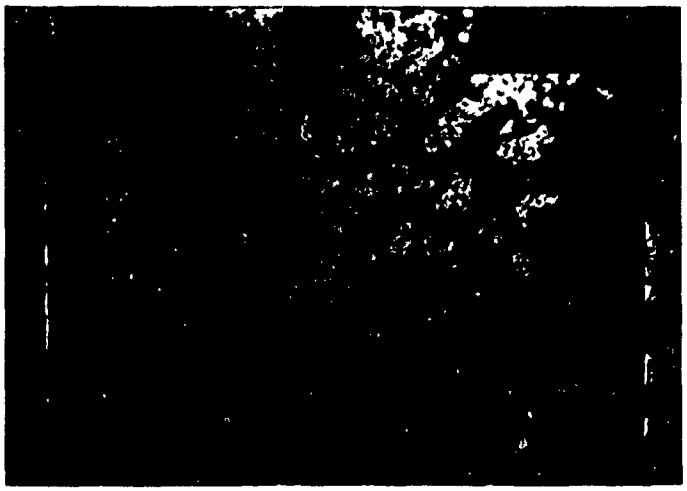

B

Figure 4.5 Transmission electron micrographs of (A) a thin **PB1** polymer film without dye (magnification = 20,000x) and (B) a thicker film containing $ZnTPPS^{4-}$ (magnification = 10,000x).

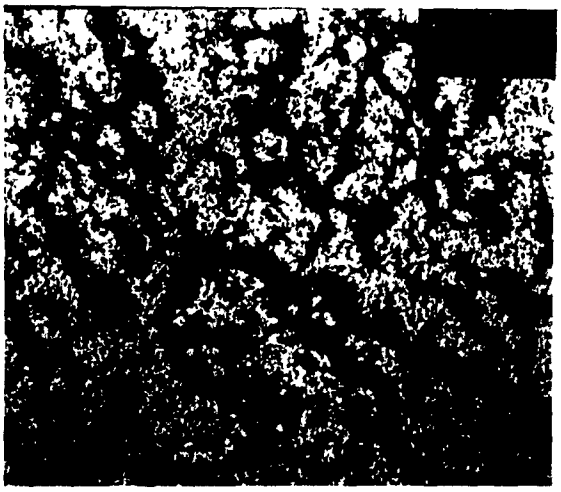

A

B

Figure 4.6 Transmission electron micrographs of a **PB1** polymer film containing $ZnTPPS^{4-}$ at (**A**) 3,000x magnification and at (**B**) 30,000x magnification.

4.3.2 Scanning Electron Microscopy

A scanning electron micrograph of the surface of a **PB1** modified electrode containing $Pt(mnt)_2^{2-}$ is shown in Figure 4.7. The cracks are a result of the removal of trapped solvent (methanol) in the film which occurred under the high vacuum process of gold sputtering prior to sample analysis. The surface has small pores of 1-3 μm diameter. The polymer modified electrode does not have a completely smooth surface. It should be noted that the polymer will swell to accomodate electrolyte solutions and alter the surface characteristics.

4.4 Photoelectrochemistry of Polymer Modified Electrodes with $M(mnt)_2^{2-}$

Photoelectrochemical measurements using visible light were conducted after the dark current had stabilized to a minimum (0.1→0.2 μA *ca.* 1-3 hours). When the polymer modified electrode was illuminated from the SnO_2 side, anodic photocurrents (2-5 uA) were recorded. A typical photocurrent-time profile is shown in Figure 4.8. The relatively slow response of the cell might be attributed to one or more of several factors including: slow diffusion of ions in the film, slow charge transport via redox reactions in the film or at the interfaces, and a reduced mobility due to the trapping of charge carriers moving across the polymer. The analysis below will to point toward a partial distinction among these factors.

In the absence of $Ni(mnt)_2^{2-}$ or $Pt(mnt)_2^{2-}$ the polymer blend films supported on SnO_2 transparent electrodes exhibit virtually no short circuit photocurrent response (100-150 nA).

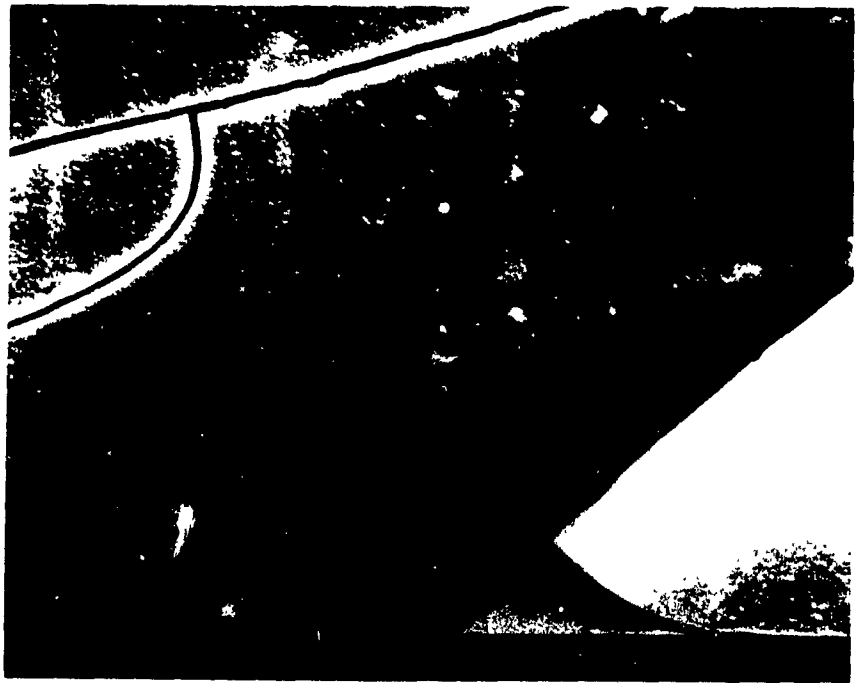

Figure 4.7 Scanning electron micrograph a **PB1** polymer film loaded with $Pt(mnt)_2^{2-}$ (magnification = 1,000 x).

Figure 4.8 Typical short circuit photocurrent-time profile of a **PB1** polymer modified electrode loaded with $Ni(mnt)_2^{2-}$ in contact with 2 mM $Fe(CN)_6^{3-/4-}$ in 0.1 M KCl.

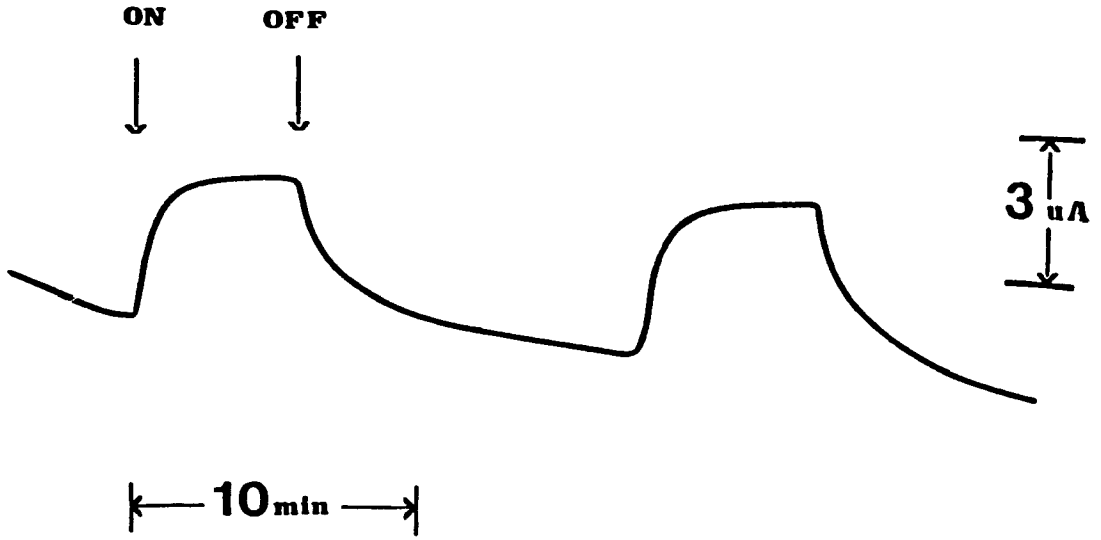

An argon ion laser, in single line mode, was used as an irradiation source in order to examine photocurrents as a function of wavelength in the vicinity of the main visible band of the complex. The resulting photocurrents are superimposed on a visible spectrum in Figure 4.9. The absorption maximum appears at 488 nm, corresponding to one of the main lines of the argon ion laser. The action spectrum maps the peak. Photocurrent increases with increasing power with slight upward curvature at high laser intensities (Figure 4.10).

The initial facts that a mechanism for the photoeffects must satisfy are the observations that the photocurrent is anodic, that it has an action spectrum matching $Ni(mnt)_2^{2-}$, and that the maleonitriledithiolate dianion is not electrochemically active in the dark while the $Fe(CN)_6^{3-/4-}$ couple is electroactive. These facts can be accommodated for by the mechanism shown in Figure 4.11. The excited state of the reduced metal maleonitriledithiolate dye transfers an electron to the SnO_2 electrode yielding $Ni(mnt)_2^{1-}$ which has an appropriate potential (0.37 V vs Ag/AgCl) to oxidize $Fe(CN)_6^{4-}$. Some excess $Fe(CN)_6^{3-}$ diffuses out of the film and the Pt counter electrode effects the reduction of Fe(III). No other reasonable sequence can account for the facts listed. A similar mechanism operates with the Pt complex.

The fact that the nickel and platinum complexes are electro-inactive in the composite film is quite surprising. This contrasts the results of the complex incorporated by ion-exchange in the QPVP films (110). The method of preparation in the latter case differs from the present preparation of the polymer film composites. The metal maleonitriledithiolate complexes appear to be bound by strong electrostatic interactions to the quaternized alkyl ammonium sites in the

Figure 4.9 Absorption spectra of PB1 polymer modified electrode loaded with $Ni(mnt)_2^{2-}$ (———) and short circuit photocurrents of a PB1 polymer modified electrode loaded with $Ni(mnt)_2^{2-}$ in contact with 2 mM $Fe(CN)_6^{3-/4-}$ in 1 M KCl when illuminated with an argon ion laser in single line mode at 100 mW (-●--●-).

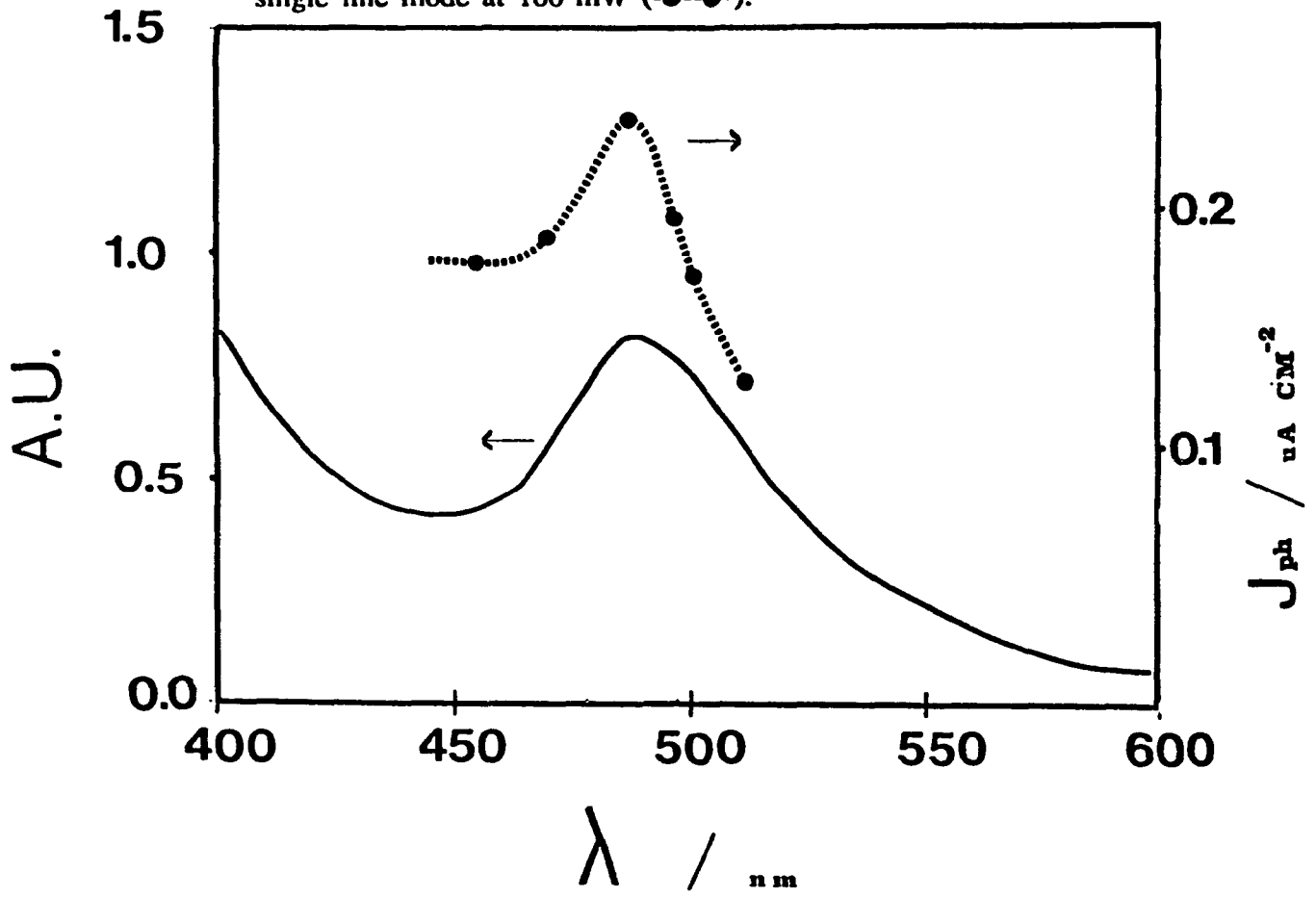

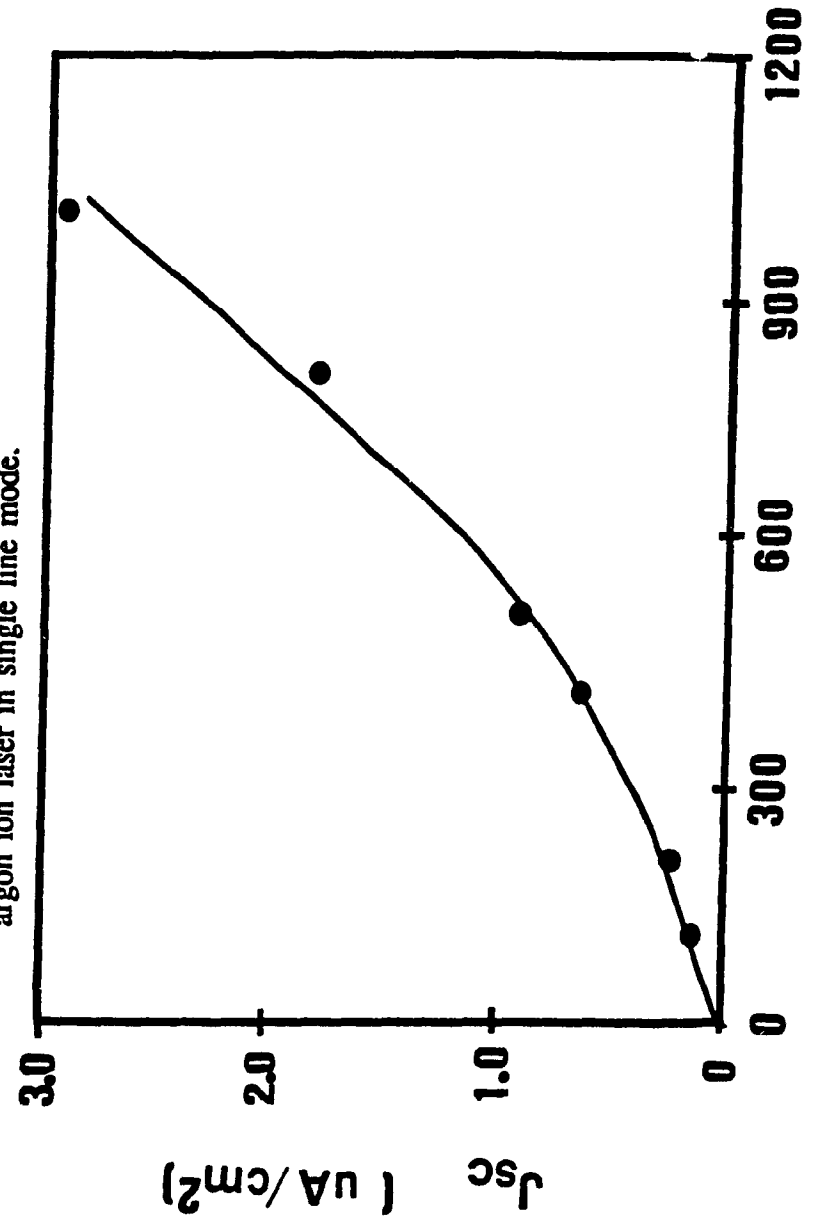

Figure 4.10 Short photocurrents of a PB1 modified electrode loaded with $Ni(mnt)_2^{2-}$ in contact with 2 mM $Fe(CN)_6^{3-4-}$ in 1 M KCl as a function of illumination intensity at 488 nm using an argon ion laser in single line mode.

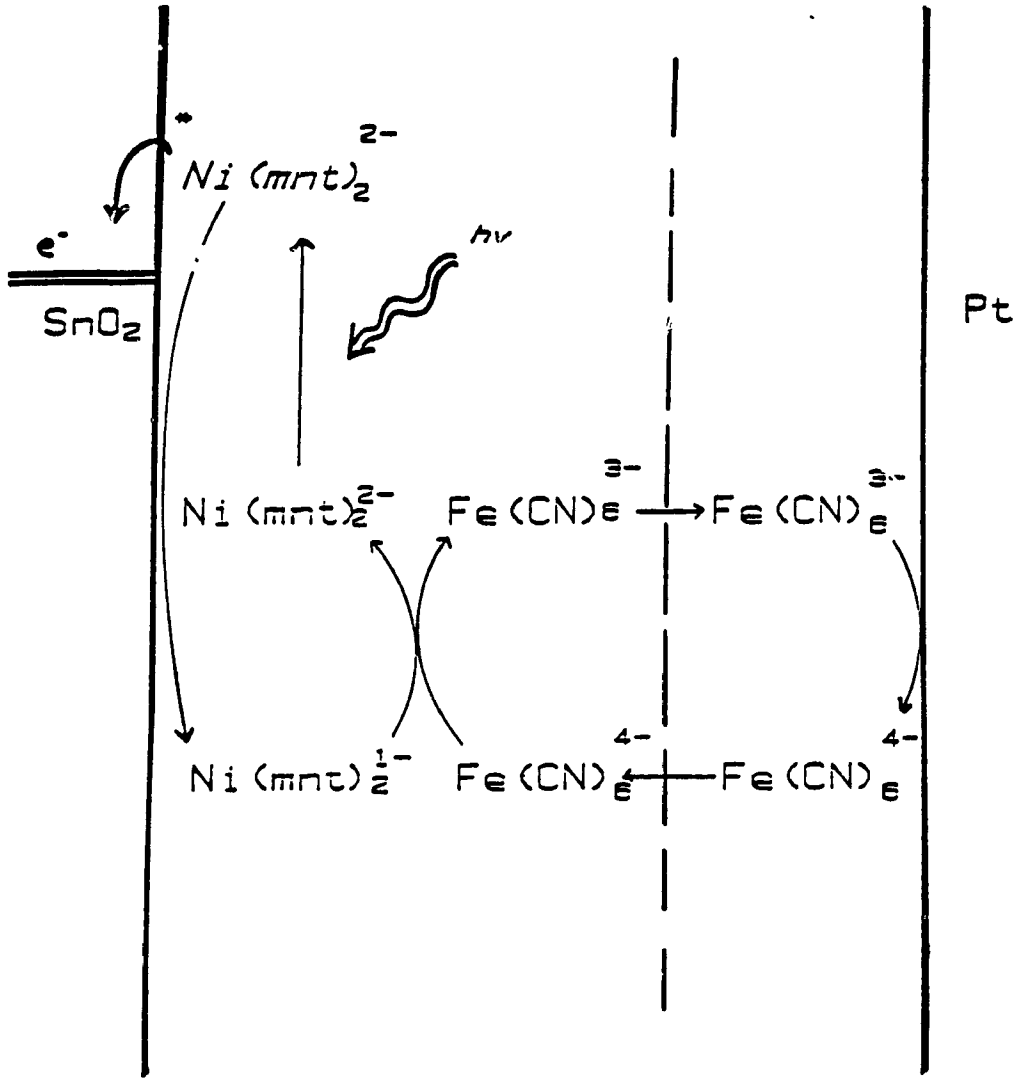

Figure 4.11 Proposed mechanism for photoeffects observed for a **PB1** polymer modified electrode loaded with $Ni(mnt)_2^{2-}$ in contact with 2 mM $Fe(CN)_6^{3-/4-}$ in 1 M KCl.

copolymer moiety of the polymer blend. Axial ligation of the complex to pyridine sites of the poly(vinylpyridine) moiety of the blend should not be discounted as possible binding sites for the strongly colored complexes. This could account for the spectral shift in the film.

Resonance raman experiments by Clark and Turtle (95) indicated that the $^1A_g \rightarrow {}^1B_{2u}$ (M→L) charge transfer transition has a greater change in the C=C bond length than the $^1A_g \rightarrow {}^1B_{2u}, {}^1B_{3u}$ (L→M) transition. Excitation of the M→L transition using visible light, as in the case of the polymer films, should lead to a greater delocalization of charge on the periphery of the ligand which would make an excited state electron more available for electron transfer to the polymer.

Figure 4.12 shows a cyclic voltammogram of the electrode under illumination which foreshadows use as a photoswitch or photodiode-like device. At potentials between 0.1 and 0.8 volts vs Ag/AgCl, the dark currents are small and irradiation in the mW/cm^2 range can turn on a current of several uA. The larger anodic photocurrents are in agreement with the proposed mechanism in Figure 4.11 (148). Localized energy states in the polymer film at these potentials may be slightly altered to allow for enhanced conduction of charge through the polymer film.

4.5 Molecular Ion-State Approach

The puzzle presented by the mechanism is how the electron is transported from the excited $Ni(mnt)_2^{2-}$ complex to the SnO_2 electrode. Two possibilities present themselves. One is energy migration from the point of excitation to the interface, with charge separation being limited to the interface. This seems unlikely. Earlier

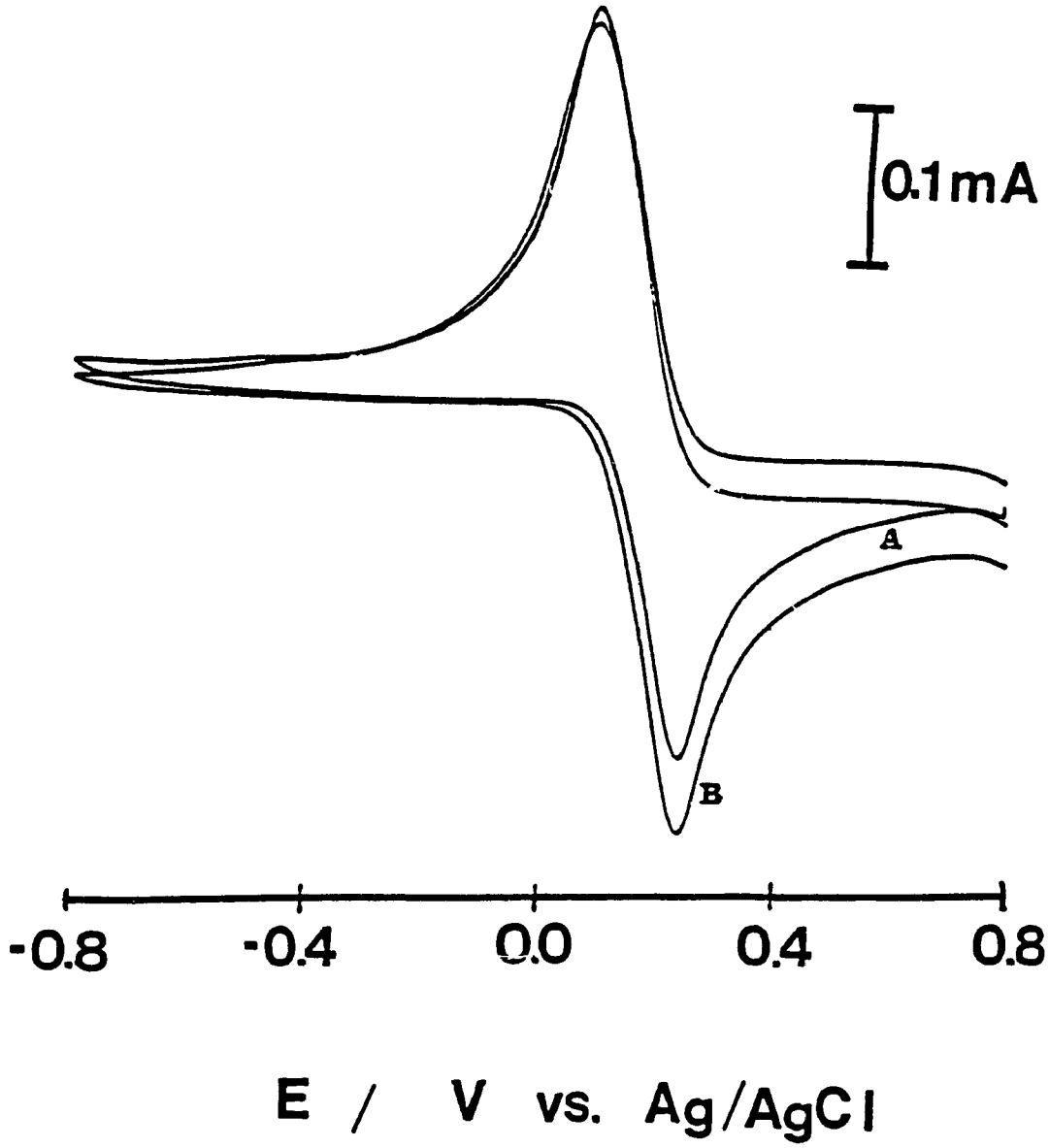

Figure 4.12 Cyclic voltammograms of a **PB1** polymer modified electrode with $Ni(mnt)_2^{2-}$ in contact with 2 mM $Fe(CN)_6^{3-/4-}$ in 1 M KCl (**A**) in the dark, and (**B**) under white light illumination. Scan rate = 5 mV/sec. Anodic currents are downward.

reports indicate short excited state lifetimes for the complex (61,62) and it is difficult to see how an exciton mechanism can be consistent with upward curvature of the current-intensity curve. The other possibility is that the excited state of $Ni(mnt)_2^{2-}$ transfers an electron to π^* levels of an aromatic ring of the polymer, and that transfer to the electrode is an analog of conductivity in polystyrene after electron injection (33). This mechanism is energetically allowed on the basis of the energy of the lowest lying excited state of the complex and the reduction potential of aromatic groups. The ^1A_g ground state of the $Ni(mnt)_2^{2-}$ complex is located at -0.1 volts versus NHE. The reduction potential of the pyridinium group lies at -0.45 volts versus NHE. Excitation to the lowest excited state of the complex adds 2.54 eV to the reduction power making transfer to the pyridinium group thermodynamically feasible.

Further support for this mechanism comes from the wavelength dependence of photocurrents in similar phthalocyanine and porphyrin films (26). In this mechanism, the slow response is related to trap controlled charge migration in this film. The magnitude of the photoresponse is dependant on the energetics of charge transfer, the lifetime of the excited state, and the polymer morphology. The highly disordered amorphous nature of this film can give rise to a large number of localized states.

The electronic states of polymeric solids arise from the weakness of intermolecular binding forces in these materials. The states result in positive and negative molecular ion states of isolated molecules. Duke and Fabish (23,24,25) developed the molecular ion state model to support their findings on charge

injection in pendant group polymers from contact-charging experiments.

The positive molecular ion states can be characterized by their ionization energy, I_g, and the negative ion states by their electron affinity, A_g. Ionization will induce changes in localized polarization of the polymeric solid. The molecular ion states can then be described as $-(A_g + P)$ and $-(I_g + P)$ for the acceptor and donor states respectively. The reorganization energy, P, is made up of collective polarizations of the polymeric environment. The molecular ion states are discrete separate states which are coupled to the polarization fluctuations of the surrounding medium rather than being localized energy-band states associated with the polymeric macromolecule. This is in contrast to the notion of bandgaps in semiconducting solids.

Molecular ion states are associated with the pendant groups of polymers. Large changes in the localized states of polymers arise from thermally induced molecular vibrations and from variations in local structure. The probability of a state energy is given by a distribution,

$$N(E) = \frac{\exp\{-(E-E^{\circ})^2/4kTP\}}{(4\pi kTP)} \qquad [4.1]$$

where T is the absolute temperature, k is Boltzmann's constant and E° is the most probable energy value. The reorganization energy, P, as described above, consists of collective polarization terms of the surrounding medium and of energies due to inner-sphere interactions involving local bond length changes (128).

Broad Gaussian distributions of localized anion (acceptor) and cation (donor) states in the polymer were consistent with the experimental findings of Duke and Fabish (24,25). Furthermore, the model predicts that these are intrinsic and localized states.

The model has been adjusted to describe the observed photoinduced electron migration in polymer films. The **PB1** polymer blend is reputed (52) to segregate into hydrophilic and hydrophobic domains. The energetic distribution of molecular ion states presented here reflects the hydrophobic domain where electron migration occurs. Duke and Fabish have shown the experimental and theoretical characterization of donor and acceptor states for atactic polystyrene and poly(2-vinylpyridine) films (23,24). They also demonstrated that the distribution of molecular ion states in polymer blends and mixtures can be described by the formula

$$N(E) = \Sigma X_i N_i(E) \qquad [4.2]$$

where X_i is the mole fraction of the individual polymers and N(E) is the double Gaussian distribution of state density. Polystyrene and poly(4-vinylpyridine) mole fractions in the hydrophobic domain of the blend are 0.6 and 0.4 respectively. The resulting distribution of molecular ion-states is shown in Figure 4.13. The diagram includes all components of the photoelectrochemical system studied. The donor and acceptor states in this figure must be considered approximate since it is assumed that the hydrophobic domains in the cast film have the same composition as the solution prior to casting and that the literature data used for the calculation of energy states relates to poly(2-vinylpyridine) (P(2-VP)). There should not be a large discrepancy between P(2-VP) and P(4-VP) even though the energy levels for the

Figure 4.13 Energy level diagram. The calculated distribution of acceptor and donor states of the **PB1** polymer blend is shown here relative to energy levels of the SnO_2 electrode, the $Fe(CN)_6^{3-/4-}$ redox couple, and the $M(mnt)_2^{2-}$ dyes used in this system. The hydrophylic domains of the polymer blend incorporates the redox couple, while the hydrophobic domain includes the styrene and PVP moieties of the polymer. The dye is believed to be at the interface of these domains.

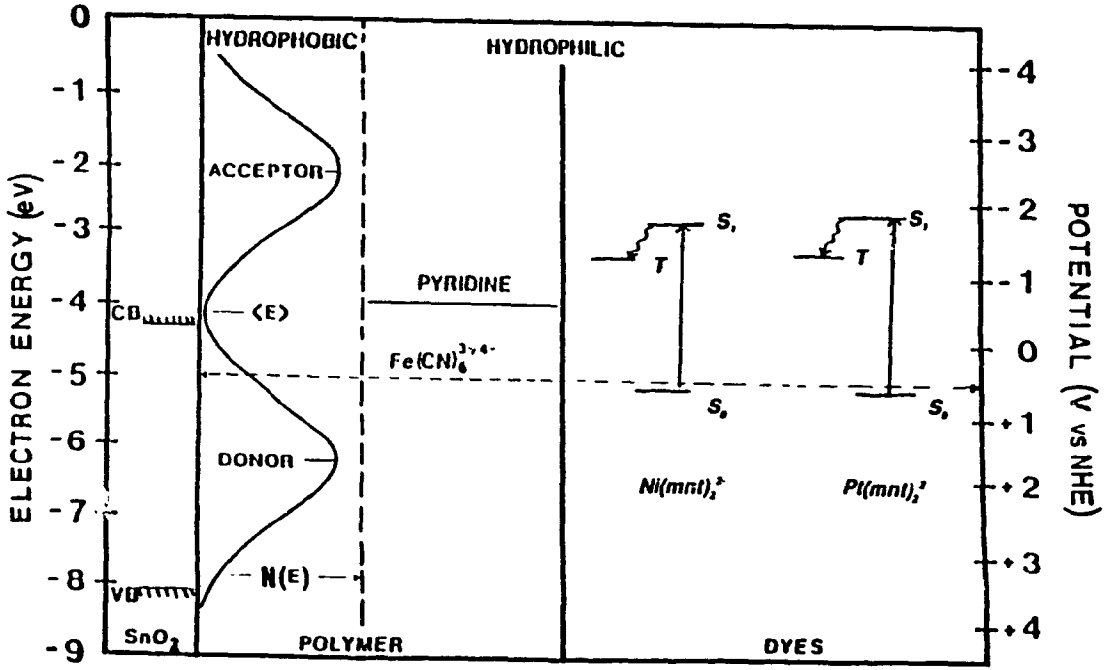

latter have not yet been established either theoretically or experimentally.

The position of the centroid <E> is an important parameter determining the feasibility of charge injection into an acceptor state of the polymer blend. A similar distribution of acceptor and donor states with a centroid at a more positive energy value would provide a larger density of acceptor states available for charge injection from the $M(mnt)_2$ chromophore. The larger density of states means that the electron "hopping" distance between adjacent sites has become shorter and electron transfer more facile.

The type of polymer used will determine the location of the centroid and the distribution of states. The hydrophilic and hydrophobic domains of the polymer blend are presented in Figure 4.13 as redox energy levels and broad band energy distributions of molecular ion states, respectively. This diagram illustrates the energetics of the mechanism shown in Figure 4.11. It is interesting to note that even though the density of available pyridine acceptor states is quite low, charge injection of electrons in pendant group polymers typically extends to distances of 4 μm (24,129,130). The $Pt(mnt)_2^{2-}$ complex parallels the nickel complex with respect to charge transport. The platinum complex has a longer excited state lifetime than the nickel and generally leads to greater photocurrents. The ratio of short circuit photocurrents for $Pt(mnt)_2^{2-}$ to $Ni(mnt)_2^{2-}$ (~1.5) does not compare with the ratio of excited state lifetime (~1000), which implies efficient electron transfer in the primary step.

The behaviour of $Pt(mnt)_2^{2-}$ and $Ni(mnt)_2^{2-}$ in this ion-exchange polymer film is similar to results obtained with ion-exchange polymer films containing zinc

porphyrins and several sulphonated metal phthlocyanines (26). In the dark the charge transport in this ion-exchange polymer blend is a diffusion limited process, while under illumination charge transport is governed by trapping of charge carriers in hydrophobic domains and by diffusion processes in the hydrophilic regions. The overall morphology of the polymer plays a significant role in the transport of charge to the electrode.

CHAPTER 5

RESULTS AND DISCUSSION III

Advanced Polymer Systems Containing $Ni(mnt)_2^{2-}$ and $Pt(mnt)_2^{2-}$

The previous chapter described the electrochemical and photoelectrochemical behaviour of the maleonitriledithiolates in **PB1** ion-exchange polymer blends. Several other electroactive polymer matrices were investigated in order to study the electrochemical and photoelectrochemical processes in the presence of the metal maleonitriledithiolates. The ion-exchange polymers include poly(4-vinylpyridine (**PVP**), and two other quaternized polystyrene based random co-polymers. Two redox polymers based on viologen groups were examined as candidate materials. Poly(pyrrole) is an electronically conducting polymer capable of anion exchange which was also used as a polymer support. $Pt(mnt)_2^{2-}$ and $Ni(mnt)_2^{2-}$ were incorporated into an insulating polycarbonate polymer for electrochemical and photoelectrochemical studies. The mechanism of charge transport in these polymer modified electrodes has been investigated in the dark and under visible light illumination. The transient behaviour of the photocurrents was treated by a trap controlled diffusion limited model from the molecular ion state model. The magnitude and time dependance of the photoresponse can be used to characterize charge transport processes.

The details of charge transport are hard to assign on a molecular level and differ for different polymer systems. However, in a number of cases simple ionic diffusion across a concentration gradient can be used to describe adequately the phenomenon of charge transport in the dark.

In polymer modified electrodes, an understanding of any apparent diffusion coefficient (D_{app}) is complicated by polymer motion, diffusion of electrolyte and solvent, and by changes in polymer layer structure with oxidation and reduction. Each polymer/dye system will be presented , reporting its electrochemical and photoelectrochemical behaviour in relation to the particular class of polymer involved (ion-exchange, redox or electronically conducting).

5.1 Polymer Modified Electrodes of Poly(4-vinylpyridine) and $Ni(mnt)_2^{2-}$.

The polymer described in chapter 4 was a blend of **P1** and poly(4-vinylpyridine) (**PVP**). The results presented in this section are based only on SnO_2 modified electrodes with **PVP** and $Ni(mnt)_2^{2-}$. Methanolic solutions of **PVP** and the metal complex were cast on optically transparent SnO_2 electrodes. The films are mechanically more rugged than the **PB1** films. They are not easily scratched, hydrophobic, and transparent red in color. The CT bands in the near-UV and visible spectrum are red shifted by 6→8 nm (Figure 5.1).

5.1.1 Electrochemistry of PVP Modified Electrodes

The solution electrochemistry of a SnO_2/**PVP** and a SnO_2/**PVP**/$Ni(mnt)_2^{2}$ electrode in background electrolyte (0.1 M KCl) is shown in Figure 5.2. The electrolyte solutions described in this section were adjusted to pH 5.0 ± 0.3 with 0.01 M HCl. There was little difference between cyclic voltammograms. A small signal due to the $Ni(mnt)_2^{2}$ in direct contact with the SnO_2 electrode is observed at an expanded scale. Strong ionic interactions and/or ligand exchange and/or axial ligation are responsible for the electroinactivity of $Ni(mnt)_2^{2}$ in these films. These

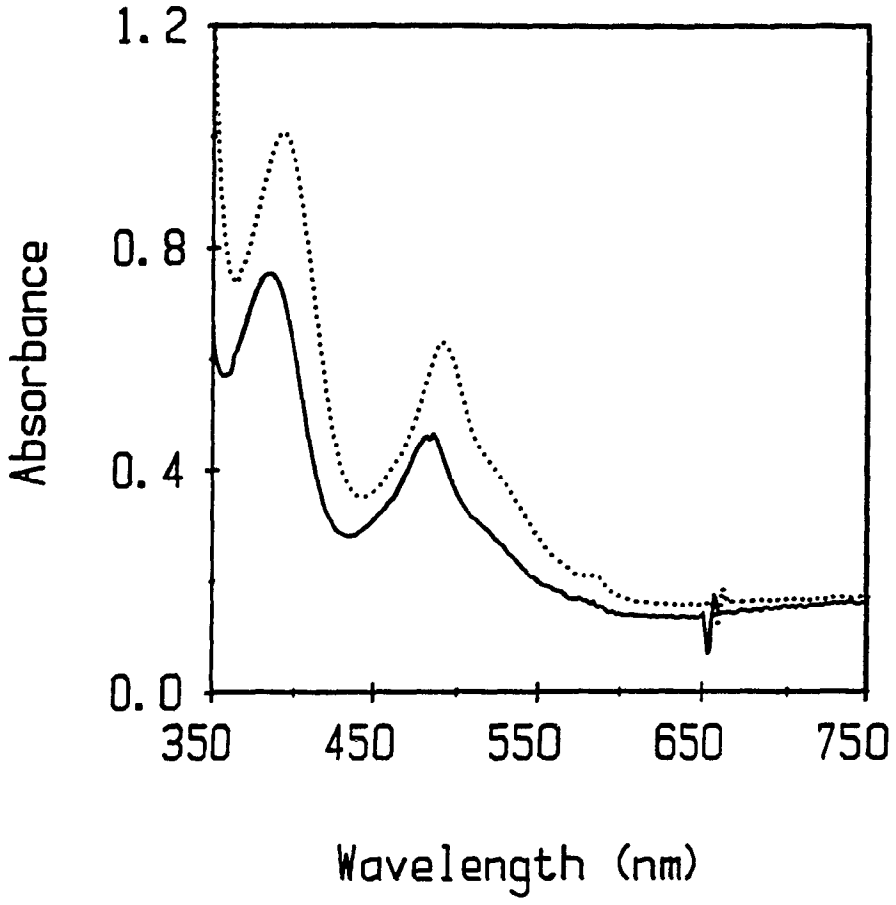

Figure 5.1 Near-UV and visible absorption spectra of $Ni(mnt)_2^{2-}$ in acetonitrile (solid line) and $Ni(mnt)_2^{2-}$ in **PVP** polymer matrix on a SnO_2 electrode.

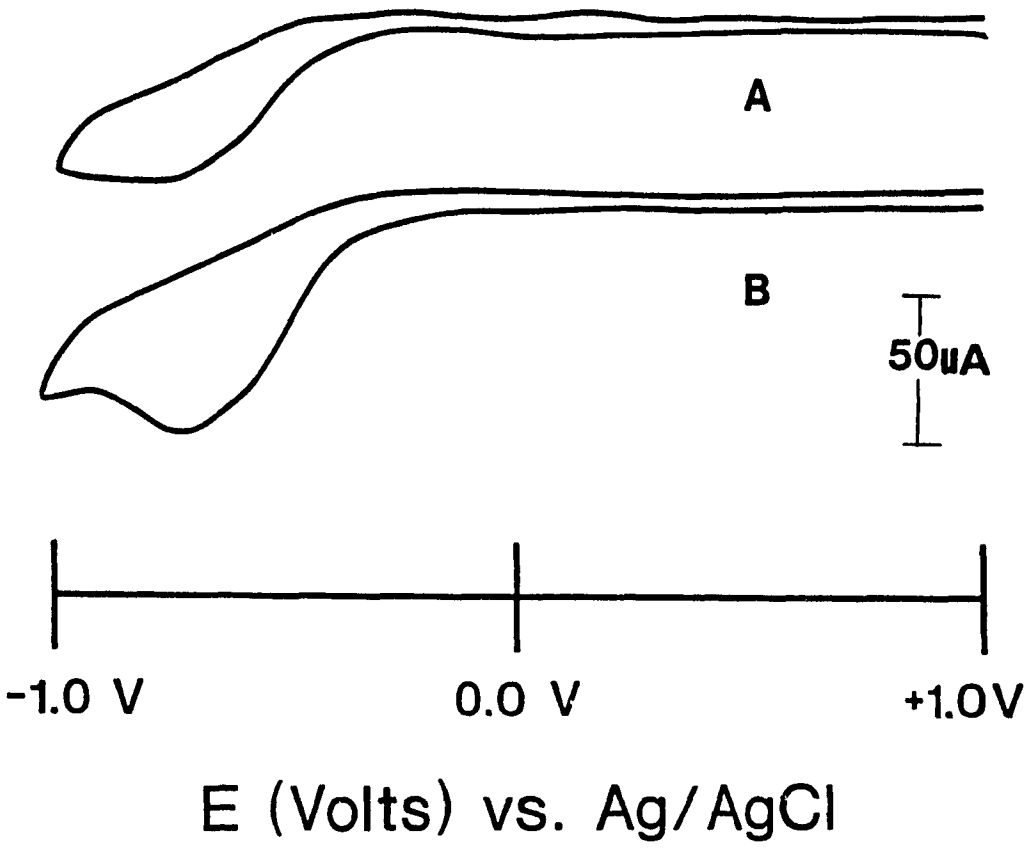

Figure 5.2 Cyclic voltammograms of (A) SnO_2/PVP/$Ni(mnt)_2^{2-}$ and (B) SnO_2/PVP in 0.1 M KCl. Scan rate = 100 mv/sec.

voltammograms are similar to the results obtained with **PB1**. The irreversible reduction of the pyridinium groups (E_{pc} = -0.8 V vs. Ag/AgCl) is the only notable voltammetric feature. These electrodes were soaked in 2 mM $Fe(CN)_6^{3-/4-}$ containing 0.1 M KCl. The hexacyanoferrate (II/III) couple was incorporated slowly into the **PVP** film (Figure 5.3). Cyclic voltammograms at different scan rates were performed and plots of peak current versus square root of scan rate were linear indicating a diffusional charge transport process in the dark (Figure 5.4) (53,54). Voltammetric data is presented in Table 5.1. The peak separation became greater with increasing scan rate, however the ratio of anodic to cathodic peak current remained fairly constant (1.0 ± 0.1). Although the polymer modified electrode behaved quasi-reversibly, sluggish kinetics were seen as the scan rate was increased from 10 to 100 mV/sec. The quantity of $Fe(CN)_6^{3-/4-}$ incorporated in the protonated **PVP** matrix is less than in the **PB1** case as indicated by integration of the voltammetric peaks at 10 mV/sec after removal from the redox solution and immersion in 0.1 M KCl. For films of similar thickness and dye content, the **PB1** film incorporated 1→2 X 10^{-5} moles/cm^3 of $Fe(CN)_6^{3-/4-}$ while the **PVP** film incorporated 8→9 X 10^{-6} moles/cm^3. The **PVP** modified electrodes did not retain the redox couple as the **PB1** polymer blend. An SnO_2/**PVP** modified electrode containing $Fe(CN)_6^{3-/4-}$ at pH=2.8 was placed in background electrolyte (pH=5.0) and voltammetrically cycled for 30 minutes (Figure 5.5). The resultant leaching of the redox couple was calculated to be 75% or 62% from the anodic and cathodic waves, respectively. The polymer blend retains 55% of the redox couple after 45 minutes in background electrolyte (section 4.2). Similar protonated **PVP** films cast

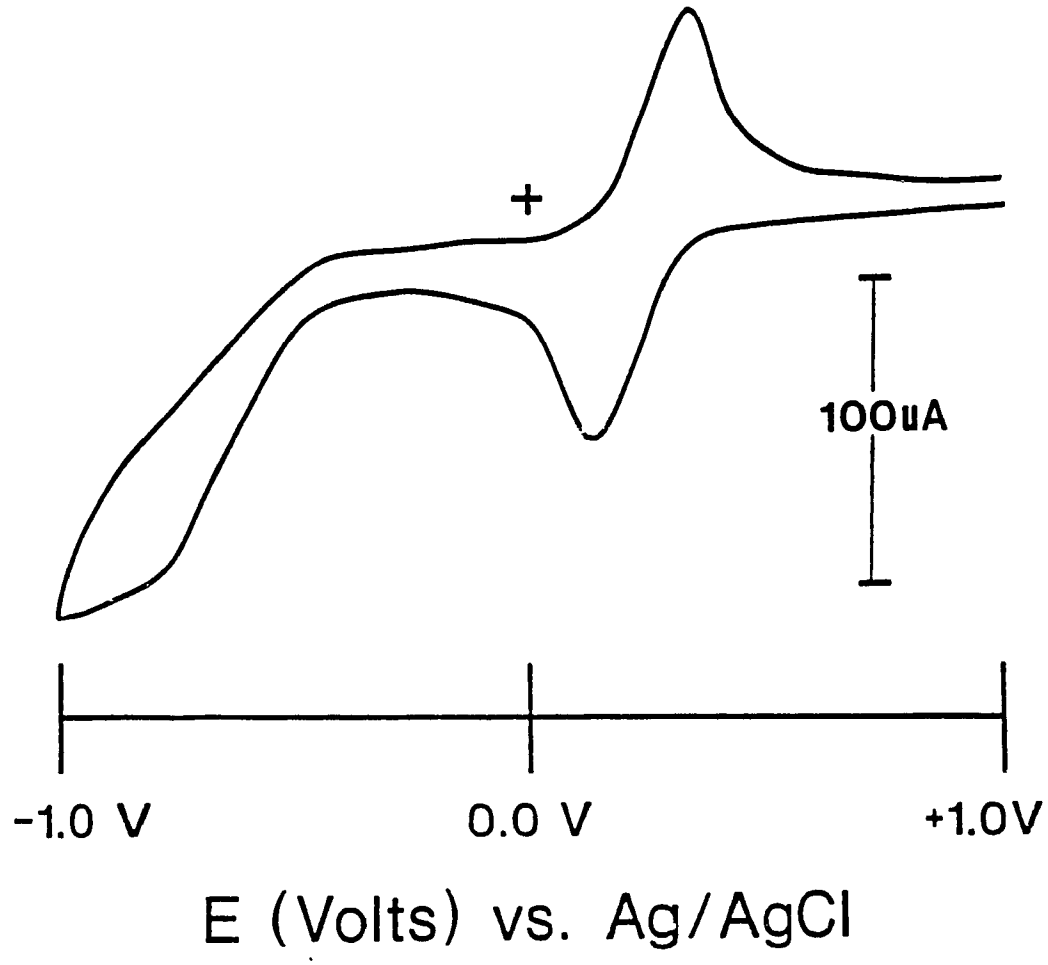

Figure 5.3 Cyclic voltammogram of a SnO_2/**PVP**/$Ni(mnt)_2^{2-}$ electrode in contact with a 2 mM $Fe(CN)_6^{3-/4-}$ in 0.1 M KCl. Scan rate = 100 mv/sec.

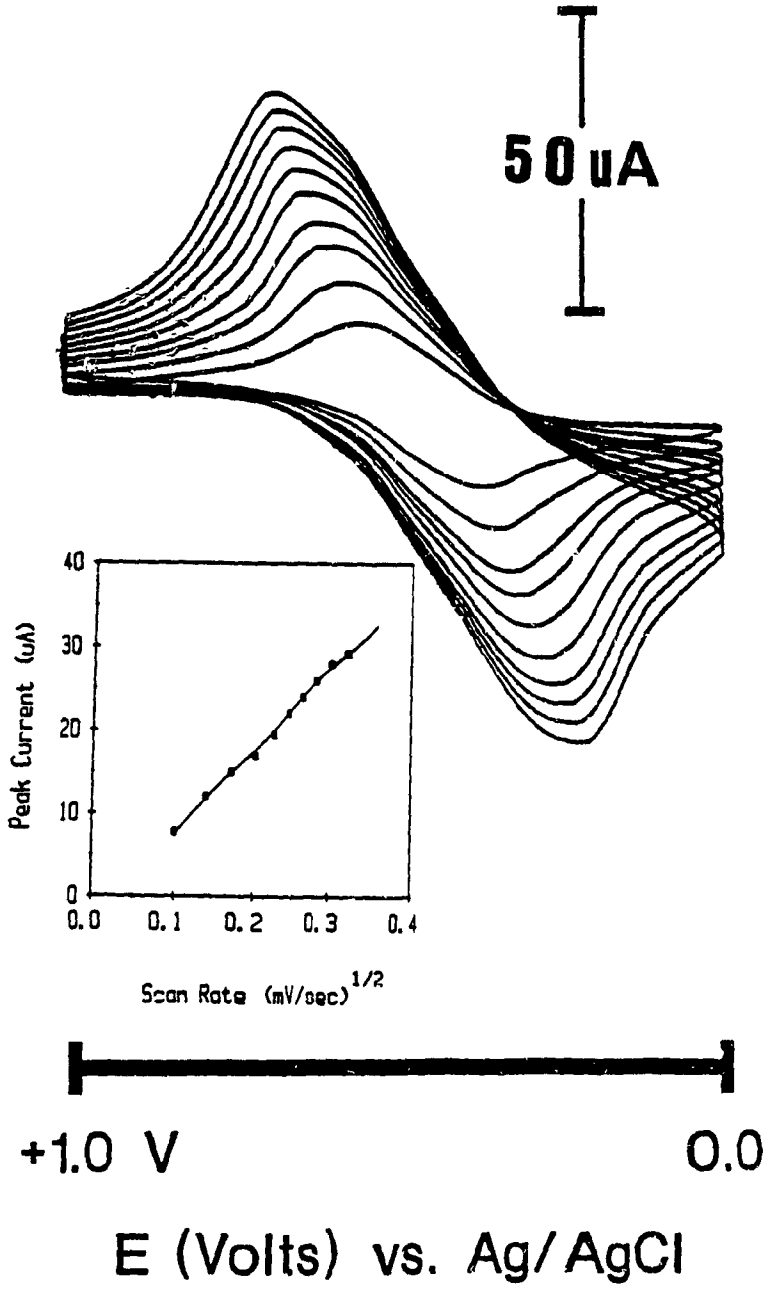

Figure 5.4 Cyclic voltammograms of a SnO_2/PVP/$Ni(mnt)_2^{2-}$ electrode in contact with a 2 mM $Fe(CN)_6^{3-/4-}$ in 0.1 M KCl. Scan rates were varied between 10 and 100 mv/sec. Inset shows plot of anodic peak current versus the square root of the scan rate.

Table 5.1 Voltammetric parameters for SnO_2/PVP/$Ni(mnt)_2^{2-}$ modified electrodes in contact with 2 mM $Fe(CN)_6^{3-/4-}$ in 0.1M KCl.

Scan rate (mV/sec)	E_{pa} [a] (V)	E_{pc} [b] (V)	ΔE_p [c] (V)	i_{pa} [d] (μA)	i_{pc} [e] (μA)	i_{pa}/i_{pc}
10	0.565	0.360	0.205	7.8	6.5	1.2
20	0.585	0.330	0.255	12.0	10.4	1.1
30	0.600	0.315	0.285	15.0	14.3	1.0
40	0.615	0.300	0.315	17.0	16.3	1.0
50	0.630	0.285	0.354	19.5	19.5	1.0
60	0.640	0.265	0.375	22.1	22.1	1.0
70	0.650	0.255	0.395	24.0	24.7	1.0
80	0.665	0.240	0.425	26.0	27.0	1.0
90	0.670	0.235	0.435	28.0	28.6	1.0
100	0.680	0.225	0.455	29.0	30.6	1.0

a) Anodic peak potential vs. Ag/AgCl
b) Cathodic peak potential vs. Ag/AgCl
c) Peak separation evaluated as (E_{pa}-E_{pc})
d) Anodic peak current
e) Cathodic peak current

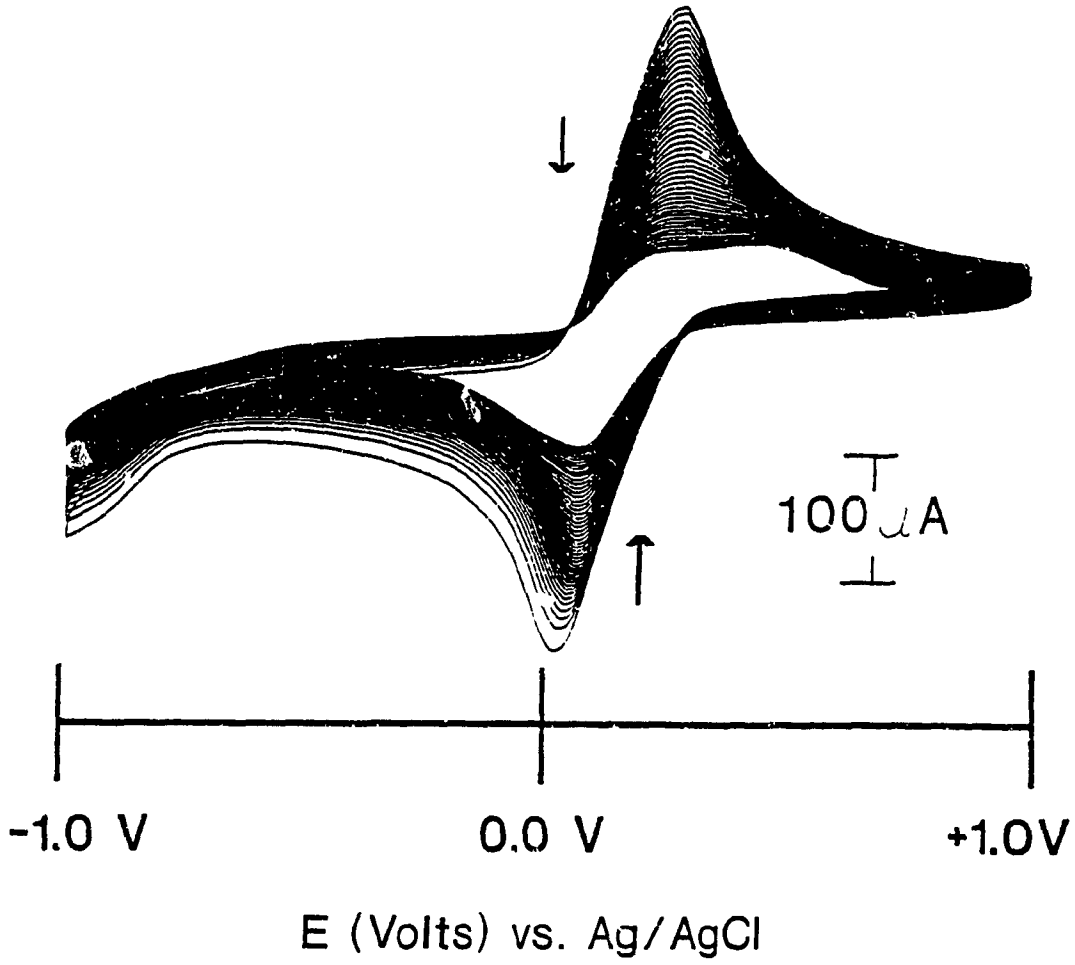

Figure 5.5 Cyclic voltammogram of a SnO_2/**PVP**/$Ni(mnt)_2^{2-}$ modified electrode containing $Fe(CN)_6^{3-/4-}$ at pH=2.8 and placed in 0.1 M KCl (pH=5.0). The resultant leaching of $Fe(CN)_6^{3-/4-}$ was monitored by cyclic voltammetry for 30 minutes. Scan rate = 100 mv/sec.

on carbon electrodes have been studied by Oyama and Anson (47,48), less leaching of $Fe(CN)_6^{3-/4-}$ was seen but no experiments were performed in a more acidic medium.

Single step chronoamperometry was used to evaluate D_{app} of $Fe(CN)_6^{3-/4-}$ in the **PVP** films. Potential steps from +0.40 → -0.40 volts vs. Ag/AgCl were performed on SnO_2/**PVP**/$Ni(mnt)_2^{2-}$electrodes; (1) soaked in $Fe(CN)_6^{3-/4-}$ for 2.5 hours, (2) rinsed with 0.1 M KCl, (3) placed in a voltammetric cell with 15 minutes wait, (4) examined by cyclic voltammetry. Subsequently, the resultant current-time decay profile was recorded (Figure 5.6). The slope of peak current versus $1/time^{1/2}$ plots were used in conjunction with the Cottrell equation [1.7] to yield apparent diffusion coefficients ranging from 2 to 4 X 10^{-9} cm^2/sec (Table 5.2). This is in good agreement with similar **PVP** modified platinum or carbon electrodes (46,48,128,129).

5.1.2 Photoelectrochemistry of PVP Modified Electrodes

The photoelectrochemical behaviour of SnO_2/**PVP**/$Ni(mnt)_2^{2-}$ electrodes was studied in solution as described in section 2.4.2. Short circuit photocurrents were measured in solutions of 0.1 M KCl and 2 mM $Fe(CN)_6^{3-/4-}$ in 0.1 M KCl. Time profiles of the anodic photocurrents are shown in Figure 5.7. The magnitude of the photocurrents is smaller than in the case of **PB1** films. A prompt photocurrent response of 6.7 ± 0.4 nA was observed for electrodes in background electrolyte alone. The response can be accounted for by generation of charge carriers in the vicinity of the semiconductor/polymer interface following the absorption of light by the metal complex. These carriers generated in the bulk of the film undergo rapid

Figure 5.6 Chronoamperometric current decay-time profile for $Fe(CN)_6^{3-/4-}$ incorporated in a SnO_2/PVP/$Ni(mnt)_2^{2-}$ electrode. Inset shows Cottrell plot of current vs. time$^{1/2}$.

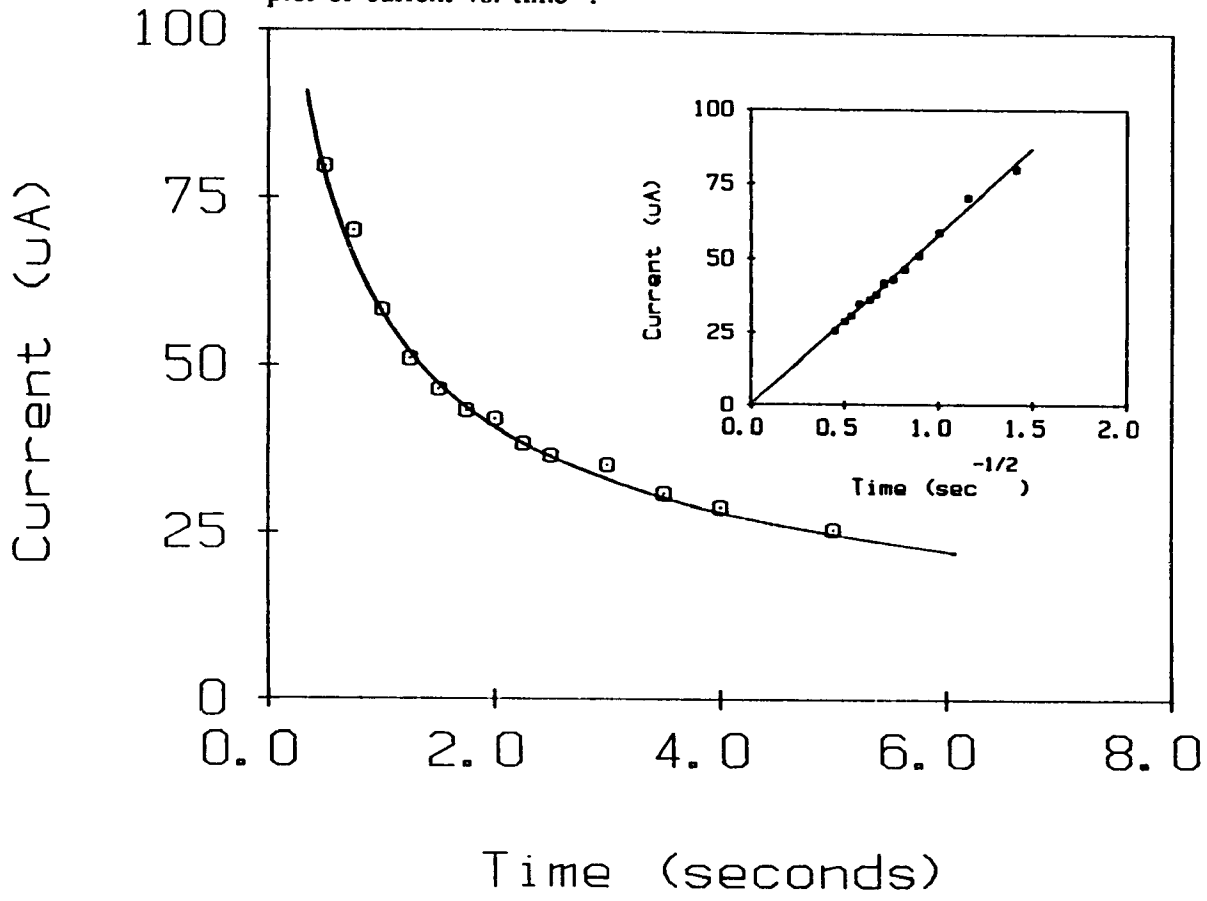

Table 5.2 Apparent diffusion coefficients of $Fe(CN)_6^{3-/4-}$ in **PVP** modified electrodes doped with $Ni(mnt)_2^{2-}$ evaluated by chronoamperometry.

Electrode	Thickness (μm)	$[Fe(CN)_6^{3-/4-}]$ (μmoles/cm^3)	D_{app} (x 10^9 cm^2/sec)
JA20	10 ± 1	9.9 ± 0.9	2.1 ± 0.4
JA21	12 ± 1	8.9 ± 0.9	3.6 ± 0.3
JA21A	15 ± 1	8.0 ± 0.8	4.1 ± 0.4

Figure 5.7 Short circuit photocurrent-time profiles for a SnO_2/PVP/Ni(mnt)$_2^{2-}$ electrode in contact with (A) 0.1 M KCl and (B) 2 mM $Fe(CN)_6^{3-/4-}$ in 0.1 M KCl. Visible light irradiation at 100 mW/cm^2 with a water filter and a UV cut-off filter (400nm).

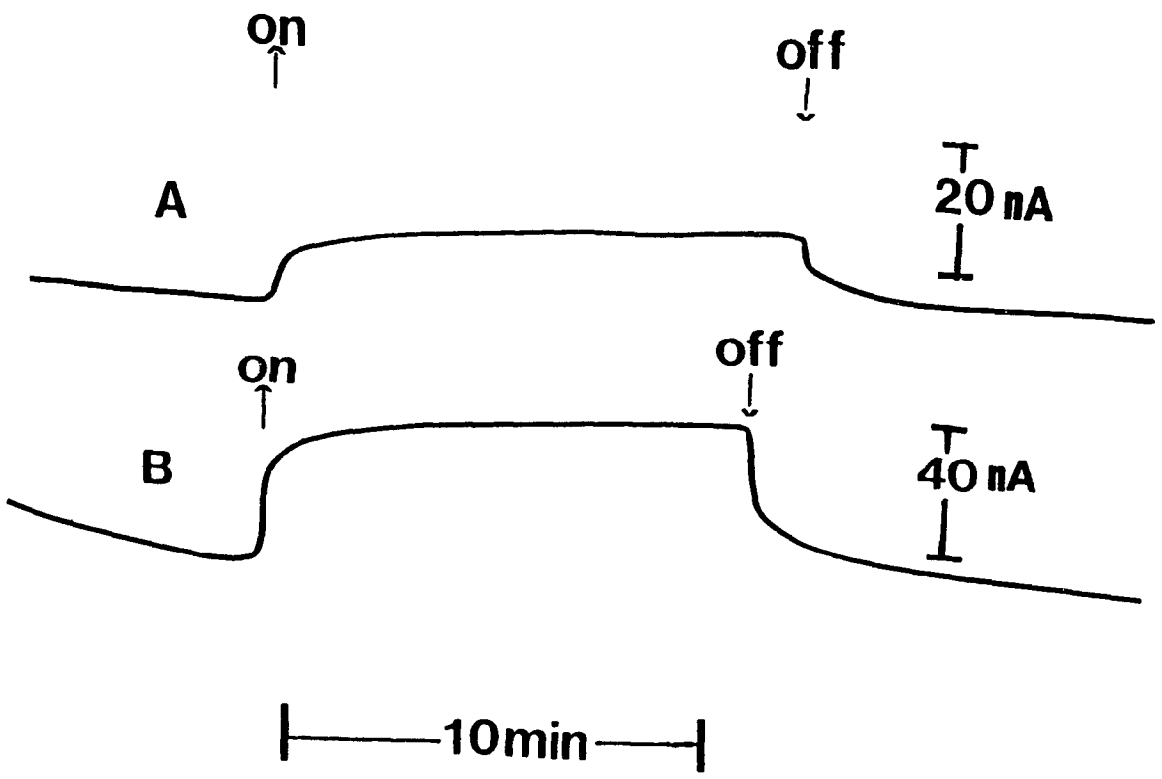

recombination and/or trapping events. The surface layer charge carriers can then rapidly transfer an electron into the conduction band of the highly n-doped SnO_2. The photocurrents in 0.1 M KCl are not as stable as the photocurrents in 2 mM $Fe(CN)_6^{3-/4-}$ since there is no redox couple available to reduce any oxidized metal complex. The decay of the photocurrent once the light source has been removed is prompt with a tailing feature indicating some thermal discharge of occupied trap sites in the polymer. The response returns to a minimal background signal.

The photoresponse from a SnO_2/**PVP**/$Ni(mnt)_2^{2-}$ electrode in 2 mM $Fe(CN)_6^{3/4-}$ is similar to that of a SnO_2/**PB1**/$Ni(mnt)_2^{2-}$ in the same medium. The photocurrents in $Fe(CN)_6^{3-/4-}$ are greater than in 0.1 M KCl alone because the redox couple can penetrate the film and participate in the reduction of oxidized $Ni(mnt)_2^{2-}$ following photogeneration of charge carriers in the bulk of the film.

The fact that the profiles are similar in **PVP** and **PB1** polymer films suggests that the **PVP** in both modified electrodes is a region where electron charge transport through pendant aromatic pyridine is possible. Further support for this mechanism is provided by results of "dry cell" experiments. The experiment consists of illuminating an SnO_2/**PVP**-$Ni(mnt)_2^{2}$/Au "cell" with either a laser or white light source. A strip of gold foil (1 cm X 2 cm) was tightly pressed against a SnO_2/**PVP**/$Ni(mnt)_2^{2-}$ with a piece of Lexan. The assembly was secured with 2 Hoffmann clamps. The cell was illuminated from the transparent SnO_2 side. Thermal effects were minimized by using a cooling fan and monitored with a thermocouple (J-type) placed next to the electrode. The photocurrent profiles at different light intensities is shown in Figure 5.8. The relationship between

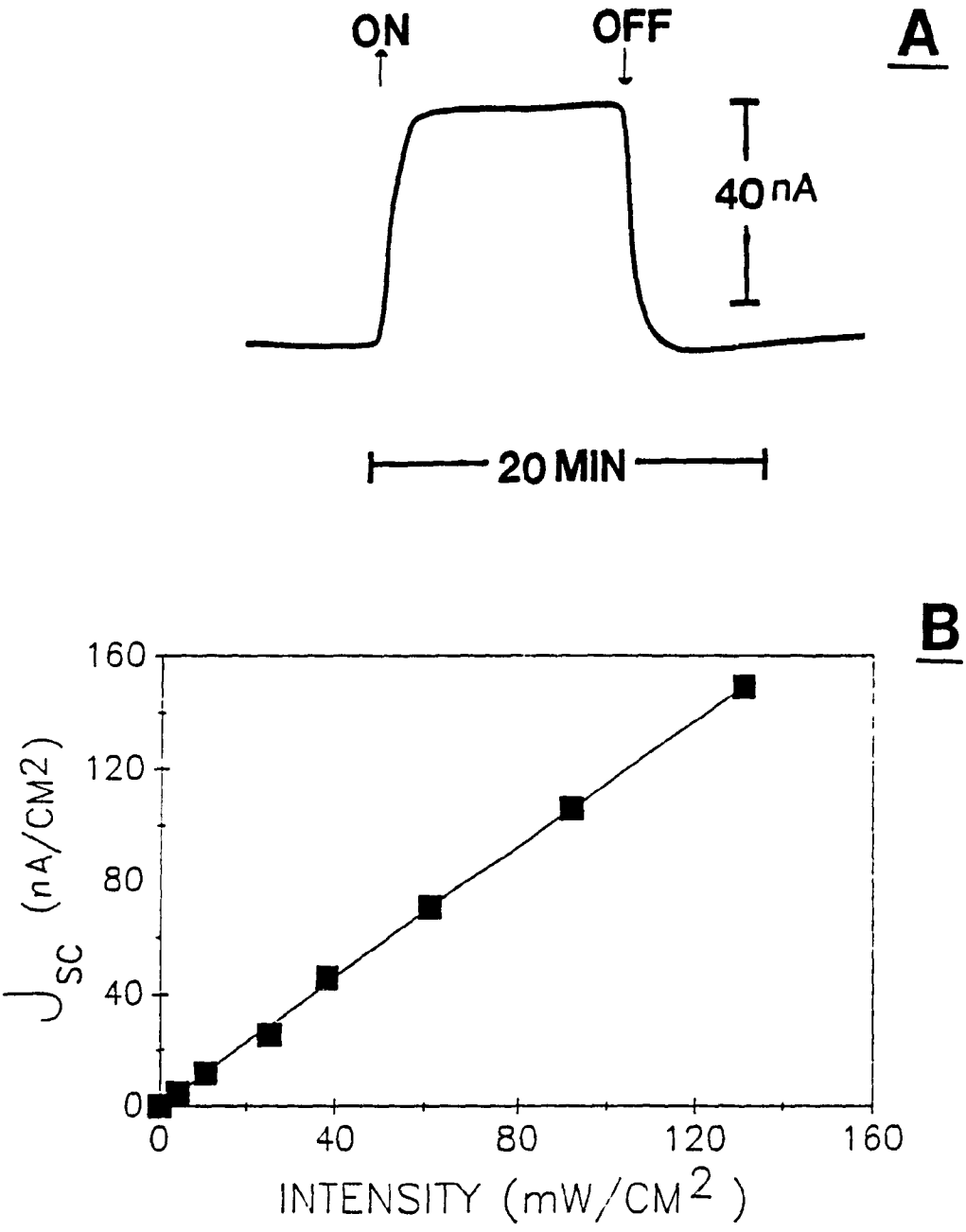

Figure 5.8 **(A)** Short circuit photocurrent-time profile for a SnO_2/PVP-Ni(mnt)$_2^{2-}$/Au "dry cell" irradiated with an argon ion laser using 60 mW at 488 nm. **(B)** Plot of short circuit photocurrent against visible light intensity.

photocurrent and light flux was determined to be linear. Photocurrents in the dry cells were much smaller than those of conventional "wet" photoelectrochemical cells. The photocurrent-time responses parallels those obtained for the wet cells. The time constants for the dry and wet cells are indistinguishable indicating that the rate-limiting process for the development of steady state photocurrents occurs in the solid **PVP** phase.

5.2 Electrochemical and Photoelectrochemical Behaviour of P2 Modified Electrodes.

P2 is an ion-exchange polymer prepared as described in section 2.2.8. It is a quaternized random co-polymer of styrene and chloromethylstyrene (see Figure 2.3). The synthesis was similar to that of **P1** except that the concentration of monomers and initiator were doubled during the initial step. The final polymer was composed of styrene, chloromethylstyrene, and quaternized moieties and was soluble in methanol. Polymer modified electrodes were prepared by drop evaporation of a 0.56% methanolic solution of **P2** onto SnO_2 conductive glass substrates. This ion-exchange polymer displayed interesting properties in comparison to the other ion-exchange polymers described above.

5.2.1 Electrochemistry of SnO_2/P2 modified electrodes

The **P2** ion-exchange polymer coated on SnO_2 electrodes was not electroactive in 0.1 M KCl from +1.0 to -1.0 volts vs. Ag/AgCl. The metal complexes were ion-exchanged into the polymer from acetonitrile or acetone solutions of the dyes. No difference was apparent attributable to the solvent used

for the ion-exchange. Composite electrodes consisting of SnO_2/**P2**/$Ni(mnt)_2^{2-}$ or SnO_2/**P2**/$Pt(mnt)_2^{2-}$ displayed voltammetric waves attributable to the maleonitriledithiolate complexes in 0.1 M KCl (Figure 5.13). A scan rate study (from 10 to 80 mV/sec) of an electrode indicated a diffusion-limited process for charge transport through the film (inset Figure 5.13). Selected voltammetric parameters are listed in Table 5.2. Other electrodes behaved similarly, but with smaller voltammetric waves. The peak separation increases linearly with the scan rate, while the half-wave potential, $E_{1/2}$, remained at a constant +0.30 ± 0.01 volts vs. Ag/AgCl. The large value of ΔE_p may represent slow electron transfer at the electrode-film interface, ohmic resistance in the film or other effects not as yet identified.

The concentration of electroactive dye was determined by integration of the area under the voltammetric wave at a scan rate of 10 mV/sec. Film thickness were measured with a micrometer. Chronoamperometry and chronocoulometry experiments were used to evaluate diffusion coefficient of $Ni(mnt)_2^{2-}$ in the **P2** films. Potential steps from +0.6 to 0.0 Volts were applied to the polymer modified electrode in 0.1 M KCl and chronoamperometric data was treated as described in section 5.1.1 using equation [1.7]. Chronocoulometric data was acquired the same way and linear Anson plots (Charge vs. time with slope *S*) were recorded for short times to ensure that the conditions for semi-infinite linear diffusion were obtained despite the limited volume of polymer film coated on the electrode. Equation 5.1 relates the slope of the plots, *S*, and the corresponding diffusion coefficient

$$D = \left[\frac{S\phi\pi^{1/2}}{2F\Gamma} \right]^{1/2} \qquad [5.1]$$

Figure 5.9 Cyclic voltammogram of a SnO_2/P2/$Ni(mnt)_2^{2-}$ modified electrode in contact with 0.1 M KCl. Scan rate = 100 mv/sec.

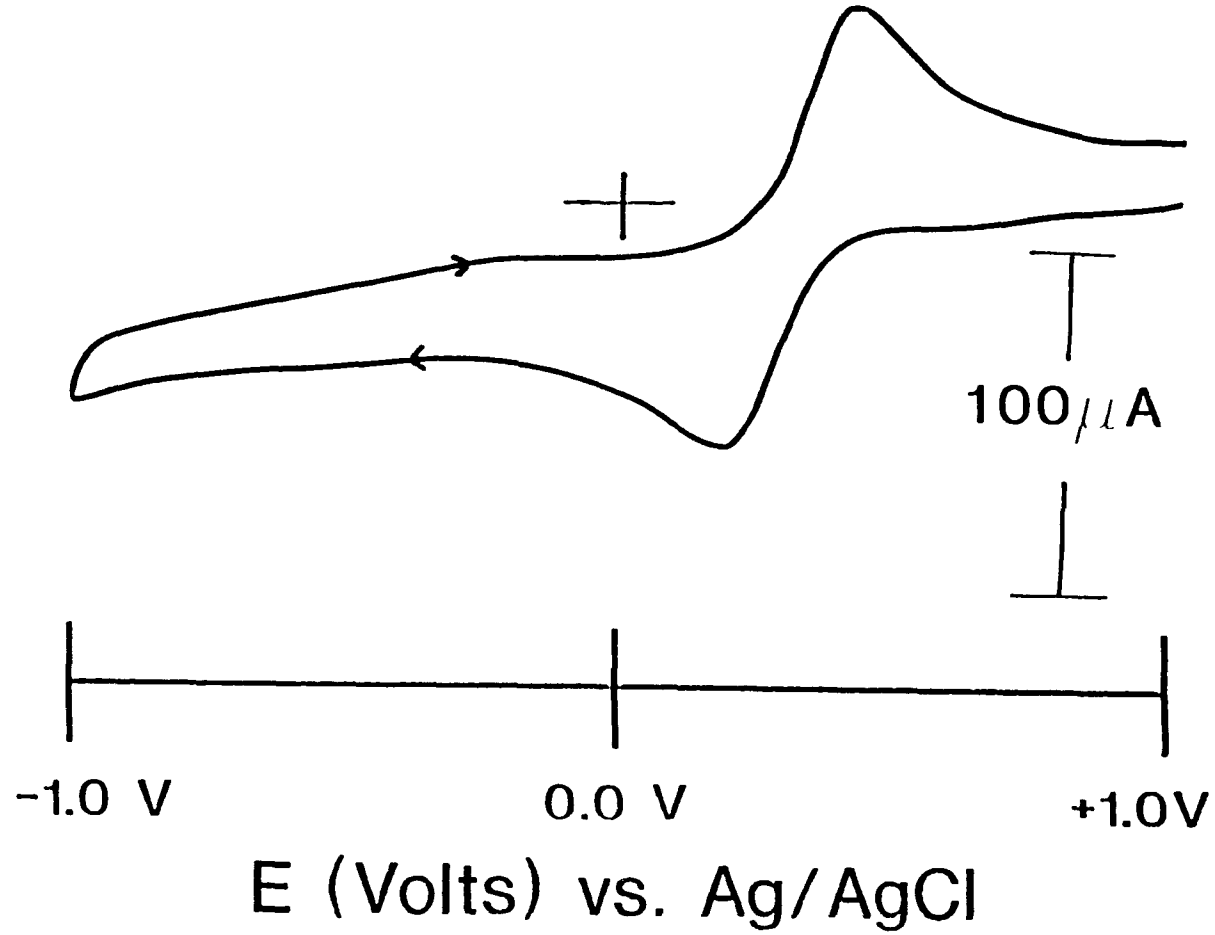

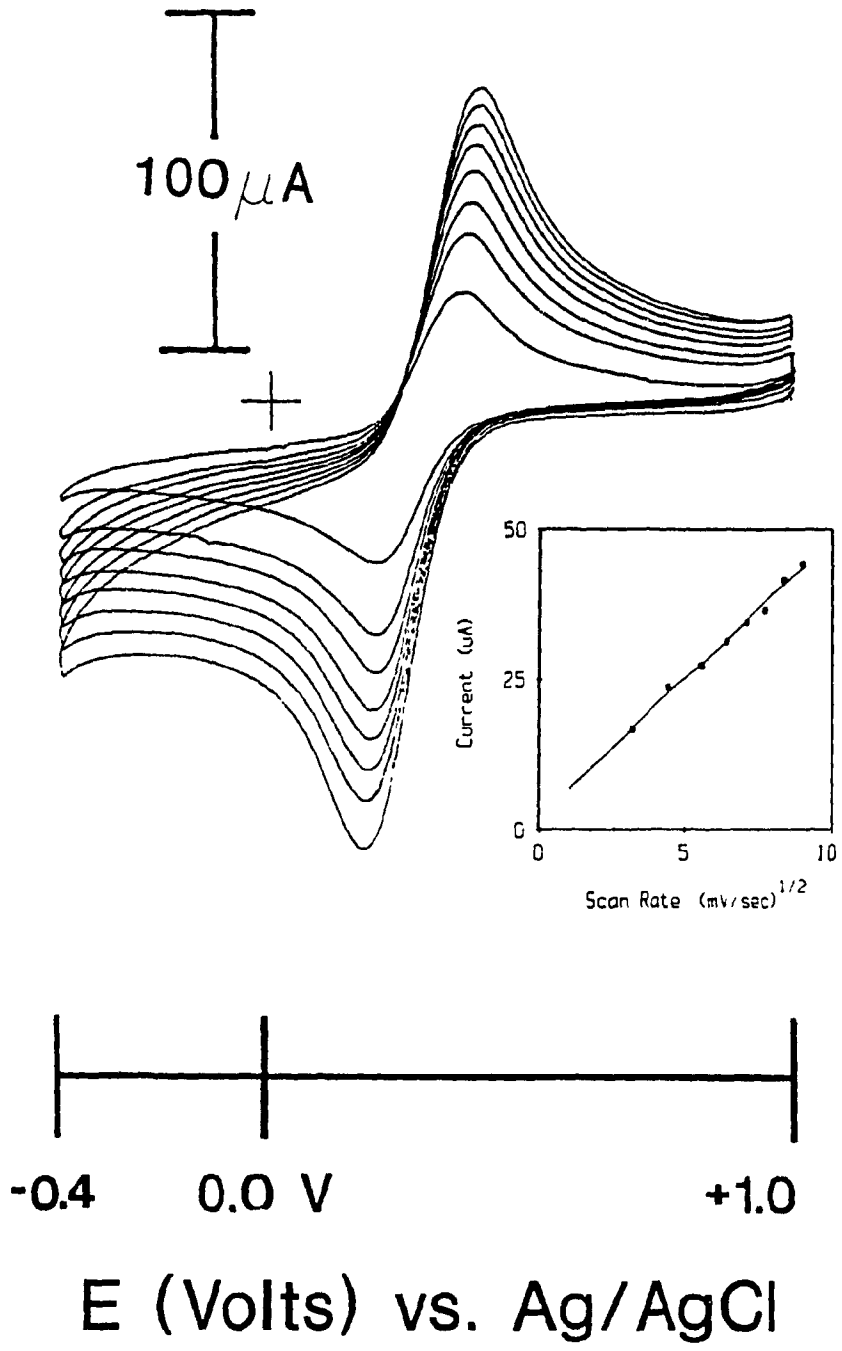

Figure 5.10 Cyclic voltammograms of a SnO_2/**P2**/$Ni(mnt)_2^{2-}$ modified electrode in contact with 0.1 M KCl. Scan rates were varied from 10→80 mV/sec. Inset shows plot of peak current versus (scan rate)$^{1/2}$.

where ϕ is the film thickness (assumed to be uniform) in cm, F is Faraday's constant, and Γ is the total quantity of diffusing reactant in the coating in mole/cm^2. A typical chronocoulometric plot is shown in Figure 5.14. Values of D_{app} obtained from chronocoulometry and chronoamperometry are listed in Table 5.3.

Table 5.3 Apparent diffusion coefficients of $Ni(mnt)_2^{2-}$ in P2 polymer films evaluated by chronocoulometry and chronoamperometry.

Electrode	D_{app} (x 10^9 cm^2/sec) (chronocoulometry)	D_{app} (x 10^9 cm^2/sec) (chronoamperometry)
AP11-1	5.4 ± 0.6	9.8 ± 1.1
AP11-2	11.5 ± 1.5	5.3 ± 0.7
AP11-3	9.6 ± 1.1	8.2 ± 0.9

Film thicknesses were measured before soaking the films in electrolyte. This can lead to errors in the determination of D_{app} since film swelling in solution may occur (52,126). These values are indicative of the order of magnitude of diffusion of these species in the film. They are slightly greater than the values obtained for $Ru(NH_3)^{2+}$ in Nafion films (135) and for $Fe(CN)_6^{3-/4-}$ in **PVP** (47,48, and section 5.1.1 of this work). The order of magnitude of D_{app} is also consistent with electron exchange controlled diffusion between fixed redox sites. It is not unlikely that both molecular motion of the $Ni(mnt)_2^{2-}$ and electron hopping contribute to the observable

Figure 5.11 Chronoamperometric current decay-time profile of a SnO_2/P2/$Ni(mnt)_2^{2-}$ electrode in contact with 0.1 M KCl. Inset shows Anson plot of charge against time$^{1/2}$.

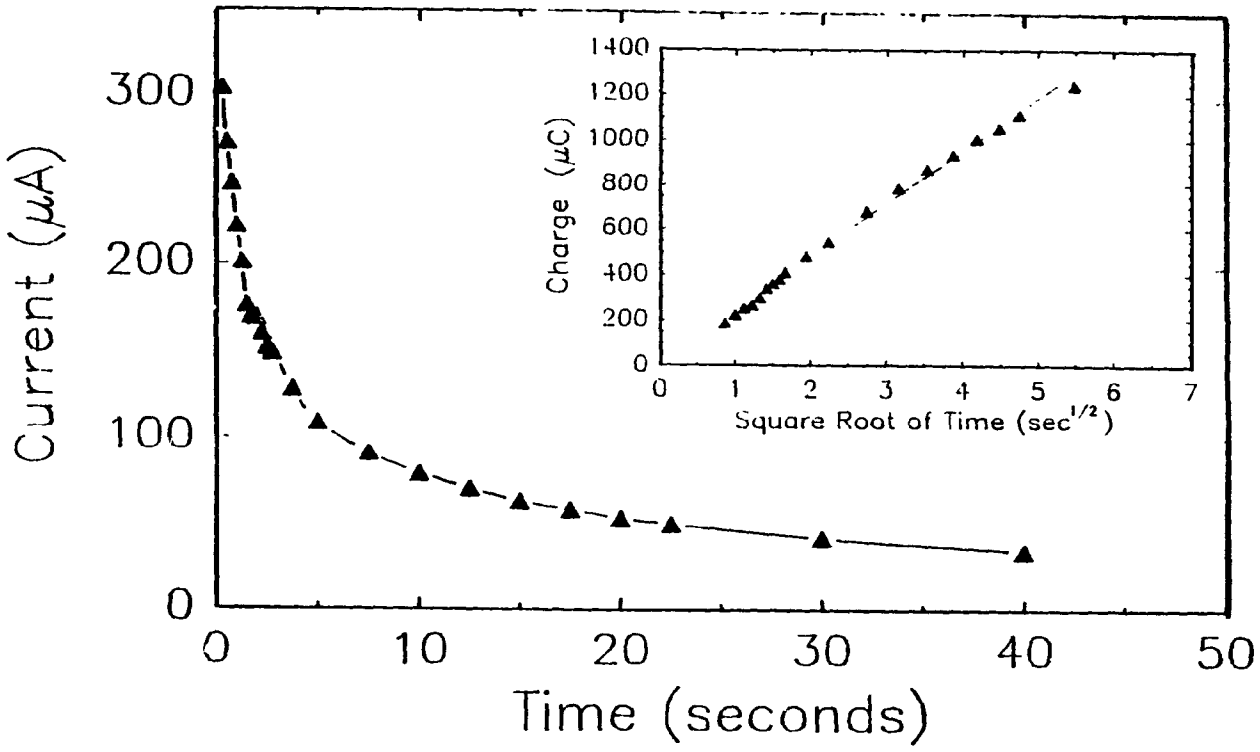

voltammetry and diffusional characteristics of this film. Nafion is an extensively studied ion-exchange polymer matrix where electron hopping between metal complexes is known to occur. Most workers agree that the morphology of the film plays a large role in diffusion. The **P2** polymer modified electrodes may possess similar morphological characteristics, with styrene and chloromethylstyrene moieties making up the hydrophobic regions and the quaternized alkylammonium sites making up the hydrophilic regions.

Additional experiments using ferri/ferrocyanide in the **P2** polymer modified electrodes were carried out by ion-exchanging $Fe(CN)_6^{3-/4-}$ for charge compensating chloride ions in the **P2** modified films. A series of voltammograms at different scan rates are presented in Figure 5.14. The redox couple exhibited quasi-reversible voltammetric behaviour. The ratio of anodic to cathodic peak currents was determined to greater than unity indicating that the more negatively charged ferrocyanide is incorporated to a larger extent than the $Fe(CN)_6^{3-}$ complex. A plot of ΔE_p vs. scan rate was determined to be linear as in the case for $Ni(mnt)_2^{2-}$ in SnO_2/**P2**/$Ni(mnt)_2^{2-}$ electrodes. This is due to the resistive component (IR) in the polymer film and is quite common in thick films on electrodes (45,46).

The charge transport behaviour of the redox couple in the film was examined by chronocoulometry and chronoamperometry using the equations presented above. Electrodes were soaked in 2 mM $Fe(CN)_6^{3-/4-}$ in 0.1 M KCl for 3 days, rinsed with distilled water, soaked in 0.1 M KCl for 2 hours, rinsed again with distilled water, then placed in a standard voltammetric cell containing only 0.1 M KCl. These steps were done to ensure that only the $Fe(CN)_6^{3/4-}$ which was in the film was

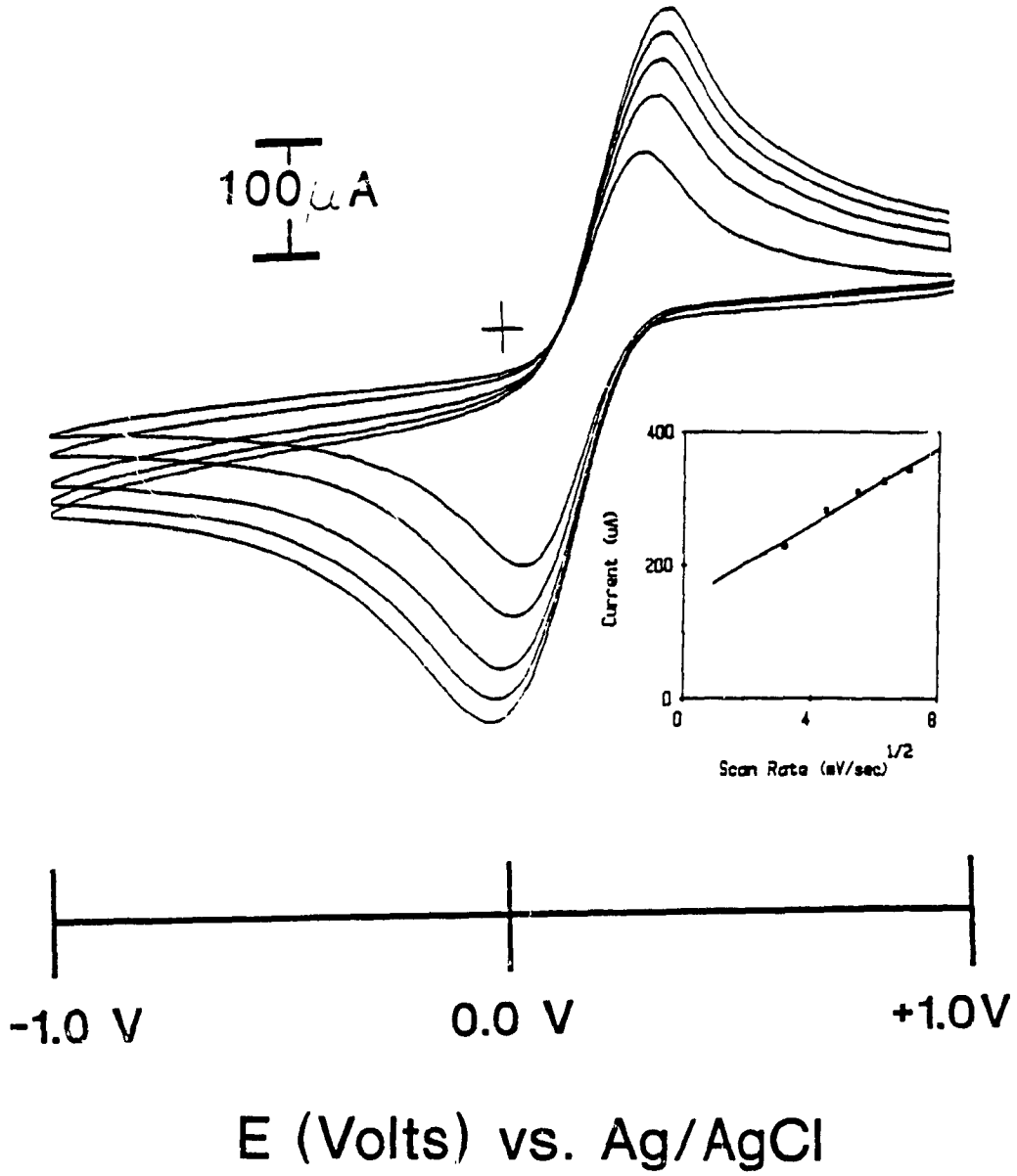

Figure 5.12 Cyclic voltammograms of a SnO_2/P2/$Ni(mnt)_2^{2-}$ modified electrode in contact with 2 mM $Fe(CN)_6^{3-/4-}$ in 0.1 M KCl. Scan rates were varied from 10→50 mV/sec. Inset shows plot of peak current versus (scan rate)$^{1/2}$.

being analyzed. A voltammogram of such an electrode prior to chronoamperometric experiments is shown in Figure 5.13. A similar shape was observed with a lesser quantity of redox couple. Both anodic and cathodic potential steps (-0.6 → +0.6 V and +0.6 → -0.6 V) were applied to the electrodes. A typical current decay and corresponding Anson plot are shown in Figure 5.14. The apparent diffusion coefficients ranged from 0.9 → 2.2 X 10^{-7} cm^2/sec with the lower values obtained for the anodic steps from -0.6 → +0.6 V indicating that the ferrocyanide species is more mobile than the ferricyanide in the film.

It is difficult to distinguish between the movement of ions through the film and charge propagation as a result of electron hopping between adjacent redox sites. The values of D_{app} for $Fe(CN)_6^{3-/4-}$ in the **P2** films appear consistent with ion movement in the film. They are roughly an order of magnitude larger than those obtained for $Ni(mnt)_2^{2-}$ in the same polymer film even though the concentration of the electroactive $Ni(mnt)_2^{2-}$ was about the same as the $Fe(CN)_6^{3-/4-}$ in the **P2** modified electrodes. These composite coatings were the only ones from the ion-exchange polymer category in this study to exhibit voltammetric waves for $Pt(mnt)_2^{2-}$ and $Ni(mnt)_2^{2-}$ in the polymer. In a way, the voltammetric characteristics of the SnO_2/**P2**/$Ni(mnt)_2^{2-}$ system resemble the results of Persaud and Langford with quaternized poly(4-vinylpyridine co-styrene) films (110). Enhanced diffusion of $Ni(mnt)_2^{2-}$ was obtained with the **P2** polymer films (D_{app} = 1 X 10^{-13} to 2.4 X 10^{-11} cm^2/sec for **QPVP** (110) modified SnO_2 electrodes versus 8.2 X 10^{-9} to 1.1 X 10^{-8} cm^2/sec for **P2** modified electrodes). This can rationalized as a lesser degree of electrostatic crosslinking between the hydrophilic sites in the **P2** polymer matrix.

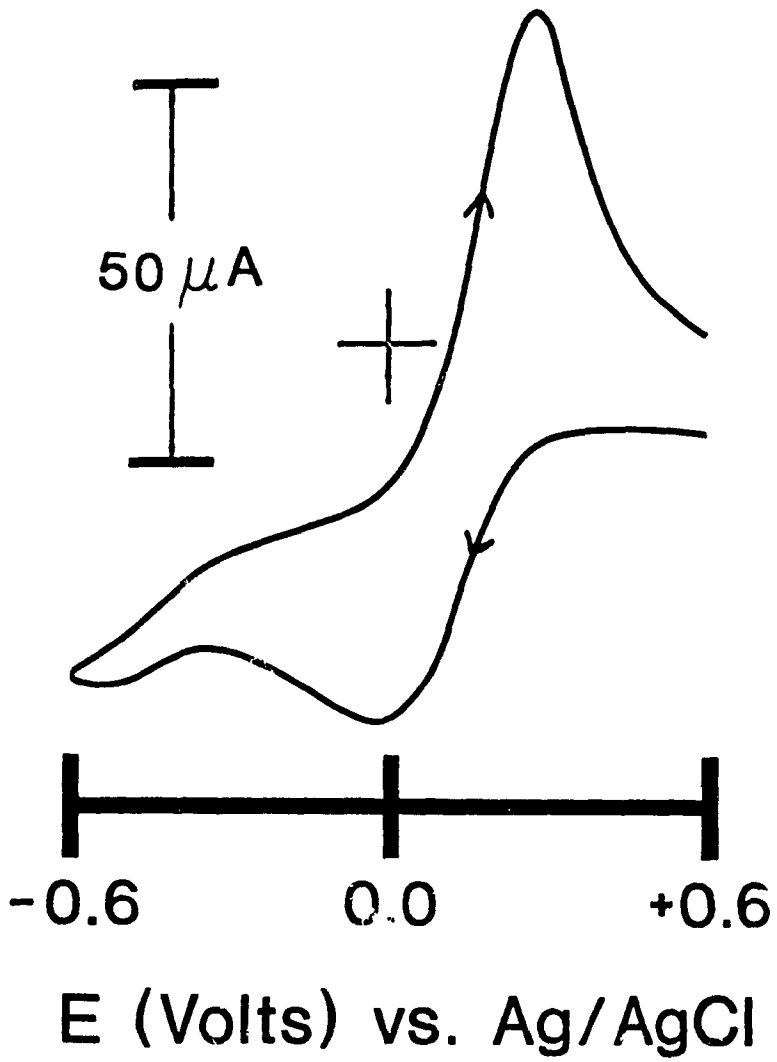

Figure 5.13 Cyclic voltammogram of a SnO_2/P2/Ni(mnt)$_2^{2-}$ modified electrode in contact with 0.1 M KCl after being soaked in $Fe(CN)_6^{3/4-}$ for 3 days, rinsed with distilled water, soaked in 0.1 M KCl for 2 hours, rinsed again with distilled water, then placed in the voltammetric cell prior to chronoamperometry.

Figure 5.14 Chronoamperometric current decay-time profile of a SnO_2/**P2**/$Ni(mnt)_2^2$ electrode containing $Fe(CN)_6^{3-/4-}$. Inset shows corresponding Anson plot of charge versus time$^{1/2}$.

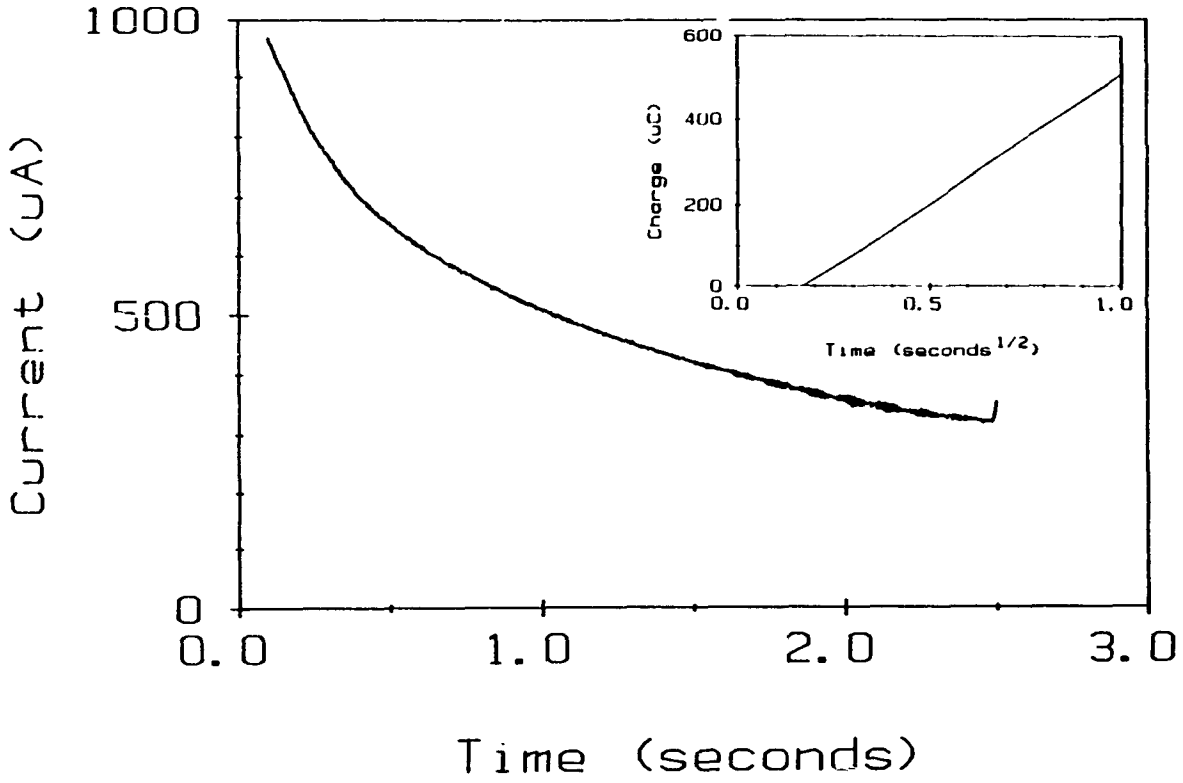

The **QPVP** polymer was probably extensively crosslinked by electrostatic interactions between cationic pyridinium groups and the anionic dyes. Salts of the pyridinium-$M(mnt)_2$ type are highly insoluble in most common organic solvents. The tetraethyl- and tetraethanol- ammonium salts of $Ni(mnt)_2^{2-}$ are quite soluble in organic solvents such as acetone, methanol and acetonitrile thereby creating solvent swollen domains in the polymer. The hydrophobic styrene and chloromethylstyrene groups may contribute to an environment which is more accommodating than the corresponding **QPVP** films. Both polymers possess different morphologies even under examination by optical microscopy. The **P2** modified electrodes appear more porous than their **QPVP** counterparts. It is evident that morphology plays a significant role in the behaviour of these polymers.

The internal morphology of the **P2** polymer films may resemble that of the **PB1** polymer blend films since the diffusion coefficients of $Fe(CN)_6^{3-/4-}$ in both these films are of the same order of magnitude. A major physical difference between the films is that the **P2** films are translucent when loaded with $Ni(mnt)_2^{2-}$ while the **PB1** polymer composites were transparent under the same conditions. The morphology of the films may be similar when placed in contact with an electrolyte solution where film swelling would occur in both cases. Peak separations for $Fe(CN)_6^{3-/4-}$ in voltammograms of the SnO_2/**P2** electrodes are larger than in the case for comparable SnO_2/**PB1** composite electrodes. This may limit photochemical processes.

5.2.2 Photoelectrochemistry of P2 Modified Electrodes Containing $Ni(mnt)_2^{2-}$ and $Pt(mnt)_2^{2-}$.

SnO_2/P2/$Ni(mnt)_2^{2-}$ electrodes were placed in 2 mM $Fe(CN)_6^{3-/4-}$ in 0.1 M KCl just prior to photoelectrochemical measurements. Continuous voltammetric cycling displayed that a limiting quantity of the redox couple was incorporated into the film within 20 minutes (Figure 5.15). Interestingly, the redox couple partitions rapidly into the film as indicated by the voltammetric waves of the first scan. A very large ΔE_p of 600 → 700 mV was noted signifying sluggish electron transfer at the polymer/electrode interface. The electrode then exhibited diffusion-limited charge transport of $Fe(CN)_6^{3-/4-}$ in the film with sluggish kinetics. This was typical for the **P2** polymer system.

Short circuit photocurrent transients are shown in Figure 5.16. In the absence of any chromophore, a small square wave response of ≈20 nA/cm² was observed for the SnO_2/P2 modified electrode in contact with $Fe(CN)_6^{3-/4-}$. Illumination of the SnO_2/P2/$Ni(mnt)_2^{2}$ electrode produced anodic photocurrents of 137→179 nA/cm² depending on the amount of $Ni(mnt)_2^{2}$ ion-exchanged in the film. These photocurrents reached a steady state value within 300 sec (usually less). The photocurrents were an order of magnitude smaller than those obtained for the **PB1** composite films described in chapter 4. The photocurrent transients displayed trap-controlled behaviour of charge carriers in the polymer. Lawrence *et al.* developed a model for trap-controlled migration of photogenerated charges in polymers of similar composition to **PB1** (131). It is not unlikely that such a model can be extended for most electroactive polymers with similar morphological characteristics. Essentially,

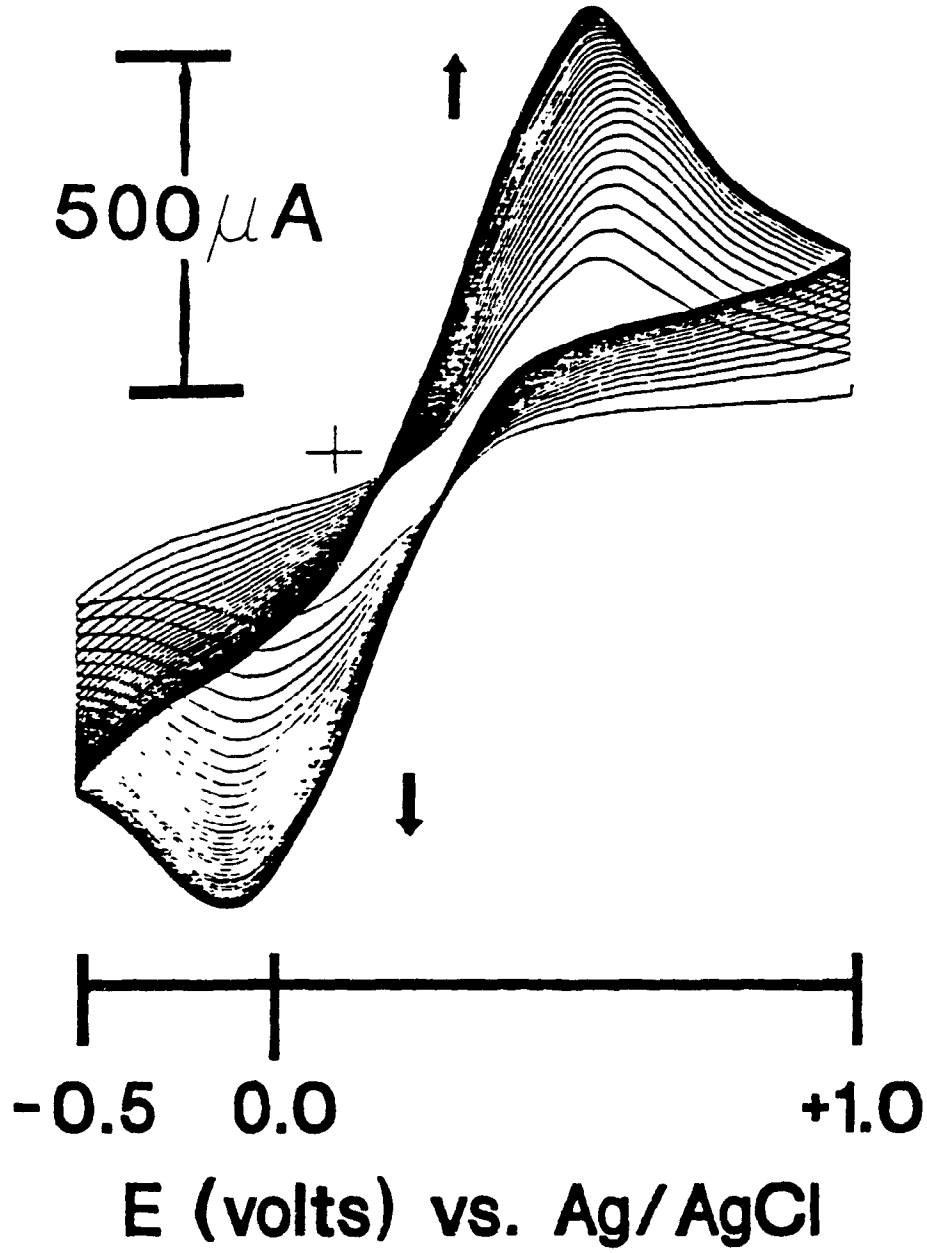

Figure 5.15 Cyclic voltammogram of a SnO_2/P2/Ni(mnt)$_2^{2-}$ modified electrode in contact with 2 mM $Fe(CN)_6^{3-/4-}$ in 0.1 M KCl prior to photoelectrochemical experiments. Maximum incorporation of $Fe(CN)_6^{3-/4-}$ requires 20 minutes. Scan rate = 100 mV/sec.

Figure 5.16 Short circuit photocurrent-time profiles for a SnO_2/P2/$Ni(mnt)_2^{2-}$ modified electrode in contact with (A) 0.1 M KCl and (B) 2 mM $Fe(CN)_6^{3-/4-}$ in 0.1 M KCl. White light illumination at 100 mW/cm² was filtered to remove UV (λ>400nm) and IR (water filter).

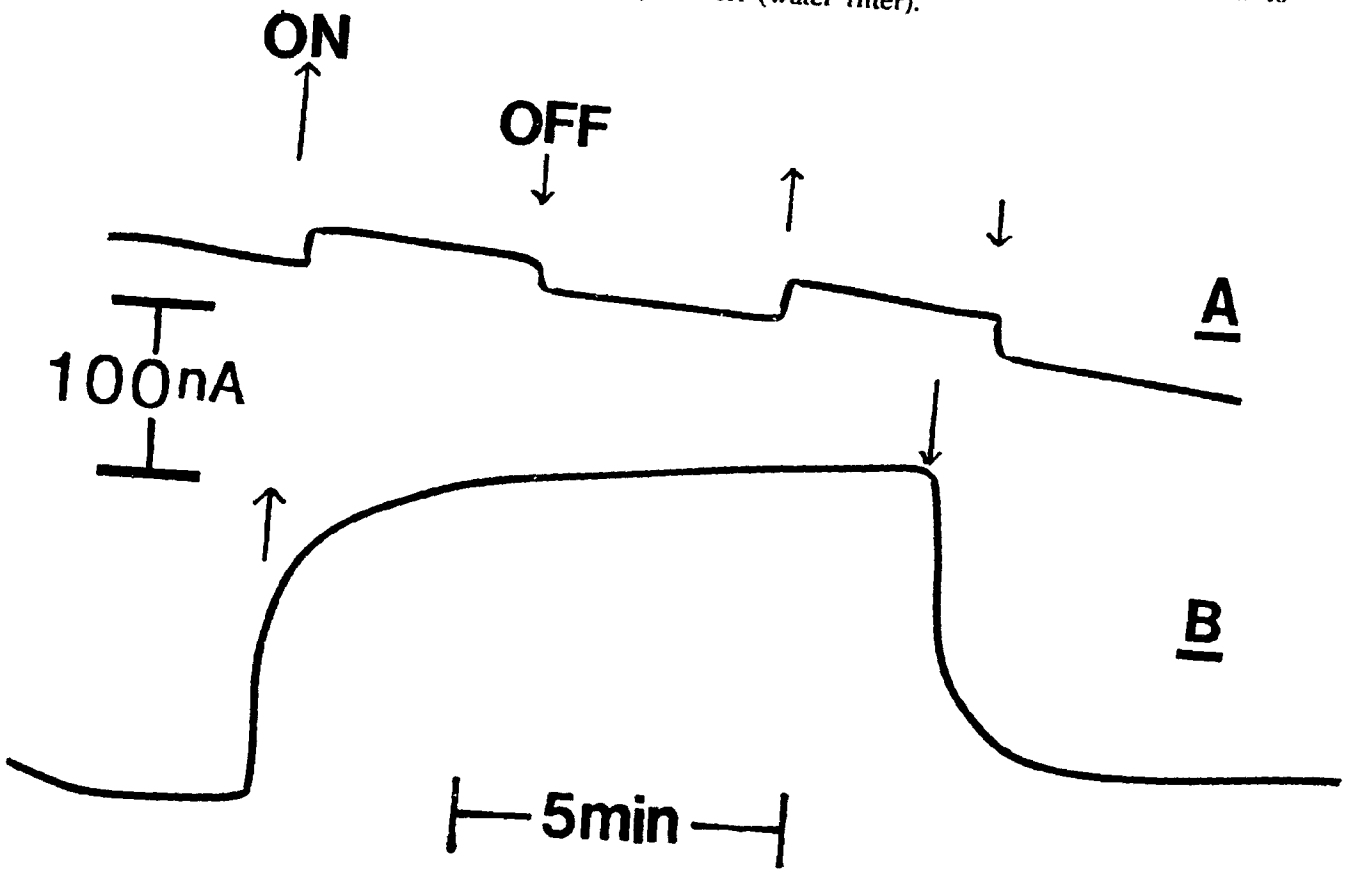

the model describes the trapping and thermal de-trapping of charge carriers from photo-excited dyes ion-exchanged into polymer matrices. The trapping and de-trapping states are a continuous distribution of localized states associated with local disorder defects of the polymer matrix. These states are intimately related to the molecular-ion states described in chapter 4.5.

The model proposes that the photocurrent rise and decay is the sum of two single exponential functions, with time constants relating the ratio of free electrons (carriers) to trapped electrons . On a molecular level, it is generally believed that electron transport proceeds through hydrophobic domains while ion transport is facile through hydrophilic domains and channels.

The **P2** polymer modified electrodes displayed some trapping characteristics as indicated by the photocurrent rise and decay transients. In this case, the chloromethylstyrene and styrene moieties of the **P2** matrix and the styrene and vinylpyridine moieties of the **PB1** polymer matrix are the hydrophobic portions of the polymers are associated with the traps. Charge trapping sites in the hydrophilic domains also exists as localized regions where electrostatic crosslinking is prominent. The time constants extracted from the fitted exponential data relate the response time of the shallow traps (τ_1) and the response time of the charge carriers through localized states (τ_2). These time constants can be related the ratio of free carriers to trapped carriers. Photocurrent rise data for SnO_2/**P2**/$Ni(mnt)_2^{2-}$ system were fitted to a exponential function yielding time constants of 2.2 sec and 48 sec for τ_1 and τ_2 respectively (Figure 5.17) (non-linear regression using the simplex method (113)). The data for the photocurrent decay fit well yielding 1.8 sec for τ_1

Figure 5.17 Short circuit photocurrent-time profiles for a SnO_2/P2/Ni(mnt)$_2^{2-}$ modified electrode in contact with 2 mM $Fe(CN)_6^{3/4}$ in 0.1 M KCl. Solid curve represents data fitted to the sum of two exponential functions.

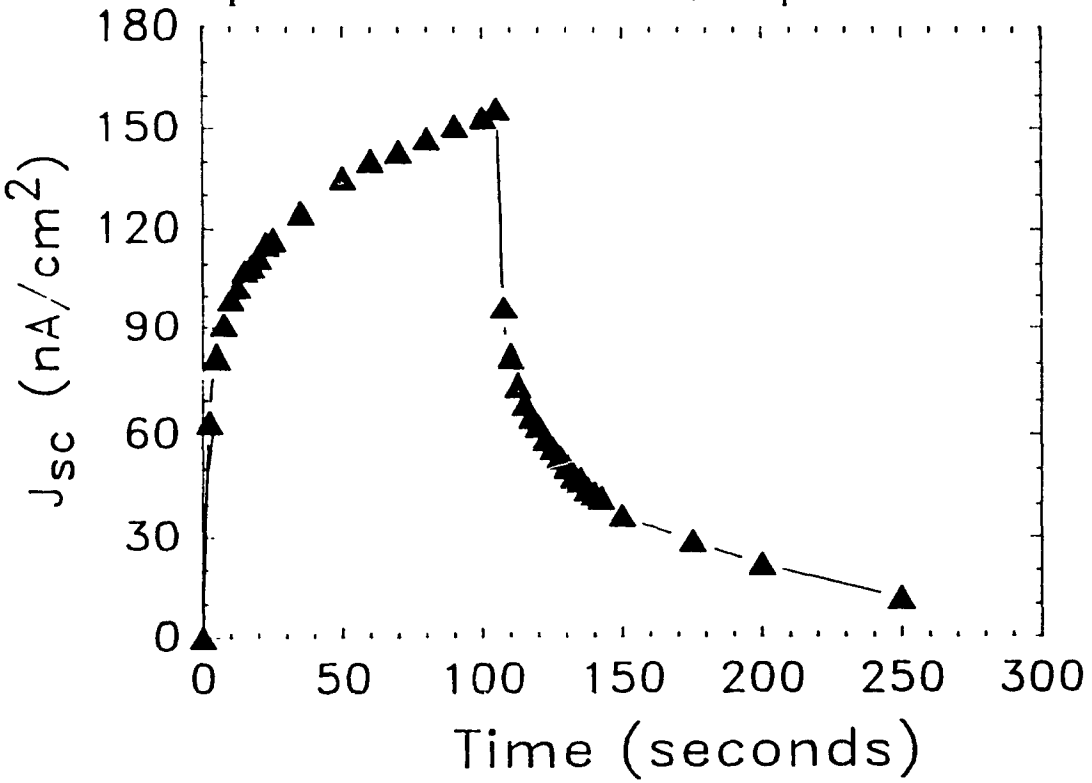

and 42 sec for τ_2. These time constants are similar for both the rise and decay indicating that the trapping and thermal de-trapping states are probably the same localized states. The photocurrent rise and decay time constants for the SnO_2/**PB1**/$Ni(mnt)_2^{2-}$ polymer films were determined by the same method. The rise in J_{sc} fit with time constants τ_1= 10.4 sec and τ_2= 72 sec. The decay of the photocurrent once light was turned off fit to the double exponential function yielding τ_1= 10.1 sec and τ_2= 173 sec (Figure 5.18). These values are consistent with a similar polymer film containing an anionic porphyrin dye, $ZnTPPS^{4-}$, examined by Ordoñez, Huang, and Lawrence (131). In the **PB1** polymer films the trapping and thermal de-trapping processes are slower but produce more photocurrent and are more probably related to the biphasic nature of the polymer blend.

The SnO_2/**P2**/$Ni(mnt)_2^{2-}$ system is a polymer composite displaying interesting ion-exchange properties and photoelectrochemical behaviour. The quaternized co-polymer appears to segregate into hydrophobic and hydrophilic domains. The hydrophobic domains are composed of styrene and chloromethylstyrene moieties. The molecular-ion state model can be adapted to approximate an energy diagram similar to Figure 4.13 using the donor and acceptor energy distributions of polystyrene. This can be done assuming that these distributions are the same for a styrene-chloromethylstyrene matrix (Figure 5.19). Charge injection from photoexcited $M(mnt)_2$'s would then proceed via energy levels associated with the styrene component located at -1.8 V versus NHE. This acceptor level is between the singlet and triplet state of the photoexcited dyes so that only the singlet state

Figure 5.18 Short circuit photocurrent-time profiles for a SnO_2/**PB1**/$Ni(mnt)_2^{2-}$ modified electrode in contact with 2 mM $Fe(CN)_6^{3-/4-}$ in 0.1 M KCl. Solid curve represents data fitted to the sum of two exponential functions

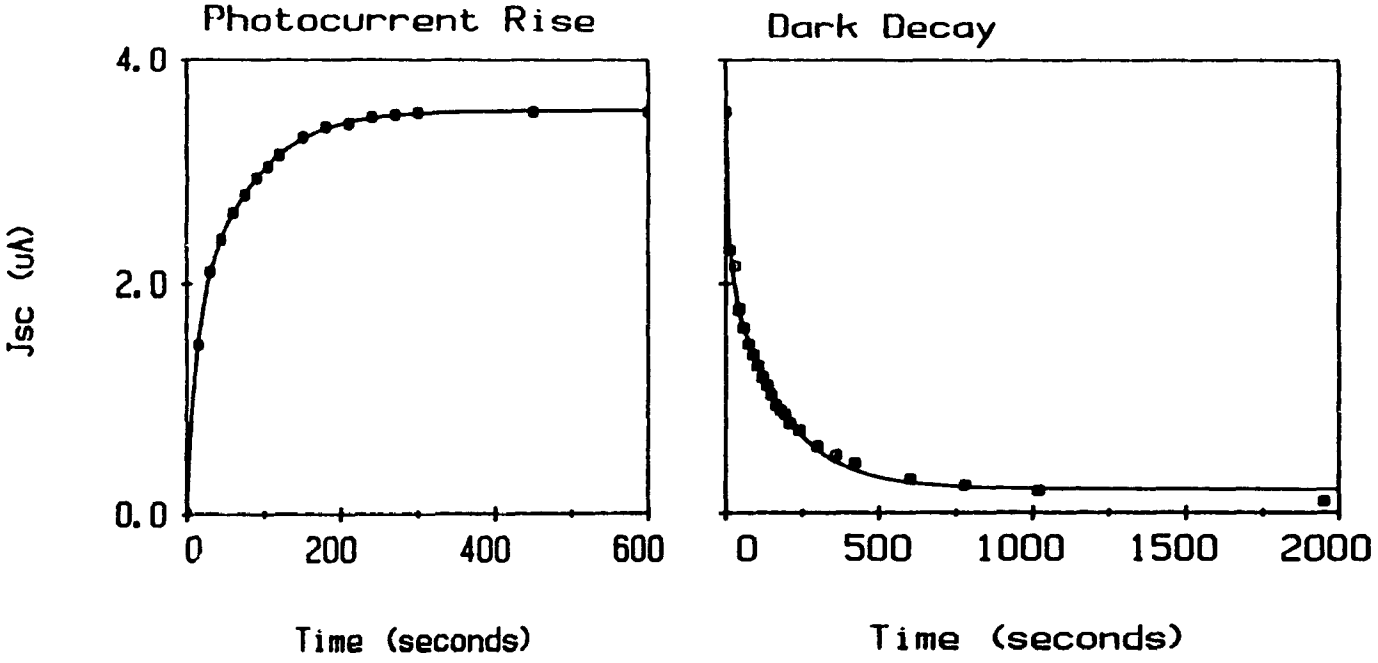

Figure 5.19 Energy level diagram for the SnO_2/P2/$M(mnt)_2^{2-}$ systems. The energy level for the chloromethylstyrene and styrene hydrophobic components of the P2 polymer were estimated from the reduction potentials of the monomers.

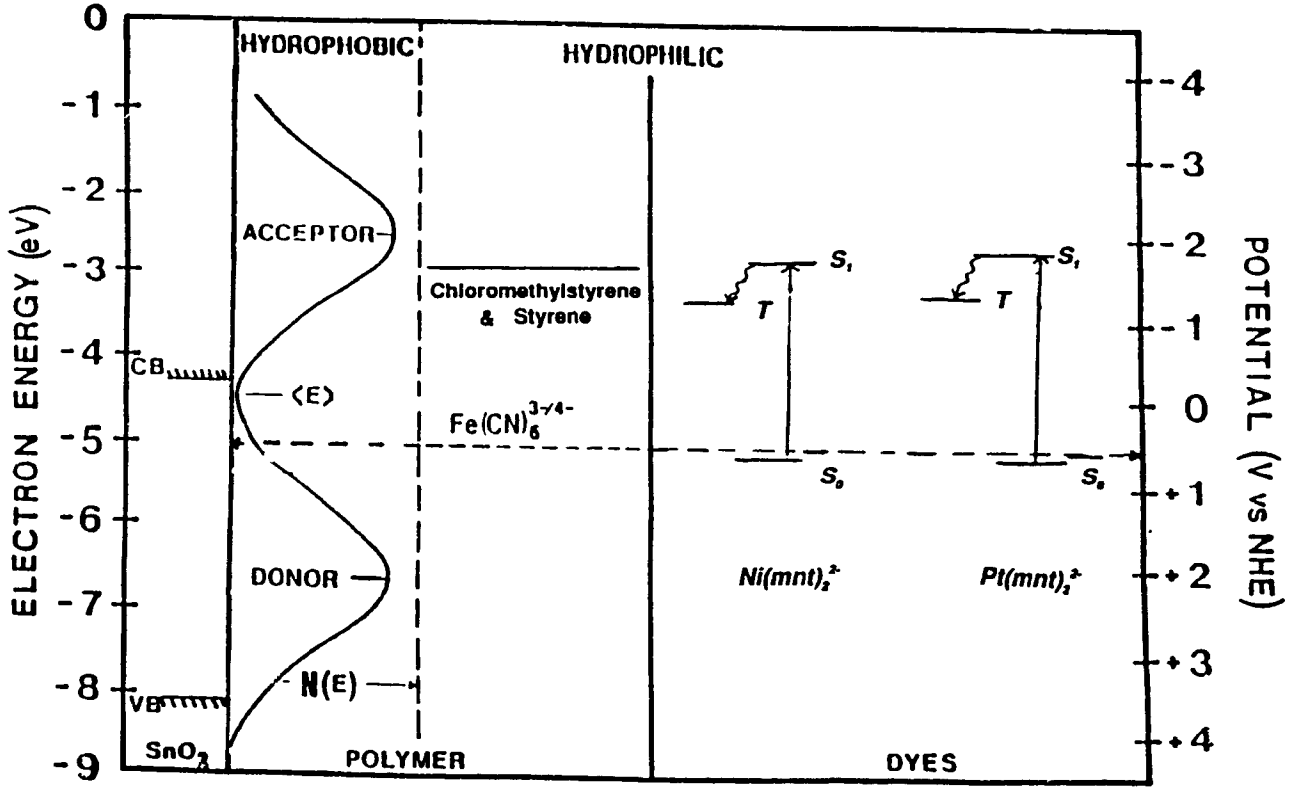

can transfer an electron in about 1 ns (or less). A limiting factor of the photocurrents is not the position of the acceptor level but the physical spacing between acceptor states. Trapping and de-trapping account for the reduced short circuit photocurrents. The results would imply to try a dye with a more reducing excited state in to get larger photocurrents with the **P2** polymer.

5.3 Electrochemistry and Photoelectrochemistry of Polymer Modified Electrodes with Ionically Conductive Polymer P4 and $M(mnt)_2^{2-}$

5.3.1 Electrochemistry of P4

This quaternized ion-exchange ternary co-polymer was synthesized according to a modification of the Anson based polymer **P1** as described in section 2.2.10. The fraction of styrene in the polymer was determined to be 25% versus 33% as in the P1 polymer case. Viscosity measurements indicated that the **P4** polymer had a higher molecular weight than the P1 polymer.

A film of the polymer was cast on SnO_2 electrodes from methanolic solution. Even at an expanded scale, the voltammetric waves normally seen for the nickel complex in the solution electrochemistry are missing. The polymer ion-exchanged the complex readily as indicated by red translucent color of the polymer coated electrode. The expected boundary layer signal is missing which indicates that the dye did not go through the polymer completely. Strong electrostatic interactions between the quaternary ammonium sites on the pendant groups of the polymer and the $M(mnt)_2^{2-}$ chromophore can account for the absence of voltammetric features.

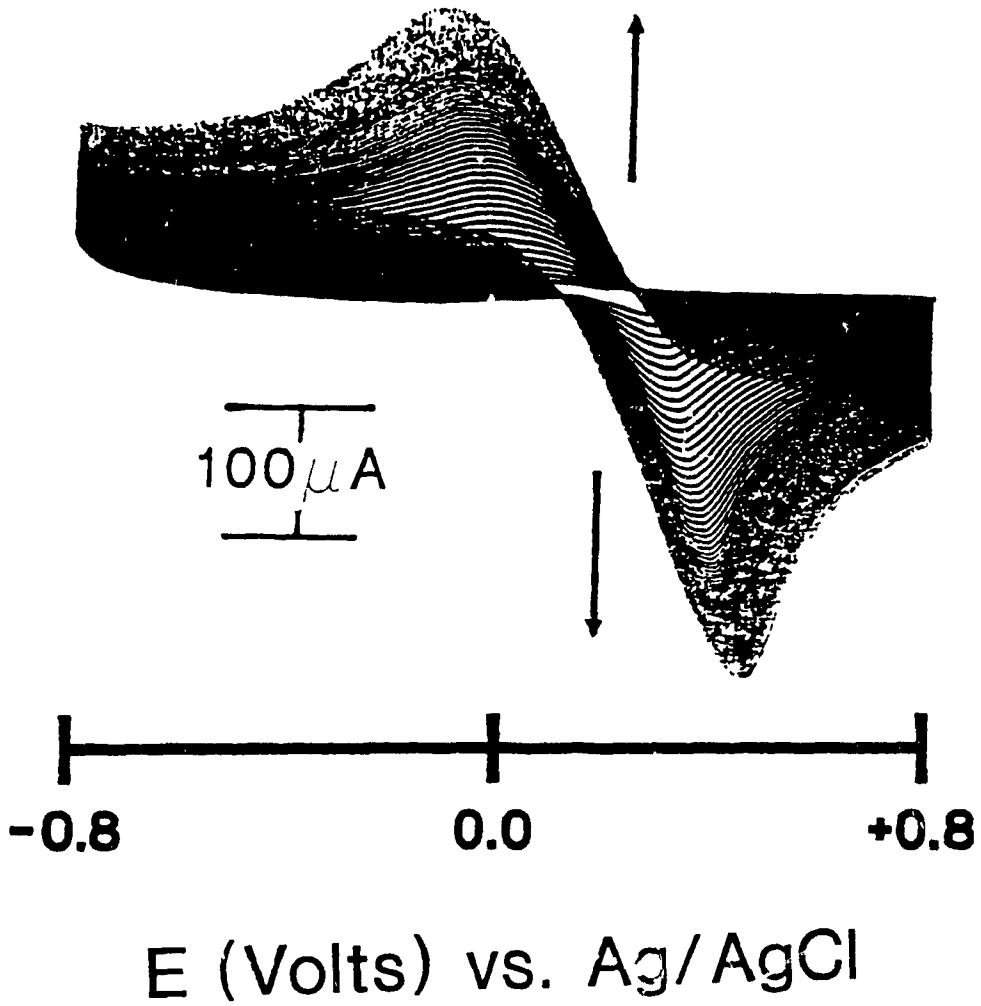

Figure 5.20 Cyclic voltammetry of a SnO_2/P4/$Ni(mnt)_2^{2-}$ modified electrode in contact with 2 mM $Fe(CN)_6^{3-/4-}$ in 0.1 M KCl. Maximum incorporation of $Fe(CN)_6^{3-/4-}$ requires 50 minutes. Scan rate = 100 mv/sec. Cathodic currents upwards.

The polymer film incorporates $Fe(CN)_6^{3-/4-}$ and broad voltammetric features of the redox couple were observed in this case. Figure 5.20 shows the incorporation of 2 mM $Fe(CN)_6^{3-/4-}$ into the film over a 50 minute time period during continuous voltammetric sweeping. The redox couple is retained for a lesser period than the **PB1** polymer when the electrode is soaked in 0.1 M KCl. The electrochemistry of the $Fe(CN)_6^{3-/4-}$ in this polymer in shown in Figure 5.21 as a function of scan rate. The inset displays a linear plot of peak current against the square root of the scan rate indicating a diffusion limited process of the ferro/ferricyanide couple. This process is sluggish and irreversible as indicated by the large ΔE_p in the scans. After leaving the electrode in $Fe(CN)_6^{3-/4-}$ for 3 days, the voltammetry shows progressively worse irreversible behaviour (Figure 5.22). These changes reflect a modification in internal morphology over this time period. This system was not as stable as the other polymer modified electrodes discussed above.

5.3.2 Photoelectrochemistry of P4

In the absence of any dye, the polymer modified electrode displayed no photocurrent. Electrodes containing either $Pt(mnt)_2^{2-}$ or $Ni(mnt)_2^{2-}$ were soaked in 2 mM $Fe(CN)_6^{3-/4-}$ in 0.1 M KCl for 1 hour prior to photoelectrochemical measurements. The short circuit photocurrents were in the range of 55-63 nA/cm^2 with a much slower rise and decay profile than the SnO_2/**PVP**/$Ni(mnt)_2^{2-}$ or SnO_2/**PB1**/$Ni(mnt)_2^{2-}$ system (Figure 5.23). The transport of charge carriers in this polymer system can be explained by a trap controlled process with low carrier mobilities. The material contains physical defects such as chain ends, hydrophilic regions and pores which result in localized electronic states. The sluggish diffusion

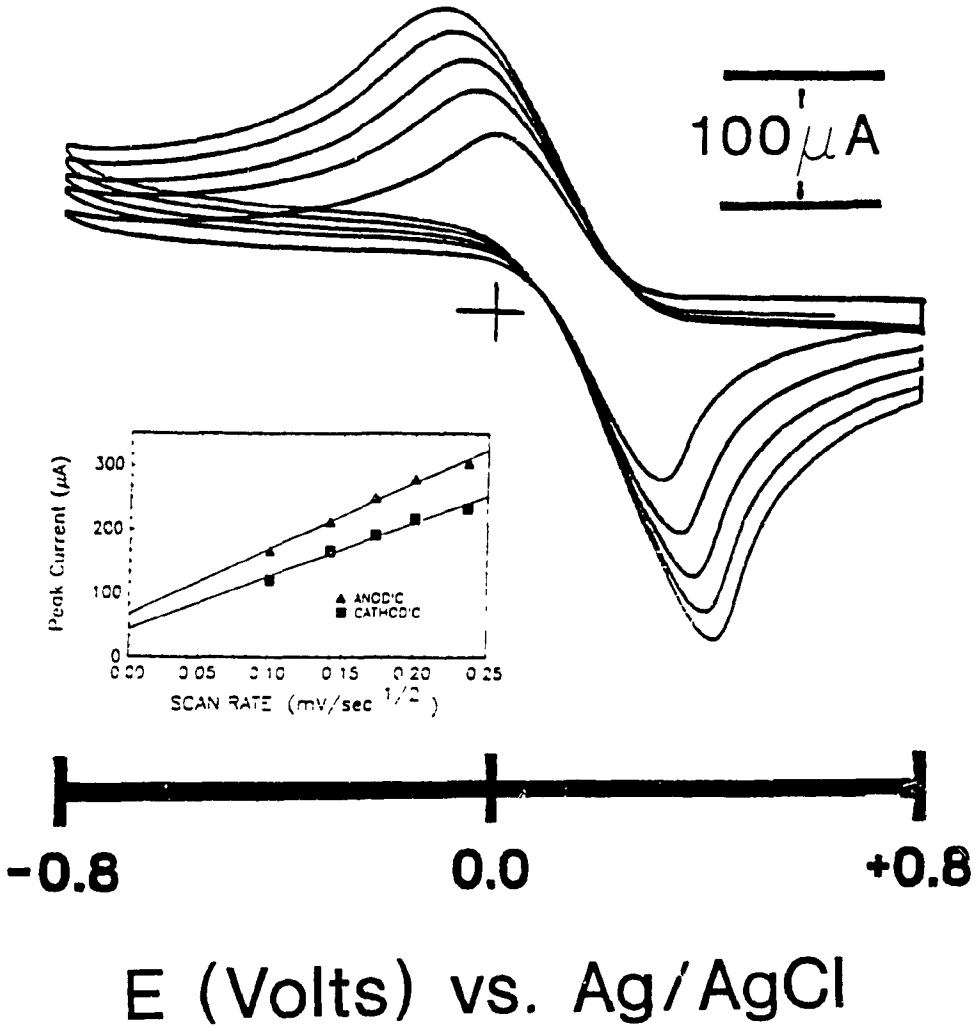

Figure 5.21 Cyclic voltammetry of a SnO_2/P4/$Ni(mnt)_2^{2-}$ modified electrode in contact with 2 mM $Fe(CN)_6^{3-/4-}$ in 0.1 M KCl. Scan rates were varied from 10→50 mV/sec. Cathodic currents upwards.

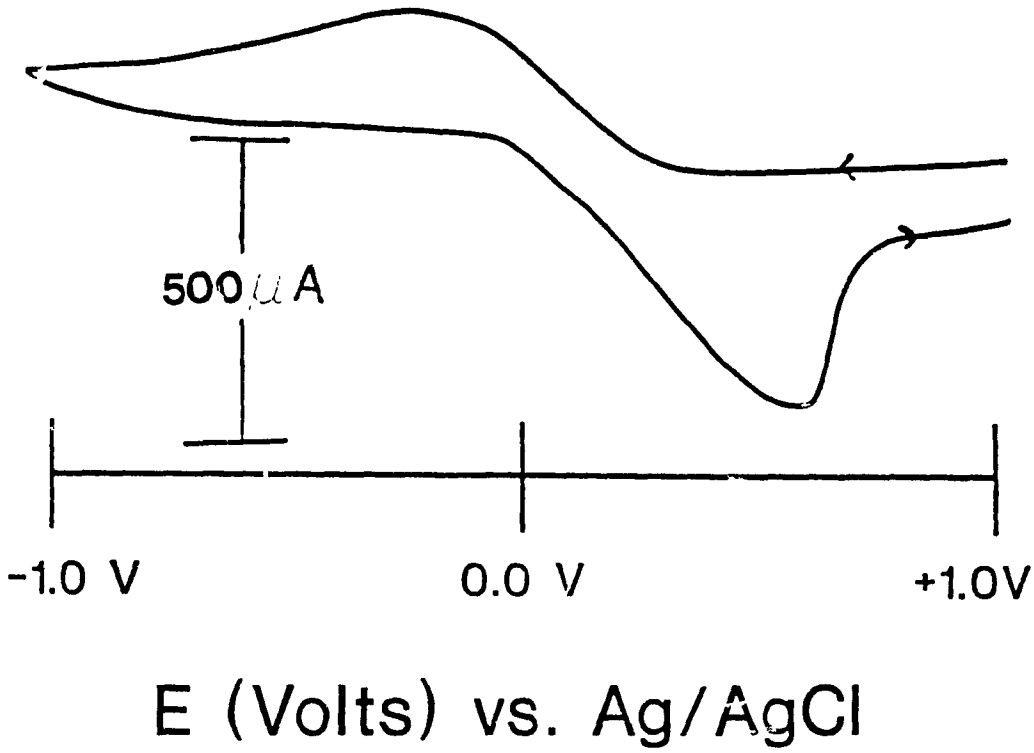

Figure 5.22 Cyclic voltammogram of a SnO_2/**P4**/$Ni(mnt)_2^{2-}$ modified electrode in contact with 2 mM $Fe(CN)_6^{3-/4-}$ in 0.1 M KCl after 3 days.

Figure 5.23 Short circuit photocurrent-time profile for a SnO_2/P4/$Ni(mnt)_2^{2-}$ modified electrode in contact with 2 mM $Fe(CN)_6^{3-/4-}$ in 0.1 M KCl.

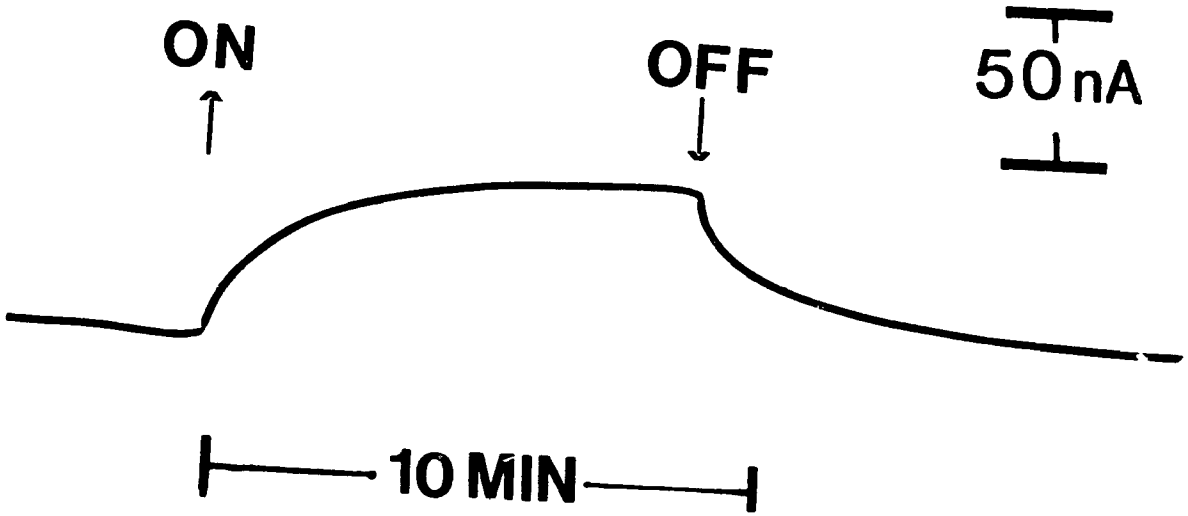

process and irreversible voltammetry of the **P4** system indicate that charge carriers (ions or electrons) are limited by the available sites for redox processes even where there exists strong electrostatic interactions of the dye to the polymer. The molecular-ion state model for this polymer is essentially that of a polystyrene based system which is similar to that of **P2** (Figure 5.19) and possesses sluggish electrochemical behaviour. The acceptor states for a purely polystyrene based polymer are slightly more positive in energy (i.e. there is a slightly greater density of sites available for electron injection). In view of the results presented here, it appears that ionic mobility and polymer morphology play an major role in the dark and photo-induced electrochemical processes for the **P4** system. The photocurrents are relatively small and sluggish for any type of useful device application.

5.4 Electrochemistry and Photoelectrochemistry of Polycarbonate Modified Electrodes Containing $Pt(mnt)_2^{2-}$ or $Ni(mnt)_2^{2-}$.

Polycarbonate resin modified electrodes containing $Pt(mnt)_2^{2-}$ or $Ni(mnt)_2^{2-}$ were prepared as described in section 2.3.2. This polymer, like nylon, is a crystalline thermoplastic with good mechanical properties. These properties stem in part from the relatively high ordering in the amorphous regions and considerable disordering in the crystalline regions (136). The electrochemistry of $Ni(mnt)_2^{2-}$ or $Pt(mnt)_2^{2-}$ is not seen in these modified electrodes in 0.1 M KCl. Even the redox couple is electrochemically silent indicating the insulating nature of the polycarbonate matrix (Figure 5.24). Under white light irradiation, small photoanodic currents ($\approx 35 \pm 5$ nA/cm^2) were recorded with charging and discharging type

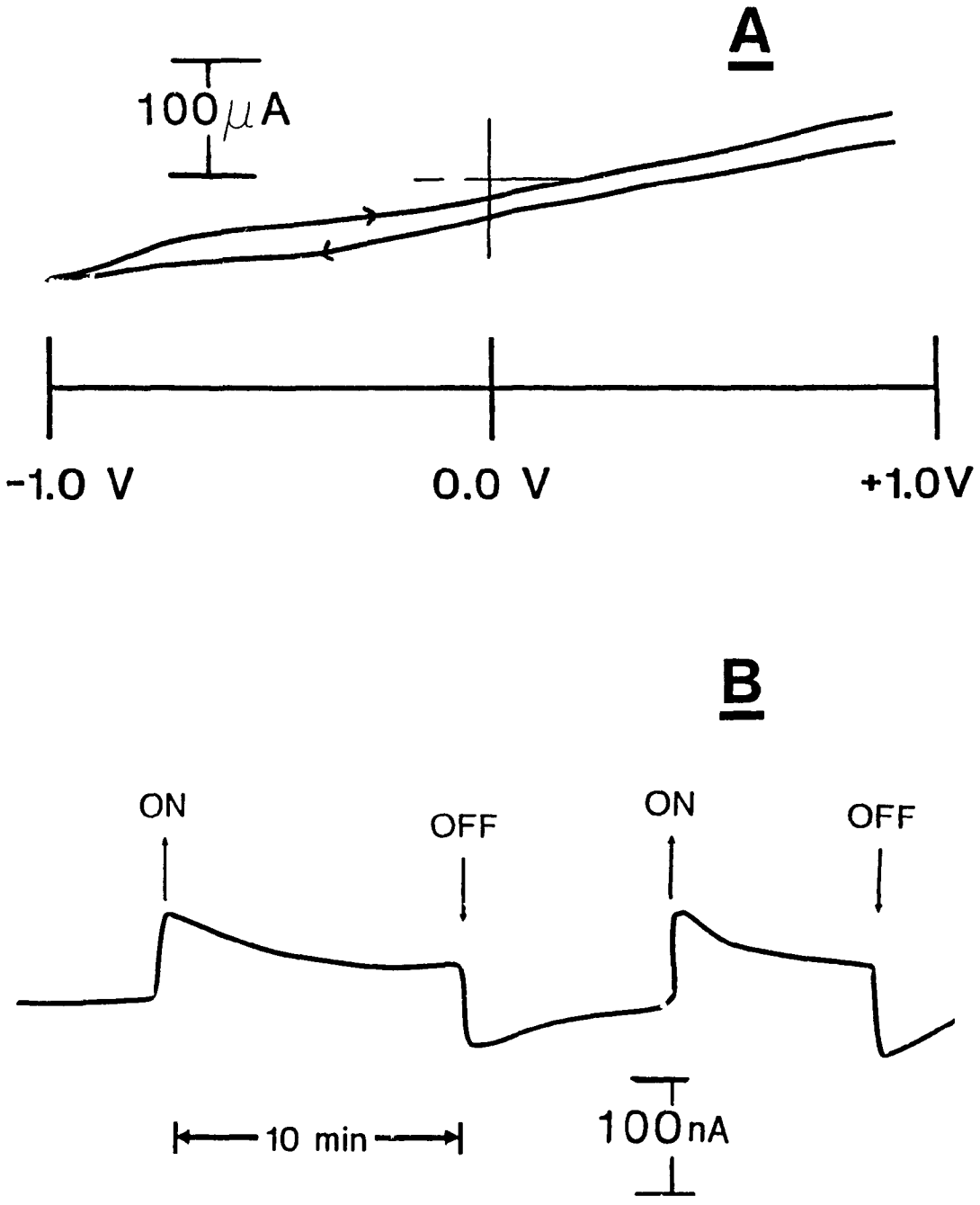

Figure 5.24 (A) Cyclic voltammogram of a SnO_2/**Polycarbonate**/$Ni(mnt)_2^{2-}$ modified electrode in contact with 2 mM $Fe(CN)_6^{3-/4-}$ in 0.1 M KCl. Scan rate = 100 mv/sec. (B) Short circuit photocurrent-time profile of a SnO_2/**Polycarbonate**/$Ni(mnt)_2^{2-}$ modified electrode in contact with 2 mM $Fe(CN)_6^{3-/4-}$ in 0.1 M KCl. White light illumination at 100 mW/cm^2 was filtered to remove UV (λ>400nm) and IR (water filter).

transients (Figure 5.24). During the light-on sequence, the charge integrated from the maximum to the steady value equals to 4.6 μC while the during the light-off process (discharging) the equivalent integration yields 4.3 μC. This behavior is analogous to the one reported by Minami *et al.* for the photoelectrochemical behaviour of copper phthlocyanine films on SnO_2 transparent electrodes (137). The transients were treated as a photo-induced electrical capacitance at the SnO_2/dye interface. Dye molecules ($Ni(mnt)_2^{2-}$ or $Pt(mnt)_2^{2-}$) in direct contact with the electrode can tranfer an electron to the SnO_2 surface. This double layer capacitance is created when the light is turned on and then discharges when the light is turned off.

These polymer films are electrical insulators with poor ionic, redox ,or electrical conduction. Polycarbonate does not possess desirable qualities for the incorporation of ionic chromophores, and the subsequent use as a photoelectrochemical device.

5.5 Electrochemistry and Photoelectrochemistry of PV1 Modified Electrodes.

The polyviologens are redox polymers which transport charge presumably by a site to site electron-hopping mechanism. **PV1** is a poly(styrene-*co*-chloromethylstyrene) pendant viologen polymer (**P3**). Benzene solutions of this polymer formed translucent yellow films on SnO_2. Viologen polymers were investigated since viologen-$M(mnt)_2$ form novel salts with inter-ion photophysical properties.

5.5.1 Electrochemistry of PV1 Modified Electrodes

The SnO_2/**PV1** polymer modified electrodes were electroactive in background 0.1 M KCl. The electroactivity arises from the viologen groups of the quaternized chloromethylstyrene sites. Figure 5.25 shows a cyclic voltammogram of an SnO_2/**PV1** electrode in background electrolyte with quasi-reversible peaks at -0.60 V and -0.74 V vs. Ag/AgCl. The anodic peak is sharper indicating adsorption of the reduced viologen species on the surface of the electrode. The polymer film became blue-violet at potentials more cathodic than -0.70 V indicating the formation of a viologen cation radical species.

Voltammetric waves for $M(mnt)_2^{2-}$ (M=Pt, Ni) in electrodes of the type SnO_2/**PV1**/$M(mnt)_2^{2-}$ were absent. The polymer electrodes did not incorporate much $Fe(CN)_6^{3-/4-}$ (Figure 5.25). This can be accounted for by the highly hydrophobic nature of this polymer. **PV1** was cast from a benzene solution. Although $Ni(mnt)_2^{2-}$ was readily ion-exchanged from acetonitrile solutions, the polymer film displayed hydrophobic qualities (poor wetting of the film surface) when placed in contact with electrolyte or the redox couple.

5.5.2 Photoelectrochemistry of SnO_2/PV1/$Ni(mnt)_2^{2-}$ Electrodes.

Despite the small quantity of $Fe(CN)_6^{3-/4-}$ incorporated into the film, small anodic photocurrents were recorded for this redox based polymer modified electrode. The square wave shape of the photocurrent transient is depicted in Figure 5.26. There appeared to be slight capacitative effects at the moment when the electrode was illuminated and when the light source was removed. This is consistent with the poor adhesion of the **PV1** polymer films to the surface of the SnO_2 electrodes.

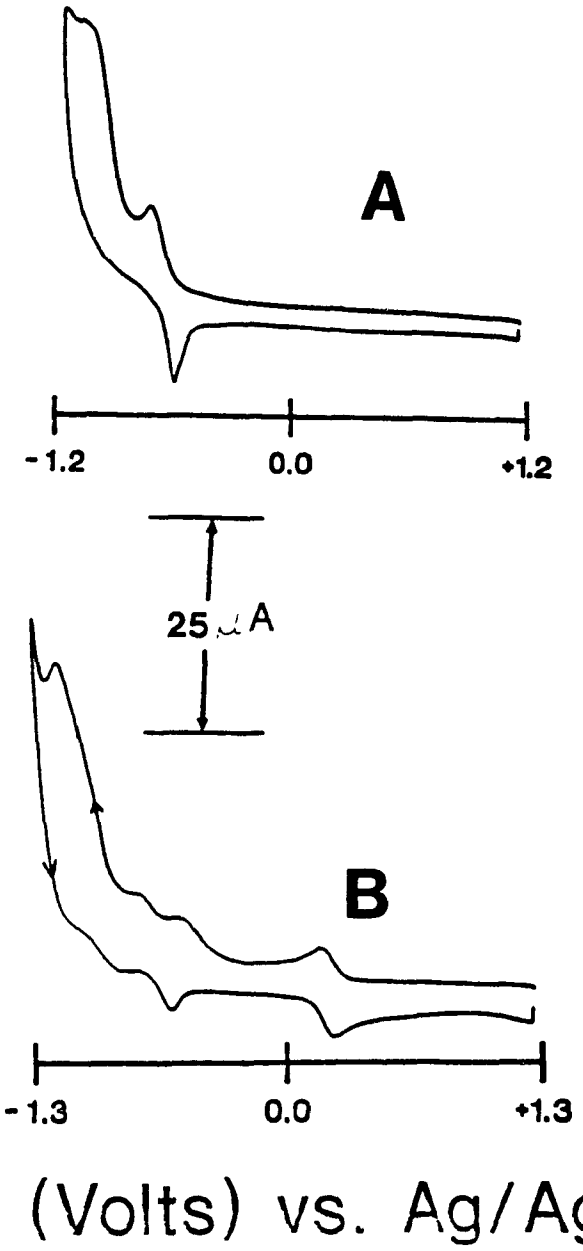

Figure 5.25 (**A**) Cyclic voltammogram of a SnO_2/**PV1** modified electrode in contact with 0.1 M KCl. (**B**) Cyclic voltammogram of a SnO_2/**PV1**/Ni(mnt)$_2^{2-}$ electrode in contact with 2 mM $Fe(CN)_6^{3-/4-}$ in 0.1 M KCl. Scan rate = 100 mv/sec. Cathodic currents upwards.

Figure 5.26 Short circuit photocurrent-time profile for a SnO_2/PV1/$Ni(mnt)_2^{2-}$ modified electrode in contact with 2 mM $Fe(CN)_6^{3-/4-}$ in 0.1 M KCl. White light illumination at 50 mW/cm^2 was filtered to remove UV (λ>400nm) and IR (water filter).

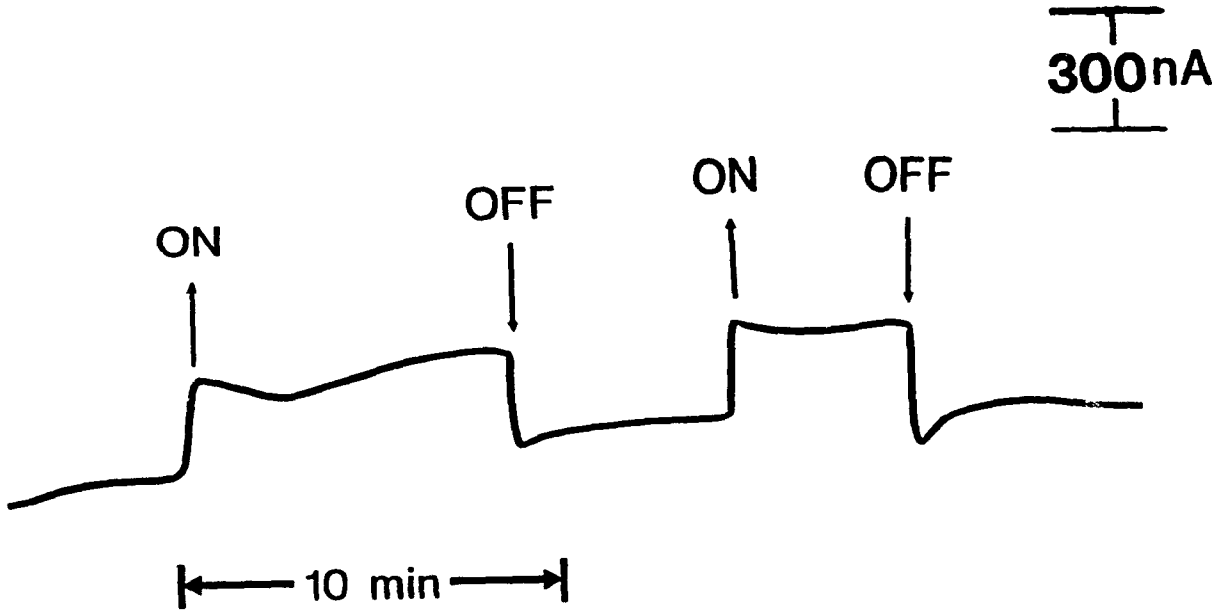

After 30 minutes of photoelectrochemical studies, the polymer film peeled away from the electrode SnO_2 surface.

Short circuit photocurrents of 320 ± 70 nA/cm^2 were recorded at a white light intensity of 50 mW/cm^2 during the period that the film remained on the electrode. The **PV1** polymer system exhibited quasi-reversible voltammetric behaviour with respect to the viologen and $Fe(CN)_6^{3-/4-}$ sites. It is possible that electrostatic interactions between the viologen and mnt complex reduced the electroactivity of the complex to a non detectable signal. The actual mechanism of the electroinactivity is unknown. The redox polymer displayed capacitative photocurrent-time transients under the experimental conditions but poor diffusion characteristics and adhesion to the electrode. The hydrophobicity of the matrix played a significant role in the poor adhesion of the film to the SnO_2 electrode. Charge transport through the **PV1** matrix is believed to occur via electron hopping between adjacent viologen sites with migration of counterions through the film being a limiting factor.

5.6 Characterization of a Redox Polymer Based on PXV Modified Electrodes Containing $M(mnt)_2^{2-}$.

Polymeric viologens with electroactive sites in the polymer backbone were prepared via a simple route as described by Factor and Heinsohn (107). Aqueous solutions of this polymer were cast on SnO_2 substrates yielding yellow films. The halogen counterions were ion-exchanged for dianionic $M(mnt)_2$'s from organic solvents. These polyviologens form interesting complexes with both $Pt(mnt)_2^{2-}$ and

$Ni(mnt)_2^{2-}$. The photophysical behaviour of viologen-mnt complexes was discussed in chapter 3. It is hoped that the interaction between these dianions and the cationic polymer would provide a suitable matrix for photoinduced electron (or charge) transfer to occur.

The molecular-ion states of poly-(p-xylyl viologen) were not studied by Duke and Fabish. However, the acceptor level for charge injection for viologen moieties would lie close to the redox potential for polymeric viologen. This value is more positive in absolute energy than pyridine levels in **PVP** or the **PB1** polymer blend. The acceptor levels will be distributed in the usual way about this average but the width of the distribution is not available.

5.6.1 Spectroscopic Characterization of PXV-$M(mnt)_2^{2-}$ Complexes.

Films on modified electrodes of the type SnO_2/**PXV**/$M(mnt)_2^{2-}$ were insoluble in most organic solvents except for DMF and DMSO. DMF was chosen as the solvent for removing the polymer and metal complex from the tin oxide substrates. Spectra were also obtained as cast films on SnO_2 substrates.

The **PXV**-bromide is a water soluble polymer which exhibited strong absorbance at 260 nm (ε=2.8 X 10^4) in good agreement with published results (λ_{max}= 260 nm, ε=2.0 X 10^4 (107)). A deoxygenated aqueous solution of the polymer could easily be reduced by adding a small amount of sodium dithionite to the cuvette (Figure 5.27). The bandshape and λ_{max} in the visible spectrum of the reduced viologen solution is very similar to that reported for reduced benzyl viologen (BV) under conditions where dimerization is prevalent. Monomeric $BV^{+\cdot}$ absorbs at 604 nm while the dimer absorbs at 540 nm (138). The λ_{max} of the

Figure 5.27 Near-UV and visible absorption spectrum of **PXV**-Br in water reduced under anaerobic conditions with $Na_2S_2O_4$.

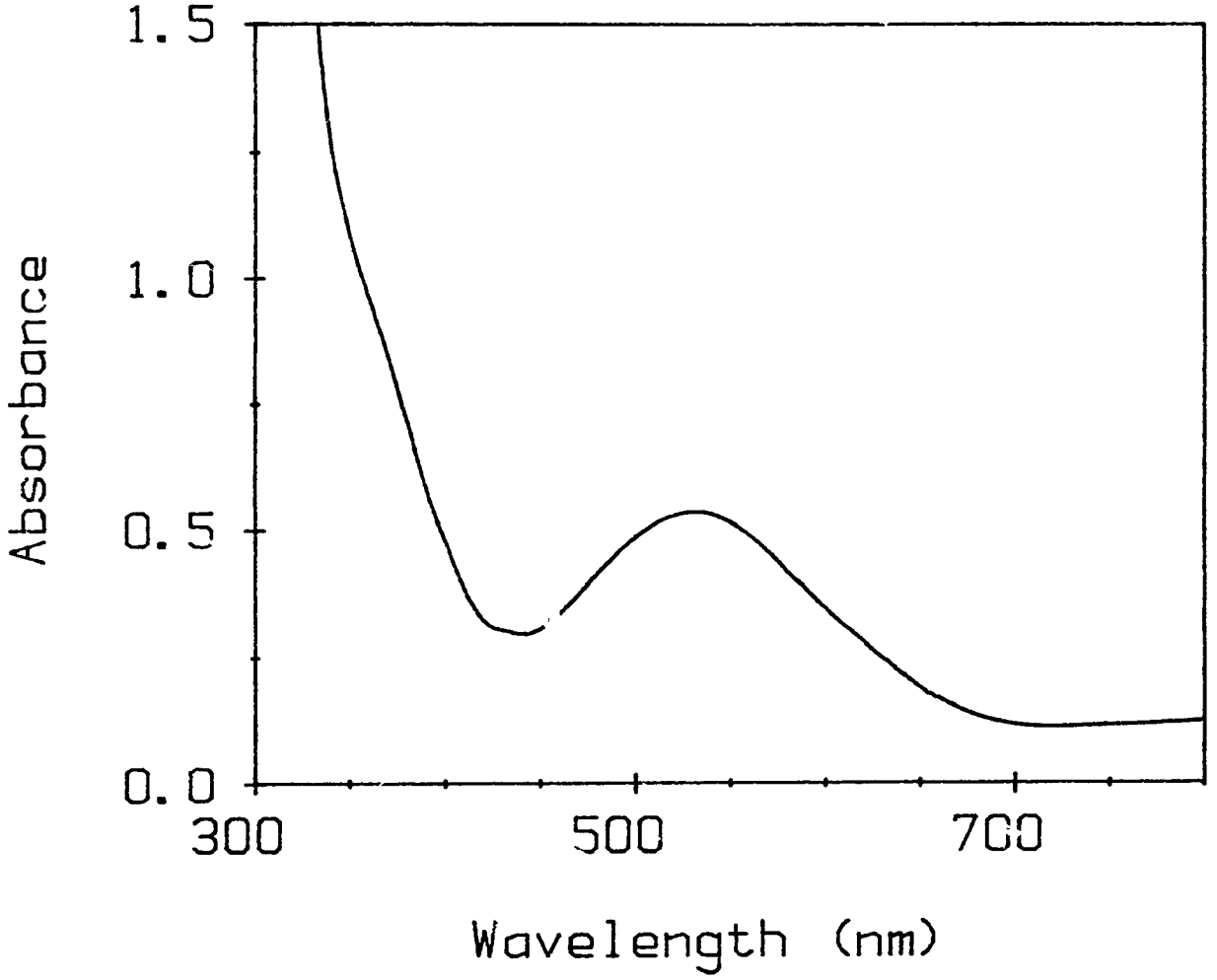

spectrum shown in FIgure 5.27 is bathochromically shifted to 532 nm indicating extensive intramolecular association of the reduced species in solution.

SnO_2/**PXV**/$Ni(mnt)_2^{2-}$ modified electrodes display absorption peaks in the visible and near-IR. The 480 nm band is attributable to the MLCT of $Ni(mnt)_2^{2-}$ and a broad band at *ca.* 890 ± 15 nm (average of 6 separate electrodes) is suggestive of a weak charge transfer band in the **PXV**-$Ni(mnt)_2^{2-}$ ion pair. No other mechanism can account for this novel band. The modified polymer film was dissolved from the electrode in DMF yielding a sharper peak in the near-IR at 896 nm (Figure 5.28). The visible spectrum of this solution displayed two peaks at 384 nm and 478 nm from CT bands of the $Ni(mnt)_2^{2}$ and a shoulder at 555 nm attributed to partially reduced viologen units in the **PXV**. This latter result is consistent with fluorescence data in chapter 3.

The vibrational spectra of **PXV** and **PXV**-$Ni(mnt)_2^{2}$ films were investigated to obtain information on the interactions in the polymer dye complex. The FTIR spectrum for **PXV** corresponded closely to a published spectrum for a similar polyviologen (139) (Figure 5.29). The most pronounced peak in the FTIR spectrum of **PXV** was attributed to ν(C=N) at 1631 cm^{-1}. Other ν(C-N) and ν(C-C) peaks at 1445 cm^{-1} and 1155 cm^{-1} were also prominent. Ion-exchange of $Ni(mnt)_2^{2}$ into the **PXV** matrix resulted in the appearance of several peaks due to the mnt with strong absorption at 2191 cm^{-1} (ν(C≡N)), 1489 cm^{-1} (ν(C=C)), and weak absorption at 1105 cm^{-1} (π(C-CN)) and at 865 cm^{-1} (ν(C-S)) (Figure 5.29). There was the appearance of new peaks at 1455, 1464, 1475, 1504, 1540, and 1575 cm^{-1}. Incorporation of $Ni(mnt)_2^{2}$ in **PXV** shifted the peaks at 1219 cm^{-1} and 1155 cm^{-1} to

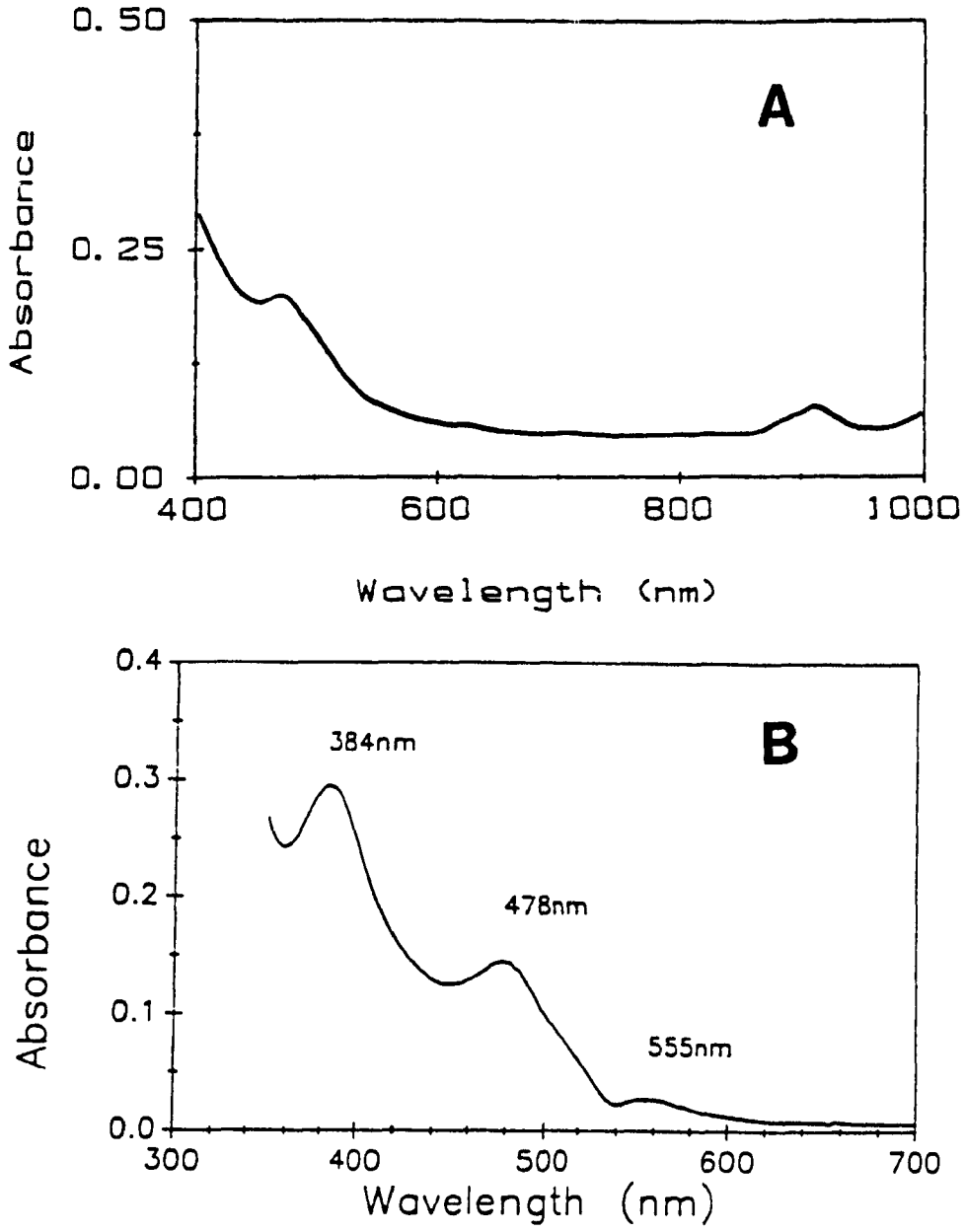

Figure 5.28 (**A**) Visible and near-IR absorption spectrum of a **PXV**/Ni(mnt)$_2^{2-}$ polymer film dissolved in DMF and (**B**) near-UV and visible absorption spectrum of same solution.

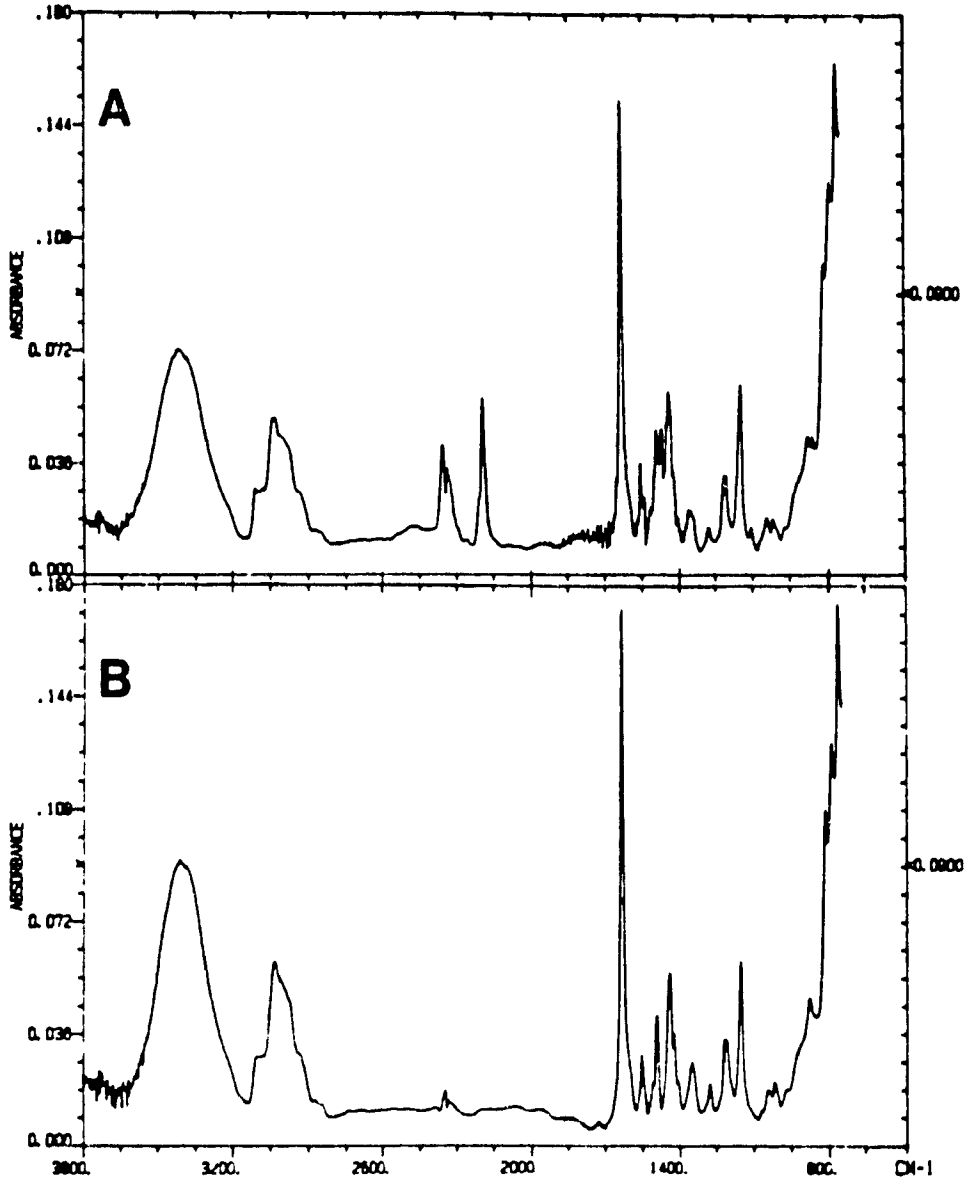

Figure 5.29 (A) FTIR spectrum of PXV/Ni(mnt)$_2^2$ on AgCl and (B) of PXV-Br on AgCl.

lower energy by 4 and 6 cm^{-1}, respectively. The distinct shifts in peak position and the appearance of additional peaks suggests that strong interactions between the $Ni(mnt)_2^{2-}$ and **PXV** exists altering the allowed modes of molecular vibration between the two molecules. This is the first reported IR spectrum for poly-(xylyl viologen) bromide and the **PXV**-$Ni(mnt)_2^{2-}$ complex.

The spectroscopic results presented in this section in conjunction with the photophysical behaviour described in chapter 3 suggests that photo-excited $Ni(mnt)_2^{2-}$ will transfer charge to viologen sites on SnO_2/**PXV**/$Ni(mnt)_2^{2}$ modified electrodes. Hopping processes would then transport the charge carriers to the SnO_2 electrode.

5.6.2 Electrochemistry of PXV Modified Electrodes.

Voltammetry of SnO_2/**PXV**/$Ni(mnt)_2^{2-}$ electrodes in 0.1 M KCl exhibited two sets of quasi-reversible waves (Figure 5.30). The first set of broad waves at E_{pa}=+0.53 V and E_{pc}=+0.03 V vs Ag/AgCl are associated with the metal complex incorporated in **PXV**. These peaks may be double peaks with the more cathodic set attributed to the CT ion-pair. In a polymer matrix, it was difficult to tell. The reduction potentials for the electroactive moieties of **PXV** was $E_{1/2}$ [$\mathbf{PXV^{2+} \rightarrow PXV^{+\cdot}}$] = -0.43 V and $E_{1/2}$ [$\mathbf{PXV^{+\cdot} \rightarrow PXV^{0}}$] = -0.84 V. These potentials are in agreement with published results (107). The presence of $Ni(mnt)_2^{2}$ voltammetric waves is in contrast with the behaviour of **PV1** in which no voltammetry for the complex was observed. A voltammogram recorded after 30 minutes in background electrolyte illustrates that the voltammetric waves diminish and become broader (Figure 5.30). These decreases have been attributed to the effects of electrostatic crosslinking and/or contraction of the film on the electrode making it less accessible to the

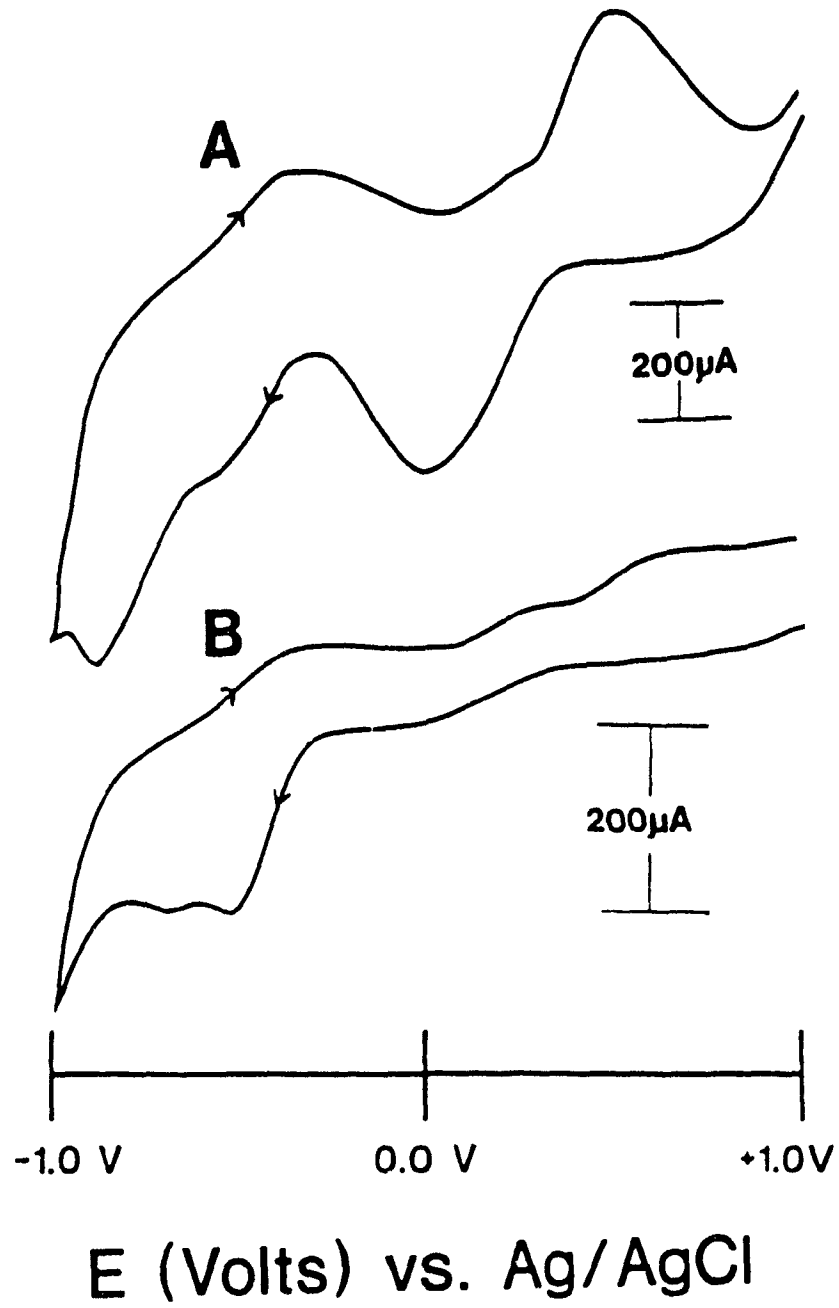

Figure 5.30 Cyclic voltammogram of a SnO_2/PXV/Ni(mnt)$_2^2$ modified electrode in contact with 0.1 M KCl (A) and after 30 minutes in solution (B). Scan rate = 100 mv/sec.

electrolyte. The complex remained in the film as indicated by the brown-red coloration of the film and lack of color in the solution.

The voltammetry of the viologen moiety of this composite polymer electrode displayed electrochromism. Cyclic voltammetry at potentials more cathodic than -0.6 V would gradually changed the film from brown-red to violet-blue ($PXV^{+\cdot}$). The original brown-red color would return only after the potential reached +0.4 V. The large peak separations coupled with the slow color change are indicative of a slow heterogeneous rate constant in the film or at the polymer/electrode interface.

The second reduction wave of viologen ($PXV^{+\cdot} \rightarrow PXV^{0}$) is known to be irreversible (119,138). Voltammetry beyond the $E_{1/2}$ for $PXV^{+\cdot} \rightarrow PXV^{0}$ led to a loss of electroactivity of the polymer. When viologen groups are reduced the coulombic repulsion between sites is lessened and the polymer chains can approach one another more closely. Partial reduction of viologen is most likely due to the presence of anionic chromophores. Moreover, the extent of solvation depend on the oxidation state of the viologen. The fully oxidized state would be more solvent swollen than the reduced state. It is likely that the loss of solvent from the polymer structure due to reduction of viologen sites would result in an increase of hydrophobic interactions and a more compact morphology.

The amount of electroactive viologen was determined by integration of the voltammetric waves. The rate of charge transport through the viologen groups of **PXV** films was determined by potential step chronoamperometry. Potentials were stepped from 0.0 V to -1.0 V for the polymer originally in the oxidized form and from -1.0 V to 0.0 V for the polymer originally in the reduced form. The apparent

diffusion coefficient was 1.4 ± 0.6 X 10^{-8} cm^2/sec for an initially oxidized film and 1.1 ± 0.5 X 10^{-8} cm^2/sec for an initially reduced film. The difference is small but consistent with morphology changes where the reduced form represents a more compact structure.

The electrochemistry of the **PXV** film is improved by the addition of $Fe(CN)_6^{3/4-}$ to the electrolyte as demonstrated by the increase in currents (Figure 5.30). The signal due to the mnt's became completely masked as the redox couple penetrated the film. The concentration of the redox couple in one film was determined to be 1.2 X 10^{-4} moles/cm^3 while the concentration of $Ni(mnt)_2^{2-}$ was 2.8 X 10^{-3} moles/cm^3 for the same electrode. $Fe(CN)_6^{3/4-}$ behaved as a quasi-reversible couple in the film with ΔE_p=200→400 mV for scan rates from 10→100 mV/sec (Figure 5.26). The electrochromic response mentioned above occurred faster. The polymer film retained only 24% of the redox couple after a 30 minute soaking in background electrolyte (Figure 5.31) The $Fe(CN)_6^{3/4-}$ can be rapidly replaced by chloride ions in the cationic sites Other porous cavities in the film can also release $Fe(CN)_6^{3/4-}$ to the solution. The charge transport process of $Fe(CN)_6^{3/4-}$ in **PXV** was examined by chronoamperometry (Figure 5.32) after soaking the film in 0.1 M KCl for 30 minutes. The D_{app} averaged for three films was 4.2 ± 0.8 X 10^{-9} cm^2/sec. D_{app} contains contributions due to the $Ni(mnt)_2^{2-}$ as well as the redox in the film This value is in the same order of magnitude for diffusion characteristics assigned to electron self-electron exchange for redox sites of ferrocene in poly(vinylferrocene) (39) and $Co(bpy)_3^{2+/3+}$ and $Ru(bpy)_3^{2+/3+}$ in Nafion (46) Charge (electron or ion) transport through these solvent swollen polymer films is generally believed to occur

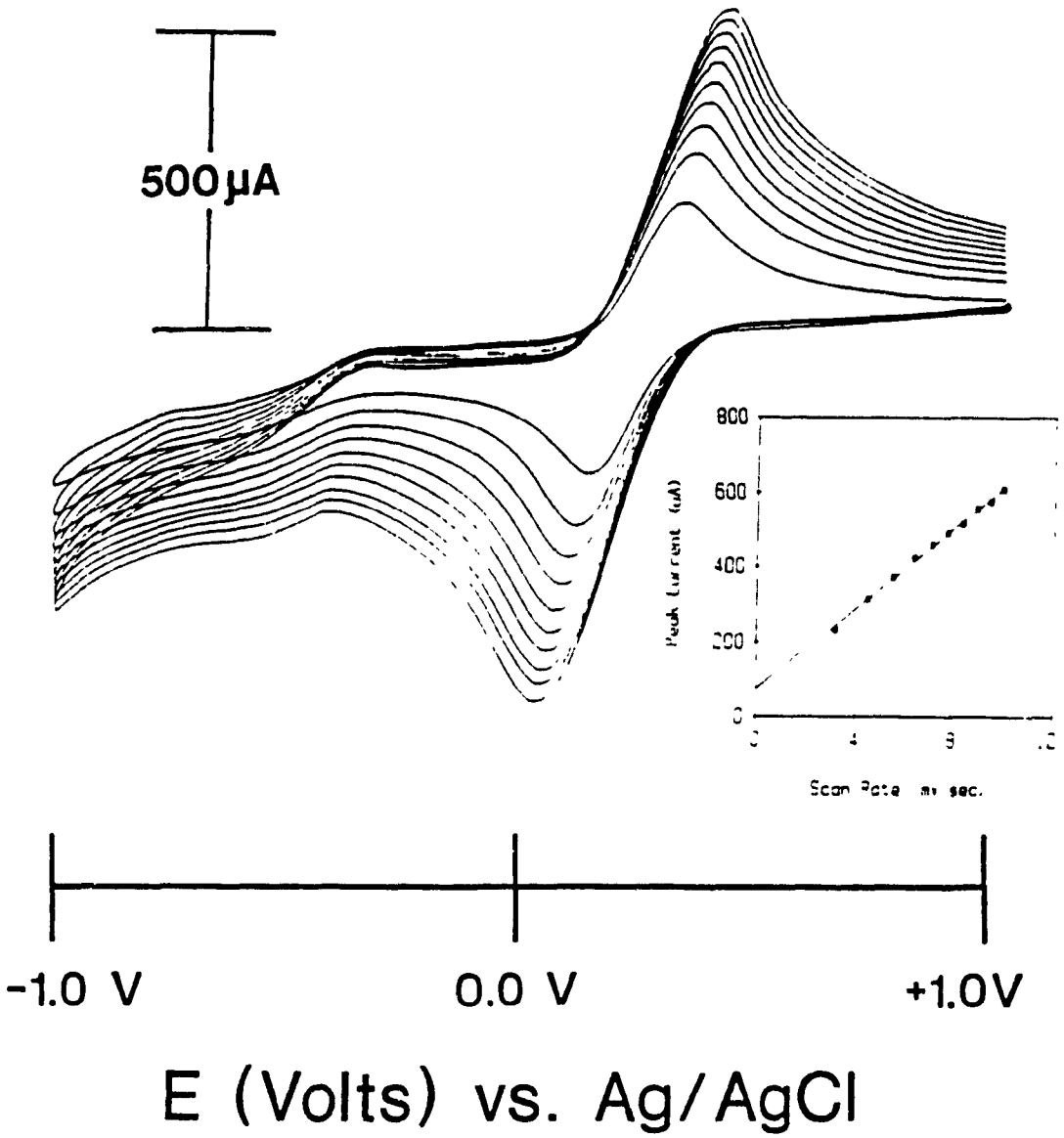

Figure 5.31 Cyclic voltammograms of a SnO_2/PXV/Ni(mnt)$_2^2$ modified electrode in contact with 2 mM $Fe(CN)_6^{3-/4-}$ in 0.1 M KCl. Scan rates were varied from 10→100 mV/sec.

Figure 5.32 Chronoamperometric current decay-time profile of a SnO_2/PXV/$Ni(mnt)_2^{2-}$ electrode containing $Fe(CN)_6^{3-/4-}$. Inset shows corresponding Anson plot of charge versus time$^{1/2}$.

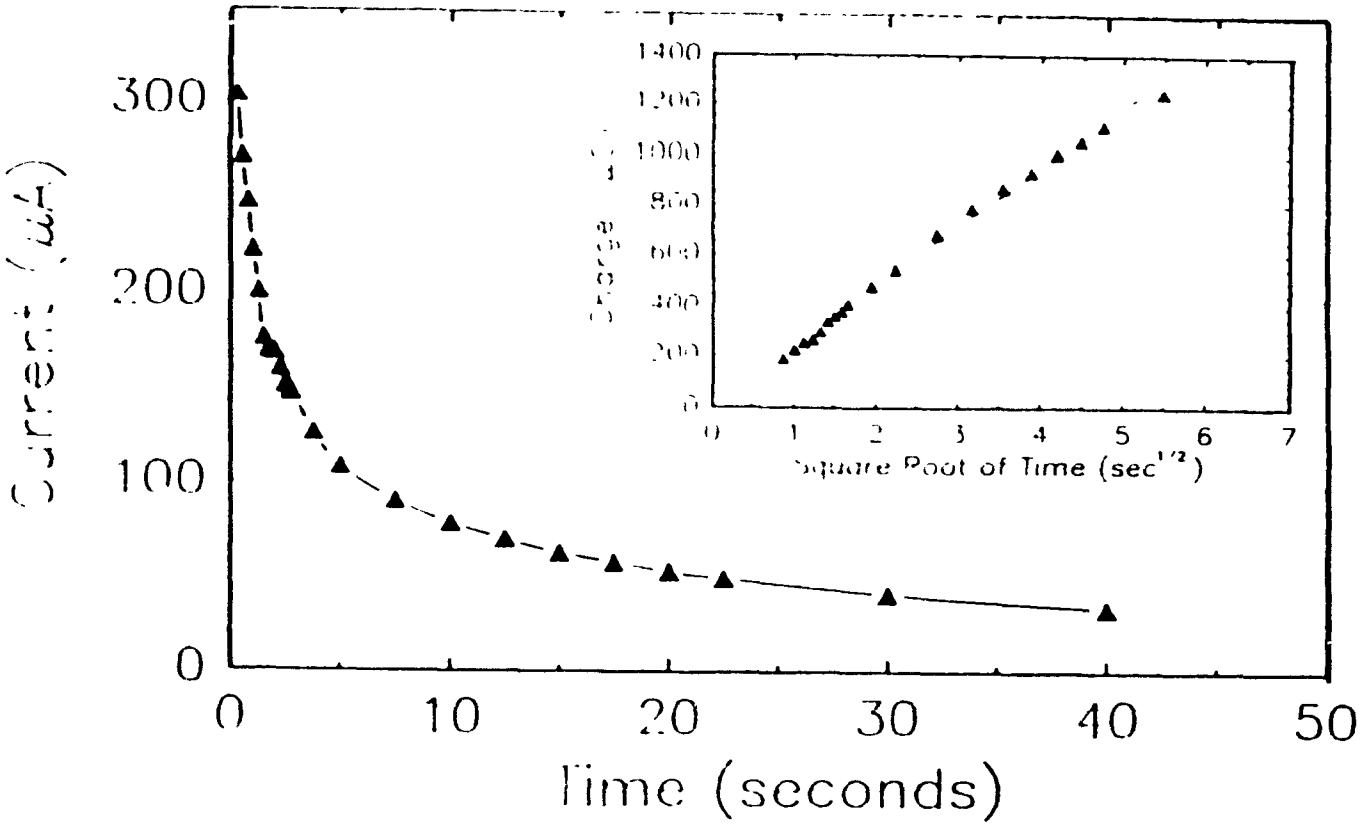

via an electron-hopping mechanism and/or by the physical diffusion of ions or redox species confined within the film (32,40-48). Both processes require concurrent uptake of counterions into the polymer matrix or expulsion or co-ions initially present in the film as an ion pair. The charge transport will be determined by the electron-transfer between adjacent redox sites, the physical diffusion of electroactive species, the motion of charge compensating counterions, the motion of solvent and the segmental motion of polymeric chains. The rate of charge transport will mainly be determined by only the slowest of these various processes and characterized by the apparent diffusion coefficient of charge transport.

PXV is a polymer with fixed redox sites which is believed to transport charge via an electron hopping mechanism. D_{app} is the sum of the diffusion coefficient D_o and the electron diffusion coefficient D_e (140-142). D_e was previously defined (equation 1.3) and is directly proportional to the concentration of redox sites available in the film. Rapid charge transport in this system (and any other one) is favored by a high density of redox exchange sites and proper alignment. For all polymers described in this study a large concentration of redox sites has an additional effect: as the concentration increases, the degree of electrostatic crosslinking between redox sites (ions) and the counterions increases, as a result the motion of solvent and segmental motion of the polymer becomes slower. Additionally physical diffusion of redox sites and/or counterions becomes sluggish. Overall the D_{app} decreases with increasing concentration. The effect of concentration on the D_{app} is strongly influenced by solvent swelling and internal polymer morphology.

5.6.3 Photoelectrochemistry of PXV Modified ELectrodes.

The photoelectrochemical behaviour of SnO_2/PXV/$Ni(mnt)_2^{2-}$ and SnO_2//PXV/$Pt(mnt)_2^{2-}$ electrodes was studied in background electrolyte and in the presence of the $Fe(CN)_6^{3-/4-}$ redox couple. In the former case, a photoresponse of ≈30 nA/cm² was observed (Figure 5.33). The photocurrent-time profile is composed of a rapid and a slow component each contributing roughly half of the photocurrent. Following charge transfer from the photo-excited dye to the viologen moiety of the polymer, the prompt response in the first 24 seconds is attributed to filling of intrinsic trap sites in the polymer matrix in addition to those created by the structural and morphological changes in the polymer during redox electron hopping through the polymeric chains. The second steady state process is related to rapid charge transport through the PXV backbone by electron hopping. Ionic movement in and out the film may also limit the photoresponse. The decay of the photoresponse in the dark was slower but similar in nature to the photocurrent rise. The dark current did not return completely to its original value indicating that thermal de-trapping of sites is very slow in this redox polymer and/or the photoresponse process induced some irreversible changes in the matrix (i.e dimerization of viologen radicals or formation of portions of completely reduced viologen).

In the presence of $Fe(CN)_6^{3-/4-}$, the photocurrent-time profile resembles a square wave response with slight capacitative effects when the light was turned on or off. The magnitude of the photocurrents was 365 ± 23 nA/cm² for a series of three electrodes at 100 mW/cm² (5 light-on/light-off cycles each). These transients

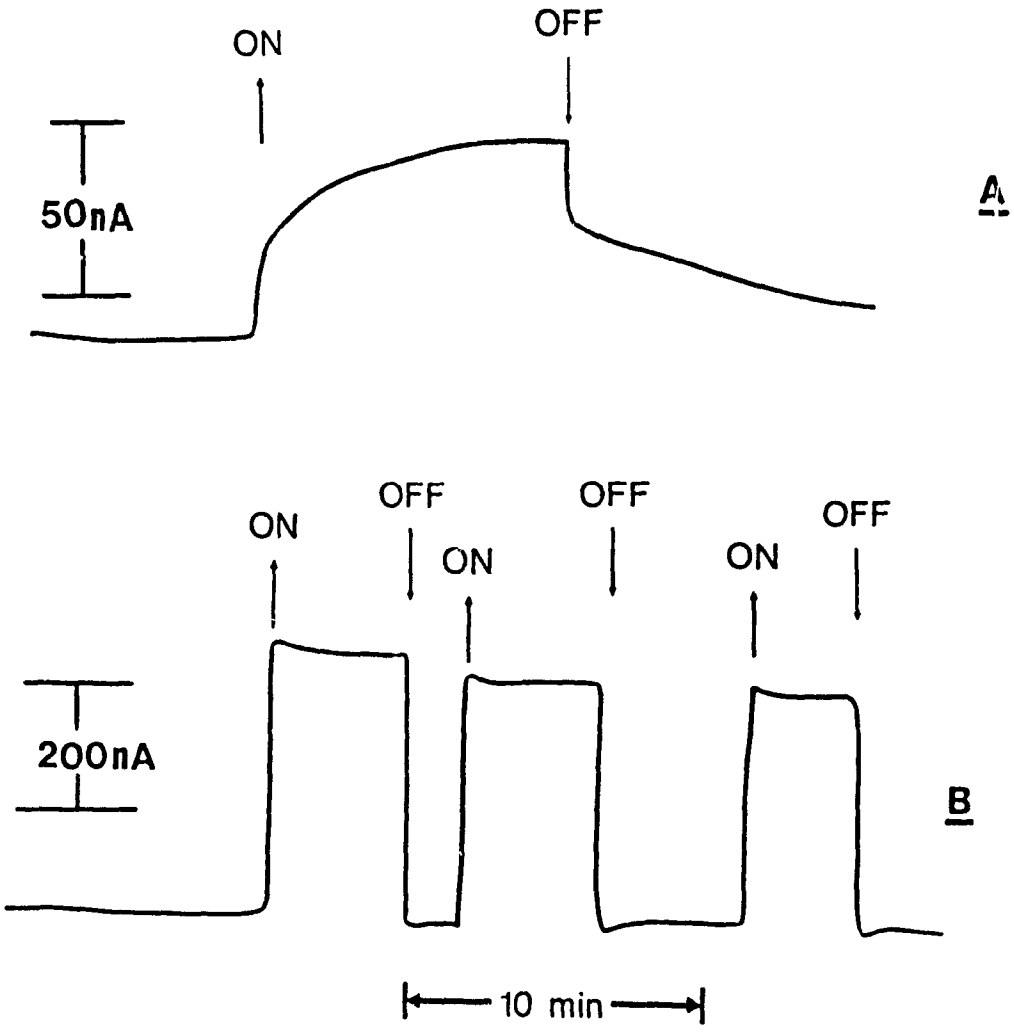

Figure 5.33 Short circuit photocurrent-time profiles for a SnO_2/PXV/$Ni(mnt)_2^2$ modified electrode in contact with (A) 0.1 M KCl and (B) 2 mM $Fe(CN)_6^{3/4}$ in 0.1 M KCl. White light illumination at 100 mW/cm² was filtered to remove UV (λ>400nm) and IR (water filter).

do not exhibit the same trapping behaviour as other electrodes described in this study. Charge transport in this polymer appears to be mediated predominately by electron hopping between adjacent redox sites in this redox polymer. First, the photoexcited anionic dye transfers an electron to the cationic viologen portion of **PXV**, followed by charge transport by electron self-exchange between adjacent redox sites of the polymer into the conduction band of the SnO_2 electrode. The oxidized chromophore is subsequently reduced by ferrocyanide incorporated in the film. Finally, the oxidized ferricyanide gets reduced at the platinum counterelectrode.

A similar mechanism operates for the platinum complex. Composite electrodes of SnO_2/**PXV**/$Pt(mnt)_2^2$ in $Fe(CN)_6^{3/4}$ were not as mechanically stable as their Ni counterpart. The polymer films dissolved off the electrodes within 30 minutes during photoelectrochemical studies. Composite electrodes of SnO_2/**PXV** + poly(ethylene oxide)/$Pt(mnt)_2^2$ improved the stability of this system to a behaviour comparable with the nickel complex.

The photoelectrochemical behaviour of **PXV** modified electrodes is a redox mediated process. The magnitude of the photocurrents is smaller than in the case of **PB1** but greater than the other polymers studied so far. There are two factors which contribute to this effect. The first is the formation of a charge transfer complex between the dye and **PXV**. The other factor is electrostatic crosslinking between redox sites and counterions (as described in the previous section) leading to structural changes which reduce the diffusion of electroactive species in the film. Redox polymers of this type would show considerable interest when blended or mixed with more hydrophobic polymers. The study of the ratio of hydrophilic to

hydrophobic character in segregated micro-domains with respect to charge transport in polymer matrices is in its infancy (123,126). An proposed energy level diagram and pathway for charge transport in the SnO_2/**PXV**/$M(mnt)_2^{2-}$ system is shown in Figure 5.34. The distribution of molecular-ion states for this polymer has not been evaluated in this or any other work.

5.7 Electrochemistry and Photoelectrochemistry of Poly(pyrrole) Modified Electrodes Containing $Ni(mnt)_2^{2-}$ and $Pt(mnt)_2^{2-}$.

Poly(pyrrole) (**PPY**) is an electronically conductive polymer consisting of linear planar α,α'- bonded chains of monomeric pyrrole units. Anodic electropolymerization of pyrrole on SnO_2 in the presence of Cl^- or ClO_4^- yielded thin green-black cationic films with one positive delocalized over 3-4 polymer units (3,28).

Many large anions such as ClO_4^- (2,3), BF_4^- (2,3), poly(4-styrenesulphonate) (143), and iron phthalocyanine tetrasulphonate (144) have been incorporated into **PPY** films by electropolymerization in the presence of the appropriate anion. Anodic electropolymerization of pyrrole in the presence of either $Ni(mnt)_2^{2-}$, $Ni(mnt)_2^{1-}$, $Pt(mnt)_2^{2-}$, $Pt(mnt)_2^{1-}$, or $Cu(mnt)_2^{2-}$ did not afford any polymeric films. $Ni(mnt)_2^{2-}$ and $Pt(mnt)_2^{2-}$ were incorporated into **PPY** films by ion-exchange for charge compensating Cl^- or ClO_4^- ions already present in **PPY**$^+$-Cl^- or **PPY**$^+$-ClO_4^- films. Polypyrrole films are known to be quite porous and the size of the holes is strongly influenced by the anions of the supporting electrolyte from which the **PPY** was prepared.

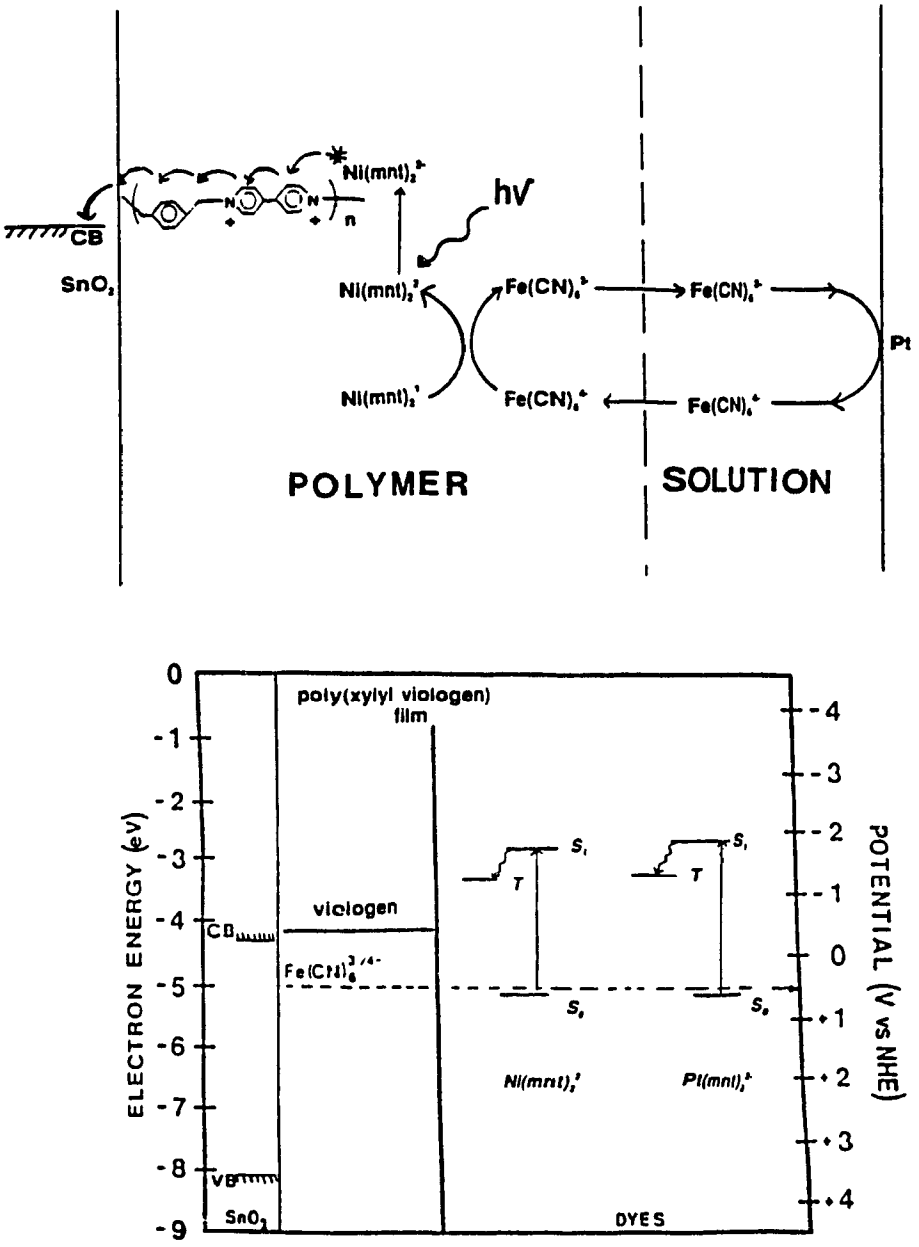

Figure 5.34 (A) Proposed mechanism for photoeffects observed for a SnO_2/PXV/$Ni(mnt)_2^{2-}$ modified electrode in contact with 2 mM $Fe(CN)_6^{3/4-}$ in 0.1 M KCl. (B) Energy level diagram. The acceptor states of the polyviologen were estimated from the reduction potential of the polyviologen. The dyes are believed to be ion-exchanged to the cationic viologen sites.

Polypyrrole-based materials have been suggested as photocorrosion inhibitors for semiconductors, and as cathode materials for novel secondary batteries. **PPY** was used as an electronically conductive cationic matrix to incorporate $Ni(mnt)_2^{2-}$ and examine the electrochemical and photoelectrochemical properties of these composite electrodes.

5.7.1 Electrochemistry of PPY Modified Electrodes Containing $Ni(mnt)_2^{2-}$.

SnO_2/**PPY**/$Ni(mnt)_2^{2-}$ modified electrodes displayed no electroactivity due to the metal complex (Figure 5.35). Electrodes of this type were red-black in color and not transparent to visible light. The capacitative current in these films is related to weakly trapped ions (ClO_4^- or $Ni(mnt)_2^{2-}$) in the film and is directly connected to the doping process (145). $Ni(mnt)_2^{2-}$ presumably interacts with the positive charge delocalized over 3-4 pyrrole units in **PPY**.

Broad electrochemical waves corresponding to the $Fe(CN)_6^{3-/4-}$ redox couple were recorded when SnO_2/**PPY**/$Ni(mnt)_2^{2}$ electrodes were placed in solutions of 2 mM $Fe(CN)_6^{3-/4-}$ in 0.1 M KCl. The peak separation was very large indicating sluggish kinetics (ΔE_p=350 mV at a scan rate of 10 mV/sec (Figure 5.35)). Only small amounts of $Fe(CN)_6^{3-/4-}$ were incorporated into SnO_2/**PPY**/$Ni(mnt)_2^{2-}$ electrodes, typically between 5.2 to 6.8 X 10^{-6} moles/cm^3. This amount is approximately an order of magnitude less than the amount of $Fe(CN)_6^{3-/4-}$ present in other polymer films described in this study. This is typically the amount of $Ni(mnt)_2^{2-}$ in **PPY** polymers. The diffusion coefficient of $Fe(CN)_6^{3-/4-}$ in **PPY** has not been determined in this work or any other study. It has been estimated to be $\approx 10^{-10}$ cm^2/sec or less (146). However the diffusion coefficient of Cl^- and ClO_4^- in **PPY** films has been

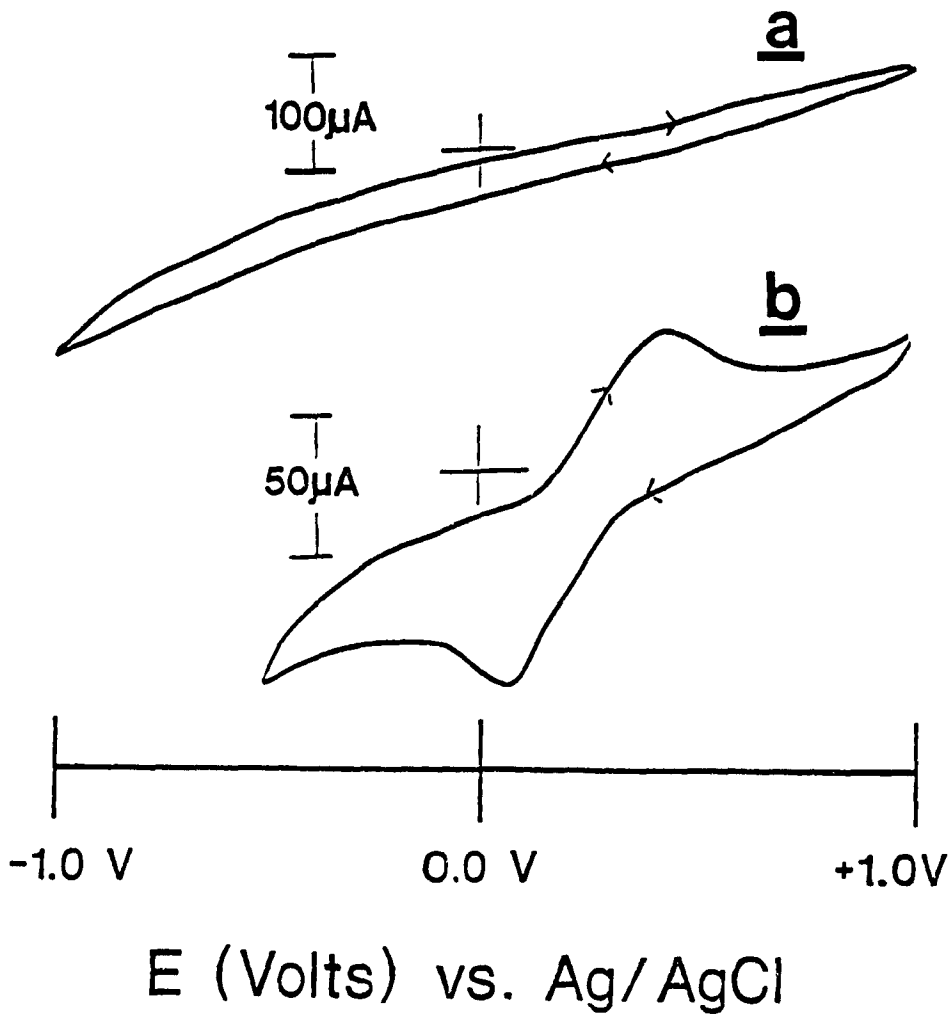

Figure 5.35 (A) Cyclic voltammogram of a SnO_2/PPY/$Ni(mnt)_2^{2-}$ modified electrode in contact with 0.1 M KCl. (B) Cyclic voltammogram of a SnO_2/PPY/$Ni(mnt)_2^{2-}$ electrode in contact with 2 mM $Fe(CN)_6^{3-/4-}$ in 0.1 M KCl. Scan rate = 100 mv/sec.

determined by Paulse and Pickup to be 3.4 X 10^{-8} cm^2/sec and 2.3 X 10^{-9} cm^2/sec respectively (146). These workers also noted that the kinetics of polypyrrole electrochemistry was limited by counterion migration rather than by diffusion.

5.7.2 Photoelectrochemistry of PPY Modified Electrodes.

Polymer modified electrodes of the type SnO_2/**PPY** exhibited no photocurrents in 0.1 M KCl and 0.24 $\mu A/cm^2$ in 2 mM $Fe(CN)_6^{3-/4-}$ in 0.1 M KCl. SnO_2/**PPY**/$Ni(mnt)_2^{2-}$ displayed a square wave like photoresponse of 1.70 ± 0.21 $\mu A/cm^2$ (3 electrodes, 5 light-on/light-off sequences each) at 100 mW/cm^2 white light irradiation (Figure 5.36). The response is reminiscent of the behaviour obtained with the **PXV** modified electrodes but not identical. The magnitude of the photocurrent is similar to the results of the **PB1** polymer blend containing $Ni(mnt)_2^{2-}$. The prompt rise and decay of the photoresponse is an indication that few sites are available for charge trapping in **PPY**/$Ni(mnt)_2^{2-}$ polymer films in contact with an aqueous 2 mM $Fe(CN)_6^{3-/4-}$ redox couple. The charge transport mechanism in this polymer can be described as follows; photoexcited $Ni(mnt)_2^{2-}$ transfers an electron to the **PPY** polymer which is an electronic conductor. This polymeric "wire" will transfer the electron to the conduction band of the SnO_2 substrate. Reduction of the oxidized dye can occur either by direct contact with a $Fe(CN)_6^{4-}$ redox ion or by a polymer assisted hopping mechanism. Reduction of the oxidized ferricyanide is accomplished at the counter electrode. The modest magnitude of the photoeffect can be explained by a combination of the porosity of the polymer, the localization of cationic charge, and the rather slow diffusion of the redox couple through the film and the film's poor optical properties.

Figure 5.36 Short circuit photocurrent-time profiles for a SnO_2/PPY/$Ni(mnt)_2^{2-}$ electrode in contact with 2 mM $Fe(CN)_6^{3-/4-}$ in 0.1 M KCl. Visible light irradiation at 100 mW/cm^2 with a water filter and a UV cut-off filter (λ>400nm).

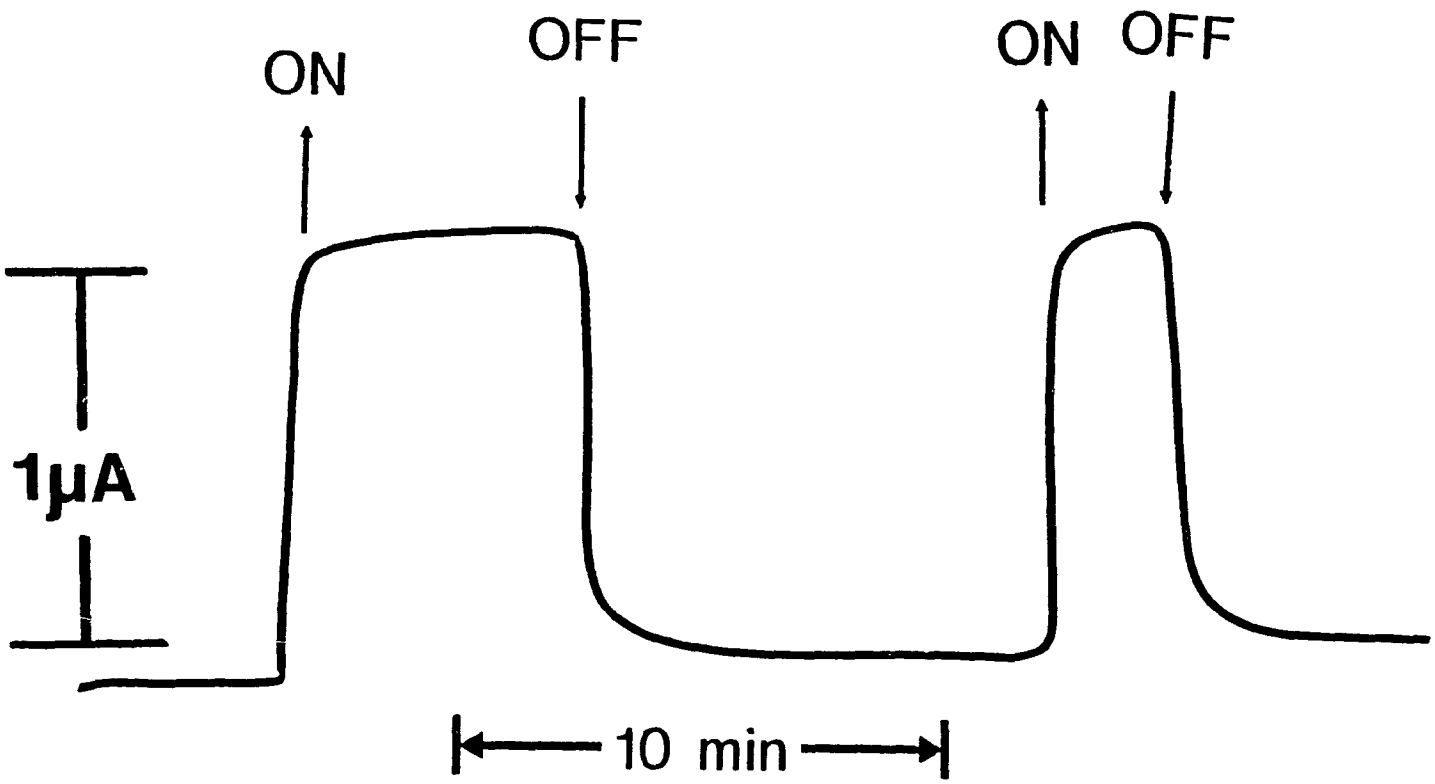

The trapping and de-trapping of photogenerated charge carriers was observed by chopping the white light source at 0.2 Hz and 0.05 Hz (Figure 5.37). During a steady state cycle the photocurrent transients reached 80% of the maximum value that was obtained when using un-modulated irradiation. The decay was similar. Using slower 0.05 Hz modulation the transients reached 95% of the value from un-modulated experiments. The shape of the photocurrent-time profiles suggests both a resistive and capacitative component (RC) involved in the filling and thermal de-trapping of localized states. It is not unlikely that these traps are quite shallow and related to the polarons and bipolarons described below.

Experiments in the absence of $Fe(CN)_6^{3-/4-}$ and supporting electrolyte were performed using "dry cells" of the type SnO_2/**PPY**-$Ni(mnt)_2^{2-}$/Au where gold was evaporated on the surface of the polymer film. Thermal effects were minimized by using a cooling fan and was monitored with a J-type thermocouple adjacent to the electrode. The dry cell was illuminated from the SnO_2 side. Photocurrent-time profiles were obtained for both white and monochromatic light (Figure 5.38). The shape of the profiles is similar to those obtained for **PVP** and **PB1** based polymers and consistent with the trapping and thermal de-trapping mechanisms proposed above. Polypyrrole is microporous with solvent-swollen polymer and solvent filled pores. Experiments in solution must account for changes in morphology due to the electrolyte and the redox couple.

The fact that the **PPY** polymer alone is photoactive is not surprising. Electronically conductive polymers with an extended π network have been studied as organic materials with a modified band structure. Electrochemically grown **PPY**

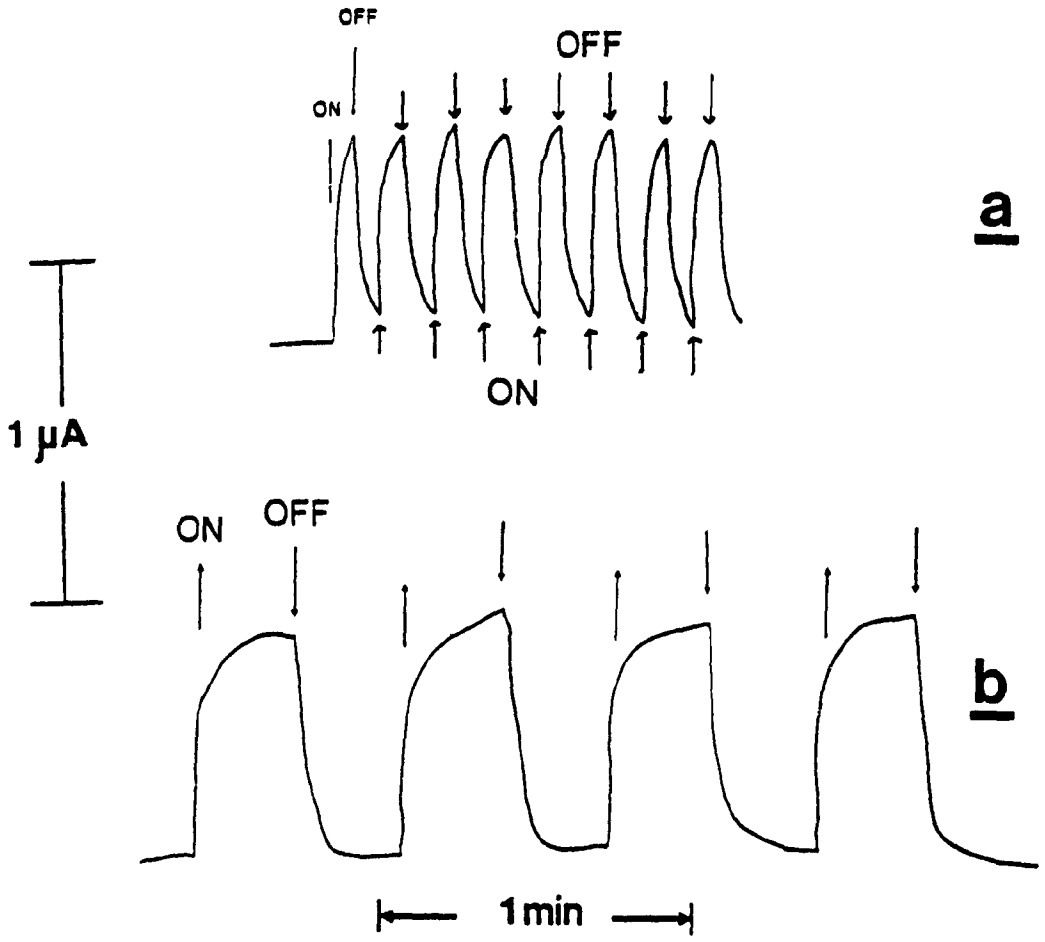

Figure 5.37 Short circuit photocurrent-time profiles for a SnO_2/PPY/Ni(mnt)$_2^{2-}$ electrode in contact with 2 mM $Fe(CN)_6^{3-/4-}$ in 0.1 M KCl. Visible light irradiation at 100 mW/cm^2 with a water filter and a UV cut-off filter (λ>400nm). Light was modulated at (a) 0.2 Hz and (b) 0.05 Hz.

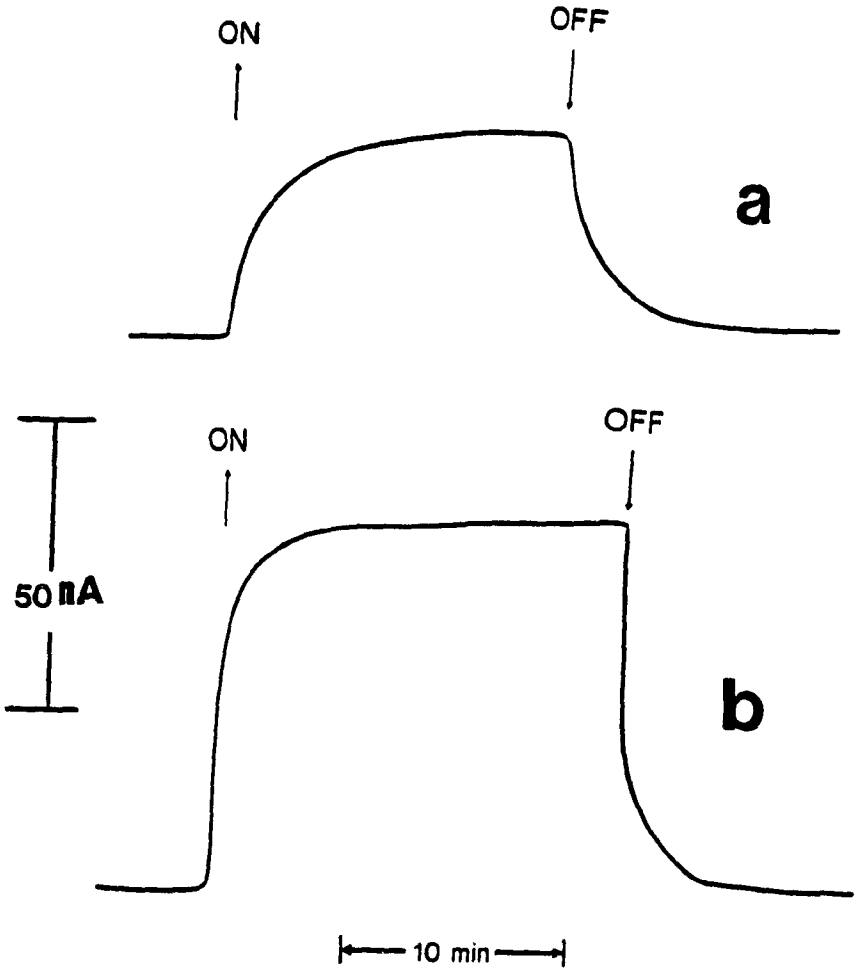

Figure 5.38 (A) Short circuit photocurrent-time profile for a SnO_2/**PPY**-$Ni(mnt)_2^{2-}$/Au "dry cell" under visible light illumination at 100 mW/cm^2 with a water filter and a UV cut-off filter (λ>400 nm) and (B) illuminated with an argon ion laser using 40 mW at 488 nm.

films have an intrinsic bandgap of ≈3.2 eV (147). Addition of $Ni(mnt)_2^{2-}$ to the polymer film creates a composite electrode with sensitizing characteristics. Transport of charge in **PPY** polymers is believed to occur by polarons at low doping levels, and via bipolarons at high dopant levels (147). Polarons are just radical ions (S=1/2) associated with a lattice distortion and the presence of localized electronic states in the bandgap are polaron states. Bipolarons are defined as a pair of similar charges (dications in this case) associated with a strong local lattice distortion (147). $Ni(mnt)_2^{2-}$, $Fe(CN)_6^{3-/4-}$ and the charge compensating counterions are dopants in the present case. It is not unlikely that there exists domains of low doping (polaron formation) and domains of relatively high doping (bipolaron formation) in composite polymer materials of this type. In polymeric materials, the charge carriers move along the polymer chains and also jump from chain to chain. The latter process is the rate limiting step which determines the conductivity and photoconductivity observed on a macroscopic scale. Interchain interactions and hopping are thus of prime importance. These polymeric materials are rather amorphous and possess a substantial amount of disorder which will reduce the efficiency of charge transport from the electrolyte/polymer interface to the polymer/SnO_2 interface. The overall reaction scheme of $Pt(mnt)_2^{2-}$ and $Ni(mnt)_2^{2-}$ in **PPY** modified electrodes is presented in Figure 5.39 in a similar fashion to energy diagrams for the other polymers.

Pyrrole was added to the **PB1**/$Ni(mnt)_2^{2-}$ casting solution and cast on SnO_2 electrodes. Polypyrrole was electrochemically grown through the pores of the polymer film to improve the electrical "contact" between the SnO_2 and the polymer.

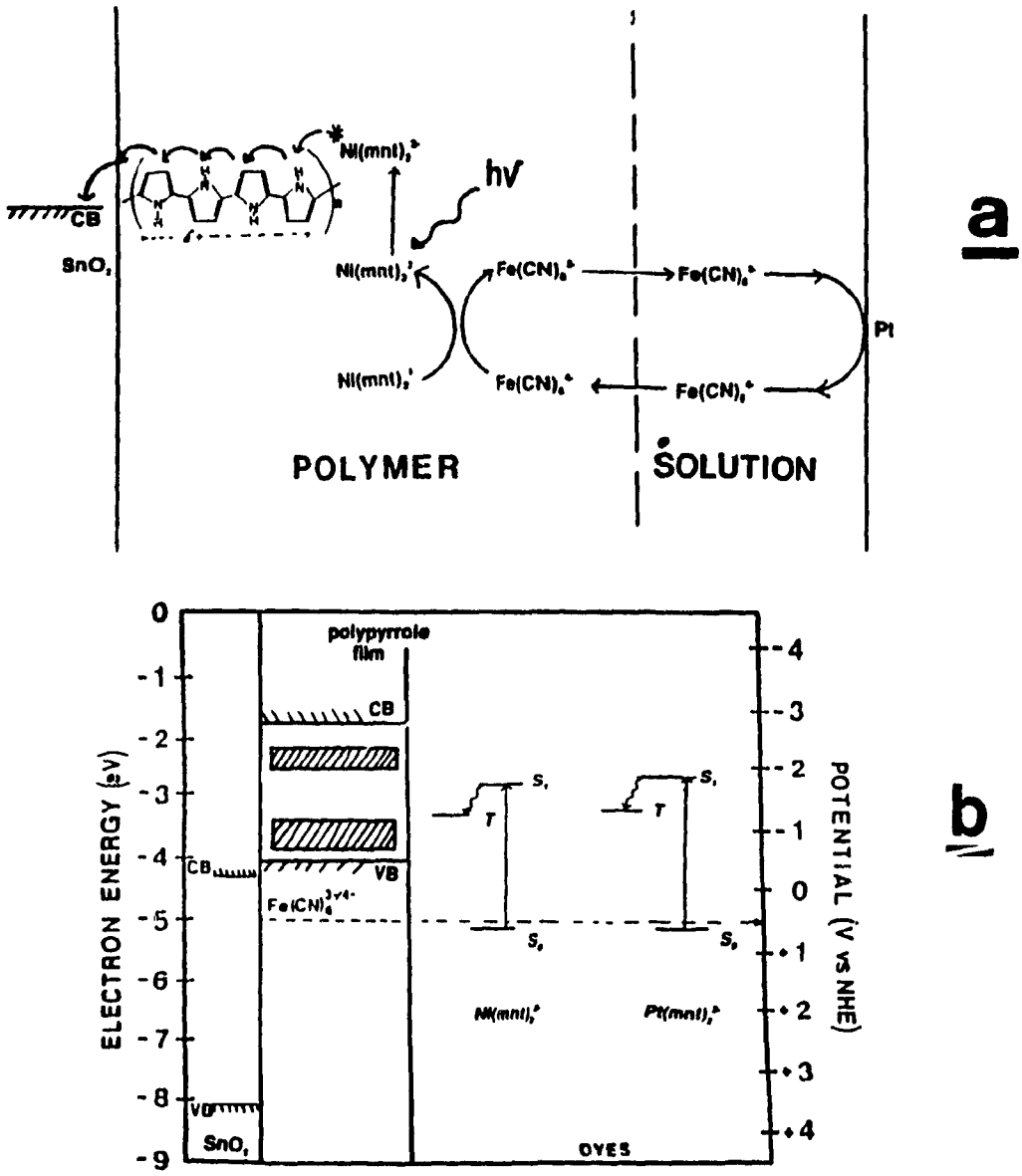

Figure 5.39 (A) Proposed mechanism for photoeffects observed for a SnO_2/PPY/$Ni(mnt)_2^{2-}$ modified electrode in contact with 2 mM $Fe(CN)_6^{3-/4-}$ in 0.1 M KCl. (B) Energy level diagram. The acceptor states of the polypyrrole were estimated from the reduction and oxidation potential of polypyrrole and the formation of polaron and bipolaron energy bands upon doping. The dyes are believed to be ion-exchanged to the cationic pyrrole sites.

The polypyrrole can be envisaged as dendrites of highly conductive material distributed through the composite electrode. The composite electrode is in effect a large area porous metal-like electrode. White light illumination of such a composite electrode (SnO_2/**PB1-PPY**-$Ni(mnt)_2^{2-}$) generated photocurrent transients of 12 μA and photocurrent-time profiles resembling the trapping and thermal de-trapping behaviour of **PB1** composite polymer films (Figure 5.40). Alternatively, electrochemically grown **PPY**-ClO_4^- on SnO_2 were coated with the same dye-polymer mixture to make a polymer soaked porous electrode. Photocurrents were smaller (7-8 μA) and the behaviour was similar to composite electrode described above. A part of the observed photocurrent is due only to the polypyrrole.

These novel composite electrodes using two polymers provide the opportunity to study the interactions between electronic and ionic conductive polymers and to investigate the possibility of large area electrodes with capacitative and resistive component.

Figure 5.40 Short circuit photocurrent-time profiles for a SnO_2/**PPY-PB1**/$Ni(mnt)_2^{2-}$ composite electrode in contact with 2 mM $Fe(CN)_6^{3-/4-}$ in 0.1 M KCl. Visible light irradiation at 100 mW/cm² with a water filter and a UV cut-off filter (λ>400nm).

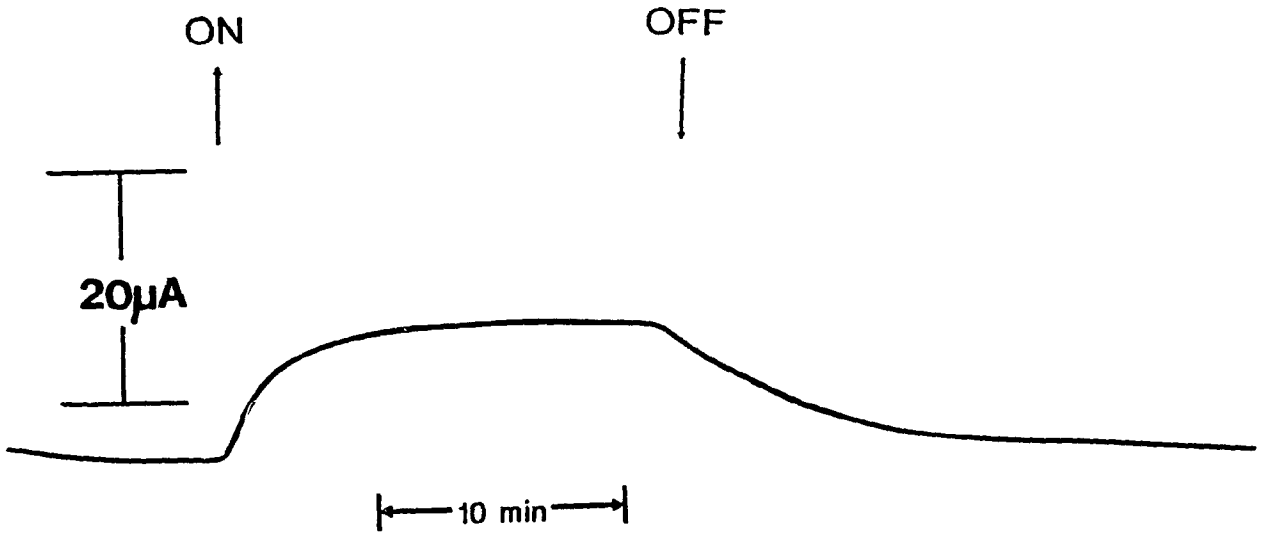

CONCLUSIONS

This work represents an extensive study on the photoelectrochemical behaviour of metal maleonitriledithiolates incorporated in electroactive polymer films on electrodes as well as their photochemical behaviour and photophysical properties in homogeneous solution.

Visible light irradiation of acetonitrile solutions of $Pt(mnt)_2^{2-}$ or $Ni(mnt)_2^{2}$ produced the monoanion as a primary photoproduct. The Pt complex was photo-oxidized more rapidly than its nickel counterpart and oxygen is believed to act as an electron acceptor in this case. Transient absorption and emission spectroscopy have indicated that the excited state lifetime of $Pt(mnt)_2^{2}$ is greater than that of $Ni(mnt)_2^{2-}$. Excitation into $L\pi \rightarrow L\pi^*$ or $L\pi \rightarrow M$ charge transfer bands produced longer lived excited states than those populated by excitation into $M \rightarrow L\pi^*$ charge transfer bands or metal centered bands of lower energy. $[MV^{2+}][M(mnt)_2^{2}]$ salts were prepared which displayed interesting photophysical properties. Irradiation into a MLCT band of the dye produces emission associated with partially reduced viologen indicating charge transfer from the metal complex to the methyl viologen acceptor. The $[MV^{2+}][M(mnt)_2^{2-}]$ complexes were used as model compounds for the photoelectrochemistry of $M(mnt)_2^{2}$'s in polyviologens.

The photoelectrochemical behaviour of polymer modified electrodes containing the dithiolene complexes was investigated to gain insight on the charge transport processes involved following irradiation of the films with visible light. Ion-exchange, redox and electronically conducting electroactive polymers were used

as supports for the chromophores. The mechanism of charge transport was evaluated for each type of polymer. Photoconduction in the polymer films was treated using a molecular-ion state model where charge carriers migrate by a trap controlled mechanism. The photogenerated carriers migrate in localized states of the polymer matrix. These states may be considered as regions which can trap or partially stabilize a charge carrier.

The high ionic mobility of electroactive species in the ion-exchange polymer blend **PB1** is an indication of good charge transport characteristics in a polymer matrix supported on a semiconducting electrode. Segregated hydrophobic and hydrophylic domains have been observed in this polymer. The dithiolene complexes are believed to be at the interface of the domains.

Several factors determine the magnitude of the observed photocurrents from these composite electrodes in contact with a redox solution. These include the diffusion of electroactive species in the film, the concentration of dye incorporated in the polymer as well as the particular morphology of the dye/polymer composite.

In order to obtain a greater photon to electron efficiency, a strategy should involve the tuning of energy levels associated with the dye, the polymer, the electrolyte, and the support. Efficient energy transfer in a dye/polymer/semiconductor composite should be acheived by organization of components as well as energetic considerations. Similar composite modified electrodes to those described here could be used as models or devices for photovoltaic and/or photocatalytic systems.

References

1 Macdiarmid, A. G.; Heeger, A. J. *Synthetic Metals*, **1980**, *1*, 101.

2 Diaz, A. F.; Kanazawa, K. K.; Gardini, G. P. *J. Chem. Soc., Chem. Comm.*, **1979**, 635.

3 Diaz, A. F.; Logan, J. A. *J. Electroanal. Chem.Interfacial Chem.*, **1980**, *111*, 111.

4 Paul, E. W.; Ricco, A. J.; Wrighton, M. S. *J. Phys. Chem.*, **1985**,*89*, 1441.

5 Rabek, J. F.; Ranby, B. *J. Polym. Sci. Part A-1*, **1974**, *12*, 273.

6 Gupta, M. C.; Gupta, A.; Horowitz, J.; Kliger D. *Macromolecules*, **1982**, *15*, 1372.

7 Takai, Y.; Mizutani, T.; Ieda, M. *Japan J. Appl. Phys.*, **1978**, *17*, 651.

8 Burkhart, R. D.; Aviles, R. G. *Macromolecules*, **1979**, *12*, 1073.

9 Webber, S. E.; Avots-Avotines, P. E. *Macromolecules*,**1971**, *14*,105.

10 Klöpper, W. *Chem. Phys.*, **1981**, *57*, 75.

11 Mort, J.; Emerald, R. J. *J. Appl. Phys.*, **1974**, *45*, 175.

12 Reucroft, P. J. In " *Photoconductivity in polymers, an Interdisciplinary Approach*", Patsis, A. V.; Seanor, D. A.;(Eds.), Technomic Publishing, Wesport, Connecticut, **1976**.

13 Aspler, J. S · Hoyle, C. E.; Guillet, J. E. *Macromolecules*, **1978**, *11*, 925.

14 Holden, D. A.; Guillet, J. E. *Macromolecules*, **1980**, *13*, 289.

15 Guillet, J. E. *"Polymer Photochemistry and Photophysics"*, Cambridge University Press, Cambridge, **1985**.

16 Dexter, D. L. *J. Chem. Phys.*, **1953**, *21*, 836.

17 Förster, T. *Amer. Phys.*, **1948**, *2*, 55.

18 Nagata, I.; Morawetz, H. *Macromolecules*, **1981**, *14*, 87.

19 Powell, R. C. *J. Chem. Phys.*, **1971**, *55*, 1871.

20 Eisenberg, A. *Macromolecules*, **1970**, *3*, 147.

21 Seanor, D. A. In *"Electrical Properties of Polymers"*, Seanor, D. A. (ed.), Academic Press, New York, **1982**, Chapter 1.

22 Bredas, J. L.; Chance, R. R.; Elsenbaumer, R. L. *J. Chem. Phys.*,**1983**,*78*, 5656.

23 Duke, C. B.; Salaneck, W. R.; Fabish, T. J.; Ritsko, J. J.; Thomas, H. R.; Paton, A. *Phys. Rev. B*, **1978**, *18*, 5717.

24 Fabish, T. J.; Duke, C. B. *J. Appl. Phys.*, **1977**, *48*, 4256.

25 Fabish, T. J. *CRC Crit. Rev. Solid State Mater. Sci.*,**Dec. 1979.**

26 Crouch, A. M.; Ordoñez, I.; Langford, C. H.; Lawrence, M. F. *J. Phys. Chem.*, **1988**, *92*, 6058.

27 Baeriswyl, D.; Harbeke, G.; Kiess, H.; Meyer, W. In *"Electronic Properties of Polymers"*, Mort, J.; Pfister, G.;(eds.), Wiley Interscience, New York, **1982**, chapter 7 and references therein.

28 Diaz, A. F.; Castillo, J. I. *J. Chem. Soc., Chem. Comm.*, **1980**, 397.

29 Wynne, K. J.; Street, G. B. *Macromolecules*, **1985**, *18*, 236.

30 Zhou. Q. X.; Kolaskie, C. J.; Miller, L. L. *J. Electroanal. Interfacial Electrochem.*, **1987**, *223*, 283.

31 Upson, D. A.; Steklenski, D. J. *U.S. Patent No. 12690*, **1980.**

32 Ohsaka, T.; Takeyoshi, O.; Oyama, N. *J. Electroanal. Interfacial Electrochem.*, **1986**, *200*, 159.

33 Kulshrestha, Y. K.; Srivastava, A. P. *Indian J. Pure Appl.Phys.* **1981**, *19*, 478.

34 David, C.; Lempereur, M.; Geuskens, G. *Europ. Polym. J.*, **1972**, *8*, 417.

35 MacCallum, J. R. *Europ. Polym. J.*,**1981**, *17*, 209.

36 Guillet, J. E., *Polymer Photophysics and Photochemistry*, Cambridge University Press, Cambridge, **1985**, chap.9.

37 Merz, A.; Bard, A. J. *J.Am. Chem. Soc.*, **1978**, *100*, 3222.

38 Schroeder, A. H.; Kaufman, F. B.; Patel, V.; Engler, J. *J. Electroanal. Chem. Interfacial Electrochem.*,**1980**, *113*, 193.

39 Chambers, J. Q. *J. Electroanal. Chem. Interfacial Electrochem.*, **1981**, *130*, 381.

40 Denisevich, P.; Abruña, H. C.; Leidner, C. R.; Meyer, T. J.; Murray, R. W. *Inorg. Chem.*, **1982**, *21*, 2153.

41 Elliot, C. M.; Redepenning, J. G.; Balk, E. M. *J.Am. Chem. Soc.*, **1985**, *107*, 8302.

42 Ewing, A. G.; Feldman, B. J.; Murray, R. W. *J.Phys. Chem.*, **1985**, *89*, 1263.

43 Andrieux, C. P.; Savéant, J.-M. *J. Electroanal. Chem. Interfacial Electrochem.*, **1980**, *111*, 377.

44 Laviron, E. *J. Electroanal. Chem. Interfacial Electrochem.*, **1980**, *112*, 1.

45 Murray, R. W. In *Electroanalytical Chemistry*; Bard, A.J., Ed.;Dekker, New York, **1984**, Vol.13, pp.191-368.

46 Abruña, H. C. *Coordination Chemistry Reviews*, **1988**, *86*, 135.

47 Oyama, N.; Anson, F. C. *J. Electrochem. Soc.*, **1980**, *127*, 247.

48 Oyama, N.; Anson, F. C. *J. Electrochem. Soc.*, **1980**, *127*, 249.

49 Nafion is a trademark of E.I. Dupont de Nemours, Inc.

50 Eisenberg, A.; Yeager, H. L. (Eds.), *Perfluro Sulfonate Ionomer Membranes*, A.C.S. *Symposium Series 180*, American Chemical Society, Washington, D.C., **1982.**

51 Besso, E.; Eisenberg, A. In *Proceedings of the Symposium on Ion Exchange Transport and Interfacial properties*, Yeo,R. S.;Buck, R. P.,(Eds.), The Electrochemical Society, New Jersey, **1981**.

52 Montgomery D., Anson F. C., *J. Am. Chem. Soc.*, **1985**,*107*,3431.

53 Bard, A. J.; Faulkner, L. R. *Electrochemical Methods, Fundementals and Applications*, Wiley, New York, **1980**.

54 Kissinger, P. T.; Heineman, W. R., In *Laboratory Techniques in Electroanalytical Chemistry*, Kissinger, P. T.;Heineman, W. R.,(Eds.); Dekker, New York, **1984**.

55 Cottrell, F. G. *Z. Physik Chem.*, **1903**, *42*, 385.

56 Chan, M. S.; Bolton, J. R. *Solar Energy*, **1979**, *24*, 561.

57 McGlynn, S. P.; Azumi, T.; Kinoshita, M. *Molecular Spectroscopy of the Triplet State*, Prentice Hall Inc., New Jersey, **1968**, p.87.

58 Harriman, A.; Porter, G.; Walters, P. *J. Chem. Soc. Faraday Trans. 2*, **1981**, *77*, 1281.

59 Hopf, F. R.; Whitten, D. G. In *"The Porphyrins VII"*, Dolphin, D. (ed.), Academic Press, New York, **1978**, 162.

60 Grätzel, M. (ed.) *"Energy Resources through Photochemistry and Catalysis"*, Academic Press, New York, **1983.**

61 Persaud, L.; Langford, C. H. *Inorganica Chimica Acta*, **1986**, *14*, 15.

62 Persaud, L.; Langford, C. H. *Inorg. Chem.*, **1985**, *25*, 3438.

63 Murray, R. W.; Ewing, A. J.; Durst, R. A., *Anal. Chem.*, **1987**, *59*,379A.

64 Chidsey, C. D.; Murray, R. W., *Science*, **1986**, *231*, 25.

65 Collman, J. P.; Marrocco, M.; Denisevich, P.; Koval, C.; Anson, F. C. *J. Electroanal. Interfacial Electrochem.*, **1979**, *101*, 117.

66 Collman, J. P.; Anson, F. C.; Bencosme, C. S.; Durand, R. R.; Kreh, R. P. *J. Am. Chem. Soc.*, **1983**, *105*, 2699.

67 Calabrese, G.S.; Buchanan, R.M.; Wrighton, M.S. *J. Am. Chem. Soc.*, **1983**, *105*, 5594.

68 Harrison, D.J.; Wrighton, M.S. *J. Phys. Chem.*, **1984**, *88*, 3932.

69 Wrighton, M.S.; Palazzotto, M.C.; Bocarsly, A.B.; Bolts, J.M.; Fischer, A.; Nadjo, L. *J. Am. Chem. Soc.*, **1978**, *100*, 7264.

70 Frank, A. In *"Energy Resources through Photochemistry and Catalysis"*, Grätzel, M. (ed.), Academic Press, New York, **1983.**

71 Chao, S.; Wrighton M.S., *J. Am. Chem. Soc.*, **1987**, *109*, 6627.

72 Chao, S.; Wrighton M.S., *J. Am. Chem. Soc.*, **1987**, *109*, 8.

73 White, H.S.; Kittlesen, G.P.; Wrighton M.S., *J. Am. Chem. Soc.*, **1984**, *106*, 5375.

74 Josowicz, M.; Janata J., *Anal. Chem.*, **1986**, *58*, 514.

75 Paul, E.W.; Ricco, A.J.; Wrighton, M.S., *J. Chem. Phys.*, **1985,** *89,* 1441.

76 Kittlesen, G.P.; White, H.S.; Wrighton, M.S., *J. Am. Chem. Soc.*, **1984,** *106,* 7389.

77 Reed, R.A.; Geng, L.; Murray, R.W., *J. Electroanal. Interfacial Electrochem.*, **1986,** *208,* 185.

78 Burns, R. P.; McAuliffe, C. A. *Adv. in Inorg. Chem. and Radiochem*, **1979,** *22*, 303.

79 Mills, W. H.; Clark, R. E. D. *J. Chem. Soc.*, **1936**, 175.

80 Bahr, G.; Schleitzer H. *Chem. Ber.*, **1957**, *90*, 438.

81 Bahr, G.; Schleitzer H. *Chem. Ber.*, **1955**, *88*, 1771.

82 Alvarez, S.; Vicente, R.; Hoffmann, R. *J.Am. Chem. Soc.*, **1985**, *107*, 6253.

83 Gray, H. B.; Williams, R.; Bernal, I.; Billig, E. *J. Am. Chem. Soc.*, **1962,** *84*, 3596.

84 McCleverty, J. A. *Prog. Inorg. Chem.*, **1968**, *10*, 49.

85 Chandramouli, G. V. R.; Manoharan, P. T. *Inorg. Chem.*, **1986**, *25*, 4680.

86 Eisenberg, R.; Ebers, J. A.; Clark, R. J. H.; Gray, H. B. *J. Am. Chem.Soc.*, **1964**, *86*, 113.

87 Mahadevan, C. *J. Crystallogr. Spectrosc. Res.*, **1986**, *16*, 347.

88 Schläpfer C. W.; Nakamoto K. *Inorg. Chem.*, **1975**, *14*, 1338.

89 Mines, I. E.; Geiger, W. E. *Inorg. Chem.*, **1973**, *12*, 1189.

90 Schrauzer, G. N.; Mayweg, V. P. *J. Am. Chem. Soc.*, **1965**, *87*, 3585.

91 Shupack, S. I.; Billig, E.; Clark, R. J. H.; Williams, R.; Gray, H. B. *J. Am. Chem. Soc.*, **1964**, *86*, 4594.

92 Sano, M.; Adachi, H.; Yamatera, H. *Bull. Chem. Soc. Japan*,**1981**, *54*, 2636.

93 Schmitt, R. D.; Maki, A. H. *J.Am. Chem. Soc.*, **1968**, *90*, 2288.

94 Geiger, W. E.; Allen, C. S.; Mines, T. E.; Senftleber, F. C. *Inorg. Chem.*, **1977**, *16*, 2003.

95 Clark, R. J. H.; Turtle, P. C. *J. Chem. Soc., Dalton Trans.*,**1977**,2142.

96 Mateinzo, J. L.; Grim, O. S.; Swartz, W. E. *J. Am. Chem. Soc.*, **1972**, *94*, 5116.

97 Hoggins, J. T.; Steinfink, H. *Inorg. Chem.*, **1976**, *15*, 1682.

98 Hennig, R.; Schlmann W.; Kisch, H. *Agnew. Chem. Int. Ed. Engl.* **1980**, *19*, 645.

99 Zeng, N.; Buckeler, J.; Kisch, H. *J. Am. Chem. Soc.* , **1985**, *107*, 1459.

100 Dooley, D. M.; Patterson, B. M. *Inorg. Chem.*, **1982**, *21*, 4330.

101 Vogler, A.; Kunkely, H. *Inorg. Chem.*, **1982**, *21*, 1172.

102 Persaud, L.; Langford, C. H. *Inorg. Chem.*, **1985**, *24*, 3526.

103 Billing E.; Williams R.; Bernal I.; Walters J. H.; Gray H. B. *Inorg. Chem.*, **1964**, *2*, 663.

104 Benson R. E.; Melby L. R.; Weiher J. F., *J. Am. Chem. Soc.*, **1964**, *86*, 4329.

105 Menschutkin N, *Z. Phys. Chem.*, **1890**, *6*, 41.

106 Spialter L., Pappalardo J. A., *"The Acyclic Tertiary Amines"*, Macmillan; New York, **1965**, pp.14-29.

107 Factor, A.; Heinsohn, G. E. *Polym. Lett.*, **1971**, *9*, 289.

108 Phillips, J.; Langford, C. H.; Koningstein, J.A.; Sassaville, R. *J. Phys. Chem.*, **1978**, *82*, 622.

109 Curtis, J. C.; Sullivan, B. P.; Meyer, T. J. *Inorg. Chem.*, **1980**, *19*, 3833.

110 Persaud, L.; Langford, C. H. *Inorg. Chem.*, **1986**, *25*, 3438.

111 Davison, A.; Edelstein, N.; Holm, R. H.; Maki, A. H. *Inorg. Chem.*, **1963**, *2*, 1227.

112 Persaud, L. *unpublished results.*

113 F-CURVE is a trademark of LEDS publishing, NC, U.S.A.

114 Watanabe, T.; Honda, K. *J. Phys. Chem.*, **1982**, *86*, 2617.

115 Vogler, A.; Kunkely, H. *J. Chem. Soc. Chem. Commun.*, **1986**, 1616.

116 Geiger, W. E. Jr.; Maki, A. H. *J. Phys. Chem.*, **1971**, *75*, 2387.

117 Wüdl, F. *J. Am. Chem. Soc.*, **1975**, *97*, 1962.

118 Mahler W. *U.S. Patent 3,398,167*, **1968**.

119 Bird, C. L.; Kuhn, A. T. *Chem. Soc. Rev.*, **1981**, *10*, 49.

120 Steckhan, E.; Kuwana, T. *Ber. Bunsenges. Phys. Chem.*, **1974**, *78*, 253.

121 Fernàndez, A.; Kisch, H. *Chem. Ber.*, **1984**, *117*, 3102.

122 Johnson, C. E.; Eisenberg, R.; Evans, T. R.; Burberry, M. S. *J. Am. Chem. Soc.*, **1983**, *105*, 1795.

123 Tsou, Y-M.; Liu, H-Y.; Bard, A. J. *J. Electrochem. Soc.*, **1988**, *135*, 1669.

124 Creager, S. E.; Fox, M. A. *J. Electroanal. and Interfacial Electrochem.*, **1989**, *258*, 431.

125 Andrieux, C. P.; Dumas-Bouchiat, J-M.; Savéant, J-M. *J. Electroanal. and Interfacial Electrochem.*, **1982**, *131*, 1.

126 Inoue, T.; Anson F. C., *J. Phys. Chem.*, **1987**, *91*, 1519.

127 Mandlebrot, B. *"The Fractal Geometry of Nature"*, W.H. Freeman, NY, NY, **1983**.

128 Lewis, T. J. *I.E.E.E. Trans. on Elec. Insul.*, **1986**, *EI-21*, 289.

129 Fabish, T. J.; Saltsburg, H. M.; Hair, M. L. *J. Appl. Phys.*, **1976**, *47*, 930.

130 Fabish, T. J.; Saltsburg, H. M.; Hair, M. L. *J. Appl. Phys.*, **1976**, *47*, 940.

131 Huang Z.; Ordoñez, I.; Lawrence, M. F., *in preparation.*

132 Gray, H. B.; Ballhausen, C. J. *J. Am. Chem. Soc.*, **1963**, *85*, 260.

133 Turro, N. J. in *"Modern Molecular Photochemistry"*, Turro, N. J.; ed.; Benjamin/Cummings Publishing, Philippines, **1978**, pg.183.

134 Carol Moralejo, *PhD. Thesis*, Concordia University, Montreal, QC, Canada, **1989**.

135 Buttry, D. A.; Anson, F. C. *J. Am. Chem. Soc.*, **1982**, *104*, 4824.

136 Billmeyer, F. W., *"Textbook of Polymer Science"*; John Wiley & Sons, NY, NY, 3rd Edition, **1984**, pg.418.

137 Minami, N.; Watanabe, T.; Fijishima, A.; Honda, K. *Ber. Bunsen-Ges. Phys, Chem.*, **1979**, *83*, 476.

138 Mayhew, S. G.; Muller, F. *Biochem. Soc. Rev.*, **1982**, *10*, 176.

139 Sato, H.; Tamamura, T. *J. Appl. Poly. Sci.*, **1979**, *24*, 2075.

140 Buttry, D. A.; Anson, F. C. *J. Am. Chem. Soc.*, **1983**, *105*, 685.

141 Buttry, D. A.; Anson, F. C. *J. Electroanal. and Interfacial Electrochem.*, **1981**, *150*, 333.

142 Dahms H. *J. Phys. Chem.*, **1968**, *72*, 362.

143 Glatzhofer, D. T.; Utanski, J.; Wegner, G. *Polymer*, **1987**, *28*, 449.

144 Bull, R. A.; Fan, F. R.; Bard, A. J. *J. Electrochem. Soc.*, **1984**, *131*, 687.

145 Tanguy, J.; Mermilliod, N.; Hoclet, M. *J. Electrochem. Soc.*, **1987**, *134*, 795.

146 Paulse, C. D.; Pickup, P. G. *J. Phys. Chem.*, **1988**, *92*, 7002.

147 Brédas, J. L.; Street, G. B. *Acc. Chem. Res.*, **1985**, *18*, 309.

148 Biro, D. A.; Langford, C. H., *Inorg. Chem.*, **1988**, *27*, 3601.